Experimental and numerical investigation of atraumatic tooth extraction biomechanics in an ex vivo swine model

by

Timothy James Gadzella

A thesis submitted in partial fulfillment of the requirements for the degree of

Doctor of Philosophy

Department of Mechanical Engineering
University of Alberta

Abstract

Tooth extraction (exodontia) is among the most common surgical procedures in healthcare, driven by the prevalence of tooth decay and periodontal disease. Traditionally, tooth extraction is completed with forceps and the exertion of combined loads about the tooth's centre of rotation. This approach widens bone surrounding the tooth root, but also may cause damage to the surrounding tissues which strongly influences patient recovery and is hypothesized to impact the survivability of implants and the remaining natural dentition. Different atraumatic extraction techniques have been developed to minimize damage, but the altered loading they impose relative to routine forceps extraction and the connection to patient outcomes is unclear. The biomechanics of the dental complex under extraction must be better understood in order to make these connections between mechanical loading and patient outcomes.

Experimental ex vivo and numerical computer models of the dental complex (a single tooth unit comprised of the tooth, periodontal ligament (PDL), and supporting bone) under vertical extraction load are proposed using partial swine incisors. First, an experimental method is developed with a novel process for preparing the swine mandibles and performing simulated extractions using a custom self-aligning experimental apparatus. Second, a generalized axisymmetric model of the swine incisor is developed using a visco-damage hyperelastic model of the PDL to represent the extraction experiments. A multi-curve inverse finite element approach is proposed to determine parameters of the PDL model from the experimental data. Both the experimental and numerical methods are then applied in a characterisation study of the biomechanics of vertical tooth extraction in relation to varying load regimes, imposed damage states, and tooth geometry. Finally, a new software interface for prescribing and recording

extraction load applied during vertical tooth extraction is proposed to facilitate implementation of the study findings with a commercially available Benex® extraction device.

Key findings from the thesis research are presented describing both a fundamental characterisation of dental complex biomechanics and applications of the developed models. The mechanical response of the dental complex to extraction load depended on both tooth geometry (root surface attachment area) and the applied extraction load, with higher loading rates and larger root surface areas causing greater peak extraction forces. The stiffness of the dental complex and tooth fracture rate also increased with load rate. A set of PDL parameters were found as a solution to the inverse finite element problem that, when implemented in the axisymmetric finite element model, predicted the stiffness and peak force of three displacement-controlled data sets from the experimental data. The application of this numerical model as a predictive tool was demonstrated for predicting new force-hold loading schemes and the predictions were validated experimentally. The model was also adapted to different geometric conditions by predicting the change in dental complex response when the PDL was damaged with a dental instrument. A proof-of-concept for the software interface was used in a benchtop ex vivo study that demonstrated the successful use of a clinical extraction device in following a prescribed load scheme.

The combined findings of the presented thesis demonstrate the importance of biomechanics in characterizing vertical tooth extraction, provide modeling tools for the development of biomechanically-based extraction procedure guidelines, and initiate the technological advancements needed to clinically implement these guidelines. Outcomes from this thesis can be directly applied to the development of improved vertical tooth extraction procedures and further investigation of the biomechanical predictors of dental complex injury.

Preface

Chapter 3 of this thesis was previously published as *Gadzella TJ, Hynkova K, Westover L, Addison O, Romanyk DL. A novel method for simulating ex vivo tooth extractions under varying applied loads. Clinical Biomechanics. 2023 Dec 1;110:106116*. I was responsible for the design of the apparatus and development of the sample preparation procedure, collecting and processing the data, and preparation of the manuscript. Kristyna Hynkova assisted in the experiments by preparing the teeth for extraction and training me in the preparation method. Lindsey Westover provided insight in manuscript preparation regarding her expertise in tissue mechanics. Owen Addison provided clinical insight in the preparation of the manuscript. Dan Romanyk assisted in the conception of the study and oversaw analysis and manuscript preparation.

Chapter 4 of this thesis has been accepted for publication in the Journal of the Mechanical Behaviour of Biomedical Materials as *Gadzella TJ, Westover L, Addison O, Romanyk DL. Inverse finite element analysis for an axisymmetric model of vertical tooth extraction.* I was responsible for the development of the finite element model and inverse finite element codes, performing the solution runs, and preparation of the manuscript. Lindsey Westover and Owen Addison provided guidance for the model development and interpretation of the results during manuscript preparation. Dan Romanyk oversaw the process conception, helped guide the development of the inverse finite element scheme, aided in the interpretation of the results, and oversaw manuscript preparation.

For Katie, my compass rose.

We arrived here by overcoming our share of hardship, heartbreak, and a world that did its best to end around us. I should have been lost a thousand times but when I look at you, I know my way home.

And for Margaret and Jensen, with whom we go joyfully into what comes next.

Dad loves you.

"He used often to say there was only one Road; that it was like a great river: its springs were at every doorstep, and every path was its tributary. 'It's a dangerous business, Frodo, going out of your door,' he used to say. 'You step into the Road, and if you don't keep your feet, there is no knowing where you might be swept off to.'" - JRR Tolkien, The Fellowship of the Ring

Acknowledgements

I would first like to acknowledge the contributions of my PhD supervisor, Dan Romanyk, to this thesis research and my personal development over the course of my studies. To say that they are immense is an understatement. Dan has always offered me the opportunity to grow as an engineering scientist, understanding for even my most expensive mistakes, a listening ear for unsolicited motorsport analysis, and genuine friendship for myself and my family. It is with incredible patience that he has taught me patience of my own for the processes of the academy and resilience to interesting problems that threaten to get us "lost in the weeds". It has been a privilege to be Dan's student and I hope to honour that privilege throughout my career.

I would also like to offer my gratitude to my supervisory committee, Dr. Lindsey Westover and Dr. Owen Addison, for helping guide my research. Lindsey has always provided an invaluable reality check for my ideas, particularly in numerical modelling of tissues, and has greatly improved this work as a result. Owen provides a frank, collegial assessment of my work from the clinical perspective that I value deeply, particularly when I have over-engineered something or strayed down a path of inquiry that leads to nowhere. I am very thankful to have had their guidance throughout my research.

There are also faculty members and staff from other faculties who I would like to acknowledge for contributing to this thesis. Dr. Michael Doschak of the Faculty of Pharmacy and Pharmaceutical Sciences and Dr. Karyne Rabey from the Faculty of Medicine and Dentistry both assisted in collecting the CT images used in this thesis. Fortunately for me, CT scanning and reconstruction are not short processes and provided me with ample opportunity to converse with and learn from them. I'm very grateful for their mentorship. Similarly, I'd like to acknowledge the tireless efforts of our research coordinator in the School of Dentistry, Maria Alexiou, for helping keep the lights on in our biomechanics lab.

I have been very fortunate to receive funding for my research from a number of sources, such as the Natural Sciences and Engineering Research Council of Canada, the Canadian Association of Dental Research and Network for Canadian Orah Health Research, the University of Alberta's President's Office, the School of Dentistry, and my home department of Mechanical Engineering. Their support has been instrumental to performing and sharing my research.

I would like to thank all the members of the Romanyk research group with whom I have worked over the last four years. Many of them will no longer trust me to pick the music (or audiobook) for a drive of any length, whether it is the long haul to a conference in Banff or a quick trip to Sherwood Park, but their camaraderie has meant a lot to me. I would like to particularly acknowledge the solidarity and friendship of Dr. Kristyna Hynkova, who was my lab partner during the COVID-19 pandemic and helped train me in preparing teeth for my experiments. Thanks, everyone.

I would like to acknowledge the support I've received from our friends and family throughout my PhD studies. I'm deeply grateful for the role all of them played in keeping me grounded through my program. I want to thank my PhD student colleagues-in-arms from the University of Calgary, Thomas Lijnse and Tiffany Dang, for their support and friendship. I'm very grateful to the AB BME conference for bringing them into my life. There are a good number of World of Warcraft players, particularly David Chavez and Olivea Dawkins, who tolerated me writing or checking solver runs between pulls and showed a great deal of sideline enthusiasm for my research. Myles Wright and Mike and Matt Mechor always made sure I had a place in the blind to get some fresh air and let off steam every spring and fall. I'm very grateful for their friendship and keen stewardship in making sure I know when my snow goose call is more likely to bring in peahens. Thank you to Eric, Geo, and the rest of House Mooney for making sure I always feel at home, even when we are far apart. My parents, Cathy and Gerry, and my sisters, KP and Ehren, have shown unwavering support for my career and love for our family for which I am eternally grateful. Finally, I have dedicated this work to my wife Katie, who is my partner in everything and whose support, encouragement, and kindness are the reasons that this thesis was completed; and our twins JJ and Maggie, whose protests at nap time are the reason it was completed with many breaks.

Table of Contents

List of Tables

List of Figures

Glossary

µCT - Micro-computed tomography. A set of imaging techniques in which projection images (gathered using x-ray) are used to construct a 3D representation of the projected body.

Axisymmetry – Demonstrates properties of rotational symmetry about an axis; 3D fields or geometries that have the same properties at a given radial position relative to a fixed axis.

CE-µCT – Contrast-enhanced micro-computed tomography. µCT images with contrast enhanced by the addition of radiopaque dyes or material.

Dental complex – The body of tissues that comprise of a single tooth and its supporting socket. Includes the enamel, dentin, cementum, and pulp of the tooth; the periodontal ligament (PDL), and the alveolar bone.

ECM – Extracellular matrix. Refers to the acellular components of a tissue that surround structural elements (fibrils, vasculature, etc.).

Exodontia – The dental practice of tooth extraction, i.e. tooth extraction performed intentionally in a clinical procedure, rather than accidentally or violently.

FE/FEA – Finite element or finite element analysis. A family of analytical techniques which solve partial differential equations (such as those that describe the resistance of physical bodies to load) over spatial domains that are subdivided or discretized into known sub-regions or "elements".

Hyperelasticity – the property of a body to store and return strain energy while undergoing large displacements that violate the assumptions of infinitesimal strain analysis.

IFEA – Inverse finite element analysis. The application of finite elements to problems in which the properties of some or all of the elements are unknown and must be determined by comparing the FEA solution to other data.

PDL – Periodontal ligament. A vascular soft tissue which occupies the space between a tooth root and the surrounding bone, providing mechanical support and attaching the tooth.

Stomatognathic system – The facial tissues and organs of the oral cavity, particularly those responsible for mastication (chewing) and speech.

Viscoelasticity – the property of a body to both store and dissipate strain energy under load, related to viscous fluid flow. Associated with the rate-dependent behaviour of materials, particularly those with fluid components.

A note on dental anatomical directions : Directions throughout are defined through the geometric centre of rotation of a tooth and oriented with respect to the dental arch. The **apical-gingival** or **apical-occlusal** axis is vertical with respect to the tooth, running along the "long axis" of the tooth from the top of the crown to the apex/root tip. The **bucco-lingual** axis is orthogonal to the apical-gingival axis, perpendicular to the apical-gingival axis and the dental arch. **Buccal** motion moves outwards (towards the cheek) and **lingual** motion is inwards (towards the tongue) with respect to the dental arch. The **mesio-distal** axis is tangential to the dental arch and orthogonal to the other two axes. **Mesial/medial** motion is towards the incisors and centreline of the arch; **distal** motion is towards the molars and away from the centreline of the arch.

1 Introduction

1.1 Background

The Canadian Dental Association (CDA) published a report titled The State of Oral Health in Canada in 2017, highlighting Canada's place in the global state of oral health affairs and identifying key areas of improvement needed to provide access to oral health care [1]. This report identified Canada as a global leader in oral health based on a number of indicators such as the decayed, missing, and filled teeth (DMFT) index. Canada's mean DMFT index for 12-year olds was 1.02, meaning that, on average, every Canadian child is affected by decay in at least one of their teeth. Canada was identified as having favourable rates of edentulism (missing teeth) among adults, with approximately 6.4% of adults reporting as fully edentulous in 2010. This figure reached up to 22% when considering only the senior population aging greater than 60. The subtext of these figures is that tooth loss is a simple reality faced by many Canadians and that the prevalence of edentulism is directly related to a large number of tooth extractions being performed in routine dental care. In 1997, 13.8% of randomly sampled dental visits to an Ontario clinic involved extraction of one or more teeth [2] – it is the inferred position of the CDA in the 2017 report that the indications underlying this prevalence have improved with water fluorination and oral health education programs, but DMFT and edentulism rates among Canadian adults suggest that tooth extraction remains one of the most common procedures performed in Canadian healthcare.

Tooth extraction (or "exodontia") is fundamentally a biomechanical process that, despite its prevalence, is not frequently studied from a biomechanical perspective nor guided by associated evidence. The biomechanics of exodontia are principally concerned with the dental complex, which is the system of tissues that supports a single tooth and comprised of the hard tissues of the tooth and the pulp chamber they surround, the alveolar bone that surrounds the tooth, and the periodontal ligament (PDL) that connects the tooth and bone [3]. Damage to all components of the dental complex are of interest to extraction biomechanics: rupture of the PDL is necessary to allow the tooth to be removed from the socket [4]; plastic deformation of the alveolar bone is required to allow for removal of the tooth and microdamage to the apical bone may occur [4] but both are negatively associated with long-term extraction outcomes [4-5]; and fracture of the tooth root during the extraction elevates the complexity, risks, and invasiveness of the extraction

procedure [5]. Routine extractions are performed with forceps, the design of which varies by tooth location, involving a consistent combination of intrusive, extrusive, bending, and rotational forces (demonstrated in Figure 1-1a and 1-1b) that are guided by a priori radiographic assessment and haptic feedback during the procedure [4-5]. The risks associated with failure in traditional forceps extraction are not trivial – fracture of the root requires more complicated, invasive periosteal flap procedures (as described by Dym and Weiss [5]) and fracture of the alveolar plates from the over-application of force is a serious traumatic injury that can take months to heal [6]. Even in a successful extraction, the damage imparted to the remaining alveolar bone is presumed to significantly impact bone resorption, which in turn influences the survivability of dental implants and the remaining natural dentition [5, 7-8]. Despite these risks, there remains no quantitative evidence-driven guideline for the forces that should be applied during routine tooth extraction. The instrumentation of forceps to provide this evidence remains challenging and has been attempted with the attachment of pressure- or strain-based instruments [9-10] or large, sensitive robotic manipulators [11] to the forceps.

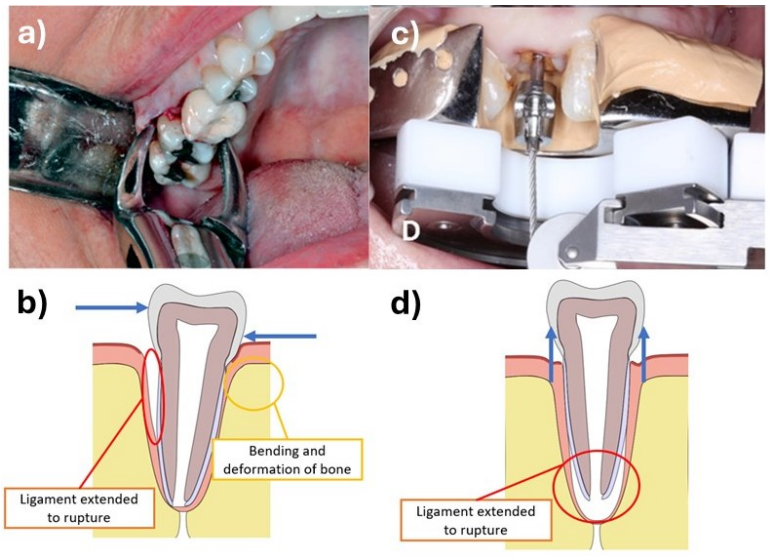

Figure 1-1: Comparison of the biomechanical principles of tooth extraction. Conventional forceps extraction (a) [4] applies combinations of moment-causing forces to rupture the PDL and deform bone (b). Vertical tooth extraction (c) [12] applies force along the axis of the tooth to extend the PDL to rupture (d). Figures a) and c) are reproduced with permission.

Alternative extraction techniques described as “atraumatic” or “minimally-invasive” have arisen to reduce the damage imparted during tooth extraction procedures and improve the associated outcomes. These techniques seek to fundamentally alter the biomechanical forces exerted on the

dental complex during tooth extraction by sectioning teeth for easier removal [13], translocating the leverage forces applied with alternative forceps designs [14], or altogether removing the twisting and rocking moments applied to the tooth in favour of purely axial traction along the tooth's root (as demonstrated in Figure 1-1c and 1-1d) [12, 15]. Split-mouth comparisons have shown promise for some of these techniques in improving clinical outcomes [14], and axial traction techniques (also known as "vertical extraction") have even been used to retrieve tooth roots that otherwise would necessitate invasive surgical removal [15]. However, the connection between these altered loads, the biomechanics of the dental complex in response, and improvements in clinical outcomes has not been fully investigated. As a result, there are no more quantitative guidelines for atraumatic extraction than there are for conventional forceps extractions, and the further development of this family of techniques is limited by the sparse nature of available data.

1.2 Thesis Structure and Objectives

Bridging the gap between dental biomechanics and evidential guidelines for atraumatic extraction procedures drives the research within this thesis, which focuses on vertical tooth extraction as a clinically-derived loading case. Studying vertical tooth extraction (such as that performed with a Benex® extraction device) offers the advantage of studying physically relevant loading regimes that are physically straightforward to replicate as force is applied in a single, known direction during the extraction. An engineering biomechanics approach is undertaken which seeks to provide a basic understanding of the dental complex's response to vertical extraction load and provide numerical models informed by this understanding as tools for further advancement. It is from this foundational understanding that changes in clinical device design and procedures can be made. To this end, the goal of this thesis is to characterise the biomechanics of tooth extraction in ways that are applicable to the development of new atraumatic extraction procedures. The thesis may be broken down into three primary objectives:

1. To experimentally characterize the mechanical behaviour of the ex vivo dental complex during controlled vertical tooth extraction and develop preliminary metrics for predicting procedure success;
2. To develop a generalizable finite element model of the dental complex that predicts the mechanics of tooth extraction for applications in future procedural and device

development and validate it using the experimental characterisation data obtained in Objective 1; and

3. To apply the findings of Objectives 1&2 towards the improvement of atraumatic exodontia procedures by augmenting a clinical device with instrumentation and feedback mechanisms allowing the further investigation of extraction procedures based on the predictions of the experimental and numerical models.

The subsequent chapters of this thesis develop both ex vivo experimental and numerical computer models for studying dental complex biomechanics. Both approaches are necessary to provide a biomechanical characterisation of vertical tooth extraction that is useful for developing new technologies: robust experimental methods provide ground truth data and validate assumptions made in the development of other models, whereas numerical models are limited by the quality of the data that informs them but allow for experimentation and iterative design at much lower costs than repeated physical testing. However, there exists a necessarily circular relationship between experimental and numerical models and the completion of Objectives 1 and 2 are correspondingly intertwined. The development of numerical models from experimental data, the application of the numerical model to the development of new ideas, and the subsequent validation of new ideas by returning to the experimental model are all demonstrated in the following chapters.

Chapter 2 of this thesis summarizes the available literature concerning the biomechanics of tooth extraction. The key features of dental complex anatomy necessary for understanding tooth extraction are introduced. A critical view of the literature describing the clinical, experimental, and numerical modeling of extraction biomechanics is adopted to develop a framework for the following chapters.

An improved ex vivo experimental method for studying vertical tooth extraction biomechanics is developed in Chapter 3 towards the completion of Objective 1. This method characterizes the biomechanics of the dental complex based on the peak force achieved during an experimentally-simulated extraction and proposes an analytical methodology to measure the instantaneous stiffness of the complete dental complex. Peak force is a metric previously used in tooth extraction studies to characterize the total energy imparted to the dental complex during an extraction [12]. Instantaneous stiffness measurement is a novel metric that provides insight into

the response of the complete dental complex to the imparted energy throughout the extraction rather than only at the end. Both mechanical metrics are investigated under different loading rates and control types (force- or displacement-controlled) for their relationships to extraction loading conditions. These loading conditions and the resulting biomechanical metrics are related to the success or failure of extractions.

An axisymmetric finite element model of the dental complex and method for determining its material parameters from experimental data towards Objective 2 is presented in Chapter 4. Material parameters describing the hyperelastic, viscoelastic, and damage behaviours of the PDL are fit to experimental data gathered in Objective 1.

Chapter 5 implements the developed methods from the preceding chapters in a characterisation study of vertical extraction biomechanics that describes the behaviour of the dental complex, validates material parameters for the finite element model (thereby completing Objectives 1&2), and demonstrates the predictive capabilities of the developed models in application to new loading schemes towards Objective 3. Root surface attachment areas are measured using micro computed tomography (μCT) to include the effects of tooth geometry in the characterization methodology developed in Chapter 3. The inclusion of the imagine data allows for statistical modeling characterizing the relationship between peak force, load rate, and tooth geometry. Contrast-enhanced μCT (CE-μCT) protocols also provides insight into the rupture behaviour of the PDL to aid interpretation of the FE model.

Chapter 6 details the design and programming of a computer interface to facilitate the application of previous chapters' findings using an instrumented clinical device, also towards Objective 3. Loading schemes developed in Chapter 5 are demonstrated with the instrumented device in benchtop ex vivo extraction tests on the swine incisor model. The response of the dental complex to loading with the instrumented device is found to be very similar to the ex vivo predictions in Chapter 5, validating the predictive capabilities of the experimental and numerical models developed in this thesis.

Chapter 7 summarizes the findings of all chapters, developing conclusions for the three objectives listed above and determining directions for future work.

References

1. Canadian Dental Association. The State of Oral Health in Canada, March 2017. Available online: https://www.cda-adc.ca/stateoforalhealth/
2. Murray H, Clarke M, Locker D, Kay EJ. Reasons for tooth extractions in dental practices in Ontario, Canada according to tooth type. International Dental Journal. 1997 Feb;47(1):3-8.
3. Chu TM, Liu SS, Babler WJ. Craniofacial biology, orthodontics, and implants. In: Basic and applied bone biology 2014 Jan 1 (pp. 225-242). Academic Press.
4. Hupp J, Ellis E, and Tucker MR. Contemporary oral and maxillofacial surgery. 7Th ed. Philadelphia, PA: Elsevier; 2019. Chapter 8: Principles of routine exodontia; p.106-134.
5. Dym H, Weiss A. Exodontia: tips and techniques for better outcomes. Dent Clin North Am. 2012;56(1):245-66. doi: 10.1016/j.cden.2011.07.002.
6. Levin L, Day PF, Hicks L, O'Connell A, Fouad AF, Bourguignon C, Abbott PV. International Association of Dental Traumatology guidelines for the management of traumatic dental injuries: General introduction. Dental Traumatology. 2020 Aug;36(4):309-13.
7. Schropp L, Wenzel A, Kostopoulos L, Karring T. Bone healing and soft tissue contour changes following single-tooth extraction: a clinical and radiographic 12-month prospective study. International Journal of Periodontics & Restorative Dentistry. 2003 Aug 1;23(4).
8. Hamed NA, Mohamed MH. Radiographic Evaluation of Bone Height Changes Around Immediately Placed Implant Retaining Mandibular Over-Denture in Atraumatic Tooth Extraction Cases. Egyptian Dental Journal. 2023 Jul 1;69(3):2035-43.
9. Lehtinen R, Ojala T. Rocking and twisting moments in extraction of teeth in the upper jaw. International journal of oral surgery. 1980 Oct 1;9(5):377-82.
10. Ahel V, Ćabov T, Špalj S, Perić B, Jelušić D, Dmitrašinović M. Forces that fracture teeth during extraction with mandibular premolar and maxillary incisor forceps. British Journal of Oral and Maxillofacial Surgery. 2015 Dec 1;53(10):982-7.

11. Riet TV, Graaf WD, Lange JD, Kober J. Analysis of movements in tooth removal procedures using robot technology. Plos one. 2023 May 18;18(5):e0285503.
12. Dietrich T, Schmid I, Locher M, Addison O. Extraction force and its determinants for minimally invasive vertical tooth extraction. J Mech Behav Biomed Mater. 2020;105:103711. doi: 10.1016/j.jmbbm.2020.103711.
13. Papadimitriou DE, Geminiani A, Zahavi T, Ercoli C. Sonosurgery for atraumatic tooth extraction: a clinical report. The Journal of Prosthetic Dentistry. 2012 Dec 1;108(6):339-43.
14. El-Kenawy MH, Ahmed WM. Comparison Between Physics and Conventional Forceps in Simple Dental Extraction. J Maxillofac Oral Surg. 2015;14(4):949-55. doi: 10.1007/s12663-015-0765-6.
15. Muska E, Walter C, Knight A, Taneja P, Bulsara Y, Hahn M, Desai M, Dietrich T. Atraumatic vertical tooth extraction: a proof of principle clinical study of a novel system. Oral Surg Oral Med Oral Pathol Oral Radiol. 2013;116(5):e303-10. doi: 10.1016/j.oooo.2011.11.037.

2 Literature Review – Dental Complex Anatomy and Tissue Biomechanics

Chapter 2 reviews the anatomy of the dental complex at the level of different tissues, their organization, and important mechanical characteristics. Salient details comparing porcine and human dental models are briefly discussed. The biomechanics of both conventional and atraumatic tooth extraction are then outlined, followed by a summary of numerical and experimental methods for modelling the periodontal ligament. Methods of coupling viscous, damage, and hyperelastic models are discussed with key examples that are important for framing the modelling work undertaken in subsequent chapters.

2.1 Dental Complex Anatomy

The dental complex refers to a subsystem of the stomatognathic system considering a single tooth and the supporting tissues. The complex consists broadly of the hard tissues of the tooth (enamel, cementum, and dentin), the pulp they contain, the alveolar bone crests that form the tooth socket, the soft tissues of the gingiva that encase the alveolar bone, and the periodontal ligament (PDL). These tissues are arranged in a layered structure surrounding the tooth (Figure 2-1a) [1] and are responsible for its mechanical stability and biological vitality.

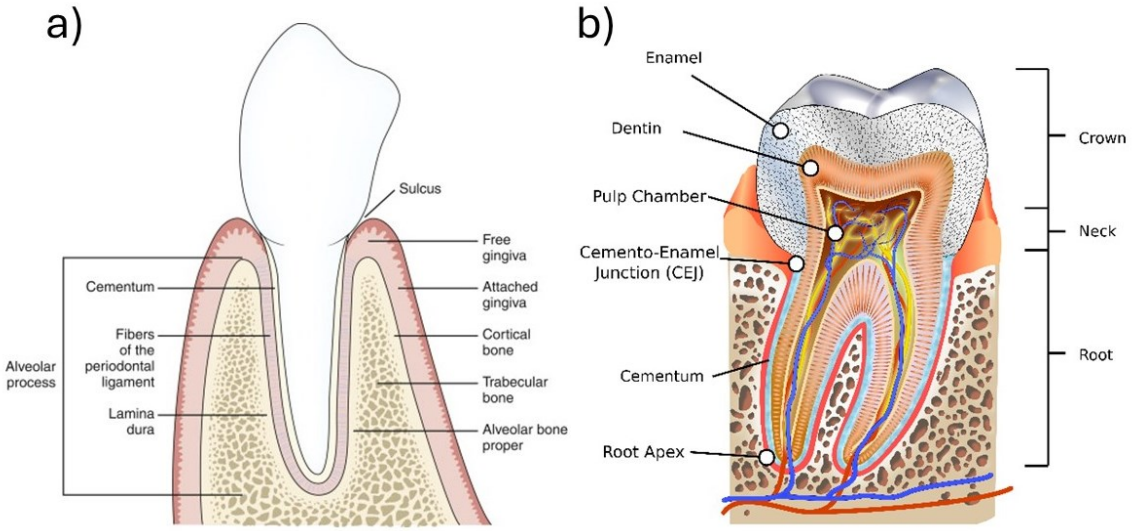

Figure 2-1: The anatomy of the dental complex, a) demonstrating the arrangement of the complex soft and hard tissues surrounding the tooth [1] (reproduced with permission); and b) the arrangement of the hard tissues in the tooth, adapted from [2] under CC-BY-SA license.

As demonstrated in Figure 2-1b, the interior arrangement of the tooth has a lamellar structure. The dentin surrounds the pulp chamber, which houses vital nerve and blood vessel tissues [3]. The enamel of the crown forms around the gingival aspect of the dentin down to the cemento-enamel junction (CEJ; the boundary which defines the crown from the root of the tooth). The dentin of the root is sheathed in cementum from the CEJ to the root apex, at which is located the apical foramen which permits the connection of the pulp tissue to the networks of the surrounding stomatognathic system.

2.1.1 Hard Tissues of the Tooth – Enamel, Dentin, and Cementum

Dental enamel is the hard lamellar tissue that forms the tooth crown, several times more dense and stiffer than the dentin it surrounds [4] with a Young's modulus of approximately 70-100 GPa

[4, 6-8]. Mechanically, the enamel is brittle and demonstrates fracture behaviour that is sensitive to crack initiation sites resulting from dental caries, tooth shape, or restorative interventions [4].

The dentin is adjacent to the pulp chamber and is composed of a mineralized matrix surrounding a tubular network of lacunae that can be visualized in radiographs [3,5]. The dentin is a cellularly active tissue supported by the pulp and a network of mineralizing cells that occupy the tubular network. It is softer than enamel (Young's modulus approx. 15-19 GPa [4, 6-8]) but still subject to brittle fracture and crack propagation, although the accumulation of microdamage localized around the tubular network and its interaction with collagen networks is hypothesized to allow for some yielding of the tissue before brittle fracture [5].

Cementum is the lamellar hard tissue that covers the surface of the dentin in the tooth root. The cementum is comprised of acellular interior layers and cellular exterior layers, but accommodates the penetration of collagen fibres (Sharpey's fibres) with varying degrees of mineralization throughout its thickness [3]. Cementum is frequently omitted from mechanical models of the dental complex because it is a thin tissue and the penetration of Sharpey's fibres can extend through it into the dentin, and it is generally accepted to be softer than the dentin and enamel (Young's modulus approx. 14 GPa [6-7]).

2.1.2 Periodontal Ligament (PDL)

The PDL is the vascular, fibrous tissue that connects the hard tissues of the tooth to surrounding bone. The structure of the PDL comprises of an extracellular matrix (ECM) which accommodates fibroblast cell activity and vasculature surrounding the collagenous fibres that connect the hard tissues [9]. Traditionally, the arrangement of the fibrous structure has been described as bundled (as evidenced in Figure 2-2) [9], but recent 3D images have been used to describe these structures as spatially-varying sheets [10] and lamellar membranes at the hard-tissue interfaces [11-12].

The function of the PDL is to distribute load applied through the dental complex from the tooth to the surrounding bone. The distribution of this loading is accommodated by the motion of the fibrous structure [11-12] which penetrates into the alveolar bone and cementum [10]. The mechanical characteristics of the PDL are complex because of its adaptive cellular nature, mechanical anisotropy primarily due to the fibrous phase, and relative softness compared to the

hard tissues. The complexities of modelling the behaviour of this tissue are discussed in detail in Chapter 2.2.2.

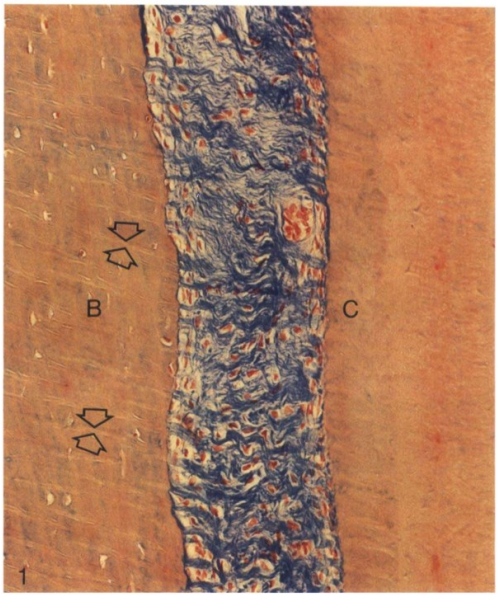

Figure 2-2: Histologically-stained transmission image of the periodontal ligament, reproduced with permission [9]. Collagen is stained in blue, with fibroblast cell nuclei stained in red. Bone [B] and cementum [C] demonstrate penetration of Sharpey's fibres originating from PDL attachment.

2.1.3 Alveolar Bone

The alveolar bone is the relatively soft, porous bone (Young's modulus 1.3-2 GPa [6,7]) that surrounds the tooth socket and lies between two stiffer, less porous cortical plates (Young's modulus 13.7 GPa [7]) defining the alveolar crest [1]. The difference between the two types of bone forming the alveolar crest is the relative porosity and trabecular orientation of the alveolar bone, although these features are not homogenous and the alveolar bone condenses slightly towards the tooth socket [1]. The alveolar crest attaches to the gingiva and PDL just inferiorly of the CEJ and is the supporting tissue of the entire dental complex. The adaptive nature of this tissue is critical for implant success and the survival of the dentition [1,16], as well as a primary consideration in orthodontic tooth movement [6-7].

2.1.4 Comparisons Between Human and Juvenile Swine Anatomy

The work presented in subsequent chapters of this thesis depends on the use of a porcine dentition model for dental biomechanics. Swine have commonly been used as subjects for

experimental models as a good analogue for human physiology [17]. Early adoption of swine models was primarily concerned with similarities to human nutritional needs, gastrointestinal processes, and cardiovascular physiology with applications of the swine model to biomechanical problems adopted later in the 20th century. Swine models offer several attractive advantages for studying dental biomechanics: the patterns of orthogenesis and fetal development are similar to humans, resulting in similar masticatory patterns; swine exhibit opportunistic omnivorous diets which, similar to humans, can accommodate almost any viable nutritious material and have similar demands on the function of the dentition; and swine exhibit rapid growth and are easy to care for, reducing the time and cost required to care for laboratory animals [18].

There are several key differences between the human and porcine dentition that must be accounted for in the use of a swine model to study dental biomechanics [18]. Transmission radiographs of juvenile swine mandibles are presented in Figure 2-3, which depict the elongation of the swine mandible relative to the human mandible. Swine teeth tend to be longer than human teeth, with larger periodontal spaces and interdental spaces to accommodate their size [18]. Swine teeth also demonstrate buccal (outward) angulation of the anterior teeth (incisors) that accommodate foraging behaviours [18]. Despite these limitations, the use of juvenile swine models for the study of dental biomechanics has proliferated [19-27] because it provides a good analog for the human dentition so long as these fundamental differences in dental complex geometry are accounted for. The primary concern for studying tooth extraction using swine models are the size and shape of the teeth and PDL space. An increase in tooth size is likely to increase the forces and energy that must be imparted to the dental complex to rupture the PDL, so the studied teeth should be selected or modified to approximate human teeth as closely as possible. Metrics for tooth size such as the root surface attachment area (RSAA) can also be used to quantify the geometry of the teeth and included in analyses as normalizing factors or covariates to eliminate or account for their impacts on biomechanical metrics. Similarly, the PDL spaces for the swine used in this thesis have a measured distance slightly greater than humans (up to 1mm) [21] that may increase the energy required to rupture the ligament. Correspondingly, the increased PDL space width may reduce the stiffness of the dental complex (these effects have not been previously studied for comparison to the human clinical extraction case). This change in geometry should be accounted for in the geometry of numerical models that represent the dental complex but is difficult to quantify post-extraction for use as a

normalizing factor (as may be done with RSAA) due to the destruction of the soft tissue during the procedure.

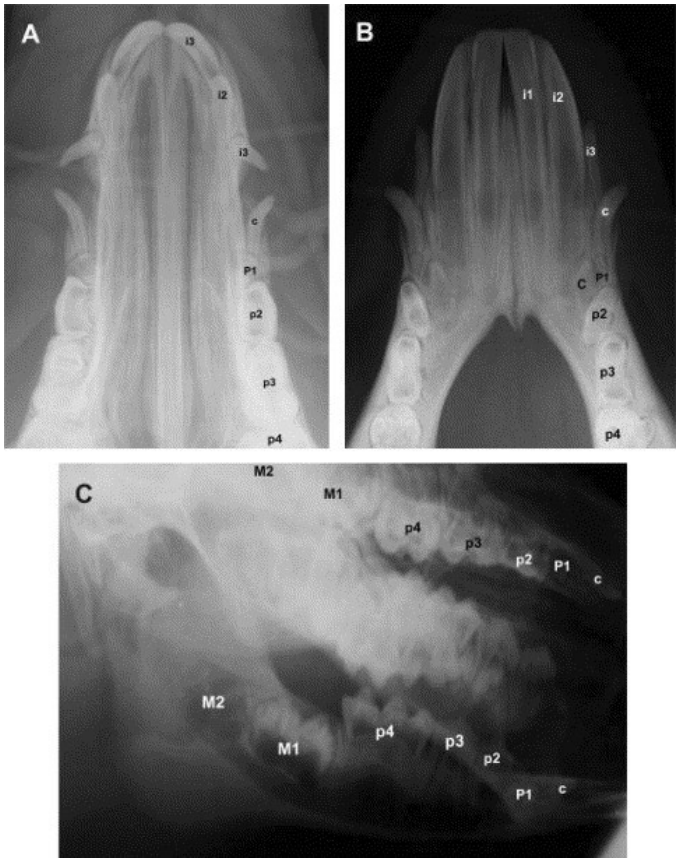

Figure 2-3: Transmission radiographs of the juvenile swine dentition, reproduced with permission [18]. a) and b) demonstrate coronal views of the anterior teeth and premolars at different gestational ages; c) a sagittal view of the mandibular and maxilary dentition, labelling molars, premolars, and canines.

2.2 Biomechanics of Tooth Extraction

The fundamental biomechanical principal of tooth extraction is the external application of force (by a clinician, via an extraction device or instrument) that causes sufficient damage to the dental complex that the tooth can be removed from the socket. Primarily, this damage is done through the extension and rupture of the PDL through motion of the tooth relative to the socket [28]. However, the other tissues are not necessarily isolated from damage. Microdamage (small-scale localized damage phenomena that affect the tissue quality without causing tissue-scale failure [29]) can accumulate in both the alveolar bone and tooth hard tissues during extraction loading. The accumulation of microdamage is a precursor to fracture in dentin [5], which can cause a

complete fracture of the tooth root that results in a portion of the tooth remaining attached to the PDL [16]. Completing the extraction in these cases requires the retrieval of the tooth root through the tooth socket or an apical access cut through the bone which is more invasive than the original procedure and increases patient recovery times [16]. Bone microdamage is caused during both the widening of the tooth socket via plastic deformation and the extension of the attached PDL during extraction movement of the tooth. This damage may also lead to a complete fracture of the alveolar ridge [28] and is of concern for the bone quality that remains at the extraction site. There is presumed to be an association between the microdamage imparted to the bone during tooth extraction and the cellular activity which governs socket healing and subsequent ossification in ways that affect the overall resorption of the alveolar crest, which threatens the survivability of implants and the native dentition. Although the healing of extraction sockets is a process that is understood at the cellular activity level [30] and microdamage has been characterized following orthodontic loading regimes [31], the microdamage occurring from tooth extraction and its connections to extraction loading has not been extensively characterized.

Conventional tooth extraction is a surgical process in which beaked forceps are inserted into the periodontal space, gripping the tooth near the CEJ, and manipulated to apply a combination of forces that rupture the PDL and widen the tooth socket through plastic deformation of the alveolar bone [28]. Generally, the primary axis of the tooth is considered to be along the apical-gingival direction along the approximate geometric centre of the pulp chamber. Relative to this axis and the orthogonal lingual-buccal and mesio-distal directions drawn through the tooth root centre of rotation, forceps can be applied to create rotational and tipping moments in addition to intrusive and extrusive translative forces in the course of an extraction. Periosteal elevators or periotomes are recommended to aid in the rupture of the PDL via insertion into the periodontal space [16, 28]. Improper application of extraction force risks fracture of the tooth or alveolar bone. In these cases, the complexity and invasiveness of the extraction procedure is immediately increased and may range from the application of leverage with an elevator [28] to resection of a periosteal flap for access to the root apex through the bone [16].

There is no quantitative guideline for the direction and magnitude of the forces applied during routine forceps extraction – extraction is guided by haptic feedback through both the hand

operating the forceps and the opposite hand, which is positioned on the dental complex surrounding the extracted tooth to reflect soft tissue away from the extraction site and gently compress the alveolar crest [28]. There have been several attempts to measure the forces applied during routine forceps extraction employing strain gauges [32] or airbags [33] to measure the pressures and forces applied to the forceps by the operating clinician. The pressure applied at the forcep grips is reported to range from 0.24-1.26 bar [33]. Reported moments applied through the forceps grips range from 0.12 – 6.08 Nm depending on tooth type and direction [29]. These metrics provide some insight into the forces applied by clinicians during routine extractions but are insufficient to provide guidelines for the protection of the surrounding bone during the procedure – pressure-based measurements do not contain directional data corresponding to the application of force to the teeth, and the relationships between applied rocking moments and tooth geometry are not sufficiently clear to connect them to deformation (and damage) of the dental complex. It is uncommon for any method of measuring tooth extraction forces to study all six degrees of motion in the dental complex during extraction [34]. This limitation is currently being challenged by advances in robotic technology for measuring extraction motions that are promising in ex vivo tests [35], but it is unclear if the size and complexity of the robotic apparatus will be successful in widespread clinical adaptation. Despite the limited data available relating biomechanical loading during tooth extraction to the damage caused to the dental complex, the desire to mitigate damage to the alveolar bone during tooth extraction in search of improved clinical outcomes has led to the development of a range of atraumatic extraction devices and techniques that alter the biomechanics of the procedure in various ways, such as:

- The insertion of periotomes deep into the periodontal space rather than separating only the gingival-most fibres [36-38];
- Sectioning of tooth roots using piezoelectric or air-driven tools to facilitate lower-force extraction of root fragments [39-42];
- Altering the leverage point applied with the forceps from the tooth's centre of rotation to the surrounding bone via Physics forceps [43-46]; and
- Vertical tooth extraction using a pulley-and-cable device called the Benex® extraction system [40, 47-48].

Similar to routine forceps tooth extraction, there are no biomechanical guidelines for the magnitudes of forces applied through atraumatic extraction techniques. Instead, these procedures are assessed on the basis of patient outcomes that are presumed to be most strongly associated with the damage caused during tooth extraction such as: self-reported patient pain during healing [36-37, 44-46, 48]; gross bone resorption around the extraction site [42, 49]; and the socket or wound size at the extraction site [36-37, 44-46, 48-49]. In some cases, biomarkers associated with healing are directly assessed in association with the extraction scenario [39, 48, 50] and radiation treatment has been proposed as a method to limit the resorptive action of associated cells [51]. Atraumatic methods are promising when compared directly with conventional forceps extraction [36-37, 39, 42-46, 48-50, 52], though without directly measuring the loading applied during the extraction, or the damage state imposed by the extraction, the connection between the altered biomechanics of the procedures and clinical outcomes is tenuous. Additional procedural outcomes, such as the time required for an extraction, can be measured [37, 44-46] that are related to the amount of force the clinician must apply, but this relationship is also not clearly defined.

A 2020 study by Dietrich et al [47] provides an exception to the uncoupling of biomechanics and atraumatic extraction procedures that is important to the subsequent chapters of this thesis. In this study, an instrumented Benex® extraction device was employed to record time traces of the vertical forces applied to extracted teeth. The advantage of studying atraumatic extraction using the Benex® device is that it provides a well-known set of boundary conditions to study the biomechanics of tooth extraction. As demonstrated in Figure 2-4, load is transmitted to the tooth root through a flexible cable and threaded insert, allowing for the application of force only along the cable direction (along the drilled pulp chamber and axis of the tooth). Tension in the cable is created by the turning of a handwheel at the handle end of the Benex® device, where the load cell measuring extraction force was located for this study. Similar to forceps tooth extraction, the only force guidance provided to clinicians during this study was based on haptic feedback received through turning the handwheel. The operating clinicians' judgement was employed to determine if tooth roots would be sectioned and extracted separately or if multi-rooted root complexes would be extracted as one unit. Pre-operative radiographs were used to estimate the root surface attachment area (RSAA) of the extracted teeth for comparison to the peak extraction forces.

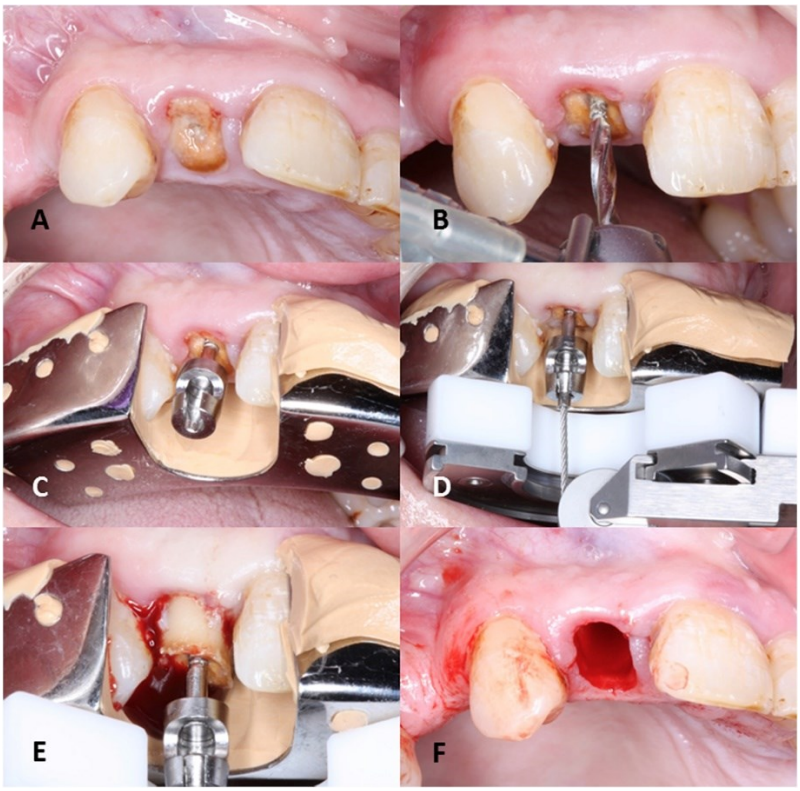

Figure 2-4: Case photos from the extraction of a single-rooted tooth with the Benex(r) vertical extraction kit, reproduced with permission [46]. Panels A-B: the crown of the tooth is removed and the pulp chamber prepared with a twist-drill; panel C: a threaded insert is placed in the pulp chamber; panel D: the Benex device is attached to the threaded insert via flexible steel cable and supported by a silicone impression on the surrounding dentition; panel E: vertical extraction force is applied to the tooth root to remove it from the socket though the cable and threaded insert; panel F: the intact post-extraction socket.

The results of the instrumented Benex® extraction study by Dietrich et al. [47] provide an important outlook for the subsequent work presented in this thesis. First, a glimpse of the biomechanical response to a known loading vector was provided despite the unprescribed loading schemes applied by the operating clinicians. The measurements demonstrated varying degrees of relaxation when the handwheel of the device is not turned, which is consistent with the characteristics of the dental complex discussed in Chapters 2.2.1 and 2.2.2. It also provides a range of peak extraction forces (41 N – 629 N) along a relatively well-known loading vector for successful human extractions, which contrasts with the forceps measurements discussed above. The study also demonstrated a moderate correlation for these peak extraction forces with the estimates of RSAA (which ranged from 50 mm^2 to 400 mm^2), indicating that the relationship

between tooth geometry and extraction biomechanics necessitates further study even when the loading vector is assumed to be purely axial.

2.2.1 Laboratory-Based Characterisation of Dental Complex Biomechanics

Many models consider the biomechanics of the dental complex in the laboratory, providing a greater degree of control over loading parameters and the condition of the studied tissue than is offered in clinical studies. Such studies tend to focus on the PDL as the primary tissue of interest for its role in tooth motion and cellular regulation of adaptive processes [13,15]. Despite its commonality in clinical practice, few laboratory models examine the mechanics of tooth extraction. Notably, these models tend to focus on the biomechanics of vertical tooth extraction as a simple but clinically-relevant load case.

A 2014 study performed by Genna and Paganelli [53] formed the basis for much of the work presented in this thesis. The purpose of the experimental aspect of the Genna and Paganelli study was to validate an interface finite element model for the PDL (discussed in greater detail in Chapter 2.2.2). Canines were extracted from sectioned mandibles of juvenile swine in a material test frame. The mandible sections were clamped rigidly to the base of the test frame and vertical displacement was applied to the tooth via an orthodontic wire passed transversally (bucco-lingually, from the lingual/interior of the dental arch to the buccal/exterior) through the crown by passing through a small hole that was drilled in the crown. Extraction experiments were performed at a rate of 2mm/min with force and displacement measured by the test frame crosshead. The resulting force-displacement curves demonstrate the typical features of soft tissue extension with a “toe-in” nonlinear region at low load, nearly linear extension of the tissue, and nonlinear stiffness approaching peak force and subsequent force decay as the tissue ruptured. Peak extraction forces ranged from 100 N to 450 N over displacements-to-peak-load of 1 mm to 4.6mm. The stiffness of the dental complexes in these extractions were estimated to fall between 20 N/mm and 150 N/mm. The success rate of this experiment was low, with only 7 extractions captured with sufficient experimental control to be used in validation of the associated numerical model. The authors hypothesized that this failure rate was due to crack initiation at the site of wire insertion based on the brittle nature and location of the observed tooth fractures but the role of the experimental fixture should also be considered. Genna and Paganelli attempted to align the axis of the canines with the loading direction visually but it is impossible to determine the extent

of eccentricity between the two directions without in situ radiographs. Any amount of eccentricity between the two directions would impose bending in the hard tissues as the tooth attempted to rotate in the socket and was resisted by the surrounding dental complex. This bending state would include significant tensile components of stress that would open crack faces and accelerate brittle fracture of the tissue.

A series of studies by Tohar, Ansbacher and colleagues [50,52] proposed an alternative method for measuring vertical extraction forces in individual roots of swine premolars. The purpose of the Tohar et al. series was to perform a split-mouth comparison determining the effect of collagenase injected into the periodontal space on extraction forces. In their work, mandibles of juvenile swine had the soft tissue (presumably only the skin and musculature, up to the gingival margin) removed and were mounted to a variable-position platform. A pair of extraction forceps were mounted to the load cell via a pin inserted between the handles with an elastic cable suspending them for gripping the teeth. The connection of the teeth to the forceps is not discussed in detail – it is assumed here for purposes of discussion that the forceps applied gripping force by some manipulation of the pin between the forceps handles. The teeth were then pulled vertically by the forceps at a rate of 10mm/min. Similar to the work by Genna and Paganelli [53], Tohar and colleagues mention a large number of fractures that occurred using this method but did not specify how many occurred. The extraction forces measured with the forceps apparatus ranged approximately from 10N to 380N across both studies in the collagenase and contralateral cases. The Tohar et al. method highlights the potential for a rigidly-aligned apparatus to introduce off-axis forces that cause teeth to fracture during experimental extraction, as well as the degree of uncertainty that can be introduced with the attachment of the instruments to the extracted teeth. These studies did not report displacements or stiffnesses measured at the test frame crosshead and the force-time traces presented in the initial study [50] demonstrate elongated toe-in regions, likely from the extension and recruitment of the elastic cable connected to the forceps handles.

A different method for extracting rat incisors proposed by Chiba et al [54-55] is alone in attempting to alter the direction of loading applied during a laboratory extraction to account for tooth geometry and is still employed in the investigation of dental biomechanics. This method studied rat incisors, which demonstrated a large degree of curvature. Rat mandibles were fixed in

a test frame and the crowns of the incisors potted in epoxy and clamped to a spinning wheel, the circumference of which was approximately aligned to the curvature of the incisor. Displacement was applied to the wheel via a cable that was wrapped around its perimeter, causing the wheel to turn and pull the incisor in a curved path relative to the fixture. Forces measured with this apparatus ranged from 2kgf to 10kgf (approximately 19.6N to 98.1N) and were found to be associated with age [54]. The most recent study employing this model demonstrated relationships among mandible mass, incisor length, and the measured forces [55]. While this experimental model demonstrated a technique for improving extraction force alignment with tooth geometry, there is a limit to the applicability of rodent models to studying atraumatic tooth extraction as rodents do not share the degree of similarity in physiology and diet to humans that is expected of swine.

The remainder of the literature concerned with measuring the mechanics of the dental complex examines other regimes of loading than those applied in tooth extraction, studying regular test geometries sectioned from the dental complex to examine the PDL in isolation [11-12, 20, 22, 24, 56-66] or examining the full dental complex in regimes related to physiological loading (such as during mastication) [19, 21, 23, 69-71] or orthodontic tooth movement [72]. The advantage of studying the sectioned dental complex is that is allows the isolation of the PDL behaviour under specific loading directions – tension [22, 24, 56-57, 60-61, 63], compression [11-12, 22, 59, 61-62, 64], shear [22, 66] – which are useful for informing constitutive models within the associated strain regimes. These models have been used to study the contribution of micromechanical structures to the behaviour of the PDL [11-12, 58-59, 65, 68-69] and characterize the viscoelastic [19-21, 24, 56, 60-62, 64-66, 69] and hyperelastic [22-24, 56-57, 61, 71] tissue response based on the assumption that the results can be generalized to the entire dental complex. This assumption is rarely studied and almost never applied to the study of tooth extraction (exceptions are discussed in Chapter 2.2.2). However, sectioned models of the dental complex also provide some insight into the local effects of structural interactions among tissues that might be informative for understanding the behaviour of tissues during tooth extraction. A 2010 study by Ho et al. [68] used atomic force microscopy to study gradients in stiffness of the dental complex traversing from the alveolar bone into the hard tissues of the tooth. The study by Ho et al. [68] study demonstrated structural changes in the organization of collagen across tissue boundaries associated with gradients in stiffness, indicating the strong relationship between the

microstructure of the tissues and the mechanical behaviour of hard-soft tissue boundaries which are often assumed to be abrupt unions among dissimilar tissues.

2.2.2 Numerical Modelling of Extraction Biomechanics

The questions that can be answered by a numerical model of the dental complex are directly influenced by the geometry, material and mesh properties, and boundary conditions that are applied in its creation [73-74]. The numerical models available in the literature reflect the range of scenarios that are examined beyond tooth extraction loading regimes, including a variety of subject-specific [25, 27, 75-99] and generalized [101-106] geometries. However, despite the importance of all tissues in the dental complex, numerical studies tend to focus almost exclusively on the properties and behaviour of the PDL with few models accounting for heterogeneity or other properties of the hard tissues [80, 90, 93]. For many problems, such as orthodontic loading, factors of the PDL behaviour such as the hyperelasticity, viscoelasticity, and damage characteristics necessary to model the rupture of the PDL are neglected [78, 80, 81-83 87-89, 99-100, 103, 105]. Each of these factors potentially influences the biomechanics of tooth extraction, even when the PDL is the primary tissue of consideration, so special attention is given to models that account for these properties as informative to the subsequent chapters of this thesis.

The micromechanical structure of the PDL is a primary consideration for modelling its complex large-strain behaviour. In general, the fibrous phase can be accounted for in the PDL material as a separate phase from the ECM as a separate term in the strain energy density function describing the material [53, 107-108]. The compressibility of the ECM (due to its fluid phase and porosity) can also be accounted for at this level, either by coupling the compressibility of the material with its strain behaviour (e.g. a hyperfoam [92]) or uncoupling them into separate dilational and distortional terms [108-109]. Viscoelastic and damage phenomena are then applied to any number of these terms in different formulations. The most complicated of these models employ strain- or strain-energy-density-time histories to determine both the viscoelastic response and damage state of the material [109-110]. It is more common to represent the viscoelastic behaviour of the PDL based on the calculation of the current stress state using a hyperelastic constitutive model and then regulate the stress in the finite element formulation by the time-history of stress [110-111]. The damage state of the overall material can then be updated and

applied to downregulate the stress state of the material. This paradigm of calculating the hyperelastic response of the material and then regulating it based on the stress-time history was proposed in the seminal text by Y.C Fung [112] which introduced the quasi-linear viscoelastic (QLV) model, which is convenient for time-discretization in finite element analysis because the relaxation function is separable from the time-history of the material stress. The QLV allows the application of simple numerical differencing schemes to update the calculated stresses at a given timestep based on a single point in the material's stress history. Different implementations of this concept (demonstrated in Figure 2-5) are discussed in greater detail below.

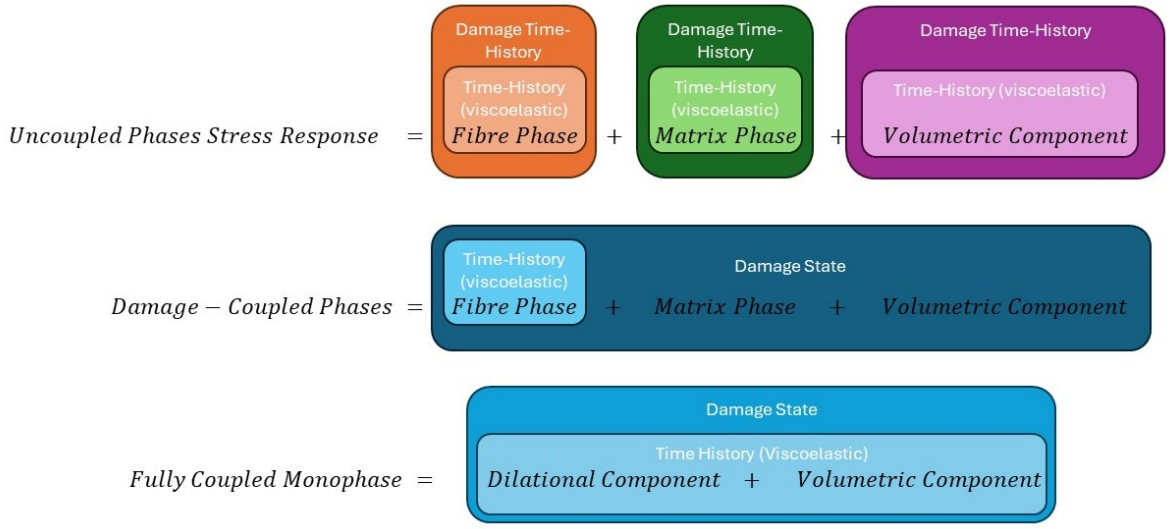

Figure 2-5: Conceptual representations for different schemes for implementing damage and viscoelastic behaviour in hyperelastic models of soft tissue. The most computationally-intensive model is in the top row, requiring separate state calculations for the damage and viscoelastic regulation of the strain-energy density of each phase which is affects the overall material stress response

A constitutive model for the PDL proposed by Natali et al [108] was not applied to a dental complex model for tooth extraction, but does demonstrate the coupling of hyperelasticity, viscoelasticity, and time-dependent damage phenomena demonstrated in the first row of Figure 2-5 (although the damage history is only considered for the fibrous phase). This model is based on exponential forms for the hyperelasticity of the fibrous and matrix phases with a single uncoupled volumetric term. The viscoelastic response of the material is assessed with convolution integrals similar in form to the QLV. The time-dependent damage response in the fibres is modeled with a separate convolution integral that maps the strain level of the material to

a series of damage “branches” with their own damage-limiting strain thresholds. The parameters describing this complex model were fit to a combination of compressive and tensile loading on samples sectioned from the dental complex. The model predicts the full range of the PDL tissue response in these regimes from the initial toe-in region to force decay following peak force leading to rupture, and demonstrates strain-rate sensitivity matching the viscoelastic behaviour of the PDL. These are highly desirable features of a numerical model applied to tooth extraction biomechanics but are offset by an immense degree of complexity. This model was implemented within custom finite element code, and implementing the additional state variables needed to model the fibrous damage in other finite element software is not a trivial task that requires changing the fundamental data stored in material or Gauss integration points within an element. Additionally, the model consists of 6 material parameters describing the hyperelastic foundation, 24 parameters for the viscous behaviour, and an additional 15 terms for describing the time-dependent damage behaviour of the fibrous phase which is a large number of parameters to be determined from experimental data in an inverse finite element process, even for uniaxial loading of simple geometries.

Another model that is capable of modelling tooth extraction but was applied to other regimes was presented by Ortun-Terrazas et al. [113]. The parameters for this material model were also determined from sectioned samples of the dental complex but were applied in this study to a genereric geometry for the complete dental complex. Subject-specific models of the full stomatognathic system and a single unit of the dental complex were created with linear models for the hard tissues to study the effects of malocclusion during several physiological loading processes. The full stomatognathic system model employed a fifth-order uncoupled Ogden (polynomial) model for the PDL, but the single dental complex model employed a coupled fibre and matrix model for the PDL [79]. The damage model was applied only for the fibrous phase of the PDL, although an additional term was added to the strain energy density function to soften the material due to “fibrous uncrimping”. This term accounts for the time-history of the deviatoric fibrous strain energy density relative to its peak value within that history. This model was also coupled with a fluid phase to account for the biphasic viscoelasticity of the PDL. The single-tooth model was loaded in combinations of intrusive and transverse loading scenarios representing mastication in maloccluded states, finding that these physiological scenarios extended the PDL material into damaging regimes. Similar to the model by Natali et al. [108],

the fibrous hyperfoam model by Ortun-Terrazas et al. [113] was implemented as custom material codes within a commercial software package and is difficult to replicate and generalize to study tooth extraction biomechanics.

A subject-specific FE model of tooth extraction was also informed by one of the few experimental models of tooth extraction developed by Genna and Paganelli in their 2014 study (discussed in detail above) [53]. The PDL is represented in these models using custom interface elements that represent a crossed structure of collagen fibres. The extensive properties of this structure are developed from the micromechanical structure of a collagen fibre during its recruitment and extension, depending on 19 parameters such as individual tropocollagen molecule stiffnesses and contour length, as well as nondimensional parameters describing the levels of the molecular structure carrying load and the molecular crosslinking stiffnesses. This model neglects the time-dependent behaviours of the tissue but predicts the large-displacement behaviour of the dental complex well when compared to the experimental force-displacement curves gathered at 2mm/min for the swine canines. The damaged phase of the force-displacement curve demonstrates brittle failure of the PDL, failing to capture the force decay that is present in the experimental data and better captured for sectioned samples by Natali et al [108]. However, the subject-specific implementations of this model were used to study a number of factors such as PDL width, soft tissue attachment after tooth luxation, and the stiffness of the cable attaching the tooth to the experimental apparatus. Similar to the other approaches discussed in this chapter, this model employed a custom solver code for a finite element solver that is difficult to directly reproduce.

2.3 Summary Discussion

The dental complex is a structure within the stomatognathic system that supports the mechanical function and vitality of the tooth. Tooth extraction is concerned with the biomechanics of this structure during combined loading with the goal of rupturing the PDL and delivering the tooth from the socket while imparting minimal damage to the remaining bone. The biomechanics of this process are hypothesized to influence patient healing, implant health, and dentition survival but the connection has not been well-investigated, limiting the evidence-informed development of new atraumatic extraction techniques.

Future work seeking to improve the characterisation of extraction biomechanics and influence clinical practice should address these key limitations as discussed in this chapter:

- The body of experimental data describing tooth extraction biomechanics is sparse and should account for various loading rates and regimes that are not well represented in the current literature;
- Experimental models of tooth extraction should have appropriate boundary conditions to ensure that the loading applied to the tooth is representative of clinical loading. Current models apply loads to the teeth in manners that do not well represent clinical tools (e.g. drilling the tooth crown and passing through wires) or are difficult to quantify and replicate (e.g. elastically-suspended forceps);
- Experimental models of vertical tooth extraction may be strongly influenced by the alignment of the dental complex to the testing apparatus, which may be contributing to extremely high rates of hard tissue fracture but have not been investigated. New methods that account for this factor should be developed;
- Numerical models of the dental complex for tooth extraction do not account for the full range of phenomena that contribute to the complex's response (i.e. damage, viscoelasticity, hyperelasticity) and the replicability of material models that are capable of capturing these behaviours is extremely poor due to their complexity and custom implementations;
- Numerical models of the dental complex depend on subject-specific geometries that are computationally intensive to generate and are not necessary for predictive modelling of new atraumatic extraction processes. Some work has been done to reduce the barriers to accessing quality models of the dental complex by providing open-source repositories of subject-specific meshes of the craniofacial complex [114] but their use as generalizable predictive models, particularly for high-strain regimes of tooth extraction or trauma, have not been investigated. The applicability and limitations of generalized models should be further investigated; and
- Current technologies for clinical tooth extraction do not facilitate investigation of extraction biomechanics. The development of new instrumentation, software, and extraction devices should provide avenues for feedback to the operating clinician allowing them to exert mechanically-informed loading control. This advancement

with contribute both to the biomechanical investigation of tooth extraction mechanics and the feasibility of implementing new techniques that are based on these mechanics.

References

1. Chu TM, Liu SS, Babler WJ. Craniofacial biology, orthodontics, and implants. In: Basic and applied bone biology 2014 Jan 1 (pp. 225-242). Academic Press.
2. Schroeder KD. Human tooth diagram-en.svg from Wikimedia Commons. Licensed under CC-BY-SA 4.0.
3. Gulabivala K, Ng YL. Tooth organogenesis, morphology and physiology. In: Endodontics (4th Edition). 2014 August (pp. 2-32). Mosby Elsevier.
4. Nejad RM, Moghadam DG, Moghadam MR, Aslani M, Moghaddam HA, Mir M. Fracture behavior of restored teeth and cavity shape optimization: Numerical and experimental investigation. Journal of the Mechanical Behavior of Biomedical Materials. 2021 Dec 1;124:104829.
5. Nalla RK, Kinney JH, Ritchie RO. On the fracture of human dentin: is it stress-or strain-controlled? Journal of Biomedical Materials Research Part A: An Official Journal of The Society for Biomaterials, The Japanese Society for Biomaterials, and The Australian Society for Biomaterials and the Korean Society for Biomaterials. 2003 Nov 1;67(2):484-95.
6. Su K, Yuan L, Du J. Bone remodeling under tooth loading. InTMS 2017 146th Annual Meeting & Exhibition Supplemental Proceedings 2017 (pp. 331-340). Springer International Publishing.
7. Su K, Yuan L, Yang J, Du J. Numerical simulation of mandible bone remodeling under tooth loading: A parametric study. Scientific reports. 2019 Oct 17;9(1):14887.
8. Zhang YR, Du W, Zhou XD, Yu HY. Review of research on the mechanical properties of the human tooth. Int J Oral Sci. 2014 Jun;6(2):61-9. doi: 10.1038/ijos.2014.21.
9. Beertsen W, McCulloch CA, Sodek J. The periodontal ligament: a unique, multifunctional connective tissue. Periodontology 2000. 1997 Feb;13(1):20-40.
10. Naveh GR, Brumfield V, Shahar R, Weiner S. Tooth periodontal ligament: Direct 3D microCT visualization of the collagen network and how the network changes when the tooth is loaded. Journal of structural biology. 2013 Feb 1;181(2):108-15.

11. Ho SP, Kurylo MP, Grandfield K, Hurng J, Herber RP, Ryder MI, Altoe V, Aloni S, Feng JQ, Webb S, Marshall GW. The plastic nature of the human bone–periodontal ligament–tooth fibrous joint. Bone. 2013 Dec 1;57(2):455-67.
12. Jang AT, Merkle AP, Fahey KP, Gansky SA, Ho SP. Multiscale biomechanical responses of adapted bone–periodontal ligament–tooth fibrous joints. Bone. 2015 Dec 1;81:196-207.
13. Fill TS, Carey JP, Toogood RW, Major PW. Experimentally determined mechanical properties of, and models for, the periodontal ligament: critical review of current literature. Journal Dent Biomech. 2011:312980.
14. Fill TS, Toogood RW, Major PW, Carey JP. Analytically determined mechanical properties of, and models for the periodontal ligament: critical review of literature. J Biomech. 2012;45(1):9-16. doi: 10.1016/j.jbiomech.2022.09.020
15. Ovy EG, Romanyk DL, Flores Mir C, Westover L. Modelling and evaluating periodontal ligament mechanical behaviour and properties: A scoping review of current approaches and limitations. Orthod Craniofac Res. 2022;25(2):199-211. doi: 10.1111/ocr.12527.
16. Dym H, Weiss A. Exodontia: tips and techniques for better outcomes. Dent Clin North Am. 2012;56(1):245-66. doi: 10.1016/j.cden.2011.07.002.
17. Bustad LK. Pigs in the laboratory. Sci Am. 1966 Jun;214(6):94-100. doi: 10.1038/scientificamerican0666-94. PMID: 5930599.
18. Oltramari PV, Navarro RL, Henriques JF, Capelozza AL, Granjeiro JM. Dental and skeletal characterization of the BR-1 minipig. The Veterinary Journal. 2007 Mar 1;173(2):399-407.
19. Papadopoulou K, Keilig L, Eliades T, Krause R, Jäger A, Bourauel C. The time-dependent biomechanical behaviour of the periodontal ligament—an in vitro experimental study in minipig mandibular two-rooted premolars. The European Journal of Orthodontics. 2014 Feb 1;36(1):9-15.
20. Huang H, Tang W, Yang YU, Wu B, Yan B. Determination of viscoelastic properties of the periodontal ligament using nanoindentation testing and numerical modeling. Journal of Mechanics in Medicine and Biology. 2016 Sep 8;16(06):1650089.

21. Romanyk DL, Guan R, Major PW, Dennison CR. Repeatability of strain magnitude and strain rate measurements in the periodontal ligament using fibre Bragg gratings: an ex vivo study in a swine model. Journal of Biomechanics. 2017 Mar 21;54:117-22.
22. Genna F, Annovazzi L, Bonesi C, Fogazzi P, Paganelli C. On the experimental determination of some mechanical properties of porcine periodontal ligament. Meccanica. 2008 Feb;43:55-73.
23. Knaup TJ, Dirk C, Reimann S, Keilig L, Eschbach M, Korbmacher-Steiner H, Bourauel C. Time-dependent behavior of porcine periodontal ligament: a combined experimental, numeric in-vitro study. American Journal of Orthodontics and Dentofacial Orthopedics. 2018 Jan 1;153(1):97-107.
24. Zhou J, Song Y, Zhang C, Shi X. Tensile creep mechanical behavior of periodontal ligament: A hyper-viscoelastic constitutive model. Computer Methods and Programs in Biomedicine. 2021 Aug 1;207.
25. Nikolaus A, Currey JD, Lindtner T, Fleck C, Zaslansky P. Importance of the variable periodontal ligament geometry for whole tooth mechanical function: a validated numerical study. Journal of the mechanical behavior of biomedical materials. 2017 Mar 1;67:61-73.
26. Huang H, Tang W, Tan Q, Yan B. Development and parameter identification of a visco-hyperelastic model for the periodontal ligament. Journal of the mechanical behavior of biomedical materials. 2017 Apr 1;68:210-5.
27. Kaiser AH, Keilig L, Klein R, Bourauel C. Parameter identification for the simulation of the periodontal ligament during the initial phase of orthodontic tooth movement. Computer Methods in Biomechanics and Biomedical Engineering. 2021 Feb 17;24(3):333-48.
28. Hupp J, Ellis E, and Tucker MR. Contemporary oral and maxillofacial surgery. 7Th ed. Philadelphia, PA: Elsevier; 2019. Chapter 8: Principles of routine exodontia; p.106-134.
29. Poundarik AA, Vashishth D. Multiscale imaging of bone microdamage. Connective tissue research. 2015 Mar 4;56(2):87-98.
30. Corredor-Gómez JP, Rueda-Ramírez AM, Gamboa-Márquez MA, Torres-Rodríguez C, Cortés-Rodríguez CJ. An intramembranous ossification model for the in silico

analysis of bone tissue formation in tooth extraction sites. Journal of Theoretical Biology. 2016 Jul 21;401:64-77.

31. Verna C, Dalstra M, Lee TC, Cattaneo PM, Melsen B. Microcracks in the alveolar bone following orthodontic tooth movement: a morphological and morphometric study. The European Journal of Orthodontics. 2004 Oct 1;26(5):459-67.
32. Lehtinen R, Ojala T. Rocking and twisting moments in extraction of teeth in the upper jaw. International journal of oral surgery. 1980 Oct 1;9(5):377-82.
33. Ahel V, Ćabov T, Špalj S, Perić B, Jelušić D, Dmitrašinović M. Forces that fracture teeth during extraction with mandibular premolar and maxillary incisor forceps. British Journal of Oral and Maxillofacial Surgery. 2015 Dec 1;53(10):982-7.
34. Beuling MG, Agterbos PC, van Riet TC, Ho JP, de Vries R, Kober J, de Lange J. Forces and movements during tooth extraction: A scoping review. Advances in Oral and Maxillofacial Surgery. 2023 Jan 7:100391.
35. Riet TV, Graaf WD, Lange JD, Kober J. Analysis of movements in tooth removal procedures using robot technology. Plos one. 2023 May 18;18(5):e0285503.
36. Sharma SD, Vidya B, Alexander M, Deshmukh S. Periotome as an Aid to Atraumatic Extraction: A Comparative Double Blind Randomized Controlled Trial. J Maxillofac Oral Surg. 2015;14(3):611-5. doi: 10.1007/s12663-014-0723-8.
37. Contractor MM, Bhate K, Londhe U, Awate S, Chhartriwala A, Samuel S. Efficacy of Periotome Versus Conventional Forceps Extraction in Socket Preservation and Reduction of Postoperative Pain: A Randomised Clinical Trial. Journal of Clinical & Diagnostic Research. 2023 Nov 1;17(11).
38. Makki AZ, Nassar AA, Alharbi WM, Bisharah WF, Alabdali MA, Alqurashi AM, Basandawa NA. Evaluation of post-extraction healing after atraumatic axial tooth extraction using Benex system II versus conventional extraction: Randomized control trial. The Saudi Dental Journal. 2021 Dec 1;33(8):923-8.
39. Mohammadi SA. Association of inflammatory markers and growth factors with radiographically assessed wound healing of extraction sockets [MSc Thesis]. Omaha (USA): University of Nebraska Medical Center; 2023. Available from: https://digitalcommons.unmc.edu/etd/754/

40. Muska E, Walter C, Knight A, Taneja P, Bulsara Y, Hahn M, Desai M, Dietrich T. Atraumatic vertical tooth extraction: a proof of principle clinical study of a novel system. Oral Surg Oral Med Oral Pathol Oral Radiol. 2013;116(5):e303-10. doi: 10.1016/j.oooo.2011.11.037.
41. Papadimitriou DE, Geminiani A, Zahavi T, Ercoli C. Sonosurgery for atraumatic tooth extraction: a clinical report. The Journal of prosthetic dentistry. 2012 Dec 1;108(6):339-43.
42. Hamed NA, Mohamed MH. Radiographic Evaluation of Bone Height Changes Around Immediately Placed Implant Retaining Mandibular Over-Denture in Atraumatic Tooth Extraction Cases. Egyptian Dental Journal. 2023 Jul 1;69(3):2035-43.
43. El-Kenawy MH, Ahmed WM. Comparison Between Physics and Conventional Forceps in Simple Dental Extraction. J Maxillofac Oral Surg. 2015;14(4):949-55. doi: 10.1007/s12663-015-0765-6.
44. Hariharan S, Narayanan V, Soh CL. Split-mouth comparison of physics forceps and extraction forceps in orthodontic extraction of upper premolars. Br J Oral Maxillofac Surg. 2014;52(10):e137-40. doi: 10.1016/j.bjoms.2014.06.013.
45. Patel HS, Managutti AM, Menat S, Agarwal A, Shah D, Patel J. Comparative Evaluation of Efficacy of Physics Forceps versus Conventional Forceps in Orthodontic Extractions: A Prospective Randomized Split Mouth Study. J Clin Diagn Res. 2016;10(7):ZC41-5. doi: 10.7860/JCDR/2016/17724.8160.
46. Irshad F, Khan UQ, Memon ZA, Punjabi SK, Zaidi SA. Use of Physics Forcep Versus Conventional Forcep in Extraction of Mandibular First Molar: Physics Forcep Versus Conventional Forcep. Pakistan Journal of Health Sciences. 2023 May 31:123-8.
47. Dietrich T, Schmid I, Locher M, Addison O. Extraction force and its determinants for minimally invasive vertical tooth extraction. J Mech Behav Biomed Mater. 2020;105:103711. doi: 10.1016/j.jmbbm.2020.103711.
48. Makki AZ, Nassar AA, Alharbi WM, Bisharah WF, Alabdali MA, Alqurashi AM, Basandawa NA. Evaluation of post-extraction healing after atraumatic axial tooth

extraction using Benex system II versus conventional extraction: Randomized control trial. The Saudi Dental Journal. 2021 Dec 1;33(8):923-8.

49. Schropp L, Wenzel A, Kostopoulos L, Karring T. Bone healing and soft tissue contour changes following single-tooth extraction: a clinical and radiographic 12-month prospective study. International Journal of Periodontics & Restorative Dentistry. 2003 Aug 1;23(4).

50. Tohar R, Alali H, Ansbacher T, Brosh T, Sher I, Gafni Y, Weinberg E, Gal M. Collagenase Administration into Periodontal Ligament Reduces the Forces Required for Tooth Extraction in an Ex situ Porcine Jaw Model. Journal of Functional Biomaterials. 2022 Jun 8;13(2):76

51. Venni Heinonen, Timo J. Ruotsalainen, Lauri Paavola, Jopi J. Mikkonen, Pekka Asikainen, Arto P. Koistinen & Arja M. Kullaa (2018) Alveolar bone remodeling after tooth extraction in irradiated mandible: An experimental study with canine model, Ultrastructural Pathology, 42:2, 124-132, DOI: 10.1080/01913123.2017.1422829

52. Ansbacher T, Tohar R, Cohen A, Cohen O, Levartovsky S, Arieli A, Matalon S, Bar DZ, Gal M, Weinberg E. A novel computationally engineered collagenase reduces the force required for tooth extraction in an ex-situ porcine jaw model. Journal of Biological Engineering. 2023 Jul 17;17(1):47.

53. Genna F, Paganelli C. Force–displacement relationship in the extraction of a porcine tooth from its socket: Experiments and numerical simulations. Journal of Mechanics of Materials and Structures. 2014 Dec 14;9(5):497-514.

54. Chiba M, Ohshima S, Takizawa K. Measurement of the force required to extract the mandibular incisor of rats of various ages. Archives of Oral Biology. 1980 Jan 1;25(10):683-7.

55. Komatsu K, Ohshima S, Chiba M. Measurement of the force required to extract the mandibular first molar from its socket in the dissected jaw of growing young rats. Gerodontology. 1990 Apr;9(1-3):3-7.

56. Oskui IZ, Hashemi A. Dynamic tensile properties of bovine periodontal ligament: a nonlinear viscoelastic model. Journal of Biomechanics. 2016 Mar 21;49(5):756-64.

57. Wu B, Fu Y, Shi H, Yan B, Lu R, Ma S, Markert B. Tensile testing of the mechanical behavior of the human periodontal ligament. BioMedical Engineering OnLine. 2018 Dec;17:1-1.
58. Ho SP, Kurylo MP, Grandfield K, Hurng J, Herber RP, Ryder MI, Altoe V, Aloni S, Feng JQ, Webb S, Marshall GW. The plastic nature of the human bone–periodontal ligament–tooth fibrous joint. Bone. 2013 Dec 1;57(2):455-67.
59. Jang AT, Chen L, Shimotake AR, Landis W, Altoe V, Aloni S, Ryder M, Ho SP. A force on the crown and tug of war in the periodontal complex. Journal of dental research. 2018 Mar;97(3):241-50.
60. Najafidoust M, Hashemi A, Oskui IZ. Dynamic viscoelastic behavior of bovine periodontal ligament in compression. Journal of Periodontal Research. 2020 Oct;55(5):651-9.
61. Shibata T, Botsis J, Bergomi M, Mellal A, Komatsu K. Mechanical behavior of bovine periodontal ligament under tension-compression cyclic displacements. European journal of oral sciences. 2006 Feb;114(1):74-82.
62. Najafidoust M, Hashemi A, Oskui IZ. Effect of temperature on dynamic compressive behavior of periodontal ligament. Medical Engineering & Physics. 2023 Jun 1;116:103986.
63. Uhlir R, Mayo V, Lin PH, Chen S, Lee YT, Hershey G, Lin FC, Ko CC. Biomechanical characterization of the periodontal ligament: Orthodontic tooth movement. The Angle Orthodontist. 2017 Mar 1;87(2):183-92.
64. Wu B, Pu P, Zhao S, Izadikhah I, Shi H, Liu M, Lu R, Yan B, Ma S, Markert B. Frequency-related viscoelastic properties of the human incisor periodontal ligament under dynamic compressive loading. Plos one. 2020 Jul 13;15(7):e0235822.
65. Wu B, Li N, Liu M, Cheng K, Jiang D, Yi Y, Ma S, Yan B, Lu Y. Construction of Human Periodontal Ligament Constitutive Model Based on Collagen Fiber Content. Materials. 2023 Oct 6;16(19):6582.
66. Toms SR, Dakin GJ, Lemons JE, Eberhardt AW. Quasi-linear viscoelastic behaviour of the human periodontal ligament. J Biomech. 2002; 35(10):1411-1415. doi: 10.1016/S0021-9290(02)00166-5.

67. Pini M, Zysset PH, Botsis J, Contro R. Tensile and compressive behaviour of the bovine periodontal ligament. Journal of biomechanics. 2004 Jan 1;37(1):111-9.
68. Ho SP, Kurylo MP, Fong TK, Lee SS, Wagner HD, Ryder MI, Marshall GW. The biomechanical characteristics of the bone-periodontal ligament-cementum complex. Biomaterials. 2010 Sep 1;31(25):6635-46.
69. Sinescu C, Duma VF, Dodenciu D, Stratul S, Manole M, Draganescu GE. Mechanical properties of the periodontal system and of dental constructs deduced from the free response of the tooth. Journal of Healthcare Engineering. 2018 Sep 17;2018.
70. Mulimani P, Popowics TE. UNDERSTANDING PERIODONTAL TISSUE RESPONSES TO MECHANICAL LOAD THROUGH THE USE OF THE PIG MODEL, SUS SCROFA. EMBRACING NOVEL TECHNOLOGIES IN DENTISTRY AND ORTHODONTICS. 2019 Mar 1;1001:86.
71. Karimi Dastgerdi A, Rouhi G, Dehghan MM, Farzad Mohajeri S, and Barikani HR. Linear momenta transferred to the dental implant-bone and natural tooth-PDL-bone contstructs under impact loading: a comparative in-vitro and in-silico study. Front. Bioeng. Biotechnol. 2020;8:54. doi: 10.3389/fbioe.2020.00544.
72. Bosiakov S, Mikhasev G. Mathematical model for analysis of translational displacements of tooth root. Mathematical Modelling and Analysis. 2015 Jul 4;20(4):490-501.
73. Romanyk DL, Vafaeian B, Addison O, Adeeb S. The use of finite element analysis in dentistry and orthodontics: Critical points for model development and interpreting results. InSeminars in Orthodontics 2020 Sep 1 (Vol. 26, No. 3, pp. 162-173). WB Saunders.
74. Cattaneo PM, Cornelis MA. Orthodontic tooth movement studied by finite element analysis: an update. What can we learn from these simulations?. Current Osteoporosis Reports. 2021 Apr;19:175-81.
75. Papadopoulou K, Hasan I, Keilig L, Reimann S, Eliades T, Jäger A, Deschner J, Bourauel C. Biomechanical time dependency of the periodontal ligament: a combined experimental and numerical approach. European journal of orthodontics. 2013 Dec 1;35(6):811-8.

76. Tuna M, Sunbuloglu E, Bozdag E. Finite element simulation of the behavior of the periodontal ligament: a validated nonlinear contact model. Journal of biomechanics. 2014 Sep 22;47(12):2883-90.
77. Knaup TJ, Dirk C, Reimann S, Keilig L, Eschbach M, Korbmacher-Steiner H, Bourauel C. Time-dependent behavior of porcine periodontal ligament: a combined experimental, numeric in-vitro study. American Journal of Orthodontics and Dentofacial Orthopedics. 2018 Jan 1;153(1):97-107.
78. Robinson D, Aguilar L, Gatti A, Abduo J, Lee PV, Ackland D. Load response of the natural tooth and dental implant: A comparative biomechanics study. The journal of advanced prosthodontics. 2019 Jun;11(3):169-78.
79. Ortún-Terrazas J, Cegoñino J, Santana-Penín U, Santana-Mora U, Del Palomar AP. Approach towards the porous fibrous structure of the periodontal ligament using micro-computerized tomography and finite element analysis. Journal of the mechanical behavior of biomedical materials. 2018 Mar 1;79:135-49.
80. McCormack SW, Witzel U, Watson PJ, Fagan MJ, Gröning F. Inclusion of periodontal ligament fibres in mandibular finite element models leads to an increase in alveolar bone strains. PLoS One. 2017 Nov 30;12(11):e0188707.
81. Uhlir R, Mayo V, Lin PH, Chen S, Lee YT, Hershey G, Lin FC, Ko CC. Biomechanical characterization of the periodontal ligament: Orthodontic tooth movement. The Angle Orthodontist. 2017 Mar 1;87(2):183-92.
82. Likitmongkolsakul U, Smithmaitrie P, Samruajbenjakun B, Aksornmuang J. Development and validation of 3D finite element models for prediction of orthodontic tooth movement. International journal of dentistry. 2018 Aug 30;2018.
83. Savignano R, Barone S, Paoli A, Razionale AV. FEM analysis of bone-ligaments-tooth models for biomechanical simulation of individual orthodontic devices. In: International Design Engineering Technical Conferences and Computers and Information in Engineering Conference 2014 Aug 17 (Vol. 46285, p. V01AT02A081). American Society of Mechanical Engineers.
84. Martinez S, Lenz J, Schweizerhof K, Schindler HJ. A variable finite element model of the overall human masticatory system for evaluation of stress distributions during

biting and bruxism. InIn10th European LS-DYNA Conference, Würzburg, Germany 2015.

85. Otani T, Kobayashi M, Nozaki K, Gonda T, Maeda Y, Tanaka M. Influence of mouthguards and their palatal design on the stress-state of tooth-periodontal ligament-bone complex under static loading. Dental traumatology. 2018 Jun;34(3):208-13.
86. Martinez Choy SE, Lenz J, Schweizerhof K, Schmitter M, Schindler HJ. Realistic kinetic loading of the jaw system during single chewing cycles: a finite element study. Journal of Oral Rehabilitation. 2017 May;44(5):375-84.
87. Nihara J, Gielo-Perczak K, Cardinal L, Saito I, Nanda R, Uribe F. Finite element analysis of mandibular molar protraction mechanics using miniscrews. European journal of orthodontics. 2015 Feb 1;37(1):95-100.
88. Barone S, Paoli A, Razionale AV, Savignano R. Computer aided modelling to simulate the biomechanical behaviour of customised orthodontic removable appliances. International Journal on Interactive Design and Manufacturing (IJIDeM). 2016 Nov;10:387-400.
89. Mehari Abraha H, Iriarte-Diaz J, Ross CF, Taylor AB, Panagiotopoulou O. The mechanical effect of the periodontal ligament on bone strain regimes in a validated finite element model of a macaque mandible. Frontiers in bioengineering and biotechnology. 2019:269.
90. Ashrafi M, Ghalichi F, Mirzakouchaki B, Zoljanahi Oskui I. Numerical simulation of hydro-mechanical coupling of periodontal ligament. Proceedings of the Institution of Mechanical Engineers, Part H: Journal of Engineering in Medicine. 2020 Feb;234(2):171-8.
91. Oskui IZ, Hashemi A, Jafarzadeh H, Kato A. Finite element investigation of human maxillary incisor under traumatic loading: Static vs dynamic analysis. Computer methods and programs in biomedicine. 2018 Mar 1;155:121-5.
92. Rahimi M, Mojra A. Numerical modeling of hyperfoam behavior of periodontal ligament in mechanical loading. In2019 26th National and 4th International Iranian Conference on Biomedical Engineering (ICBME) 2019 Nov 27 (pp. 82-87). IEEE.
93. Liao Z, Chen J, Zhang Z, Li W, Swain M, Li Q. Computational modeling of dynamic behaviors of human teeth. Journal of biomechanics. 2015 Dec 16;48(16):4214-20.

94. Gei M, Genna F, Bigoni D. An interface model for the periodontal ligament. J. Biomech. Eng.. 2002 Oct 1;124(5):538-46.
95. Genna F. A micromechanically-based, three-dimensional interface finite element for the modelling of the periodontal ligament. Computer Methods in Biomechanics and Biomedical Engineering. 2006 Aug 1;9(4):243-56.
96. Qian L, Todo M, Morita Y, Matsushita Y, Koyano K. Deformation analysis of the periodontium considering the viscoelasticity of the periodontal ligament. Dental Materials. 2009 Oct 1;25(10):1285-92.
97. Karimi Dastgerdi A, Rouhi G, Dehghan MM, Farzad Mohajeri S, and Barikani HR. Linear momenta transferred to the dental implant-bone and natural tooth-PDL-bone contstructs under impact loading: a comparative in-vitro and in-silico study. Front. Bioeng. Biotechnol. 2020;8:54. doi: 10.3389/fbioe.2020.00544.
98. Dezzen-Gomide AC, de Carvalho MA, Lazari-Carvalho PC, de Oliveira HF, Cury AA, Yamamoto-Silva FP, de Freitas Silva BS. A three-dimensional finite element analysis of permanent maxillary central incisors in different stages of root development and trauma settings. Computer methods and programs in biomedicine. 2021 Aug 1;207:106195.
99. Limjeerajarus N, Sratong-On P, Dhammayannarangsi P, Tompkins KA, Kamolratanakul P, Phannarus K, Osathanon T, Limjeerajarus CN. Determination of the compressive modulus of elasticity of periodontal ligament derived from human first premolars. Heliyon. 2023 Mar 1;9(3).
100. Tuna M, Sunbuloglu E, Bozdag E. Finite element simulation of the behavior of the periodontal ligament: a validated nonlinear contact model. Journal of biomechanics. 2014 Sep 22;47(12):2883-90.
101. Natali AN, Pavan PG, Scarpa C. Numerical analysis of tooth mobility: formulation of a non-linear constitutive law for the periodontal ligament. Dental Materials. 2004 Sep 1;20(7):623-9.
102. Su MZ, Chang HH, Chiang YC, Cheng JH, Fuh LJ, Wang CY, Lin CP. Modeling viscoelastic behavior of periodontal ligament with nonlinear finite element analysis. Journal of Dental Sciences. 2013 Jun 1;8(2):121-8.

103. Ou KL, Chang CC, Chang WJ, Lin CT, Chang KJ, Huang HM. Effect of damping properties on fracture resistance of root filled premolar teeth: a dynamic finite element analysis. International endodontic journal. 2009 Aug;42(8):694-704.
104. Karimi A, Razaghi R, Biglari H, Rahmati SM, Sandbothe A, Hasani M. Finite element modeling of the periodontal ligament under a realistic kinetic loading of the jaw system. The Saudi Dental Journal. 2020 Nov 1;32(7):349-56.
105. Gupta M, Madhok K, Kulshrestha R, Chain S, Kaur H, Yadav A. Determination of stress distribution on periodontal ligament and alveolar bone by various tooth movements–A 3D FEM study. Journal of oral biology and craniofacial research. 2020 Oct 1;10(4):758-63.
106. Otani T, Koga T, Nozaki K, Kobayashi Y, Tanaka M. Mechanical effects of distributed fibre orientation in the periodontal ligament of an idealised geometry. Computer Methods in Biomechanics and Biomedical Engineering. 2020 Nov 10;24(7):701-9.
107. Maceri F, Marino M, Vairo G. A unified multiscale mechanical model for soft collagenous tissues with regular fiber arrangement. Journal of biomechanics. 2010 Jan 19;43(2):355-63.
108. Natali, A. N., Carniel, E. L., Pavan, P. G., Sander, F. G., Dorow, C., and Geiger, M. (April 22, 2008). A Visco-Hyperelastic-Damage Constitutive Model for the Analysis of the Biomechanical Response of the Periodontal Ligament. ASME. J Biomech Eng. June 2008; 130(3): 031004. https://doi.org/10.1115/1.
109. Fard AM, Vakili-Tahami F. Fibrous soft tissues damage evaluation with a coupled thermo-visco-hyperelastic model. International Journal of Non-Linear Mechanics. 2020 Jan 1;118:103260
110. Huang H, Tang W, Tan Q, Yan B. Development and parameter identification of a visco-hyperelastic model for the periodontal ligament. Journal of the mechanical behavior of biomedical materials. 2017 Apr 1;68:210-5.
111. Narooei K, Arman M. Generalization of exponential based hyperelastic to hyper-viscoelastic model for investigation of mechanical behavior of rate dependent materials. Journal of the mechanical behavior of biomedical materials. 2018 Mar 1;79:104-13.

112. Fung, YC. Biomechanics: mechanical properties of living tissues. 2nd Ed. New York (USA). Springer New York; 2013. Chapter 7, Bioviscoelastic Solids; p242-314.
113. Ortún-Terrazas J, Cegoñino J, Del Palomar AP. In silico study of cuspid'periodontal ligament damage under parafunctional and traumatic conditions of whole-mouth occlusions. A patient-specific evaluation. Computer methods and programs in biomedicine. 2020 Feb 1;184:105107.
114. Gholamalizadeh T, Moshfeghifar F, Ferguson Z, Schneider T, Panozzo D, Darkner S, Makaremi M, Chan F, Søndergaard PL, Erleben K. Open-Full-Jaw: An open-access dataset and pipeline for finite element models of human jaw. Computer Methods and Programs in Biomedicine. 2022 Sep 1;224:107009.

3 Development of an Ex Vivo Model for Characterising Vertical Tooth Extraction

The following chapter details an ex vivo experimental method for testing the extraction biomechanics of partial swine incisors. A self-aligning apparatus is proposed that uses linear and rotational motion elements to reduce the out-of-axis loads applied in simulated vertical tooth extraction. A pilot study using various rates of force- and displacement-controlled loading is performed. This method provides the data used for solving an IFEA problem for PDL parameters under extraction load in Chapter 4 and serves as the basis for the characterisation study performed in Chapter 5. A version of this chapter has been published as:

Gadzella TJ, Hynkova K, Westover L, Addison O, Romanyk DL. A novel method for simulating ex vivo tooth extractions under varying applied loads. Clinical Biomechanics. 2023 Dec 1;110:106116.

3.1 Introduction

Tooth extraction (exodontia) is one of the most common surgical procedures in health care, being carried out in a reported 5–14 % of all dental clinic attendances [1-4]. Although considered a minor surgical procedure, exodontia inevitably results in damage to the surrounding bone and soft tissues. Most procedures involve the use of instruments such as elevators and forceps to apply prying forces to the rupture the periodontal ligament and release the tooth from its socket [5-6]. The application of these forces causes plastic deformation to the alveolar bone and can result in fractures of the tooth and/or bone which influences how the site heals [7]. More complicated tooth extractions can require further deformation of the alveolar complex to allow a path of removal for the tooth [8-9], with healing outcomes correlated to the invasiveness of the surgery [9].

Following exodontia, the alveolar bone can remodel exhibiting a resorptive pattern that can pose risks to: the survivability of the adjacent dentition; the ability to support a prosthesis comfortably; and the availability of bone to receive an osseointegrated dental implant [6,8,10]. The nature of trauma at the time of tooth extraction can limit opportunity for immediate [6,10-12] and delayed implant placement [11], and elective surgical extractions can often reduce intraoperative trauma [12-13]. Several techniques and devices have been developed to perform 'atraumatic' exodontia to improve healing outcomes. However, these techniques have largely been assessed based on short-term clinical measurements such as the incidence of operative trauma [14-19] or procedure duration [13,16-19]. Data describing the mechanical nature of tissue trauma and its relationships to these outcomes are scarce. An exception has been data collected from load-cells connected to a Benex® device (Helmut Zepf, Seitingen-Oberflacht, Germany), which is designed to remove teeth axially and reduce damage to the alveolar cortical plates. It was used to record in vivo force-time data from clinical extractions [19]. The peak forces ranged from 41 N to 629 N and were correlated with estimates of the root surface attachment area from planar radiographs, demonstrating an increase in extraction force as the root surface area increased [19]. Studying extraction forces in vivo provides important insight to the force magnitudes and loading rates applied during this form of exodontia.

Laboratory-based experimental approaches to study exodontia may provide insight to extraction mechanics but are also limited in the literature. One such approach was proposed by Genna and

Paganelli [20] where swine canines were extracted from mandibles clamped firmly in a test frame with orthodontic wires passed transversely through the crown as a point of load application. Peak forces in this study ranged from 100 N to 450 N with approximate dental complex stiffnesses ranging from 20 N/mm to 150 N/mm. Force-displacement data was used to validate a viscoelastic damage finite element model representing the periodontal ligament. However, 25 of the attempted 40 extractions were unsuccessful (i.e. resulted in tooth fractures as opposed to an extracted tooth) which may have been due to potential misalignment of the specimen to the load frame and/or stress concentrations resulting from drilling into the tooth crown.

Other engineering models of dental trauma relate to the anticipated load and displacement regimens for tooth extraction without directly modelling the process. These models are informed by uniaxial tests in compression or tension on coupons cut from the tooth-PDL-bone junction [21-23] and have been used to model loading of the dental complex under traumatic loading. The loads considered in these studies are generally intrusive rather than extrusive to the teeth, such as from simulated falls or direct intrusive impacts [24-26]. Associated models demonstrate appropriate ranges of tooth displacements and applied forces but the relationships between these modes of injury and extraction trauma are unproven.

The purpose of this study is to present a novel ex vivo test method for simulated tooth extractions that has a high degree of experimental control and will enable better understanding of the relationships between the mechanics of exodontia and damage accumulation in the alveolar complex. Critical features of the proposed method are that the experimental apparatus and supporting analysis of the data are sufficiently robust to characterize non-linear behaviours of the dental complex that may influence the success or failure of extraction (e.g. viscoelasticity). Peak extraction force and stiffness are examined as potential metrics for predicting extraction success or failure that encapsulate these aspects of the dental complex mechanical response. The preliminary experimental work performed tests using a range of rates through displacement-control, load-control, and clinically-informed intermittent loading in a pilot study on swine incisors to investigate extraction mechanics. . The ability of the proposed method to capture mechanical outcomes (peak force and stiffness) and their relationships to extraction success or failure is demonstrated.

3.2 Methods

Tissue samples for this study were mandibles taken from Duroc X swine aged 8-12 months. Animals were sacrificed as part of the surgical research initiative at the University of Alberta. Thirteen (13) mandibles were obtained from these animals post-mortem under a secondary-use exemption provided by the University of Alberta Research Ethics Office (REO Reference 2021.006 Romanyk(2019.046)) (n=25). Mandibles were frozen at -24 °C immediately after collection and thawed for 24 hours prior to testing. Testing was carried out at room temperature with a paper towel soaked in PBS placed over the tissue to maintain hydration while not being handled. Mandibles were sectioned to an approximate root length of 15 mm and potted in dental stone to be attached to the apparatus. Threaded anchors and an attachment cable from a Benex® atraumatic extraction kit (Helmut Zepf, Seitingen-Oberflacht, Germany) were used to connect the incisors to the test frame crosshead. Further detail surrounding sample preparation can be found in Appendix A.

Vertical tooth extraction was simulated by applying tension to the tooth through a cable, which was attached to the tooth through a threaded anchor (Helmut Zepf, Seitingen-Oberflacht, Germany) aligned with the primary axis of the tooth. The sample was fixed by the custom test apparatus (Figure 3-1a) to an Instron E3000 ElectroPuls material test frame (Instron, Norwood, USA). This allowed for control over the direction of extraction forces because the cable, in conjunction with the self-aligning base, does not provide bending or torsional resistance (Figure 3-1c). This apparatus is described in Appendix A.

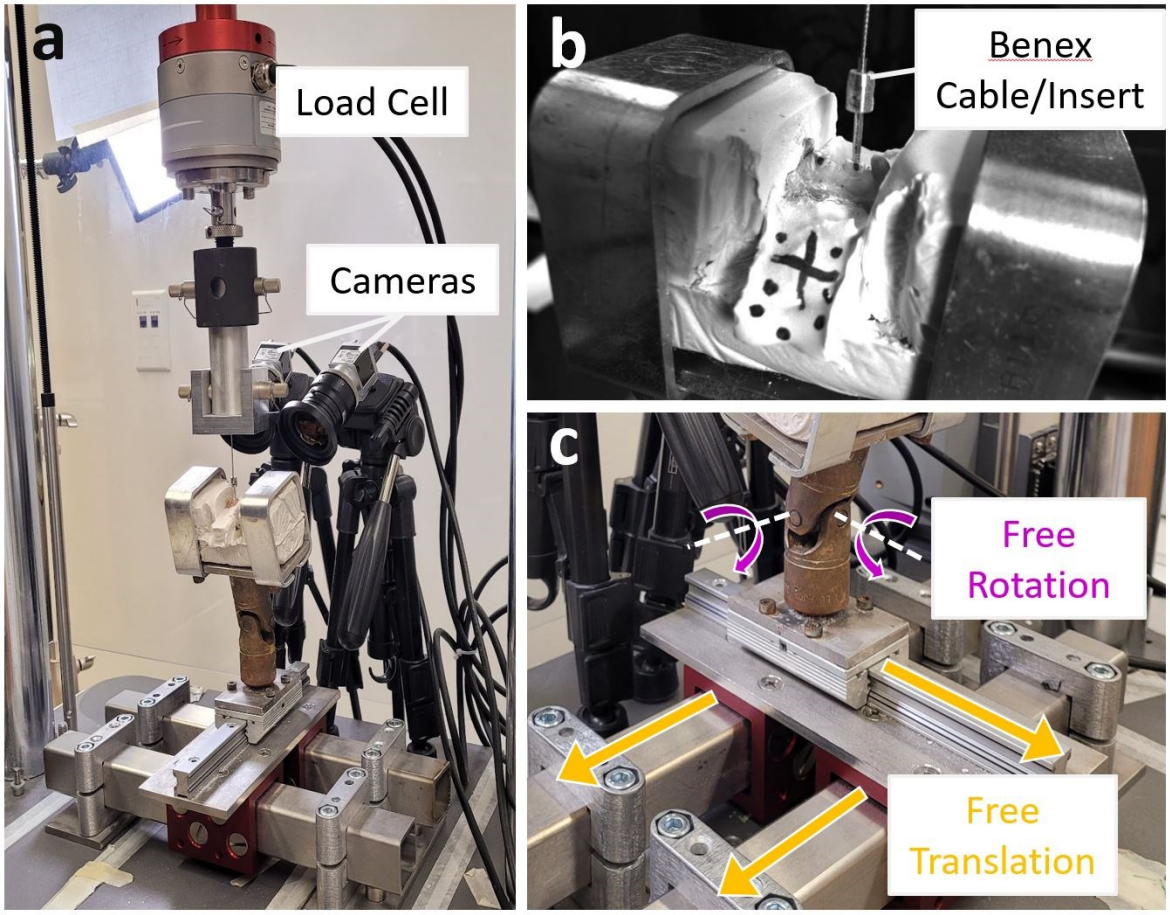

Figure 3-1: The self-aligning test apparatus inside the test frame, showing: a) the entire test apparatus. Force and displacement measurements are taken by the load cell and crosshead at the top of the image; b) image of a sample attached to the test apparatus with aluminum clamps. The incisor is attached to the crosshead with a screw implant and cable; c) an enlarged view of the self-aligning system motion elements. A monorail with bearing carriage and two square sleeve carriages provide linear motion (yellow arrows) and the universal joint allows for two axes of rotation (purple arrows).

Two different loading rates were tested using both force and displacement control: 0.2 mm/min (DC1) and 2 mm/min (DC2) rates for displacement control, and 10 N/min (FC1) and 100 N/min (FC2) for force control. The 100 N/min rate was estimated as a near-equivalent to 2 mm/min extractions based on the force-displacement curves produced by Genna and Paganelli [20] when simulating extractions of swine canines. Correspondingly, 10 N/min and 0.2 mm/min rates were selected as a tenfold reduction achieving quasi-static loading.

A fifth load scheme, an intermittent ramp-hold scheme (IC), was included for comparison with clinically representative loading using the Benex device, where the operator activates the device

intermittently based subjectively on their clinical judgement [19]. The need to change grip, reverse direction, or wait for tissue relaxation all cause interruptions to the load applied during tooth extraction. To simulate this loading, 0.25 mm displacements were applied at a loading rate of 2 mm/min with 10s constant-displacement dwell periods between each loading interval. This loading scheme was derived from force-time traces collected from a clinical study [19] and pilot data collected using the ex vivo system. The clinical data demonstrated brief ramp periods with hold periods approximately 10s in duration. It was determined from pilot data that a single ramp-hold cycle should consist of a 0.25 mm displacements over a range of 2 mm to ensure complete extraction. Table 1 demonstrates the relationships among all five test schemes.

Table 3-1: Organization of the five test schemes used to extract central incisors in the study (n=25). Intermittent displacement tests were performed using a single load rate (2mm/min) during ramp periods.

Control Type	Group 2	Group 1
Displacement	2 mm/min (5 tests)	0.2 mm/min (5 tests)
Force	100 N/min (5 tests)	10 N/min (5 tests)
Intermittent Displacement	2mm/min ramp, 10 second dwell (5 tests)	

Five incisors were extracted for each of the five test schemes (n=25). For all mandibles, the left central incisor was extracted first and the test order of load schemes was randomized.

3.2.1 Test Procedure

Potted samples were attached to the self-aligning system using aluminum clamps. The load cell was connected to the threaded anchor in the subject incisor with slack in the system so that the self-aligning base could be moved to improve alignment. Two Basler area-scan cameras (Basler AG, Ahrensburg, Germany) were used to capture each extraction test at an acquisition period of 9ms (capture rate of 110fps) with an image resolution of 960x600 pixels. Calibration image sets were captured regularly between test sessions using a 2.20 mm grid.

From a slack position, tests were initiated with a 1 mm/min preloading ramp to a maximum preload of 20 N. Immediately upon reaching 20 N, the system switched into the appropriate load scheme for the test. The specified rate was applied until the load dropped below 10 N, indicating that the tissue was no longer resisting load. Peak forces were extracted from the force-time data in MATLAB. The minimum, maximum, and median peak force values for each of the five load schemes were compared directly. Statistical comparisons of peak extraction forces based on load scheme or extraction order were not included because of the limited sample size for this initial study.

Tested samples were removed from the apparatus and visually assessed for failed extraction. Failed extractions due to tooth fracture were visually evident at this point. Extractions were classified as failed after removal from the dental stone if a noticeable bone fracture was observed. Thus, extractions were classified as failed if a) the dental tissue fractured, resulting in failure to remove the tooth root (Figure 3-2a); or b) the tooth root was removed but bone fracture was observed upon examination of the mandible sample.

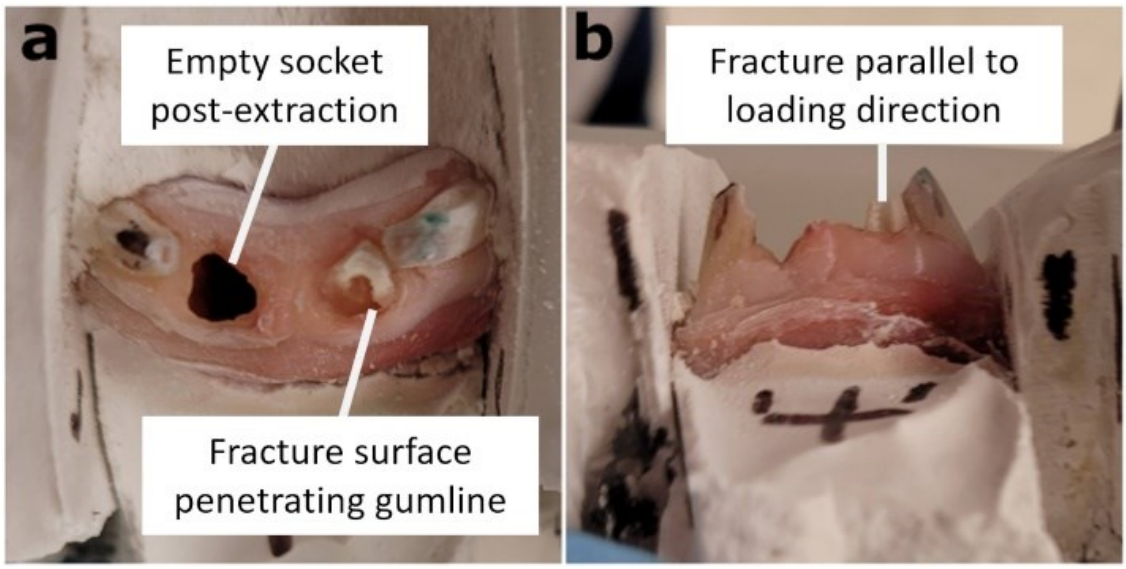

Figure 3-2: a) Top view and b) front view of a swine mandible sample fixed in dental stone post-extraction. The left central incisor has fractured at the crown reaching below the gingival margin into the dentin. The right central incisor socket cavity is shown.

3.2.2 Stiffness Analysis

Instantaneous stiffness of the dental complex was assessed in a separate analysis to demonstrate the sensitivity of the proposed testing method and investigate dental complex stiffness as a

mechanical variable associated with tooth extraction success. The stiffness analysis was performed only for continuous-loading tests with a tissue-loading region identified through video analysis so that system alignment motion was omitted from the analysis. The video analysis that identified these periods is described in Supplemental Material S1. The video-measured displacements confirmed trends in the crosshead data wherein alignment occurred at low forces, with tooth displacement relative to the dental stone dominating after the alignment phase (Figure A-3). The force-displacement data lying between the point where tissue loading became dominant and the peak load for the test were extracted. The data in these regions demonstrated nonlinear behaviour, requiring an instantaneous stiffness measure rather than a linear fit. The data were filtered in MATLAB using a moving average windowing filter with a filter width of 101 samples. A sliding window regression function, movingslope() [27], was used to calculate the instantaneous stiffness at every point in the curve over a 21-sample sliding window. The displacements were then normalized by dividing by the displacement recorded at peak load giving a range from 0 to 1 where 0 represented the start of tissue-dominated loading and 1 represented the point of peak load. The Shape Language Modelling toolbox for MATLAB [28] was used to evaluate the stiffness value from the calculated slopes across 1000 common points in the normalized range. The FC1 and DC1 stiffness curves (0.2mm/min and 10N/min) were then filtered with the moving-average filter again because they demonstrated greater sensitivity to noise in the original signal.

The K-means algorithm was applied to perform curve clustering on the normalized stiffness curves in MATLAB. The kmeans() function was set to identify 4 clusters (matching the number of applied load schemes) with 50,000 replicates to determine if trends in the stiffness curves could be identified independent of the applied load scheme. The resulting best set of clusters was then related to the original loading schemes as a probability of each load scheme being grouped into a specific cluster.

3.3 Results

Independent of the control scheme used, regions of system self-alignment in the low-load (approximately <50 N) regions are seen in the force-displacement results measured in all trials (Figure 3-3). One extraction at 100 N/min was removed due to a premature failure at the interface between the screw and tooth. Five failed extractions were retained in the dataset: two

(10 N/min, 100 N/min) due to bone fractures and three (2 mm/min, Intermittent) due to tooth root fractures.

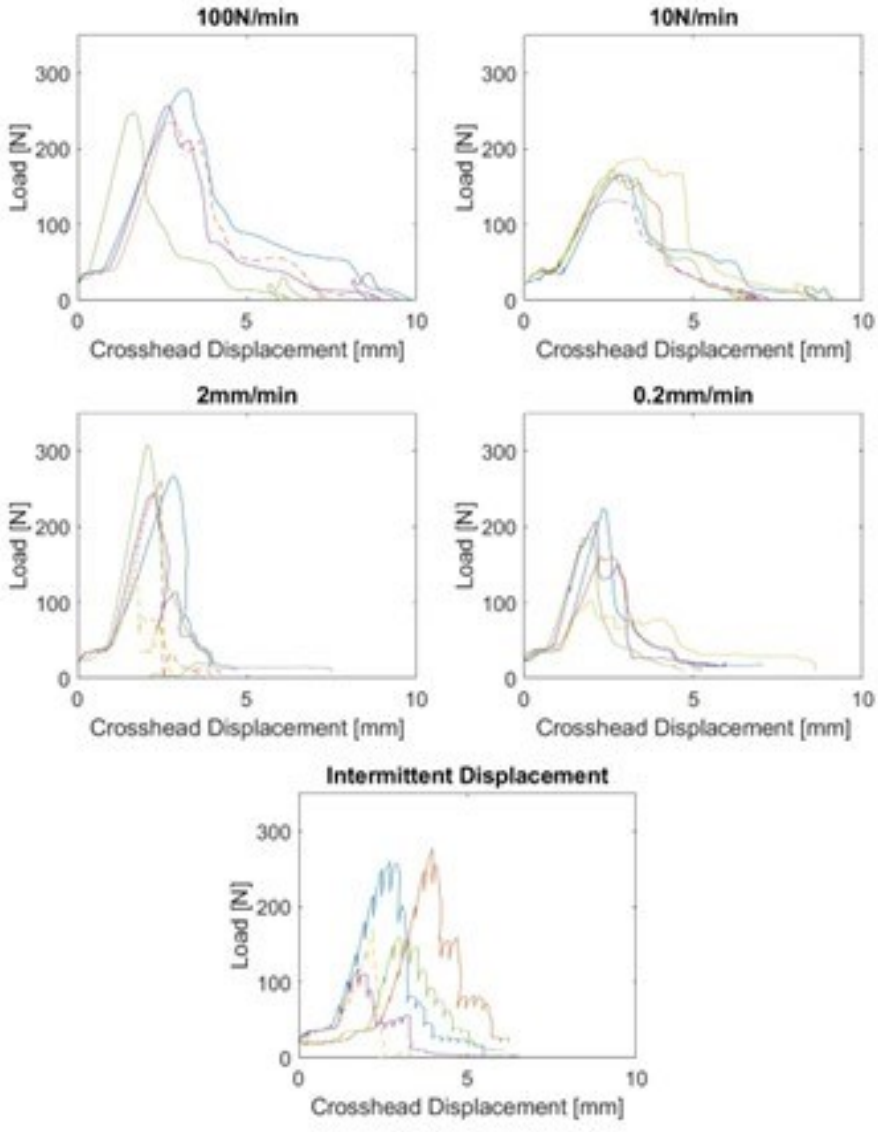

Figure 3-3: Plots of force vs displacement for 'tooth extractions' organized by control scheme. Top left: traces from 100 N/min extractions. Top right: traces from 10N/min extractions. Centre right: traces from 0.2 mm/min extractions. Centre left: traces from 2 mm/min extractions. Bottom centre: traces from the intermittent-displacement extractions. Each colour indicates a separate extraction (n=24) with dashed lines indicating failed extractions. Curves are not corrected for preload (displacement is zero at 20 N).

High-load regions are extended in the 10 N/min curves when compared to all other control schemes, with forces approaching and maintaining near-peak forces across greater displacements. Peak forces in each trial occurred between 2-5 mm of crosshead displacement. Force relaxations are evident in the intermittent displacement load curves. During ramp periods

prior to peak load, the load rapidly returns to the previous level and continues to increase. The intermittent force-displacement curves after peak load display distinctive rounding of the curves during ramp periods.

3.3.1 Peak Extraction Forces

Peak extraction forces ranged from 101.9 N to 308.9 N (Figure 3-4). Median extraction forces for the FC2 and DC2 load schemes were higher than the FC1 and DC1 schemes . The median value for the intermittent loading extractions was between the FC2/DC2 and FC1/DC1 continuous schemes at 171.2 N (Table 3-2).

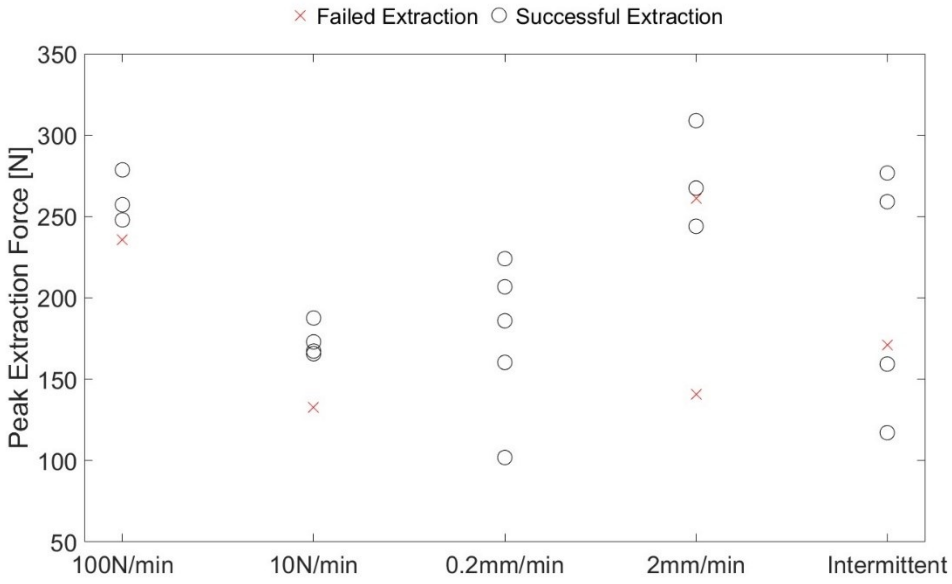

Figure 3-4: Scatter plot of peak extraction force categorized by load scheme type. Failed extractions are demarked with an X marker to demonstrate their contributions to widening the distributions downwards.

Table 3-2: Characteristic values of the peak extraction forces obtained from simulated swine tooth extractions

a) Peak force (N) characteristics, including failed extractions

Group	100N/min	10N/min	0.2mm/min	2mm/min	Intermittent
Median	252.5	167.3	185.9	261.2	171.2
Min	235.6	132.5	101.9	140.6	117.1
Max	278.6	187.6	224.0	308.9	276.7

b) Peak force (N) characteristics with failed extractions excluded

Group	100N/min	10N/min	0.2mm/min	2mm/min	Intermittent
Median	257.2	170.1	185.9	267.4	209.2
Min	247.8	165.7	101.9	244.0	117.1
Max	278.6	187.6	224.0	308.9	276.7

3.3.2 Stiffness Analysis

13 continuous-loading extractions with loading periods dominated by tooth movement were analyzed for instantaneous stiffness clustering. The k-means algorithm with four clusters identified two different primary clusters and two single-curve clusters (Figure 3-5a). The FC1 and DC1 extractions were identified from the FC2 and DC2 extractions by the clustering algorithm as demonstrated in the zero-probability associated with these clusters in Figure 3-5b. The FC1/DC1cluster demonstrates overall lower stiffness magnitudes (below 150 N/mm) and gradual reductions in stiffness up to peak load. The FC2/DC2 cluster is characterized by higher stiffness magnitudes reaching 150 N/mm – 200 N/mm and a rapid decrease in stiffness leading to peak load.

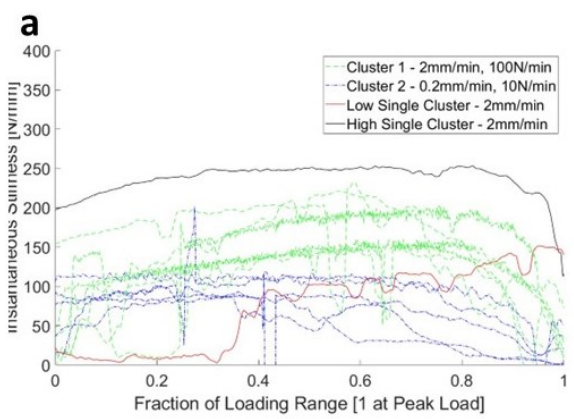

	3	2	1	4
0.2mm/min	0	1	0	0
10N/min	0	1	0	0
2mm/min	0.2	0	0.6	0.2
100N/min	0	0	1	0

Figure 3-5: a) Instantaneous stiffnesses of video-confirmed loading periods of dental complex loading, normalized to peak load. Stiffness curves are identified by cluster using the K-Means algorithm and differentiated by colour: Green indicates the higher-stiffness, FC2/DC2 cluster; Blue indicates the lower-stiffness, FC1/DC1 cluster; and black and red indicate the single-curve clusters composed of 2 mm/min FC2 extraction traces. b) Heat map demonstrating the probability of a test from each continuous load scheme being identified in a cluster (p=0.0-1.0). Clusters are arranged in columns by colour – Clusters 1 & 2 (blue and green) are the FC1/DC1 and FC2/DC2 clusters, 3 & 4 the single-curve clusters.

Both single-curve clusters belonged to 2 mm/minute extractions. One curve was identified by having much higher stiffness values overall (black single-curve cluster in Figure 3-5), ranging between 200 N/mm and 250 N/mm before reaching peak load. The other curve was identified due to a prolonged period of near-zero stiffness followed by a rapid increase in stiffness, reaching an overall magnitude more characteristic of the high-load cluster near 150 N/mm (red single-curve cluster in Figure 3-5).

3.4 Discussion

The presented work proposes an approach to study the biomechanics of tooth extraction in a mechanically controlled environment that resulted in consistent extraction success (i.e. 19/24 extractions without perceptible tooth or bone fracture). A preliminary comparison of mechanical response among continuous and intermittent loading schemes is presented. Peak extraction forces were related to load rate during tooth extraction. Successful extractions from the 2 mm/min and 100 N/min groups experienced peak forces ranging from 244 N to 309 N, which has no overlap with the range of successful extractions for the 0.2 mm/min and 10 N/min loading schemes that spanned 102 N to 224 N. These results are consistent with the general understanding that the dental complex, particularly the periodontal ligament, is viscoelastic [29-31] and should provide

greater resistance to higher-rate loads. This sensitivity is an important finding for the presented study because it demonstrates the proposed method is sufficiently sensitive and robust to capture differences in the nonlinear mechanical response of the tested complex.

Intermittent loading did not reduce peak forces and fracture risk relative to the continuous load schemes in this pilot study. Peak forces from intermittent-loading trials range from the second-lowest overall at 117 N to the third-highest at 277 N. Stress relaxation during hold periods for these tests was identifiable, but large increases in force still occurred during loading periods. Feedback control was not exerted in this basic comparative study – extractions were performed following a set scheme unaffected by the system response, which may not represent the loads applied by a clinician. Further work should investigate different control schemes utilizing variable rate controls or threshold-based logic to further investigate the role of tissue relaxation in extraction mechanics.

Peak extraction forces measured with this ex vivo swine model align well with the available clinical measurements despite several key differences in the ex vivo swine and in vivo human clinical models. Extraction forces measured ex vivo range from 102 N to 309 N, well inside the envelope of forces (41 N – 629 N) observed in the clinical extraction study performed by Dietrich et al [19]. The similarity between these models should be interpreted cautiously given the geometric differences between the swine and human models, ex vivoparticularly the buccal angulation and length of swine incisors relative to the matching human anatomy. Additionally, the clinical study included multi-rooted teeth that were only sectioned when deemed necessary by the clinician, resulting in a greater range of tooth geometries in the human model. To limit the influence of geometry in the current study, the apices of the swine teeth were removed before testing. However, the exclusion of the root apex may reduce the peak extraction forces by decreasing root surface attachment area while limiting the range of attachment areas across the studied teeth. It is unsurprising given these differences that the human clinical data varies more than the ex vivo swine model, but it is important that the models share a degree of similarity. When comparing the ex vivo swine and human clinical modelthethe relatively small ranges of peak force exhibited within ex vivo groups compared to the clinical data indicate the high level of consistency achieved during the preparation and testing phases of this study compared to a clinical sample. Future work will focus on a robust characterization of the swine dental complex

geometry to investigate its relationship with extraction mechanics and generalizability to a clinical model.

The key mechanical results of this study agree with previous experimental results obtained by Genna and Paganelli [20]. The peak forces obtained at 2 mm/min in the current study range from 141-309 N, and are within the range reported by Genna and Paganelli at the same rate (100-450 N). Genna and Paganelli also reported overall stiffness values for the dental complex between 20 to 150 N/mm, which align with the overall magnitudes of the clusters identified in this study at the same loading rate. The notable differences between the experimental approaches are that the prior study extracted whole swine canines [20] rather than the partial incisors, and that the application of the self-aligning apparatus in the present study resulted in a higher percentage of successful extractions. The self-aligning apparatus also improves the mechanical control of the experiment by applying vertical forces with minimal induced bending in the tooth root. Stiffffness analysis identified several trends among the different loading schemes. The K-means algorithm was able to objectively distinguish the stiffness curves between loading rates while blinded to the applied load schemes, demonstrating the importance of load rate to the dental complex mechanical response and the system's sensitivity to these systematic changes. The underlying differences in curve shape and magnitude, such as the approximately 50 N/mm increases in stiffness over the loading range demonstrated by the FC2/DC2 cluster (green in Figure 5a) and the tendency of stiffness in all clusters to decay approaching peak force, are indicators for the mechanical nonlinearity of the dental complex. The viscoelasticity of the periodontal complex is well-established [29-31] and likely contributes to the overall higher stiffnesses in the FC2/DC2 cluster compared to the FC1/DC1cluster. Two stiffness curves from the 2 mm/min test group were identified as their own distinct clusters based on shape and overall magnitude. The high-magnitude single-cluster was more similar in shape to the other DC2 curves but was shifted upwards, exceeding the maximum stiffness of all other curves in this study and those found by Genna and Paganelli [20], whereas the lower single-cluster had a much different shape than all other curves. The inclusion of only continuous-loading trials with successful video analysis limited the number of tests included in the stiffness analysis but was necessary given the intentional design of the apparatus to displace to ensure vertical extraction.

One limitation of the study is that surface-level displacement measurements cannot differentiate the contributions of different tissues in the dental complex to the overall mechanical response. However, this compromise allows for the analysis of the complete dental complex during extraction rather than small sections of tissue. Additionally, this study was performed using tissue samples that were frozen and thawed. The effect of freezing on soft tissues remains contentious, but this storage method was necessary given the intermittent availability of tissue samples. The video analysis was subject to limitations of camera lighting and feature occlusion but is an important analysis tool. Future work can improve on displacement measurements in video by adjusting the camera fixtures to provide greater similarities between views and implementing spherical targets to provide a more consistent shape for tracking across large rotations.

3.5 Conclusion

This study presents a self-aligning test apparatus which seeks to minimize eccentric loads that can be associated with undesirable hard tissue fractures. A basic pilot study comparing different continuous loading rates and an intermittent loading scheme during simulated tooth extractions was performed on swine incisors. Peak forces differed among extractions at different continuous loading rates. Intermittent loading did not reduce peak extraction forces. Higher rates continuous loading demonstrated higher stiffnesses of the tooth-PDL-bone complex than lower rates continuous loading. The results of this study suggest that the control of load rate during tooth extraction is important, laying the foundation for future work towards improving wound site healing and immediate implant placement.

References

1. Broers DLM, Dubois L, de Lange J, Su N, and de Jongh A. Reasons for tooth removal in adults. Int Dent J. 2021;72(2022):52-57.
2. Schneider C, Zemp E, Zitzmann NU. Dental care behaviour in Switzerland. *Swiss Dent J*. 2019;129(6):466-478.
3. Cunha MAGM, Lino PA, Santos TRD, Vasconcelos M, Lucas SD, Abreu MHNG. A 15-Year Time-series Study of Tooth Extraction in Brazil. *Medicine (Baltimore)*. 2015;94(47):e1924. doi: 10.1097/MD.0000000000001924.
4. Murray H, Locker D, Kay EJ. Patterns of and reasons for tooth extractions in general dental practice in Ontario, Canada. *Community Dent Oral Epidemiol*. 1996;24(3):196-200. doi: 10.1111/j.1600-0528.1996.tb00841.x.
5. Hupp J, Ellis E, and Tucker MR. Contemporary oral and maxillofacial surgery. 7Th ed. Philadelphia, PA: Elsevier; 2019. Chapter 8: Principles of routine exodontia; p.106-134.
6. Dym H, Weiss A. Exodontia: tips and techniques for better outcomes. *Dent Clin North Am*. 2012;56(1):245-66. doi: 10.1016/j.cden.2011.07.002.
7. Adeyemo WL, Ladeinde AL, Ogunlewe MO. Influence of trans-operative complications on socket healing following dental extractions. *J Contemp Dent Pract*. 2007;8(1):52-9.
8. Leblebicioglu B, Hegde R, Yildiz VO, Tatakis DN. Immediate effects of tooth extraction on ridge integrity and dimensions. *Clin Oral Investig*. 2015;19(8):1777-84. doi: 10.1007/s00784-014-1392-1.
9. Fickl S, Zuhr O, Wachtel H, Bolz W, Huerzeler M. Tissue alterations after tooth extraction with and without surgical trauma: a volumetric study in the beagle dog. *J Clin Periodontol*. 2008;35(4):356-63. doi: 10.1111/j.1600-051X.2008.01209.xHämmerle and Tarnow, 2018).
10. Becker W. Immediate implant placement: treatment planning and surgical steps for successful outcomes. *Br Dent J*. 2006;201(4):199-205. doi: 10.1038/sj.bdj.4813881.
11. Blanco J, Carral C, Argibay O, Liñares A. Implant placement in fresh extraction sockets. *Periodontol*. 2000. 2019;79(1):151-167. doi: 10.1111/prd.12253.
12. Hämmerle CHF, Tarnow D. The etiology of hard- and soft-tissue deficiencies at dental implants: A narrative review. *J Periodontol*. 2018;89 Suppl 1:S291-S303. doi: 10.1002/JPER.16-0810.

13. Sharma SD, Vidya B, Alexander M, Deshmukh S. Periotome as an Aid to Atraumatic Extraction: A Comparative Double Blind Randomized Controlled Trial. *J Maxillofac Oral Surg*. 2015;14(3):611-5. doi: 10.1007/s12663-014-0723-8.
14. Papadimitriou DE, Geminiani A, Zahavi T, Ercoli C. Sonosurgery for atraumatic tooth extraction: a clinical report. *J Prosthet Dent*. 2012;108(6):339-43. doi: 10.1016/S0022-3913(12)00169-2.
15. El-Kenawy MH, Ahmed WM. Comparison Between Physics and Conventional Forceps in Simple Dental Extraction. *J Maxillofac Oral Surg*. 2015;14(4):949-55. doi: 10.1007/s12663-015-0765-6.
16. Patel HS, Managutti AM, Menat S, Agarwal A, Shah D, Patel J. Comparative Evaluation of Efficacy of Physics Forceps versus Conventional Forceps in Orthodontic Extractions: A Prospective Randomized Split Mouth Study. *J Clin Diagn Res*. 2016;10(7):ZC41-5. doi: 10.7860/JCDR/2016/17724.8160.
17. Hariharan S, Narayanan V, Soh CL. Split-mouth comparison of physics forceps and extraction forceps in orthodontic extraction of upper premolars. *Br J Oral Maxillofac Surg*. 2014;52(10):e137-40. doi: 10.1016/j.bjoms.2014.06.013.
18. Muska E, Walter C, Knight A, Taneja P, Bulsara Y, Hahn M, Desai M, Dietrich T. Atraumatic vertical tooth extraction: a proof of principle clinical study of a novel system. *Oral Surg Oral Med Oral Pathol Oral Radiol*. 2013;116(5):e303-10. doi: 10.1016/j.oooo.2011.11.037.
19. Dietrich T, Schmid I, Locher M, Addison O. Extraction force and its determinants for minimally invasive vertical tooth extraction. *J Mech Behav Biomed Mater*. 2020;105:103711. doi: 10.1016/j.jmbbm.2020.103711.
20. Genna F, Paganelli C. Force–displacement relationship in the extraction of a porcine tooth from its socket: experiments and numerical simulations. *Journal Mech Mat Struct*. 2014; 9(5):497-514.
21. Natali AN, Pavan PG, Carniel EL, Dorow C. A transversally isotropic elasto-damage constitutive model for the periodontal ligament. *Comput Methods Biomech Biomed Engin*. 2003;6(5-6):329-36. doi: 10.1080/10255840310001639840Bergomi M, Cugnoni J, Galli M, Botsis J, Belser UC, Wiskott HW. Hydro-mechanical coupling in the

periodontal ligament: a porohyperelastic finite element model. *J Biomech*. 2011;44(1):34-8. doi: 10.1016/j.jbiomech.2010.08.019.

22. Bergomi M, Cugnoni J, Botsis J, Belser UC, Anselm Wiskott HW. The role of the fluid phase in the viscous response of bovine periodontal ligament. *J Biomech*. 2010;43(6):1146-52. doi: 10.1016/j.jbiomech.2009.12.020.Ortún-Terrazas et al, 2019;
23. Dezzen-Gomide AC, de Carvalho MA, Lazari-Carvalho PC, de Oliveira HF, Cury AADB, Yamamoto-Silva FP, Silva BSF. A three-dimensional finite element analysis of permanent maxillary central incisors in different stages of root development and trauma settings. *Comput Methods Programs Biomed*. 2021;207:106195. doi: 10.1016/j.cmpb.2021.
24. Karimi Dastgerdi A, Rouhi G, Dehghan MM, Farzad-Mohajeri S, Barikani HR. Linear Momenta Transferred to the Dental Implant-Bone and Natural Tooth-PDL-Bone Constructs Under Impact Loading: A Comparative in-vitro and in-silico Study. *Front Bioeng Biotechnol*. 2020;8:544. doi: 10.3389/fbioe.2020.00544.
25. Ortún-Terrazas J, Cegoñino J, Santana-Penín U, Santana-Mora U, Pérez Del Palomar A. A porous fibrous hyperelastic damage model for human periodontal ligament: Application of a microcomputerized tomography finite element model. *Int J Numer Method Biomed Eng*. 2019;35(4):e3176. doi: 10.1002/cnm.3176.
26. John D'Errico (2021a). Movingslope(). Matlab Central File Exchange, retrieved July 30th, 2021. Available from: https://www.mathworks.com/matlabcentral/fileexchange/16997-movingslope
27. John D'Errico (2021b). SLM – Shape Language Modeling. Matlab Central File Exchange, retrieved July 30th, 2021. Available from: https://www.mathworks.com/matlabcentral/fileexchange/24443-slm-shape-language-modelingOvy et al, 2022;
28. Ovy EG, Romanyk DL, Mir CF, Westover L. Modelling and evaluating periodontal ligament mechanical behaviour and properties: A scoping review of current approaches and limitations. *Orthod Craniofac Res*. 2022:25(2):199-211. doi: 10.1111/ocr.12527
29. Fill TS, Toogood RW, Major PW, Carey JP. Analytically determined mechanical properties of, and models for the periodontal ligament: critical review of literature. *J Biomech*. 2012;45(1):9-16. doi:10.1016/j.jbiomech.2022.09.020

30. Fill TS, Carey JP, Toogood RW, Major PW. Experimentally determined mechanical properties of, and models for, the periodontal ligament: critical review of current literature. *Journal Dent Biomech*. 2011:312980. doi:10.4061/2011/312980

4 Development of an Axisymmetric Finite Element Model for Simulating Vertical Tooth Extraction

This chapter describes the construction of an axisymmetric finite element model for simulating vertical tooth extraction including the generation of the model geometry, mesh, and applied boundary conditions. A multi-curve formulation of an inverse finite element analysis (IFEA) problem is proposed and solved using pilot data from the experimental study performed in Chapter 3. This model provides the numerical basis for the characterisation study performed in Chapter 5. At the time of this thesis preparation, a version of this chapter has been accepted for publication in the Journal of the Mechanical Behaviour of Biomedical Materials as:

Gadzella TJ, Westover L, Addison O, Romanyk DL. Inverse finite element analysis for an axisymmetric model of vertical tooth extraction.

4.1 Introduction

Tooth extraction is one of the most common surgical procedures, related to an estimated 5-14% of dental clinic attendances [1-4] and with a range of indications from dental decay to financial need [1,5-6]. Despite its commonality, the biomechanics of tooth extraction are not well understood. This is a limitation on the development of atraumatic extraction techniques, which alter the biomechanics of the extraction procedure to reduce the trauma caused to the remaining bone. Trauma and damage to the remaining bone is negatively associated with the preservation of the surviving dentition, patient recovery times, and subsequent implant retention [7-11]. For example, conventional extraction using forceps employ leverage to grip the tooth root externally and to apply combinations intrusive and transverse forces. These coupled forces cause bending in the bone and tooth that expands the socket but is also directly linked to damage [7]. In extreme cases, this damage accumulates to cause fracture in the tooth or bone. Alternatively, the Benex® vertical extraction system seeks to apply a purely axial force along the tooth root via a threaded insert along the centre axis of the tooth, rupturing the periodontal ligament (PDL) and releasing the tooth while minimizing damage to the bone (Figure 1). The difference in biomechanical loading from combined intrusion/bending forces applied with to the purely axial loading applied with the Benex® device is fundamental to the atraumatic nature of the procedure, despite the biomechanical characteristics of the dental complex being poorly understood in either case. This study focuses on tooth extraction using the Benex® device because it has been successfully employed in the clinic with instrumentation to measure extraction forces [12]. Additionally, recent work has sought to better investigate the biomechanics of loading with this device in an ex vivo laboratory model using swine incisors as a pre-clinical model for human tooth extraction [14].

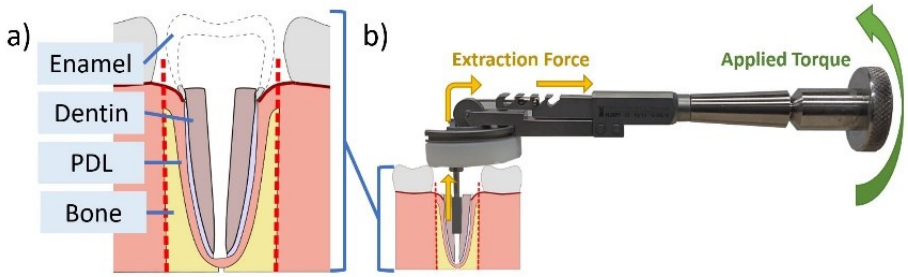

Figure 4-1: The application of forces to a single-rooted tooth with the Benex(R) device: a) the anatomy of the dental complex with the enamel of the crown removed to provide access to the internal root; b) the application of force to the tooth root with the Benex® device resting on the nearby dentition.

There are many available experimental [13-18] and numerical [19-23] models characterizing the biomechanics of the dental complex. These models relate to implant stability [24,25], adaptive remodelling [26,27], or mastication [22, 28]. Generally, they represent the hard tissues of the tooth and bone as homogeneous bodies and focus on the mechanical role of the PDL [20-22, 27-28]. The teeth of interest are loaded intrusively (i.e. simulating mastication) [21-22, 26-28] or transversally (such as in orthodontic tooth movement or malocclusion) [21-22, 27] and are validated against experiments that load the dental complex in the corresponding directions [22, 27] or data collected from small coupons cut from the dental complex [21, 27]. Comparatively few studies examine the behaviour of the dental complex in the extrusive regimes relating to tooth extraction [29], trauma [30] or rupture of the PDL [16,23]. Among the models representing these schema relevant to tooth extraction are three key limitations: they often depend on the use of custom solvers or material models that cannot be replicated [21-3, 29]; they are validated with data gathered from tests on "coupons" or small, regular samples cut from the dental complex and therefore their validity for modelling tooth extraction is unclear [21-23]; and/or they are computationally-expensive subject-specific models that may not be suitable for representing a broad range of extraction cases [22, 29]. However, the available models have demonstrated the importance of modeling hyperelastic [13,15,20-23, 28], viscoelastic [13,16-19, 28], and damage characteristics [15,21-23,30] of the PDL in each loading case. An aim of the presented study is to address each of these important characteristics in loading regimes relevant to tooth extraction while addressing the limitations of previous models.

The primary challenge in modelling tooth extraction is the poor suitability of the available biomechanical data and models for the extraction case based on the above-listed criteria, which in turn limits the design of new extraction techniques and devices. Recent experimental work [14] characterizes the biomechanics of vertical tooth extraction through highly-controlled ex vivo methods. Numerical modelling informed by these experimental findings provides an alternative to studying extraction biomechanics at lower cost and resource intensity compared to the original experiments. The purpose of this study is to propose a generic FE model of the dental complex that can predict the biomechanics of tooth extraction. The proposed FE model has several features that directly address the limitations in the present state of the art: the model uses material constants that are determined from experimental tooth extractions that closely approximate the clinical case rather than generalizing properties obtained in a small-scale test on isolated tissue samples; uses material constants determined from several experimental data sets simultaneously rather than attempting to select a representative case; and is formulated using only material models natively available in an accessible solver with elements specifically formulated for finite strains. The model complexity is reduced by constructing an axisymmetric representation of an experimental tooth extraction model that minimizes the required computational power and solving a multi-curve formulation of the inverse problem for its material properties. Specifically, the axisymmetric representation of the ex vivo swine dental complex (assuming a planar geometry than can be revolved around the long axis of the tooth) was selected for this model to reduce the mesh size required to represent the dental complex. This is advantageous for modeling complex phenomena with minimal computational expense. For example, reducing the meshed volume with an axisymmetric assumption allows greater refinement at active sites such as tissue interfaces than could be accommodated in a 3D mesh. The use of the axisymmetry here is enabled by the approximately-conical shape of the incisors extracted in the previous ex vivo study [14]. The axisymmetric assumption depends on a simplified, fixed representation of the tooth geometry that can be represented as a revolved geometry. The axisymmetric representation of the dental complex can only then be used to approximate the response of the single-rooted, approximately axisymmetric tooth geometry to loading that can also follows the conditions of axisymmetry (as in vertical tooth extraction). In order to predict the biomechanics of the dental complex in various loading conditions, the model parameters are determined in an inverse finite element process based on three different loading

regimes. Within each loading regime, the model is optimized to fit a cluster of data obtained in separate trials. This introduces variability to the data set but also ensures that the model parameters describe a range of extraction cases effectively (rather than deriving parameters from a single representative extraction test). This process is aimed at providing physically-relevant model of the dental complex that can be used as a translational tool in further design and clinical investigation.

4.2 Methods

4.2.1 Experimental Data Collection

Force-time data from a previous ex vivo study of extraction mechanics utilizing swine incisors was used for model development [14]. Mandibles from juvenile swine were cut in a way that truncated the central incisor root length to approximately 15mm (Figure 2a) to be approximately equivalent to an adult human incisor with in-tact apex. Swine teeth are commonly used as a preclinical biomechanical model for approximating human biomechanics [13-15, 31] due to similarities in dental growth and diet between juvenile swine and humans. The experimental model established in the ex vivo study attempts to limit the influence of the curved geometry of swine incisors by truncating the roots superior to the apex [14], although the increased PDL space width presence in the swine model must be accounted for in the application of the preclinical model results. Samples were potted in dental stone and attached to a self-aligning apparatus inside a universal test frame (Figure 2b). Extraction load was applied to the teeth through a threaded insert included in the Benex® kit (Figure 2c) to closely emulate clinical loading. Force-time data from three displacement-controlled schemes were used in the finite element study: 2mm/min, 0.2mm/min, and intermittent periods of 2mm/min loading with 10 second hold periods. Loading rates were determined in the previous ex vivo study [14] based on previous ex vivo and clinical test data [12, 15], The previous study [14] included tests at force-controlled rates but only displacement-controlled tests were included in this finite element study to ensure numerical stability of the model during IFEA solution runs. Only data from successful extractions in which the tooth was delivered from the socket without fracture to the tooth or bone on visual inspection were included because the axisymmetric FE model was not currently trained to model fracture to the hard tissues (the primary mechanism of extraction failure). One 0.2mm/min extraction trace was also excluded because it was found to lie below an envelope of

the 95% confidence interval of the other successful extraction curves due to much lower stiffness of the dental complex and early rupture. This curve was excluded to avoid artificial reduction in the overall stiffness of the model and shortening of the rupture time. The exclusion analysis is presented in Appendix B.

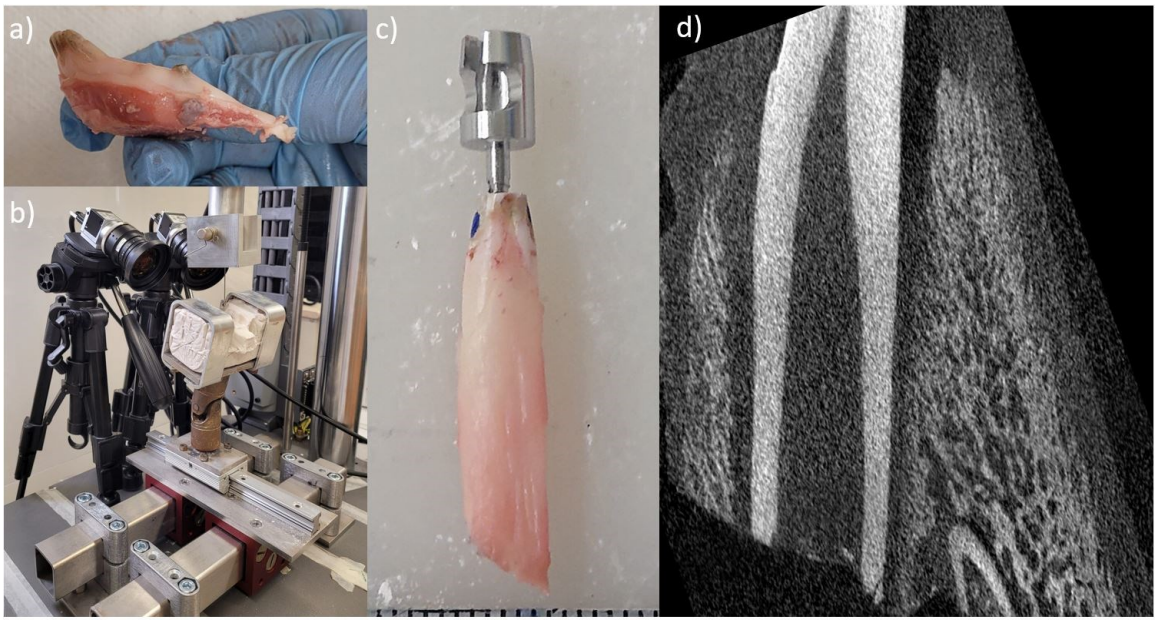

Figure 4-2: Ex vivo model used in previous experimental work [14]: a) A swine mandible section with the central incisors; b) the experimental apparatus used for data collection, with self-aligning elements retaining the potted sample and Benex® cable connection; c) An example of an extracted incisor with the embedded Benex® screw; and d) CT slice showing the arrangement of hard tissues (tooth and bone) in the dental complex

Experimental data required additional preparation for curve fitting because of the self-aligning motion of the apparatus in the original experiments. Each sample underwent a different amount of self-alignment motion which is captured in the displacement-time curve, resulting in a range of force-time curves that could not be accurately assessed with a single finite element solution. The force-time data from each curve above 50N was then moved to a common transition time to simultaneously account for extended periods of self-alignment motion that varied in length [14] and move the curves to a common time domain for curve fitting in the tissue extension phase above 50N. This analysis was necessary to perform the multi-curve analysis but enforces the assumption that the tissue state in every trial was identical at the 50N transition because the loading prior to this point was not included in the optimization error function. The 50N transition point was selected because it was observed that self-alignment motion was complete in all trials

below this point with minimum loss of information during the tissue extension phase of motion. This process is further detailed in Appendix B.

4.2.2 Geometry

Four material bodies were used to represent the dentoalveolar complex from the previous ex vivo experiments [14] (identified by colour in Figure 4-3): the Benex® screw, dentin (representing the entire tooth body), the PDL, and bone. These bodies are arranged concentrically from the long axis of the tooth root and are approximately conical (Figure 4-2d), allowing their representation in an axisymmetric model. The geometry of a central swine incisor was estimated based on post-extraction computed tomography (CT) scans of the extracted teeth and measurements taken with digital calipers during extraction. An approximate diameter of 5mm was determined from the caliper measurements with an outward draft angle of 1 degree towards the crown. The root attachment length of 15mm determined the height of the PDL and bone bodies, with an additional 4mm of height for the tooth material representing the residual crown. The PDL width of 1mm could not be determined from post-extraction scans but was determined by a previous study on swine from the same source [31].

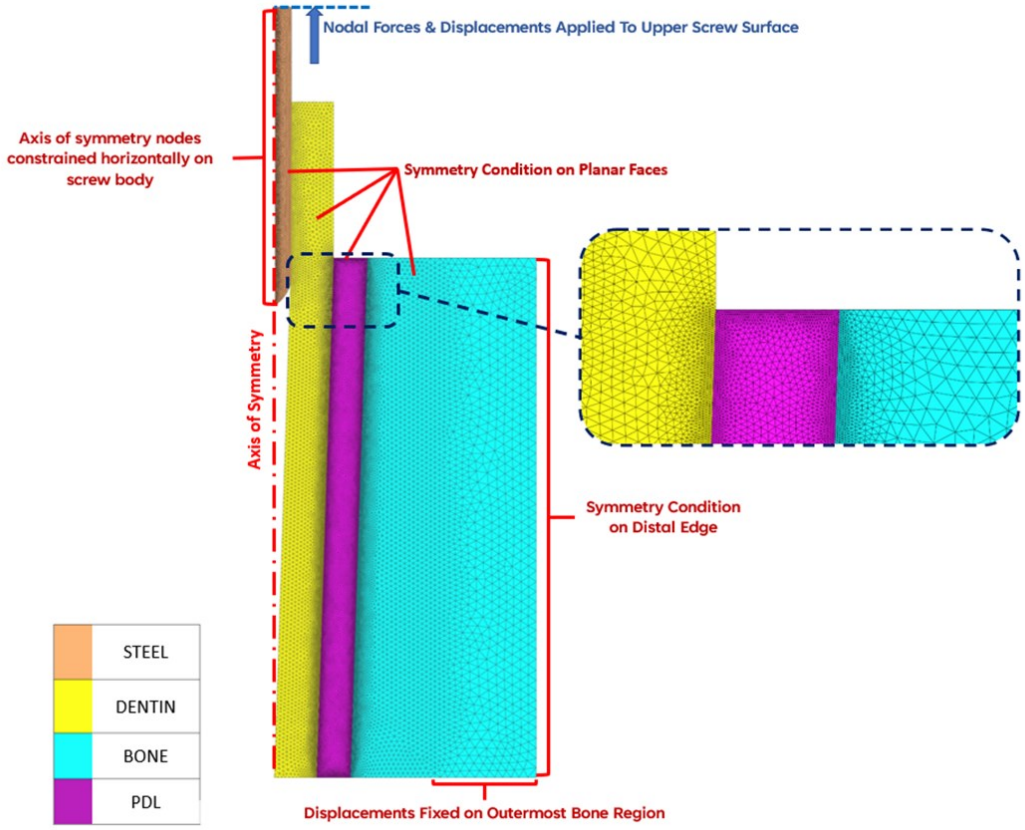

Figure 4-3: The generated mesh and axisymmetric boundary conditions. Inset: enlarged view of the mesh refinement at the borders of the PDL body (purple) with the tooth (yellow) and bone (cyan)

A 1mm screw diameter was modelled, neglecting the depth of threads and their contact with the tooth body. This simplification is appropriate for this modelling case as failed extractions such as those resulting from a root fracture initiating at the screw interface were omitted from inclusion in the study. For the axisymmetric case, alveolar bone plates and complex geometry in interdental spaces were not modelled. Instead, two large regions of bone were modelled: one 2.5mm wide representing the bone nearest the tooth root, and the second 3mm wide representing the interaction of tissues far from the tooth root. This simplification limits the study to only examining the behaviour of the PDL joint rather than the accumulation of damage and deformation in the entire alveolar complex.

4.2.3 Mesh

The model mesh was generated in SALOME 9.7 [32] using 4-node tetrahedral elements. The target mesh element sizes per body are given below in Table 1 with smaller mesh sizes used for the PDL, tooth, and nearby bone with larger mesh sizes further from this active area. The PDL boundary local refinement size of 0.02mm was determined through a mesh sensitivity investigation of the PDL boundary element size and its influence on overall peak force and time to peak force (Appendix D). This analysis examined the principal strain behaviour of elements in two locations and the simulation end time (at peak force) as variables sensitive to reductions in mesh size to the limit of the mesh solver stability. At an interface element size of 0.02mm (the lowest the solver could accommodate), the relative changes in principal strain and end time were less than 10%. The resulting number of elements per body were 20,385 (screw), 47,412 (tooth), 101,979 (PDL), and 70,926 (bone) for a total of 240,702.

Table 4-1: Target element size for the axisymmetric model

PDL Body	0.05mm	**PDL Boundaries (local refinement)**	0.02mm
Screw Body	0.05mm	**Tooth Body**	0.1mm
Near Bone Body	0.12mm	**Distant Bone Body**	0.2mm

Mesh nodes were shared across all material boundaries rather than implementing contact elements using the "weld" function in FEBio to share nodes between adjacent elements at the material boundaries. In this way, the bodies were modeled as a single continuous mesh with properties that varied by body (or material, e.g. steel). Local refinement was applied to all boundaries of the PDL because it was anticipated to be the highest-strain body. An example of the results of this refinement are demonstrated in Figure 3. The NETGEN 1D-2D-3D algorithm incorporated in SALOME was used to generate the mesh to these specifications without local curvature optimization, resulting in a mesh with 240,702 tetrahedral elements.

4.2.4 Boundary Conditions

The FEBio environment [33] was selected for this model because it is specifically formulated for large-deformation soft tissue models and includes viscoelastic and damage models for hyperelastic materials. Symmetry boundary conditions were applied to both sets of planar faces to enforce axisymmetry (Figure 4-3). Another symmetry condition was applied to the vertical

surface of the bone most distal to the axis of symmetry. The model was constrained by fixing the nodes in the distal bone at the inferior-most surface in all directions. The centre axis of the screw body lying along the axis of symmetry was also constrained in the two horizontal directions. Nodal displacements are applied to the uppermost surface of the screw body to load the model.

4.2.5 Material Models

The screw and hard tissues were modelled as linear elastic, homogeneous, and isotropic materials. Elastic moduli and Poison's ratios for steel (e.g. AISI 4140), dentin [16,25,26,30] and bone [16,25,26] are provided in Table 2. Both the dentin and bone material models employed a strain-based damage model with a threshold principal strain of 0.05. The selected damage strain is higher than those strains at which crack propagation or local fracture could be anticipated for hard tissues [34-36], but was assigned to provide "softening" of high-strain elements at tissue interfaces. This feature was applied to provide numerical stability in the place of contact elements between bodies, which demonstrated poor stability due to their near-parallel orientation to the direction of loading.

Table 4-2: Material properties for the isotropic Hookean materials included in the FE model

Screw (steel)	$\boldsymbol{E = 190\ GPa}$ $\boldsymbol{\nu = 0.30}$
Tooth (dentin)	$E = 18.6\ GPa$ $\nu = 0.31$ $\epsilon_{DAMAGE} = 0.05$
Bone	$E = 1.37\ GPa$ $\nu = 0.30$ $\epsilon_{DAMAGE} = 0.05$

The PDL was modeled as an uncoupled viscoelastic damage model in FEBio, which constructs a material model with three components: viscoelasticity, damage, and an underlying hyperelastic constitutive model. Viscoelasticity of the PDL tissue is a well-documented nonlinear phenomenon [13,17,19] and the rate-sensitivity of the dental complex has already been

demonstrated in the experimental data for the ex vivo swine model [14]. A quasi-linear viscoelastic (QLV) model is used to represent the viscoelasticity of the PDL in this model with a single relaxation constant and time g and τ for a Prony-series relaxation function. The QLV is a desirable model for simplifying the nonlinear viscoelasticity of the PDL so that it can be modeled alongside other complex phenomena [37] such as the hyperelastic and damage behaviour of the PDL and is an appropriate approximation for the continuously-increasing (e.g. non-cyclical) loading applied in this study:

$$G(t) = g_0 + g * \exp(-t/\tau) \qquad [1]$$

A damage model is included for the PDL in order to predict the rupture of the tissue necessary for tooth extraction. A quintic polynomial with strain-energy density (SED) criteria governs the damage variable D based on limits SED_min and SED_max using the quintic polynomial damage model in FEBio:

$$D(\psi) = \begin{cases} 0 & \psi \le SED_{min} \\ x^3(10 - 15x + 6x^2) & SED_{min} < \psi \le SED_{max} \\ 1 & SED_{max} < \psi \end{cases} \qquad [2a]$$

$$x = \frac{\psi - SED_{min}}{SED_{max} - SED_{min}} \qquad [2b]$$

The Arruda-Boyce model [37] was selected as the hyperelastic basis for the PDL because it employs a statistical representation of chain recruitment to model the behaviour of distributed fiber networks with only 3 parameters (initial modulus μ, chain number N, and bulk modulus k). This property allows the Arruda-Boyce model to represent the highly-variable structure of the PDL with a small set of parameters and has been demonstrated to be effective at representing similarly complex tissues [38-40]. The strain energy density function Ψ for this hyperelastic material is governed in FEBio by the 1st invariant of the Cauchy-Greent strain tensor I_1 and Jacobian J:

$$\Psi = \mu \sum_{i=1}^{5} \frac{C_i}{N^{i-1}} (I_1^i - 3^i) + \frac{1}{2} k (\ln J)^2 \qquad [3]$$

4.2.6 Setup of the inverse problem

The goal of solving the inverse FE analysis (IFEA) problem was to obtain material parameters for the PDL from multiple force-time curves simultaneously. The finite element model was loaded in a linear ramp to 50N at the experimental transition time determined in the preparation of the experimental data (Supplementary Material S1), beyond which it was loaded at the specified experimental scheme until rupture. The auto-time stepper in FEBio was allowed to make 40 reductions in time-step to resolve errors or rupture before terminating the solution.

The error function optimized for the IFEA problem is as follows:

$$\boldsymbol{Error} = \sum_{i=1}^{n}[(\boldsymbol{SSE_i}/\boldsymbol{10^5})\boldsymbol{\Delta t^2_{peak,\,i}}\boldsymbol{\Delta F^2_{peak,i}}] \qquad \textbf{[4]}$$

where SSE_i is the sum of squares error between curve i and the FEA response; Δt_(peak,i) is the difference between the FEA simulation endpoint and the endpoint of the ith curve; ΔF_(peak,i) is the difference between the force at the FEA simulation endpoint and the peak force of the ith experimental curve; and n is the number of experimental curves. A coefficient of 10-5 was included to help reduce the magnitude of the SSE values, which were un-normalized and thus very large due to the large number of points along each curve.

The error function was minimized using a bounded version of the Nelder-Mead algorithm in MATLAB [42]. Preliminary investigations found that the optimization error function discontinuities (introduced by truncating the force-time data to above 50N) and nonlinearities (due to the number of parameters and their interactions) were poorly suited to gradient-based optimization methods. The Nelder-Mead algorithm was found to be more robust to the nonlinearities of the selected optimization function but required the use of the additional algorithms to enforce the boundary conditions [42]. The GIBBON toolbox was used to interface the MATLAB algorithms with FEBio [43]. The seven material parameters that were optimized were for viscoelasticity (g and τ in Equation 1), damage (SED_max and SED_min in Equation 2b), and the Arruda-Boyce model (μ,N, and k in Equation 3). Each parameter used an initial guess from within the range of values present in the literature where available (Table 4-3). Bounds were set for physicality (e.g. preventing negative, non-physical values). Upper bounds were set for g and the SED limits to avoid non-physical values. The upper bound for SED_max was set to be approximately 5 times greater than the estimated total area under the curve of

available PDL models in the literature [15,18]. The upper bound for SED_min was set to the minimum of SED_max to avoid overlap. The upper limit for g was set to 1 to limit the dominance of viscoelasticity relative to the underlying hyperelastic model. The function tolerance for convergence was set to 1E-03 and the variable vector tolerance to 5E-04. All IFEA solution runs were performed on an Intel Xeon W-2245 processor with an available 256GB of RAM. However, up to three processes could be run simultaneously based on computational capacity and problem formulation.

Table 4-3 Initial guess and boundary values for the parameters included in the IFEA optimization

Parameter	g [n.u.]	τ [s]	μ [MPa]	N [n.u.]	k [MPa]	SED_{min} [mJ/mm³]	SED_{max} [mJ/mm³]
Initial Guess	**0.50**	**20**	**0.5**	**10**	**10**	**0.1**	**5**
Lower Bound	0.001	0.001	0.001	0.001	0.001	0.001	0.5
Upper Bound	1	∞	∞	∞	∞	0.5	10

4.3 Results

The resulting PDL parameters from each load case are demonstrated in Table 4.

Table 4-4:Resulting parameter values from the IFEA optimization for each load case and averaged across all cases

Parameter	0.2mm/min	2mm/min	Intermittent	Average
g [n.u.]	0.570	0.586	0.527	**0.561**
τ [s]	20.7	19.3	20.4	**20.1**
μ [MPa]	0.450	0.505	0.463	**0.472**
N [n.u.]	9.51	9.58	10.6	**9.90**
k [MPa]	10.2	9.70	9.63	**9.84**
SED_{min}	0.246	0.129	0.250	**0.208**
SED_{max}	5.86	5.71	6.20	**5.92**

PDL parameters show good agreement across all three independently-fit cases. Some parameters did not vary far from the initial guess which is understandable given that these values were estimated from a range of previously-published models [16, 25, 26]. A sensitivity analysis

(presented in Supplement S2) demonstrated that the FEA results are sensitive to local changes in these values and their interactions. The peak force and time at peak force demonstrated the greatest sensitivity to initial modulus μ, tending to change 1-3.5% with 10% variations around the IFEA solution. The solution was slightly less sensitive to N and k, with percent changes tending to be <3% over the 10% parameter variations except in the 2mm/min solution, which demonstrated up to 7% end point sensitivity. The sensitivity to g varied from no sensitivity for the intermittent case up to 3.5% sensitivity for the other cases.

The force-time response of the IFEA solutions fit well to the time-adjusted experimental data. Peak forces, times at peak force, and overall curve shape fall within the ranges defined by the experimental data (Figure 4-4). Relaxation during hold periods is evident in the intermittent-displacement case, matching well to the relaxation at low force levels but underestimating relaxation at higher forces. The coefficient-averaged solution performs similarly well for all three cases, including the intermittent case. There is a slight discrepancy between the endpoint of the intermittent displacement IFEA solution and coefficient-averaged solution, likely due to a reduction in SED_max from 6.20 to 5.92 between curves. However, both curves adequately predict peak force (within 5N of each other) and the overall time to peak force.

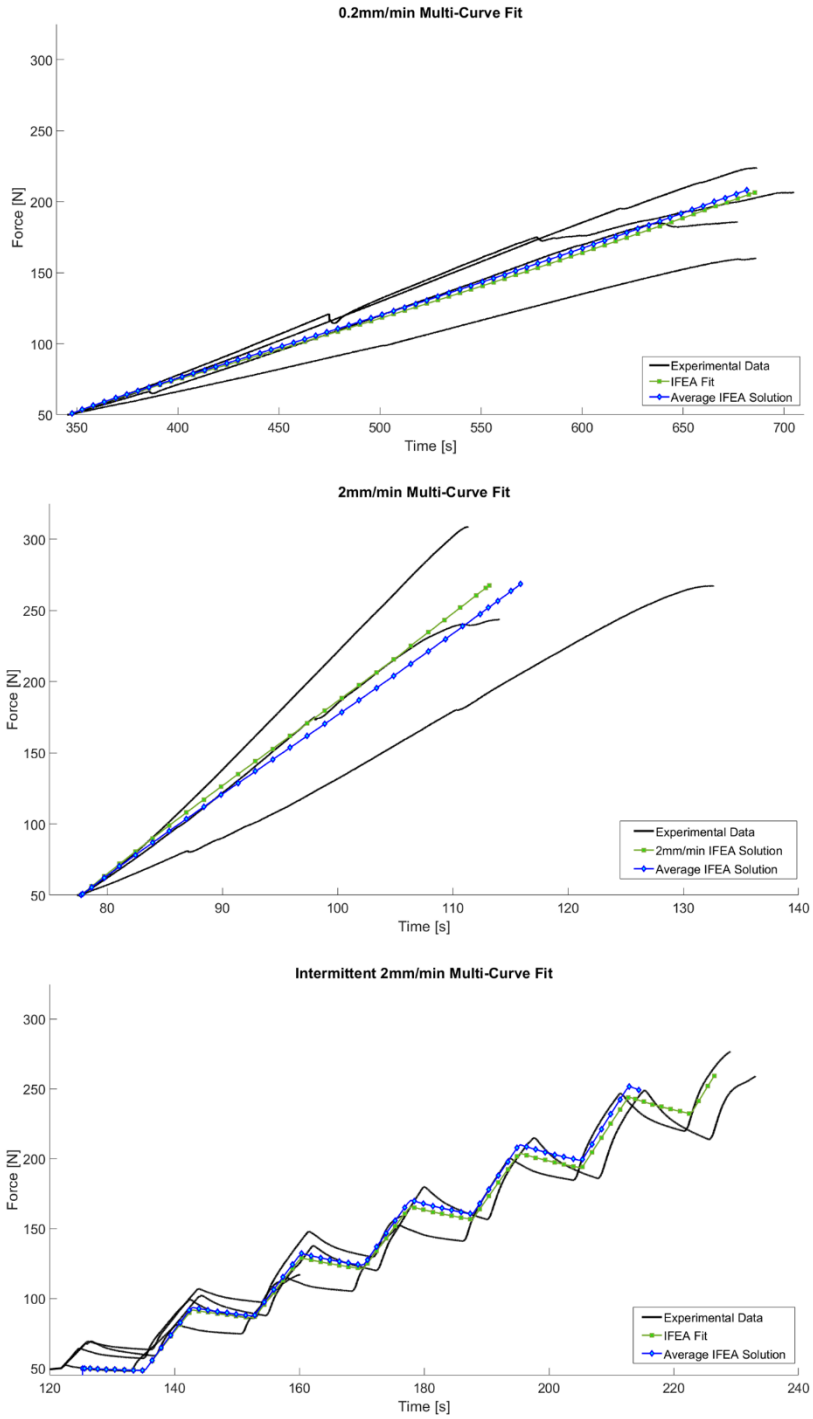

Figure 4-4: Force-time comparison of time-adjusted experimental data to IFEA solutions for each case (green) and the coefficient-averaged solution across all three cases (blue). Top: results for 0.2mm/min loading; Centre: results for 2mm/min loading; Bottom: results for 2mm/min intermittent loading

Examining the element behaviour of the PDL body confirms that the damage and rupture of this tissue govern the peak force response of the FEA model. Strain evolves throughout the loading of the dental complex in the PDL body (Figure 4-5), beginning with localisation at the proximal-occlusal corner nearest the tooth and threaded insert. As these strains evolve the elements are damaged and a rupture front forms which rapidly ends the simulation. In all cases this rupture behaviour causes the simulation to abort as the tooth body becomes completely detached from the PDL and results in the peak force predictions presented in Figure 4-4.

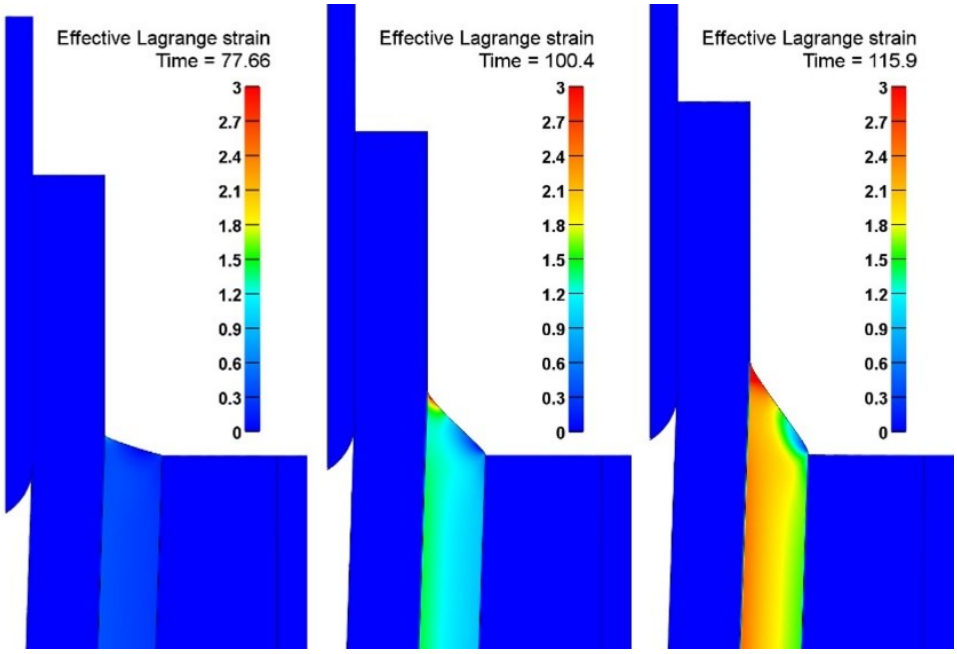

Figure 4-5:Evolution of effective Lagrange strain in the occlusal PDL during loading at 2mm/min. Left: Lagrange strain at 50N transition point; Centre: strain field during loading; Right: strain field immediately before element failure ending the simulation

4.4 Discussion

The purpose of this study was to develop an axisymmetric FE representation of an experimental swine incisor model to study the biomechanics of vertical tooth extraction. The goals of the study pursuant to this purpose were to represent a generalized geometry and material models for the dental complex and determine material parameters for the PDL using groups of experimental data. This model will be used to predict and design new experimental loading schemes that can be further investigated for implementation towards biomechanically-validated practices in atraumatic tooth extraction. Towards this intended purpose, the model was trained on, and is intended to predict, the behaviour of an ex vivo swine experimental model and the interpretation

of the results towards extractions in human should be approached with caution, The ex vivo swine model is a necessary preclinical step required before introducing new extraction loading practices to the clinic. This model in particular is a predictive tool that will allow for the in silico testing of new load schemes (e.g. using a stiffness or force-limited adaptive control scheme) using the Benex® device in the swine model, which has been developed previously as a pre-clinical method for investigating the biomechanics of single-rooted, low-curvature tooth roots during extraction [14].

The PDL parameters resulting from the IFEA optimization and corresponding force-time responses suggest that the axisymmetric model can represent the dental complex for the purposes of studying vertical tooth extraction biomechanics. The force-time FEA curves fit the experimental data well in terms of both curve shape and prediction of peak force (Figure 4-4). Additionally, internal parameters such as strain evolution in the PDL follow patterns that may be reasonably expected given the loading and model geometry (Figure 4-5). There is good agreement between the IFEA solution and experimental data in the amount of relaxation that occurs at low force levels in the intermittent displacement solution, but the relaxation at higher force levels is underestimated. This is a limitation of the single-term quasi-linear viscoelastic model that may be addressed by the addition of a nonlinear viscoelastic model or more quasi-linear terms. However, the sensitivity of the IFEA solution endpoint to the material parameters indicates that including the Δ terms to peak force and time at peak force are appropriate. A limitation of the multi-curve method is that it is difficult to quantify the agreement between all curves and the IFEA solutions simultaneously outside the optimized error function values. However, the solution parameter sets presented in this study results in the lowest error values across different initial guesses.

There is a notable difference between the IFEA solution behaviour at peak load and the experimental data. The experimental data contains information regarding the decay of force during removal of the tooth that is removed during pre-processing (Supplement S1). The finite element simulation ends at peak force, as the formation of a rupture front causes the force sustained by the structure to drop rapidly to zero. This is a common limitation for visco-hyperelastic damage models that model the complete rupture of a tissue and is demonstrated in other attempts to model tooth extraction [29]. This behaviour is a limitation of the implicit

dynamics solver used in FEBio and may be improved through explicit dynamics and further stability controls.

The similarity of PDL parameters across independently-fit load cases suggest that the parameters are physically representative and can be used in further predictive studies. This is a critical aspect of the model's performance and is promising for its application as a predictive tool representing the actual dental complex response outside the three test cases used to identify the PDL parameters. The agreement between the coefficient-averaged solution and ranges of experimental data further demonstrate this principle. The slight discrepancy between the IFEA and coefficient-averaged solution endpoints in the intermittent displacement case are understandable, as damage-limiting strain energy is reduced by approximately 5% between cases and strongly determines the endpoint of the simulation. This difference is a limitation of the study but based on the commonality among cases. It is anticipated that increasing the number of fit curves in each load group will improve the predictive performance of a coefficient-averaged solution. Future work will seek to demonstrate this improvement as more extraction data becomes available but the ability to predict multiple instances of tooth extraction data across load schemes remains one of the strengths of this study. The predictive ability of the physically-representative model derived with this approach will also be investigated.

There are a number of numerical models potentially suitable for modelling tooth extraction via the rupture of the PDL but they vary in formulations in such a way that meaningful comparison to the presented study is challenging. Direct comparison to the micromechanical interface elements in previous work [29] is impractical because their model parameters are constructed directly from the measured properties of collagen rather than homogeneous continuum properties representing the overall tissue. However, the presented axisymmetric model predicts the rising-force behaviour at 2mm/min with similar efficacy to the previous study and demonstrates the same rapid decay in force following peak force prediction [29]. The low computational intensity of the axisymmetric model developed in this study allowed its validation against three different loading schemes whereas the previous work [29] neglects the rate-dependency of the dental complex's behaviour. The other models developed from small sample testing employ small modulus values from 4 kPa to 30 kPa [21,23] but both are multi-phase coupled models that represent fibre and ground substance recruitment very differently from the uncoupled Arruda-

Boyce model presented in this study. In general, however, modulus values for the PDL from the broader literature range from several kPa to 100 MPa [19], which certainly accommodates the initial modulus value of 0.47 MPa determined in this study. Similarly, the range of viscoelastic constants (0.005 to 0.91) and relaxation times (0.0025 s to 583 s) available in similar models of the PDL [23,26] also accommodate the values determined in this study. Differences in experimental model, constitutive model, and loading type must be accounted for but the parameter values determined in this study agree with other models overall where such comparison is possible.

The axisymmetric model proposed in this study is also an improvement on the current state of the art in tooth extraction modelling in that it has relatively low computational requirements and functions in an open-source environment. For example, the subject-specific model proposed by Genna and Paganelli reportedly required 3 hours for a functional evaluation [29]. A single evaluation of the axisymmetric model proposed in this study ranged from 20-45 minutes, allowing the large number of functional evaluations necessary for the IFEA process. Other high-fidelity numerical models suitable for studying tooth extraction use ABAQUS or other paid-license software with customized code [29,21], the replication of which poses a formidable challenge where at all possible. Although the IFEA process presented in this study requires a MATLAB license, the model can be implemented in FEBio with no additional plugins or custom code. Additionally, this model uses a generalized geometry rather than computationally-intensive subject specific models.

The generalized geometry employed in the axisymmetric model presents some limitations for the interpretation of the model results. The distributions of stress and strain in the generalized bodies, especially the large regions of bone, should be interpreted carefully because there may be features that influence how these bodies deform away from the PDL joint. Specifically, the shape of the alveolar plates is neglected and modeled as a continuous volume and the thread geometry and interface of the Benex® screw is simplified. Both features would limit the application of the axisymmetric assumption to the model and would be important to applying the model to predict fracture in the hard tissues of the dental complex. However, the presented model is fit only to data taken from successful experimental extractions and would require further development of the hard tissue models and geometries to be appropriate for modeling these phenomena.

Additional future work based on the presented model will investigate the parameterization of the model geometry to capture simple geometric variations between cases (e.g. adjusting the overall tooth root length and diameter) and the development of subject-specific models that capture the contributions of (and damage to) all tissues in the dental complex. However, both of these extended proposals detract from the predictive purpose of the presented model because they require imaging of specific teeth. Such models cannot be used to predict the response of a new load scheme for a broad range of specimens, which is the purpose of the model developed here. Future work will investigate these generalized predictive capabilities of this model for its application in designing clinical devices and procedures.

In addition to geometric limitations, the generalized material models employed for the tooth root and bone limit the ability of this model to assess tissue damage resulting from the extraction process. The strain-governed damage model was implemented to simulate compliance of the interfaces (entheses) between the PDL and the hard tissues. This model for the entheses was necessary because of the poor performance of contact elements at these surfaces and is physically realistic in concept (that strain at the fibrous, lamellar interfaces will result in damage and softening of the tissues) but is not appropriate for crack propagation through the tissue. Future work may investigate applying more complex models of the hard tissues (such as those that account for structural anisotropy, crack propagation, and fluid phase movement) to better model the different forms of damage accumulation in the tooth and bone. Such a model would necessarily capture the heterogeneity of tissues in subject-specific geometries which limit the predictive usefulness of the model as discussed above and limit the applicability of the axisymmetric assumptions.

4.5 Conclusion

This study presents an axisymmetric model of the swine dental complex during vertical tooth extraction. The axisymmetric model employs a combination of isotropic Hookean models, strain- and strain energy density-governed damage models, and a visco-hyperelastic model for the PDL to simulate the mechanical response of the dental complex to extraction load. Parameters for the PDL model were determined by solving an inverse finite element problem independently for three displacement-controlled extraction schemes. The key outcome of this study is the resulting material parameters, which reflect the physically-representative nature of the developed model in

the similarity in magnitudes across the three fit cases. A coefficient-averaged solution across the three cases predicts both the force-time curve shape and peak force in all three of the source cases, critically demonstrating that the similarity is a characteristic of the model's representation of the underlying biomechanical system rather than a numerical artefact of optimization. The proposed axisymmetric model using these material parameters represents an advancement in the replicability and accessibility of finite element models for tooth extraction. Although this model was developed to represent a specific ex vivo preclinical case, it will be applied in future work developing vertical extraction procedures in iterative design processes. Using the proposed FE model in place of intensive subject-specific models will reduce the computational and financial costs of preclinical testing of new loading procedures.

References

1. Broers DLM, Dubois L, de Lange J, Su N, and de Jongh A. Reasons for tooth removal in adults. Int Dent J. 2021;72(2022):52-57.
2. Schneider C, Zemp E, Zitzmann NU. Dental care behaviour in Switzerland. Swiss Dent J. 2019;129(6):466-478.
3. Cunha MAGM, Lino PA, Santos TRD, Vasconcelos M, Lucas SD, Abreu MHNG. A 15-Year Time-series Study of Tooth Extraction in Brazil. Medicine (Baltimore). 2015;94(47):e1924. doi: 10.1097/MD.0000000000001924.
4. Murray H, Locker D, Kay EJ. Patterns of and reasons for tooth extractions in general dental practice in Ontario, Canada. Community Dent Oral Epidemiol. 1996;24(3):196-200. doi: 10.1111/j.1600-0528.1996.tb00841.x.
5. Broers DLM, Dubois L, de Lange J, Brands WG, Lagas MBD, et al. How dentists and oral and maxillofacial surgeons deal with tooth extraction without a valid clinical indication. PLoS ONE. 2023;18(1):1-10. doi: 10.1371/journal.pone.0280288
6. Hiltunen K, Vehkalahti MM. Why and when older people lose their teeth: A study of public healthcare patients aged 60 years and over in 2007-2015. Gerodontology. 2023; 40: 326-333. doi: 10.1111/ger.12657
7. Dym H, Weiss A. Exodontia: tips and techniques for better outcomes. Dent Clin North Am. 2012;56(1):245-66. doi: 2010.1016/j.cden.2011.07.002.
8. Papadimitriou DEV, Geminiani A, Zahavi T, Ercoli C. Sonosurgery for atraumatic tooth extraction: a clinical report. J Prosthet Dent. 2012;108:339-343
9. Sharma SD, Vidya B, Alexander M, Deshmukh S. Periotome as an aid to atraumatic extraction: a comparative double blind randomized controlled trial. J Maxillofac Oral Surg. 2015;14(3):611-615.
10. Hariharan S, Narayanan V, Soh CL. Split-mouth comparison of physics forceps and extraction forceps in orthodontic extraction of upper premolars. Br J Oral Maxillofac Surg. 2014;52(10):e137-40. doi: 10.1016/j.bjoms.2014.06.013.
11. Muska E, Walter C, Knight A, Taneja P, Bulsara Y, Hahn M, Desai M, Dietrich T. Atraumatic vertical tooth extraction: a proof of principle clinical study of a novel system. Oral Surg Oral Med Oral Pathol Oral Radiol. 2013;116(5):e303-10. doi: 10.1016/j.oooo.2011.11.037.

12. Dietrich T, Schmid I, Locher M, Addison O. Extraction force and its determinants for minimally invasive vertical tooth extraction. J Mech Behav Biomed Mater. 2020;105:103711. doi: 10.1016/j.jmbbm.2020.103711.
13. Fill TS, Carey JP, Toogood RW, Major PW. Experimentally determined mechanical properties of, and models for, the periodontal ligament: critical review of current literature. Journal Dent Biomech. 2011:312980. doi:10.4061/2011/312980
14. Gadzella TJ, Hynkova K, Westover L, Addison O, Romanyk DL. A novel method for simulating ex vivo tooth extractions under varying applied loads. J Clin Biomech. 2023;110:106116. https://doi.org/10.1016/j.clinbiomech.2023.106116.
15. Genna F, Annovazzi L, Bonesi C, Fogazzi P, Paganelli C. On the experimental determination of some mechanical properties of porcine periodontal ligament. Meccanica. 2008; 43:55-73. doi: 10.1007/s11012-007-9094-2.
16. Karimi Dastgerdi A, Rouhi G, Dehghan MM, Farzad Mohajeri S, and Barikani HR. Linear momenta transferred to the dental implant-bone and natural tooth-PDL-bone contstructs under impact loading: a comparative in-vitro and in-silico study. Front. Bioeng. Biotechnol. 2020;8:54. doi: 10.3389/fbioe.2020.00544.
17. Ovy EG, Romanyk DL, Flores Mir C, Westover L. Modelling and evaluating periodontal ligament mechanical behaviour and properties: A scoping review of current approaches and limitations. Orthod Craniofac Res. 2022;25(2):199-211. doi: 10.1111/ocr.12527.
18. Toms SR, Dakin GJ, Lemons JE, Eberhardt AW. Quasi-linear viscoelastic behaviour of the human periodontal ligament. J Biomech. 2002; 35(10):1411-1415. doi: 10.1016/S0021-9290(02)00166-5.
19. Fill TS, Toogood RW, Major PW, Carey JP. Analytically determined mechanical properties of, and models for the periodontal ligament: critical review of literature. J Biomech. 2012;45(1):9-16. doi: 10.1016/j.jbiomech.2022.09.020
20. Gei M, Genna F, Bigno D. An interface model for the periodontal ligament. J Biomech Eng. 2002;124:538-546. doi: 10.1115/1.1502664.
21. Ortún-Terrazas J, Cegoñino J, Santana-Penín U, Santana-Mora U, Pérez Del Palomar A. A porous fibrous hyperelastic damage model for human periodontal ligament: Application of a microcomputerized tomography finite element model. Int J Numer Method Biomed Eng. 2019 Apr;35(4):e3176. doi: 10.1002/cnm.3176.

22. Ortún-Terrazas J, Cegoñino J, Pérez Del Palomar A. In silico study of cuspid' periodontal ligament damage under parafunctional and traumatic conditions of whole-mouth occlusions. A patient-specific evaluation. Comput Methods Programs Biomed. 2020 Feb;184:105107. doi: 10.1016/j.cmpb.2019.105107.
23. Natali AN, Carniel EL, Pavan PG, Sander FG, Dorow C, Geiger M. A visco-hyperelastic-damage constitutive model for the analysis of the biomechanical response of the periodontal ligament. J Biomech Eng. 2008 Jun;130(3):031004. doi: 10.1115/1.2900415.
24. Cicciù M, Cervino G, Milone D, Risitano G. FEM Investigation of the Stress Distribution over Mandibular Bone Due to Screwed Overdenture Positioned on Dental Implants. Materials (Basel). 2018;11(9):1512. doi: 10.3390/ma11091512
25. Rao S, Arora H, Hameed S. A Three dimensional Finite Element Analysis of Stress Distribution in the Cortical Bone in Single Tooth Implant and Post Core-treated Tooth subjected to variable Loads. Int J Prosthodont Restor Dent 2017;7(1):8-16.
26. Su, K., Yuan, L., Yang, J. et al. Numerical Simulation of Mandible Bone Remodeling under Tooth Loading: A Parametric Study. Sci Rep. 2019;9:14887. doi: 10.1038/s41598-019-51429-w
27. Tuna M, Sunbuloglu E, Bozdag E. Finite element simulation of the behavior of the periodontal ligament: a validated nonlinear contact model. J Biomech. 2014;47(12):2883-90. doi: 10.1016/j.jbiomech.2014.07.023
28. Karimi A, Razaghi R, Biglari H, Rahmati SM, Sandbothe A, Hasani M. Finite element modeling of the periodontal ligament under a realistic kinetic loading of the jaw system. The Saudi Dental Journal. 2020 Nov 1;32(7):349-56
29. Genna F, Paganelli C. Force–displacement relationship in the extraction of a porcine tooth from its socket: experiments and numerical simulations. Journal Mech Mat Struct. 2014;9(5):497-514.
30. Dezzen-Gomide AC, de Carvalho MA, Lazari-Carvalho PC, de Oliveira HF, Cury AADB, Yamamoto-Silva FP, Silva BSF. A three-dimensional finite element analysis of permanent maxillary central incisors in different stages of root development and trauma settings. Comput Methods Programs Biomed. 2021;207:106195. doi: 10.1016/j.cmpb.2021.106195.

31. Houg KP, Camarillo AM, Doschak MR, Major PW, Popwics T, Dennison Cr, Romanyk DL. Strain Measurement within an Intact Swine Periodontal Ligament. Journal of Dental Research. 2022;101(12):1474-1480. doi: 10.1177/00220345221100234
32. CEA, EDF, Open Cascade. SALOME 9 (Version 9.7). Issy-le-Moulineaux : Open Cascade. (2024). [Accessed June 24, 2020]. Retrieved from salome-platform.org.
33. Maas SA, Ellis BJ, Ateshian GA, Weiss JA: FEBio: Finite Elements for Biomechanics. J Biomech Eng. 2012;134(1):011005
34. An B, Zhang D. An analysis of crack growth in dentin at the microstructural scale. Mech Behav Biomed Mater. 2018; 81:149-160
35. Korabi, R., Shemtov-Yona, K., Dorogoy, A. Rittel D. The Failure Envelope Concept Applied To The Bone-Dental Implant System. Sci Rep. 2017;7:2051. doi: 10.1038/s41598-017-02282-2
36. Salem M, Westover L, Adeeb S, Duke K. An Equivalent Constitutive Model of Cancellous Bone With Fracture Prediction. J Biomech Eng. 2020; 142(12):121004. doi: 10.1115/1.4047080
37. Puso MA, Weiss JA: Finite element implementation of anisotropic quasi-linear viscoelasticity using a discrete spectrum approximation. Journal of Biomechanical Engineering, 120(1):62-70, 1998.
38. Arruda, EM and Boyce, MC. A three-dimensional constitutive model for the large stretch behaviour of rubber elastic materials. J Mech Phys Solid. 1993; 41(2):389-412. doi: 10.1016/0022-5096(93)90013-6
39. Sangpradit K, Liu H, Dasgupta P, Althoefer K, Seneviratne LD. Finite-Element Modeling of Soft Tissue Rolling Indentation. IEEE Transactions on Biomedical Engineering. 2011; 58(12):3319-3327. doi: 10.1109/TBME.2011.2106783.
40. Liu Y, Kerdok AE, Howe RD. A nonlinear finite element model of soft tissue indentation. International symposium on medical simulation. 2004 Jun 17; 67-76. Berlin, Heidelberg: Springer Berlin Heidelberg.
41. Marchesseau S, Tobias Heimann T, Chatelin S, Willinger R , Delingette H. Fast porous visco-hyperelastic soft tissue model for surgery simulation: Application to liver surgery. Progress in Biophysics and Molecular Biology. 2010; 103(2–3):185-196. doi: 10.1016/j.pbiomolbio.2010.09.005.

42. D'Errico, J. fminsearchbnd, fminsearchcon (), MATLAB Central File Exchange (2023). Available from: https://www.mathworks.com/matlabcentral/fileexchange/8277-fminsearchbnd-fminsearchcon
43. Moerman, KM. GIBBON: The Geometry and Image-Based Bioengineering Add-On. J Open Source Softw. 2018;3(22):506. doi: 10.21105/joss.00506

5 Characterisation of Vertical Tooth Extraction Mechanics and Prediction of Force-Hold and Damaged Loading Scenarios

In this chapter, both the numerical and experimental methods described in Chapters 3 & 4 are applied to the biomechanical characterisation of the dental complex during extraction load. The application of these methods, with additional statistical and imaging techniques, is demonstrated towards fulfilling Objectives 1 & 2 of this thesis. Additional simulations are performed using the developed axisymmetric model towards predicting the biomechanics of force-hold loading with intact and damaged PDL states, demonstrating the capabilities of the model as a procedural design tool and validating its findings by re-applying the experimental method and comparing the results. This investigation leads towards the fulfilment of Objective 3 and provides the basis for interface development in Chapter 6.

5.1 Introduction

Tooth extraction is among the most common procedures in dental medicine with a range causes and indications (e.g. tooth decay) [1-5]. Despite its importance to clinical practice, there is very little literature available characterising the biomechanics of tooth extraction in clinical [6-9], numerical [10-11], or experimental laboratory models [12-13]. The scarcity of biomechanical data contrasts with growing interest in atraumatic tooth extraction, a family of techniques that alter application of load to the extracted tooth to reduce the damage caused to the remaining bone and gingival tissue. Techniques for atraumatic extraction include the sectioning of teeth with piezoelectric or air-driven tools [14-16]; severing the periodontal ligament (PDL) with elevators, luxators, or periotomes [14-21]; or application of novel loading devices such as Physics forceps [18, 23-25] or the Benex® vertical tooth extraction device [9,15,22]. Biomechanical data describing the forces or displacements applied in these studies is rarely collected despite the biomechanical nature of each technique's departure from conventional extraction, either in the mechanism by which loading is applied to the dental complex or the damage induced in the dental complex to assist in retrieval of the tooth root. The metrics by which these techniques are commonly assessed are clinical in nature, and include measures such as socket depth or gingival rupture size [14,17,20-25], self-reported pain [20-25], or procedure time [15, 21, 23-25]. It is less common for alveolar bone resorption [16-17] or cellular response [14, 22, 26] to be measured following tooth extraction, although these metrics could most closely be associated with differences in biomechanical load based on the hypothesis that the loading nature determines the extent of the damage and subsequent resorption response.

The lack of congruency among biomechanical measurement and clinical outcomes is associated with the technically difficulty of collecting biomechanical data in clinical models of tooth extraction. Traditional forceps are difficult to instrument and limit the amount of data that can be gathered measuring the forces applied to the dental complex during traditional tooth extraction. Methods such as attaching airbags [6,7] or strain gauges [8] to forceps can distinguish between grip pressure and rotational moment, but do not provide directional data needed to understand how the force interacts with the dental complex. This information is critical to understanding the extraction behaviour of the dental complex because it dictates the distribution of load throughout the dental complex, determining factors such as the location of PDL rupture, tooth fracture, and bone damage. For example, the study by Ahel and colleagues [7] characterized moments in

different axes applied at forceps grips. The load induced in the tissues of the dental complex depends greatly on both the forceps geometry and the forceps location relative to the tooth's centre of rotation as both bodies behave as moment arms transforming the forces applied by the clinician. Neither geometry was characterized. Vertical tooth extraction with the Benex device affords an opportunity to overcome such limitations because the only force intentionally applied to the tooth root is along its long axis and the configuration of the device's components facilitates the inclusion of a load cell that can measure the extraction force [9]. However, current extraction procedures are guided through a combination of haptic feedback mechanisms and clinician discretion [27] because of lacking biomechanical data related to clinical outcomes that may inform procedures in real time. It is generally stated that the alveolar ridge is preserved as much as possible without describing exactly how this is achieved with the application of conventional forceps [17], loading a tooth until "significant resistance" is met with a Benex® device [9], or forces that are "slow and steady… until the tooth becomes loose" with Physics forceps [18]. Although the effectiveness of these atraumatic techniques has been studied on the basis of clinical outcomes [18, 20-22], a link to foundational descriptive biomechanical data prevents further improvements to protocols and devices.

Laboratory-based experimental methods for simulating tooth extraction in ex vivo animal models are promising for providing insight into extraction biomechanics but are scarce. Experimental models for characterising biomechanics in the dental complex tend to focus on the mechanical behaviour of the periodontal ligament (PDL) in small, isolated tissue sections in uniaxial loading regimes to inform constitutive models [27-41]. The entire dental complex response has also been examined in occlusal-apical or buccal-lingual loading directions to replicate physiological or orthodontic loading [42-47]. Few experimental models focus on the load directions and displacement magnitudes required to characterize tooth extraction. Models of tooth extraction on the complete dental complex [10,12-13,47-48] predominantly consider vertical tooth extraction because the loading vectors are known but have been limited in the range of load regimes studied [11,47-48], sample size [12], and applicability to the human clinical model [13]. Recent experimental work has sought to improve on laboratory-based experimental methods for mounting ex vivo swine samples in testing apparati by introducing self-aligning motion elements to reduce off-axis forces acting on the tooth root [12]. In general, these experiments are limited in their capacity to characterize the tooth geometry and its influence on the complex response as

well as the mechanisms of tissue rupture underlying the overall dental complex response. Post hoc analyses of residual PDL have been performed in clinical models to examine cell viability for re-implantation [49] and bone resorption [50], but the rupture behaviours of the PDL have not been assessed alongside a rigorous characterization of their underlying extraction mechanics.

The scarcity of biomechanical data drives limitations in numerical models that characterize the dental complex for understanding tooth extraction. Reflecting the nature of the collected experimental data, numerical models of the dental complex tend to model orthodontic [51-55] or physiological [56-64] processes, which share little in loading direction and magnitude with the forces applied during tooth extraction (such as 400N compressive/intrusive masticatory loads [60] or 0.5N - 3N mesial-distal/transverse orthodontic loads [53] vs. up to 620N extensive/extrusive loading for vertical tooth extraction [9]). Models that are suitable for understanding tooth extraction include high-strain formulations that account for tissue viscoelasticity and damage in the PDL [10, 65-66]. However, these models suffer from high computational costs due to their reliance on subject-specific mesh generation and the application of custom solver code and material subroutines. These computational costs make these models difficult to use as generalized tools for studying tooth extraction procedures in a broader population. Recently, an axisymmetric model was proposed with PDL parameters fit to pilot data collected at three different loading regimes [11] and demonstrated that a shared solution among three different displacement-controlled load groups performed well at explaining the experimental data. Although this model is promising as a low-computational-cost alternative for modelling tooth extraction, it is also limited by a sparse supporting data set. Robustly validated, accessible, and appropriate numerical models continue to be elusive but are critical tools for the future development of atraumatic extraction technologies and techniques.

The current study addresses the limitations of experimental and numerical characterisation of tooth extraction by extending the findings of previous studies in extraction biomechanics with new methods and towards new lines of inquiry. The addition of new data characterising the dental complex under extraction load provides the opportunity for more thorough characterization of the interactions between loading rate and tooth geometry, and to image the post-extraction PDL to gain new insight into its role in tooth extraction biomechanics. This improved data also allows for improved validation of PDL parameters in a generalized

axisymmetric model of the dental complex than is offered in previous research [11]. These improved characterizations are then applied to study two new factors in tooth extraction. First, the prediction of dental complex behaviour under a force-controlled loading to a threshold force which is then maintained ("force-hold loading") is demonstrated as an application of the generalizable numerical model as a design tool for a new procedure based on the findings of the mechanical experiments. Second, the model is used to predict the behaviour of the dental complex under force-hold loading with imposed PDL damage, which has been the basis for many atraumatic extraction techniques but the biomechanical effect of which has never been rigorously studied. The purpose of this combined approach is to provide a robust characterisation of the dental complex response to extraction load with demonstrated applications in the predictive modelling of different extraction scenarios.

5.2 Methods

5.2.1 Mechanical Tooth Extraction Experiments

The general approach to mechanically testing ex vivo samples under simulated vertical tooth extraction and design of the experimental device has been presented and validated in a previous study [12]. Briefly, the mandibles of juvenile swine were acquired under a secondary-use exemption provided by the University of Alberta Research Ethics Office (REO Reference No. ETR65) and cut ex vivo to isolate the central incisors at an approximate root length of 15mm. Samples were then potted in dental stone and attached to a custom self-aligning apparatus within a material test frame (Instron E3000, Instron, Norwood, USA). Both central incisors from each specimen were extracted under various load rates and schemes to observe the effects of different loading on extraction mechanics. The current study duplicated the experimental design of the previous pilot study [12], but doubling the sample size per group to n=10 by completing an additional 25 experimental extractions for a total of 50. The tested load schemes were continuous displacement control at 0.2mm/min and 2mm/min, continuous force control at 10N/min and 100N/min, and intermittent displacement control at 2mm/min with displacement-held dwell periods. Extractions were determined to be successful if the incisor was removed from the socket without visually recognizable fracture to the tooth or surrounding bone.

The video-assisted stiffness analysis from previous work [12] was repeated using load-displacement data from all successful continuous-loading extractions with video tracking in the

pool of 49 attempts [12]. The video analysis aided in isolating periods of self-alignment from tissue extension in the crosshead-measured force and displacement curves. These curves were used to calculate the instantaneous stiffness through the loading periods of each extraction. Instantaneous stiffness curves were input to a K-means algorithm in MATLAB to identify clusters in the stiffness data based on stiffness magnitude and curve shape. In doing so, the K-means algorithm presented patterns in the instantaneous stiffness while being blinded to the underlying load regime. The probability of a stiffness curve from an extraction at a given load rate being sorted into each curve was calculated after the K-means algorithm to assess if the patterns driving the cluster sorting corresponded to the loading rate and control scheme. The robustness of this method for sorting stiffness curves and their relationship to the underlying load rate is further detailed in Appendix E.

5.2.1.1 Post-Extraction Imaging of Tooth Surfaces and Residual PDL

Post-extraction images of the incisors were gathered to allow for the accurate measurement of tooth root surface attachment area (RSAA) as a metric describing tooth geometry. Contrast-enhanced (CE) images were also collected for some teeth to provide 3D representations of the residual PDL that were examined for patterns or features that may relate to the mechanics of the PDL rupture behaviour. Teeth from all successful extractions in the continuous-loading and intermittent displacement cases were scanned with x-ray microcomputed tomography (μCT) at a nominal resolution of 9 micron following extraction. All images were obtained in a Skyscan 1076 CT scanner with a 1mm aluminum filter at 90kV and 100μA of source voltage and current, respectively. All scans were reconstructed in the Skyscan NRecon v1.6 software with default levels of ring artefact, beam hardening, and smoothing corrections. 21 incisors from the original pilot study were imaged with a contrast-enhanced μCT protocol (CE- μCT) whereby incisors were fixed in 10% buffered formalin and then stained in a 10% by-weight solution of mercury chloride in water for 24 hours prior to imaging. The remaining 20 incisors were imaged at the same resolution but were only fixed in formalin prior to imaging.

Reconstructed μCT image stacks were cropped in FIJI ImageJ to exclude the volume surrounding the sample tubes in which the teeth were imaged and thereby reduce memory load before being imported to Materialise Mimics (Version 25, Materialise, Leuven, Belgium) for segmentation and analysis. Images were segmented semi-automatically using the region grow

algorithm to capture the outer geometry of the tooth's hard tissue surface. Three-dimensional open and close morphological operations were performed with 26-voxel connectivity to smooth the masks. Slice editing with interpolation was performed by hand where needed to improve the coverage of the segmentation masks where the region-growth algorithm had caused the masks to overlap at tissue boundaries or include small, disconnected bodies due to noise. This procedure was also applied to capture the geometry of the soft tissue in the CE-μCT scans.

Three-dimensional bodies were generated from the segmentation in MIMICS and were exported to 3-Matic (Version 17, Materialise, Leuven, Belgium) for RSAA measurement and examination of PDL rupture patterns. The freehand triangle selection tool was used to select the entire surface of the tooth below the boundary of PDL attachment. The resulting surface was exported to a separate part, the surface area of which was taken to be the root surface attachment area (RSAA) for that tooth. Soft tissue bodies from CE-μCT scans were examined to qualitatively identify patterns in the PDL rupture behaviour across the full set of extracted teeth. No comparisons of soft tissue behaviour were made between groups.

5.2.1.2 Statistical Analysis of Peak Forces

Peak force data from successful extractions in the continuous-loading and intermittent displacement loading cases were normalized by the RSAA obtained with CT imaging and examined for significant differences among groups using a Kruskall-Wallis test in MATLAB with a Tukey's Honestly Significant Difference post-hoc test. In order to further investigate the relationship between RSAA and peak extraction force, mixed linear models were fit to the peak force, load scheme group, and RSAA data in MATLAB. This modelling method allowed the introduction of random and covariate effects to the ordinal load group data, facilitating a quantitative assessment of the influence of RSAA on peak extraction force while accounting for differences between load schemes. Pairwise comparison of these models with the "lmmodelcompare()" MATLAB command using different combinations of omitted and included terms allowed for the isolation of the most likely effective model. For example, the evolution of the models compared for peak extraction force based on simulated follows in Eq. 1:

$$Peak\ Force = C + \sum \mathrm{B}_i X_{Codified\ Group} + \gamma * RSAA + Zu_{RSAA} + \epsilon \qquad \text{Eq. 1a}$$

$$Peak\ Force = C + \sum \mathrm{B}_i X_{Codified\ Group} + \gamma * RSAA + \epsilon \qquad \text{Eq. 1b}$$

$$Peak\ Force = C + \sum \mathrm{B}_i X_{Codified\ Group} + \epsilon \qquad \text{Eq. 1c}$$

$$Peak\ Force = C + \gamma * RSAA + \epsilon \qquad \text{Eq. 1d}$$

where C is the model intercept; B_i the coefficients corresponding to the codified extraction group $X_{Codified\ Group}$; Z and u_{RSAA} the coefficients and distribution representing randomness in RSAA; γ the covariant coefficient for RSAA; and ϵ the residual error in the model. To arrive at the optimal model, Eq. 1a could be compared to Eq. 1b. If Eq. 1b is simulated to perform better, it can be pairwise compared to both Eq. 1c and Eq. 1d to determine which factors are necessary in the model.

5.2.2 Numerical Study

The acquisition of new experimental data provided an opportunity to better validate a low-computational-cost, generalizable finite element model of the dental complex for modelling tooth extraction and predicting the biomechanical response of the dental complex to new extraction procedures. An axisymmetric representation of the dental complex has already been developed [11], and the purpose of the current study was to better validate this model using the larger data. An axisymmetric model of the dental complex consisting of the Benex insert, tooth, PDL, and bone was loaded in the FEBio finite element environment [67] to simulate the vertical extraction forces applied in the experimental model. The material model for the PDL was a visco-damage-hyperelastic model based on the Arruda-Boyce hyperelastic model with strain energy density (SED) function given in Eq. 2:

$$\Psi = \mu \sum_{i=1}^{5} \frac{C_i}{N^{i-1}} (I_1^i - 3^i) + \frac{1}{2} k (\ln J)^2 \qquad \text{Eq. 2}$$

The default quasi-linear viscoelastic formulation in FEBio [67] was used to represent the viscoelasticity of the PDL based on an exponential relaxation function given in Eq. 3:

$$G(t) = g_0 + g * \exp(-t/\tau) \qquad \text{Eq. 3}$$

Finally, the damage of the PDL was governed by a quintic polynomial (Eq. 4a) with SED thresholds SED_{max} and SED_{min} determining the limits of the damage function (Eq. 4b):

$$D(\psi) = \begin{cases} 0 & \psi \leq SED_{min} \\ x^3(10 - 15x + 6x^2) & SED_{min} < \psi \leq SED_{max} \\ 1 & SED_{max} < \psi \end{cases} \quad \text{Eq. 4a}$$

$$x = \frac{\psi - SED_{min}}{SED_{max} - SED_{min}} \quad \text{Eq. 4b}$$

The result was a set of seven parameters that are used to fit the force-time response of the FE model to the experimental data: initial modulus μ, chain number N, and bulk modulus k for the hyperelastic model (Eq.1); relaxation constant g and tine τ for viscoelasticity; and damage-limiting strain energy density thresholds SED_{max} and SED_{min}.Force-time curves for each successful extraction in a single displacement-controlled test group were fit at once, accommodated by the method of aligning each force-time curve at a common transition past 50N. Successful extractions from the 0.2mm/min, 2mm/min, and intermittent displacement load groups were selected for the inverse finite element analysis (IFEA) problem. Outlier curves were isolated and omitted by examining the 95% confidence intervals for the force-time curves of each load group.

The error function minimized in the IFEA problem consisted of the product of the sum-of-squares error for a single experimental curve to the FE model response, the square of the peak force difference between the experimental and FE model curves, and the square of the time-at-peak force difference. These errors were summed for every curve in a load scheme group to achieve a single error function for the group which is minimized using the constrained Nelder-Mead algorithm in MATLAB [68] and the GIBBON interface between FEBio and MATLAB [69]. The initial guess for each test group was determined from a range of values available in the PDL modelling literature. The model coefficients resulting from each independent group fit were averaged and the resulting FE model response compared to the averaged response obtained from the previous study [11].

5.2.3 Application of the Finite Element Model to Predicting Force-Hold Loading Response and the Effect of PDL Damage

5.2.3.1 Investigation of force-hold extraction schemes

The purpose of this section of the study was to demonstrate the application of biomechanical models of tooth extraction towards developing new extraction loading schemes. Previous work found peak extraction forces for extractions at 0.2mm/min ranged from 102N to 224N with no extraction failures, with higher forces and increased extraction failure risk at higher loading rates [12]. It was hypothesized that loading the dental complex to a constant force threshold between 150N and 225N (near the upper limit of the 0.2mm/min force range) would result in significant creep displacement due to the viscoelasticity of the PDL, and that the strain energy accrued during creep would be sufficient to rupture the PDL and extract the tooth. The proposed target force range was also below the lowest successful extraction forces at 100N/min and 2mm/min observed in previous work [12]. Within this target force range, higher loading rates (e.g. 100N/min) are applied to reach the target force rather than increasing until extraction success, hypothetically reducing the risk of extraction failure but maintaining relatively short extraction times. To investigate this hypothesis, two force thresholds of 175N and 200N were selected because they were below the maximum force for the upper limit of the 0.2mm/min load group and below the minimum successful extraction force of 244N for the higher-rate 100N and 2mm/min groups. Swine incisors were extracted using the established ex vivo method to investigate these force-hold schemes. Six incisors for each force threshold (n=12) were extracted in a randomized order. In order to limit the test time, force holds were maintained for 500 seconds before the loading was again increased at 100N/min until extraction. Simulation of this loading scheme using the axisymmetric finite element model established in previous work [11] predicted that rupture of the PDL and subsequent delivery of the tooth would occur during this constant force-hold period at both 175N and 200N force-hold levels.

5.2.3.2 Investigation of damage initiation influence on force-hold extractions

A secondary set of experiments were conducted to further demonstrate the application of both numerical and experimental methods for the predictive modelling of different tooth extraction scenarios. This section of the study modeled the changes of the ex vivo swine dental complex response to mechanical damage of the PDL under force-hold loading. The damage scenario

selected for this section of the study is that imposed by the insertion of a flexible periotome (TBS Dental, Union, NJ, USA) inserted into the PDL space to an approximate depth of 4mm. Insertion of a periotome to both the apical and gingival ends of the PDL space was studied in this section. Gingival insertion of an instrument to the PDL space is a common method for severing the PDL before extraction [10,12,20,22] but the biomechanical effect of this action has not been closely examined. Insertion of a periotome to the PDL space from the root apex is not typically possible but was available due to the sectioning of mandibles during sample preparation. Although not clinically representative, this damage case was studied as an analogue for apical decay, resorption, or trauma.

Damage occurring from PDL insertion was modelled in FE simulations as zones of elements with reduced damage capacity relative to the rest of the PDL. The exact nature of the damage induced by the periotome insertion cannot be characterized without pre-extraction imaging that may damage the tissue and influence the response of the tissue to load. The PDL body was remeshed to contain a damaged zone with a depth of 2.5mm, 5mm, and 7.5mm to represent a range of damaged volumes that could result from the periotome insertion, with damaged volume depth defined from the apical or gingival extent of the bone body (Figure 5-1). Damage was induced in these zones by creating a gradient in the damage-limiting SED_{max} from the outer edge to the main PDL body, with the capacity at the outer edge reduced to 0%, 50%, or 75% of the nominal value for the PDL. The field variable tool in FEBio was used to assign reduced SED_{max} values to the elements in the damaged volume. The model displacement-time response for each of the three damage depths and threshold levels was simulated for both the apical and gingival damage cases (total of 18 simulations) with a 100N/min ramp to a force threshold of 175N. Following the initial investigation, additional meshes were generated for modelling damage to the gingival margin of the PDL by creating gaps in the mesh at depths of 2.5mm, 5mm, and 7.5mm. In these meshes, the damaged zone depth was maintained at 0.25mm. Damage thresholds were manipulated over the same range from 0-75%.

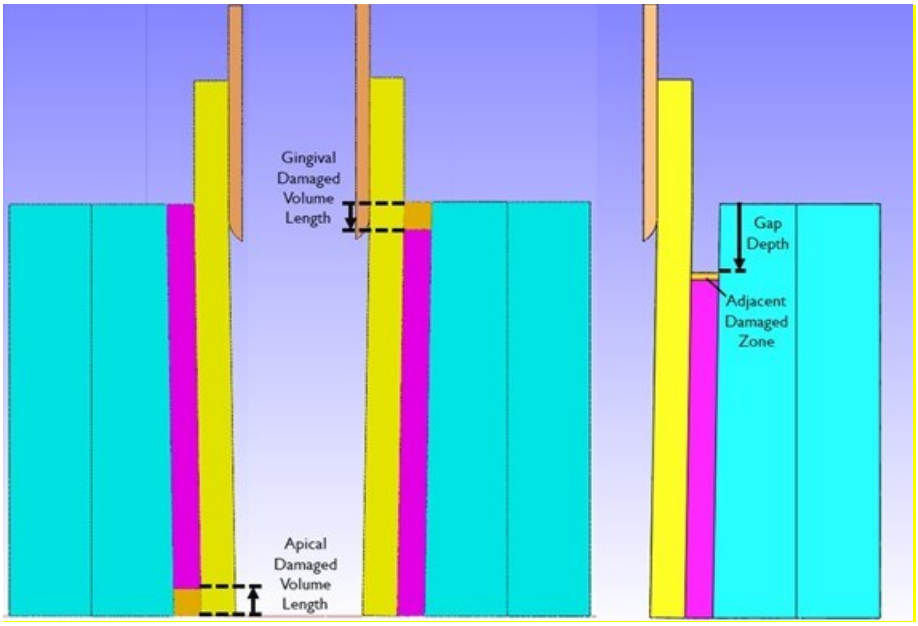

Figure 5-1: Planar views of the axisymmetric dental complex model with the damaged PDL volume at the apical and gingival sides

Experimental extractions were performed to examine the predictive power of the FE model in the damaged cases. The flexible periotome was marked to the desired insertion depth of 4mm with a permanent marker. In the apical damage case, the periotome was inserted to this depth following the circumference of the exposed perioodontal space. In the gingival damage cases, a scalpel was used to create a gingival flap that was peeled back with tissue forceps to expose the alveolar bone crest around the central incisors. The periotome was then inserted to the 4mm depth following the shape of the alveolar crest around the incisor (Figure 5-2). Three tests were performed for each of the apical and gingival damage cases (total of 6) at a 175N target force threshold.

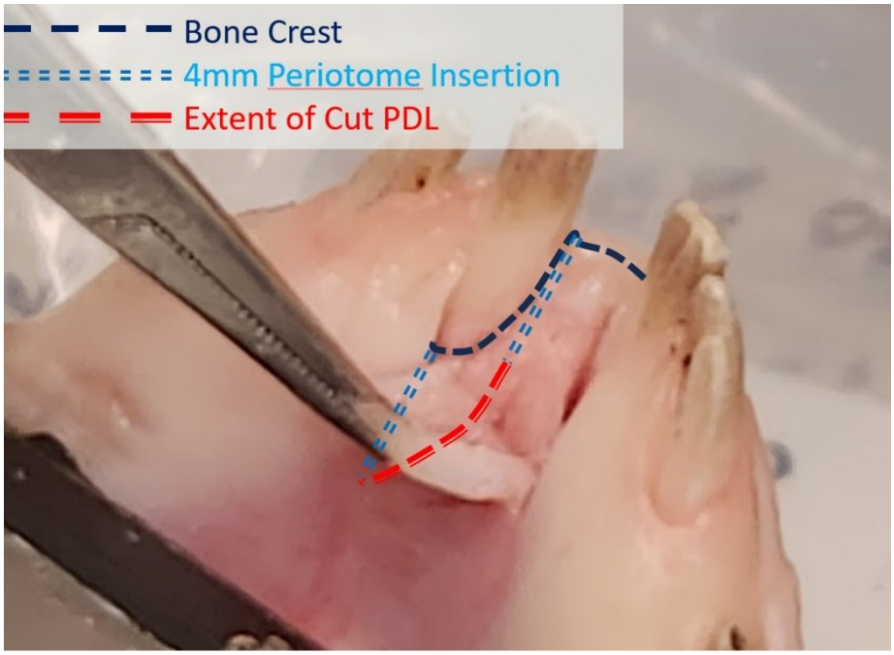

Figure 5-2: Diagram of the apical margin of the alveolar bone with path followed by the insertion of a flexible periotome to a depth of 4mm

5.3 Results

5.3.1 Mechanical Tooth Extraction Experiments

Twenty-five extractions were simulated with continuously-increasing or intermittent-displacement loading and combined with the data from the previous work [12] for a total of 49 simulated extractions across all five load scheme groups. One extraction from previous work was omitted due to a failure of the interface between the Benex® extraction screw and the tooth root that was determined to be unrepresentative of a clinical extraction failure (i.e. mechanism failure vs. successful extraction or failure of the dental complex). The crosshead force-displacement data from these tests is demonstrated in Figure 5-3. Further results consider the results of the previous study and this study as a single combined data set.

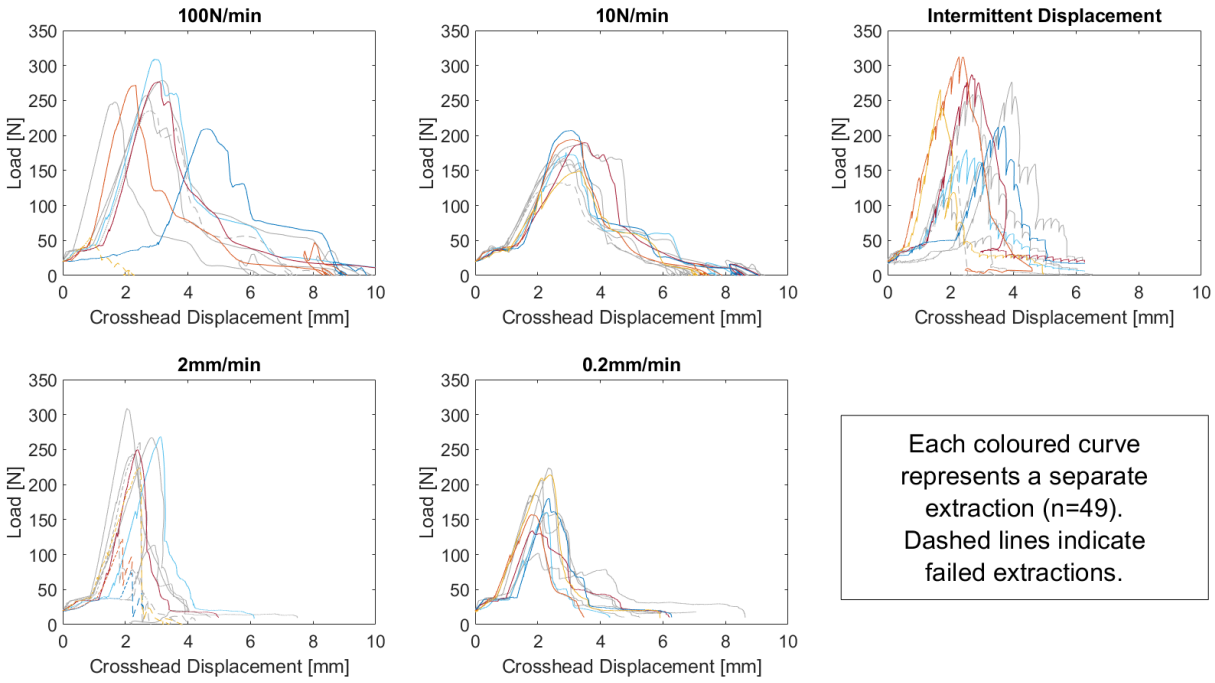

Figure 5-3: Crosshead force-displacement curves for the complete study (n=49), plotted by load scheme group. Curves from the previous study [12] are coloured grey. Dashed curves indicate failed extractions due to tooth or bone fracture.

5.3.1.1 Statistical Analysis of Peak Forces

The distribution of RSAAs for successful extractions with post-hoc imaging is demonstrated in Figure 5-4. RSAA values range from 183mm^2 to 434mm^2. The distribution appears to be approximately symmetrical about an RSAA of 300mm^2 and does not appear to contain any systematic trends (e.g. skew or multiple peaks/means) that will influence the normalization of peak forces.

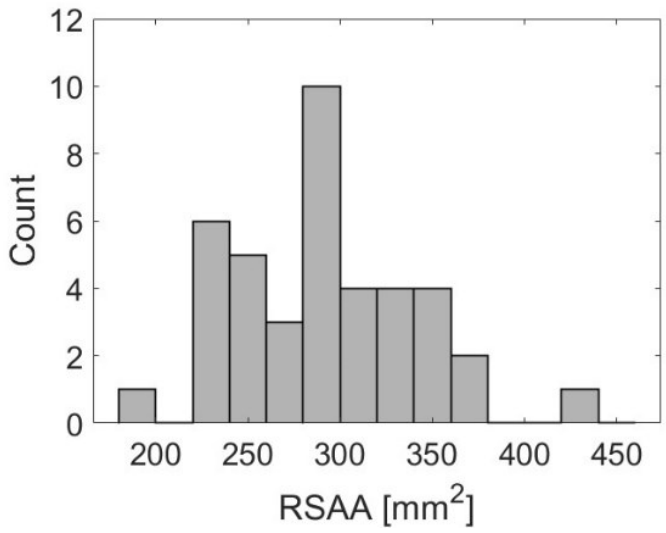

Figure 5-4: Histogram demonstrating the distribution of root surface attachment areas (RSAA) across 40 successful ex vivo extractions

Peak forces from successful extractions gathered from each test group are compared in Figure 5-5. An overall significant effect of load group was found among normalized peak forces for successful extractions ($p < 0.01$). The Tukey HSD post-hoc test found significant differences between both 2mm/min and 100N/min load groups when compared individually to the 10N/min and 0.2mm/min groups ($p < 0.05$). No groups were found to differ significantly from the intermittent displacement loading group because the distribution of these peak forces spans the range of peak forces from all other groups, even when normalized to RSAA.

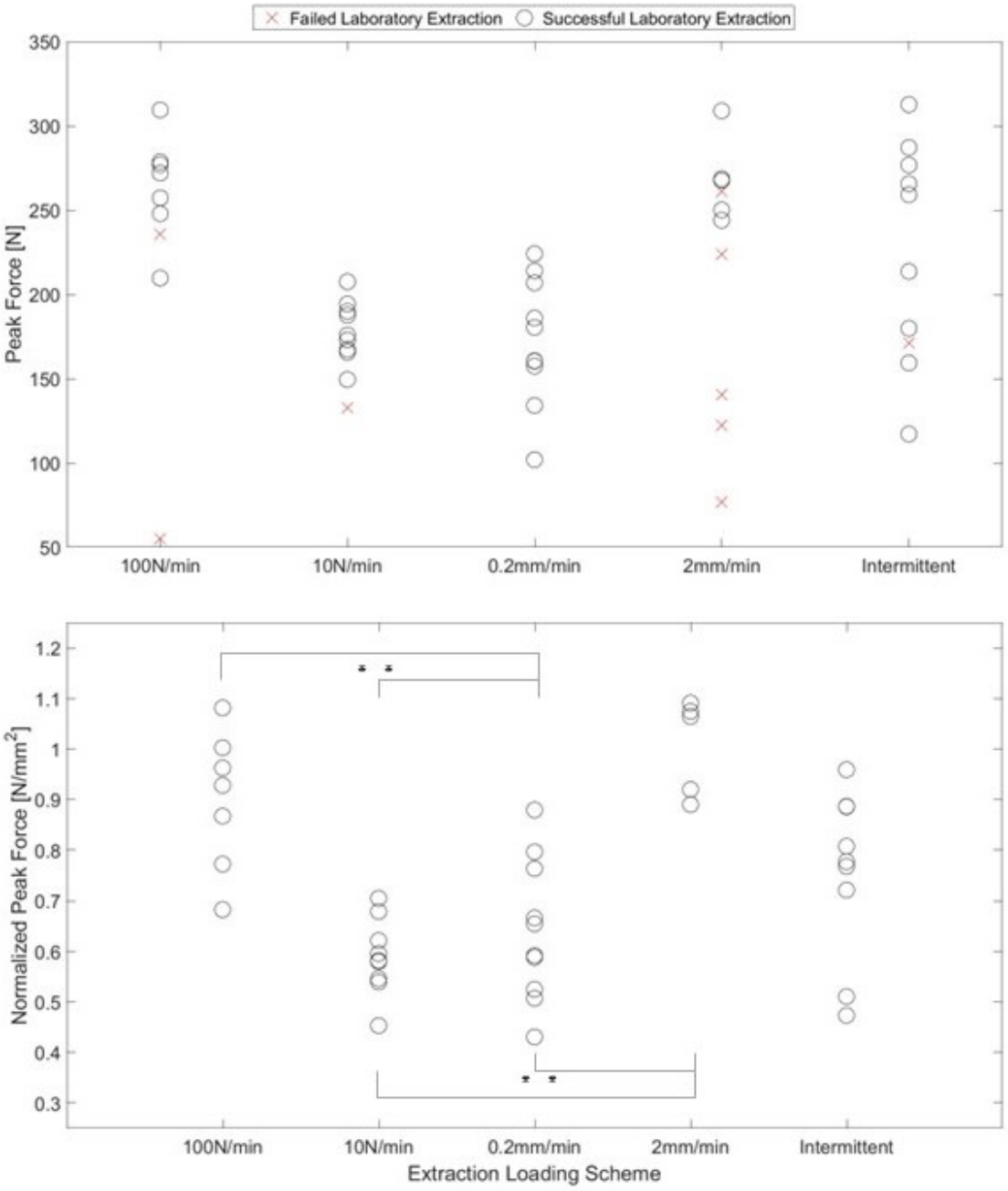

*Figure 5-5: Peak forces from ex vivo tooth extractions, un-normalized and including failed extractions (above) and normalized to RSAA for successful extractions (below). ** - comparisons with significant differences determined by Tukey HSD post-hoc, $p < 0.05$*

The linear model predicting peak force determined by the comparative analysis had a reported R^2 = 0.623 and is represented by:

$$Peak\ Force = C + \sum \mathrm{B}_i X_{Codified\ Group} + \gamma * RSAA + \epsilon$$

where $C = 140.9N$

$$\mathrm{B_i} = [-108.3\mathrm{N}, \quad -98.3\mathrm{N}, \quad -55.8\mathrm{N}]$$

$$X = binary\left(\left[\frac{10N}{minute} \quad \frac{0.2mm}{minute} \quad Intermittent\right]^T\right)$$

and $\gamma = 0.475N/mm^2$.

Similar to the findings of the comparison among normalized groups, the linear model analysis also grouped the 2mm/min and 100N/min groups together (represented by the intercept constant C). Each of the 0.2mm/min, 10N/min, and intermittent test groups were determined to have the individual coefficients B_i. The effect of RSAA variations are represented by the covariate coefficient γ of 0.475N/mm^2. The fit of this model to the peak force and RSAA data is presented in Figure 5-6.

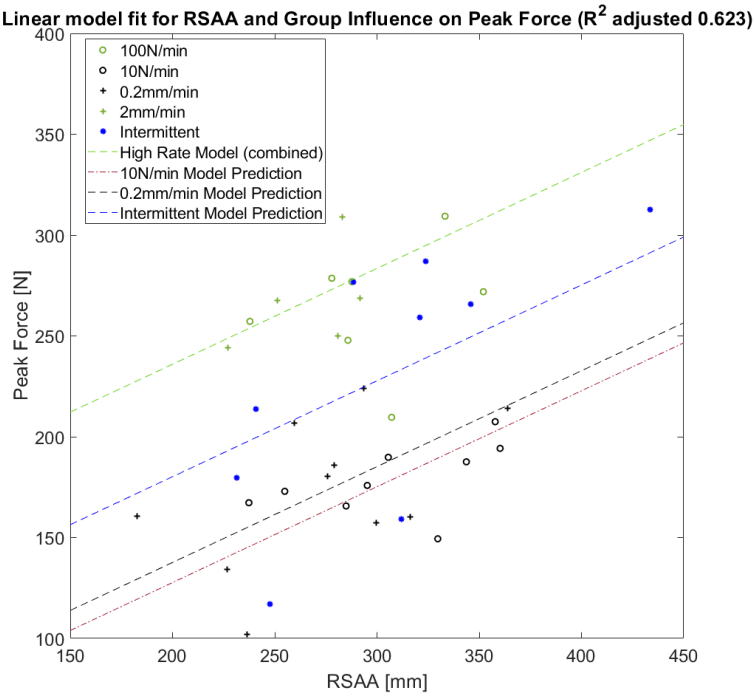

Figure 5-6: Scatter plot of RSAA and peak force for successful extractions. Linear model is represented for each significant loading group with RSAA covariance.

5.3.1.2 *Success rates*

The greatest risk of failed extraction in this study was in the 2mm/min loading group, which had five failures among 10 simulated extractions. The next-highest failure rate was in the 100N/min group (2 failures), followed by the 10N/min and intermittent groups (1 failure each). The 0.2mm/min group had no failed extractions.

5.3.1.3 *Stiffness analysis*

21 successful continuous-loading extractions with successful video analysis were identified in this study. Figure 5-7 demonstrates the results of the K-means analysis and the likelihood of an extraction from each load group being sorted into a given cluster.

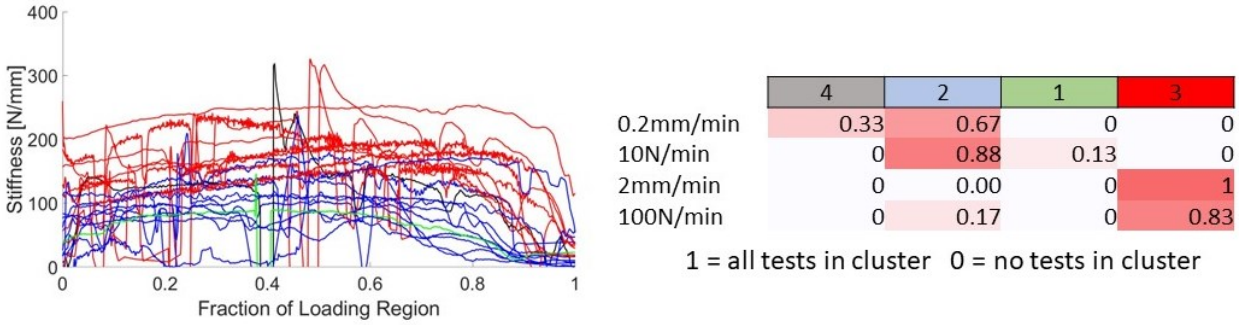

Figure 5-7: a) Instantaneous stiffness curves, sorted by cluster obtained from the K-means algorithm. Fraction of loading region is from video-identified onset of tissue loading to peak force; b) likelihood of a stiffness curve being sorted into a given cluster (identified by colour and number).

The K-means analysis clearly identifies two primary clusters of stiffness with two single-curve clusters interspersed. The higher of the two clusters (red in Figure 5-7) consists entirely of extractions performed at 2mm/min and 100N/min. The lower of the main clusters (blue in Figure 5-7) is comprised mostly of 0.2mm/min and 10N/min extractions with a single associated 100N/min stiffness curve. The overall trends between the two clusters are similar to the previous work [13] in that both demonstrate gradual increases in stiffness over time before dropping off towards peak load. This trend is more pronounced for the higher of the two main clusters, with larger decay ranges for the lower cluster. Interestingly, the rise-and-fall pattern is most pronounced for the 100N/min curve among those in the lower main cluster.

5.3.1.4 Post-Extraction Imaging of Tooth Surfaces and Residual PDL

Contrast-enhanced CT scanning (CE-µCT) was used to quantitatively assess the patterns of PDL rupture that occurred during tooth extraction. Two primary patterns were identified: large areas of denudement of the tooth surface from PDL tissue, and the formation of tissue flaps. Generally, denuded tissue areas occurred in the apical third of the tooth root. Flaps formed throughout the tissue body surrounding the tooth root.

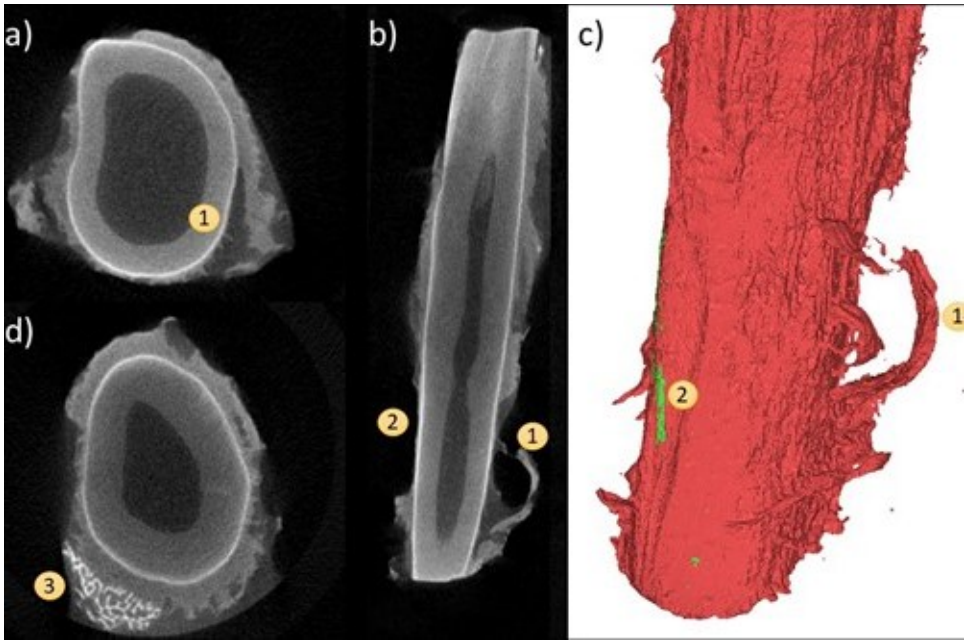

Figure 5-8: Coronal (a), frontal (b), and 3D reconstruction views (c) of a "flap" pattern of PDL rupture (1) observed with CE-µCT. Opposite is an area of rooth denudement without a flap (2); A coronal view near the apex (d) showing a small fragment of attached bone (3).

The flap pattern appears to originate with rupture at the tooth surface (Figure 5-8a, right), extending apically to the root of the flap (Figure 5-8b and 5-8c). There is a significant area of denudement opposite this flap (Figure 5-8b and 5-8c). Immediately apical and adjacent to this area is a small volume of detached alveolar bone (Figure 5-8d) that was not visible during initial post-extraction assessment. This is the only instance of bone remaining attached to the tooth that was observed in this study.

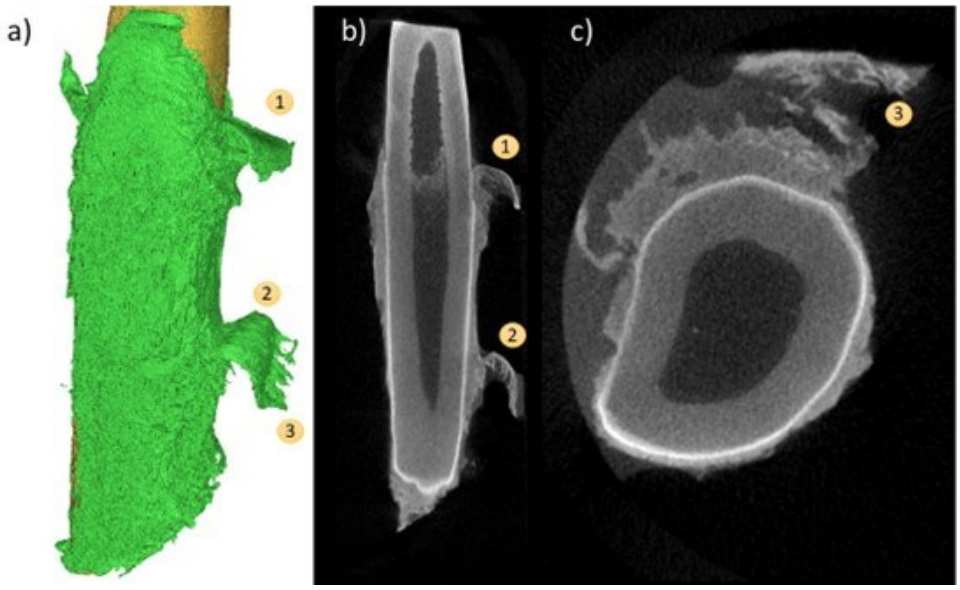

Figure 5-9: 3D reconstruction view (a) and saggittal view (b) of two colinear instances of the "flap" pattern, one gingival occurrence (1) and one mid-apical (2). Fibrous patterns (3) are visible in the coronal view of the tooth (c)

Figure 5-9a also demonstrates the flap phenomenon, with two pronounced flaps evident on the buccal side of the tooth. The gingival-most flap appears next to the partially-denuded cemento-enamel junction (CEJ). The apical-most flap appears adjacent to a region of partial but incomplete tissue thickness reduction (Figure 5-9b) and also demonstrates fibrous strands that appear to be the result of tissue rupture (Figure 5-9c).

5.3.2 Numerical Study

The PDL parameters resulting from the IFEA study are demonstrated in Table 1. Similar to previous work establishing this IFEA method [11], there are strong similarities among parameters determined from each of the three load cases. Both viscoelastic parameters and chain link number, N, and initial modulus, μ, vary around the coefficient averages determined previously. Bulk modulus k and SED_{max} vary more compared to the previous coefficient average (up to 28%), especially in the intermittent loading case. The coefficient averaged solution for the present study reflects this similarity across all parameters except SED_{max}, which is slightly higher (6.26mJ/mm^3 from 5.92mJ/mm^3).

Table 5-1: PDL material parameters obtained from IFEA solutions for three displacement-controlled loading schemes. Previous averaged solution from [11].

	g	τ	μ	N	k	SED_{min}	SED_{max}
0.2mm/min	0.562	21.9	0.422	10.7	7.86	0.696	5.04
2mm/min	0.520	19.6	0.502	10.2	9.78	0.111	6.22
Intermittent	0.455	19.9	0.470	10.3	11.0	0.195	7.53
Current Averaged Solution	0.512	20.5	0.464	10.4	9.55	0.334	6.26
Previous Avg. at Reduced Sample Size [11]	0.561	20.1	0.472	9.90	9.84	0.208	5.92

The variations in PDL parameters among the IFEA solutions, coefficient-averaged solution from previous work [11], and the current averaged solution are evident in the force-time responses compared in Figure 5-10. Across all three cases, the performance of the IFEA solutions is good at explaining the overall distributions of the experimental data. In each load case, there is a slight variation in FE response among the IFEA solution and the two coefficient-averaged solutions in terms of both curve shape and peak force. Differences in curve shape are most pronounced in the 0.2mm/min group, with the IFEA solution underpredicting both averaged solutions. The differences in time to peak force and peak fore are most pronounced in the intermittent loading case, with the coefficient-averaged solutions predicting earlier rupture and lower peak force than the IFEA solution as a result of their relatively reduced SED_{max} values.

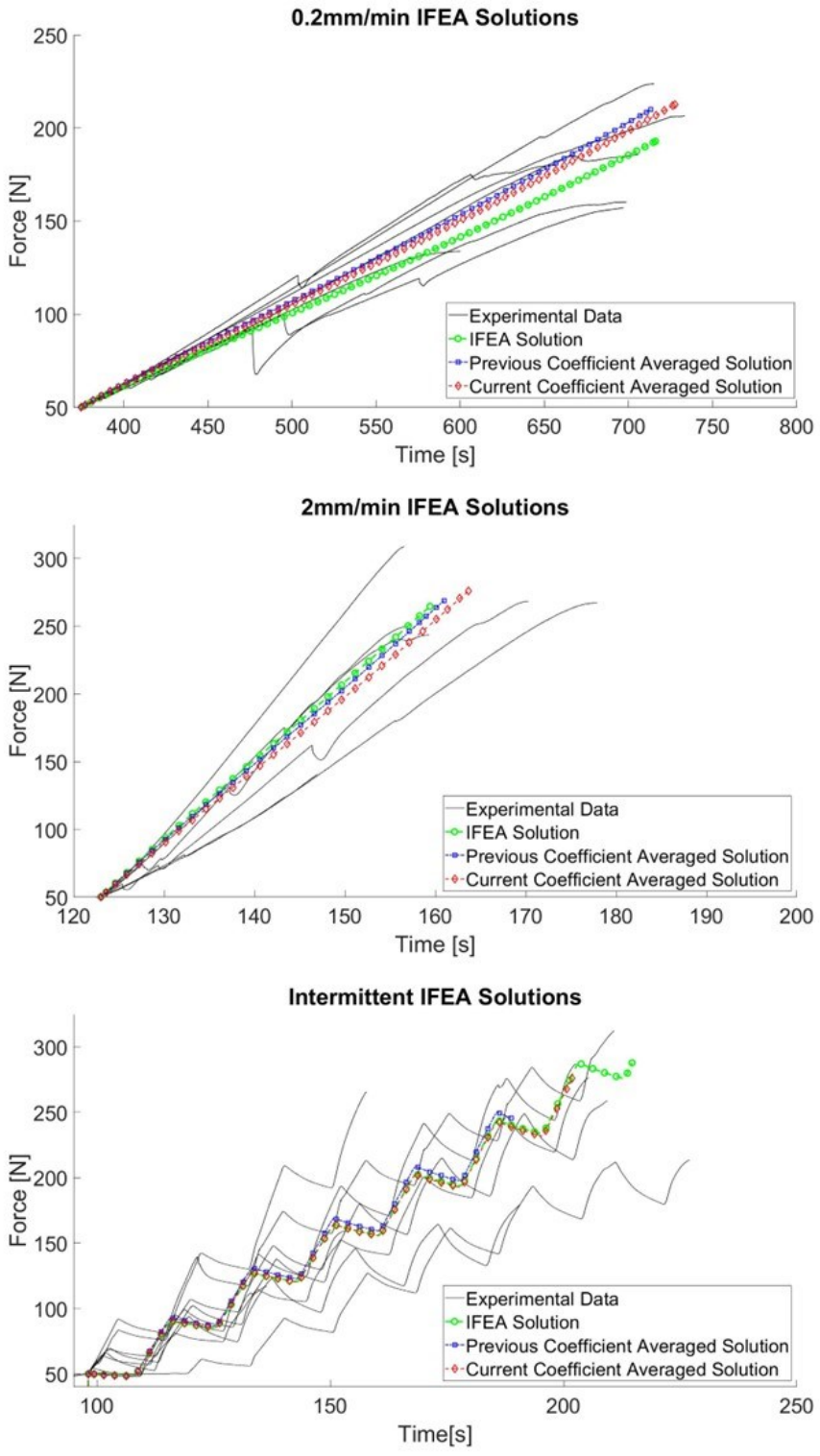

Figure 5-10: Force-time trace comparison among IFEA solutions and experimental data for 0.2mm/min (top), 2mm/min (centre), and intermittent displacement (bottom) cases.

5.3.3 Investigation of force-hold extraction schemes

Crosshead data collected during the 175N and 200N force-hold tests (Figure 5-11) demonstrates the self-alignment behaviour of the apparatus at low forces, indicated in the large millimeter-scale displacements that occur concurrently with periods of low force. After system alignment, the dental complex response to the force-hold loading can be categorized into three categories: tests which ended during the initial 100N/min ramp; tests which ended during the force-controlled hold; and tests which ended during the post-hold increase in loading. Tests ended due to either tooth extraction or fracture of the tooth root in all three categories (indicated by red markers in Figure 5-11).

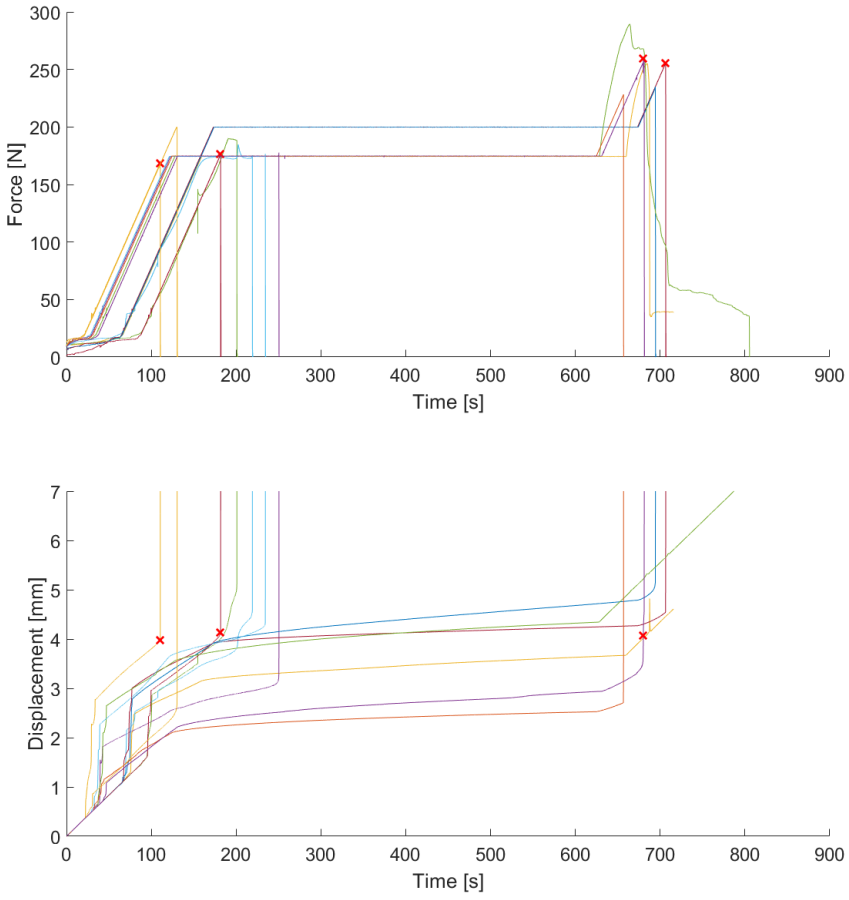

Figure 5-11: Force-time (above) and displacement-time (below) crosshead data collected during force-hold ex vivo extractions. Each pair of coloured curves is a single extraction. Red "X" marks indicate the point at which an extraction failed due to tooth root fracture.

The displacement-time behaviour of the force-hold extractions demonstrates creep in varying degrees. Some extractions match the FE prediction well in that they appear to reach equilibrium within the 500 s hold period, whereas others continuously displace and do not reach this equilibrium state before the end of the period. This behaviour does not appear to depend on the force threshold applied.

5.3.4 Investigation of damage initiation influence on force-hold extractions

Displacement-time data from both the experimental and numerical models of PDL damage are demonstrated in Figures 5-12 and 5-13. The finite element study demonstrated that the time of rupture depended very strongly on the depth and capacity of the damaged PDL volume but the shape of the displacement-time curve (i.e. dental complex stiffness) did not. Only FEA curves from the 4mm damage volume depth are demonstrated for clarity. All experimental curves are adjusted to share a common transition time from apparatus self-alignment to tissue extension with the finite element results.

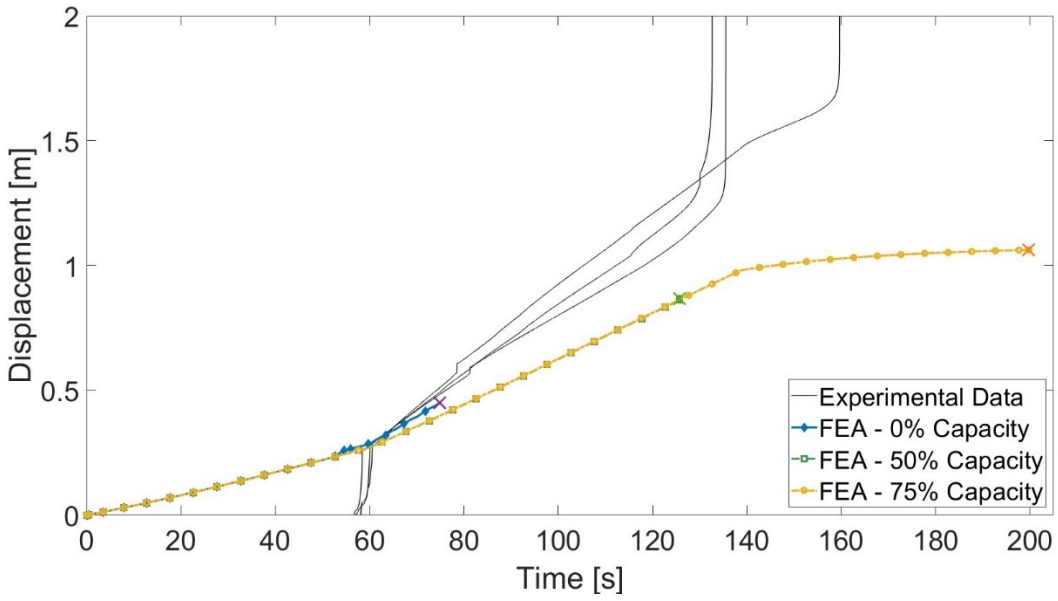

Figure 5-12: Comparison of displacement-time traces gathered with experimentally-modeled damage of the gingival PDL and finite element simulations. 'X' markers indicate PDL rupture ending the simulation in finite element results.

When the apical PDL is damaged, only one experiment lasted to the 175N force hold (Figure 5-13). Both other extractions were completed during the 100N/min ramp just prior to the force-

hold transition. The finite element results predict a range of behaviours from a period of force-hold before rupture at 75% damage capacity to a very early rupture during the load ramp for 0% capacity. The shape of the finite element curves underpredict the displacements seen in the experimental curves, indicating that the system stiffness is much lower in the experimental model. However, the rupture times in the experimental curves agree well with those predicted by the finite element model.

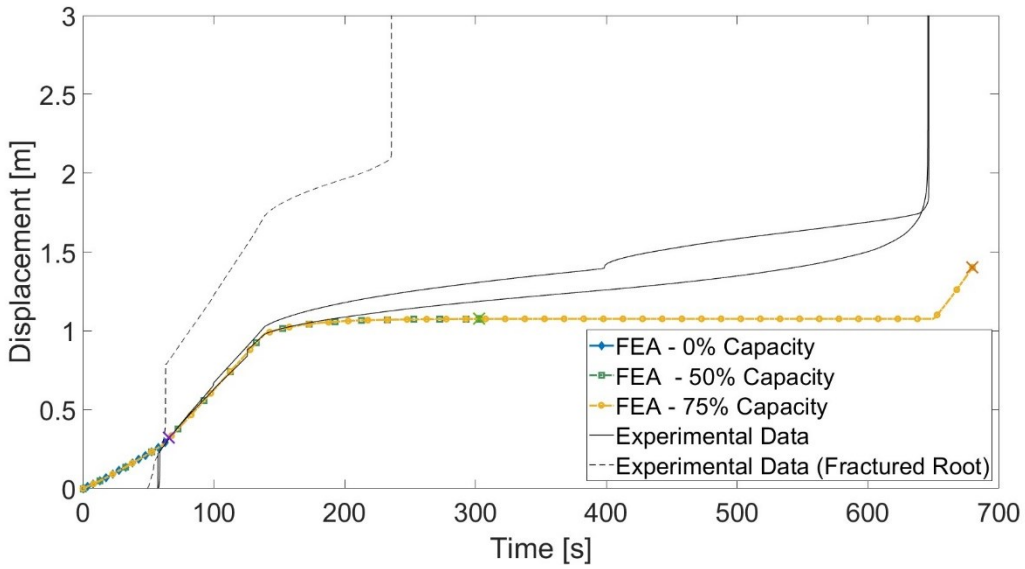

Figure 5-13: Comparison of displacement-time traces gathered in experimentally-modeled damage of the apical PDL and finite element simulations. 'X' markers indicate PDL rupture ending the simulation in finite element results.

One experimental extraction in the apically-damaged PDL case failed to due fracture of the tooth root. The other two experimental extractions demonstrated continuous creep over the force-hold period before extraction just prior to the end of the 500s period. The finite element results predicted all three of extraction in the initial loading, force-hold, and post-hold loading at 0%, 50%, and 75% damage capacity respectively. Again, the dependence of the system stiffness on damage capacity for this fixed volume appears to be low and the FEA results underpredict the displacement in the experimental model. Consistent with the apically-damaged case, the experimental rupture time lies within the region predicted by the 50% and 75% capacity damaged FEA results.

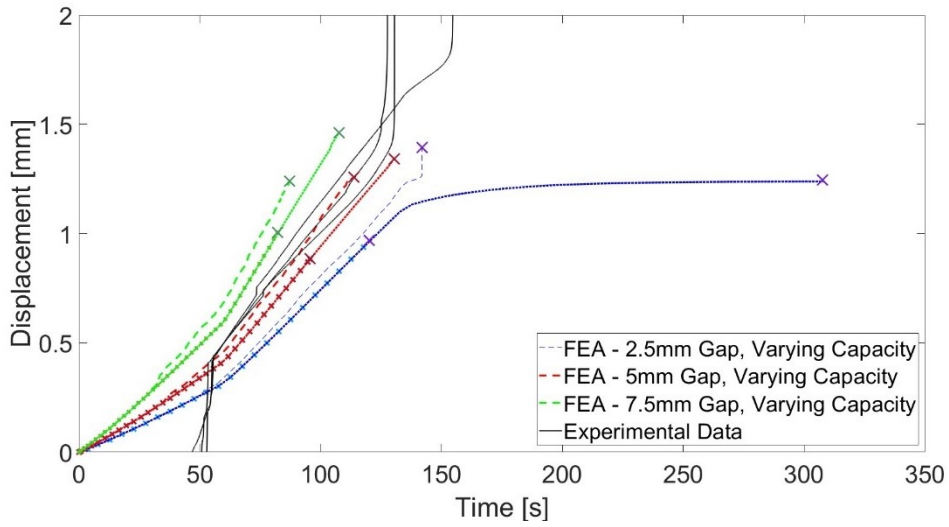

Figure 5-14: Comparison of experimental force-hold displacement curves for apically damaged PDL with FEA results representing gaps imposed at the damage site. 'X' markers indicate PDL rupture ending the simulation in finite element results.

Introducing a gap at the apical edge to represent damage better simulates the stiffness of the experimental model, evidenced by the alignment of the experimental curves with the FEA results (Figure 5-14). For each gap depth, the trend is consistent that varying damage capacity varies the predicted tissue rupture time. The experimental rupture times and displacement rates fall between the 2.5mm and 5mm gap data series. There also appears to be a slight interaction between damaged volume capacity and gap depth, with the 2.5mm gap results presenting the greatest range of predicted rupture times. Introducing the gap also introduces a slight sensitivity in curve shape to the damage capacity but stiffness is dominated by the gap depth.

5.4 Discussion

The purpose of the presented study was to characterize the biomechanical response of the dental complex to vertical tooth extraction and demonstrate the application of a relevant numerical model to predict ex vivo model response under previously-unexamined [12] loading scenarios. A set of continuous- and intermittent-displacement loading tests were performed to expand an available data set for statistical analysis and FE material parameter generation. The resulting models demonstrate that peak force and stiffness depend on load rate; that tooth geometry represented by RSAA also determines peak force; and that a single set of PDL material parameters gathered from independent load case IFEA solutions reasonably predict the force-

time response of the dental complex to displacement-controlled vertical extraction load. The application of the FE model as a predictive tool was demonstrated by predicting the displacement-time behaviour of the ex vivo experimental model under force-hold loading. Simple changes to the mesh geometry and material parameters were also demonstrated to predict the effects of imposing mechanical damage to the PDL on dental complex biomechanics during vertical tooth extraction.

Collecting an expanded data set characterising continuously-increasing force- and displacement-controlled loading permitted a thorough characterisation of the ex vivo swine dental complex response to these loading regimes. The addition of imaging measures for RSAA provided important additional data to this characterization. Significant differences among the peak forces measured in the 10N/min and 0.2mm/min lower rate groups and the 100N/min and 2mm/min higher rate groups were found after normalization by RSAA. Intermittent displacement loading did not demonstrate significant differences from any group in the post-hoc analysis. However, a mixed-methods model analysis returned a simple linear model for peak force based on loading rate with a covariant for RSAA, and in this model a significant coefficient for intermittent loading compared to the high-rate baseline model (in addition to coefficients for the low-rate group) was found to be significant but with half the reduction in peak force of the lower-rate groups. This finding is more consistent with an intuitive understanding of PDL viscoelasticity than the Kruskal-Wallis post hoc suggestion that intermittent loading has no effect on load rate in that energy dissipated by intermittent relaxation of the tissue may reduce the overall peak force, but the higher rate at which the tissue is loaded between relaxation periods still results in higher peak force than a quasi-static load. The description of peak extraction force portrayed by these models clearly illustrates the importance of load rate in determining peak extraction force, which aligns well with the viscoelasticity of the PDL which has been extensively characterised in other loading regimes [65-66,71-72].

The quantification of the influence of load-rate dependence with the inclusion of individual tooth geometry (RSAA) is an important finding of this study. Previous clinical measurements of extraction forces and RSAA have shown a moderate correlation during non-prescribed loading applied with a Benex® device [10]. The linear model proposed in this study quantifies the importance of geometry relative to load rate: the range of RSAA determined in this study

(183mm^2 to 434mm^2) corresponds to an approximate change in peak force of 120N, similar in magnitude to the anticipated 98.3-108N changes reductions in peak force anticipated by reducing the load rate from a higher rate to 0.2mm/min or 10N/min. Notably, the range of RSAAs measured in this study is consistent with those measured for single- and multi-rooted teeth in a clinical study utilising the Benex® device (52-400mm^2) [9]. This degree of similarity is promising for the applicability of the ex vivo swine model in predicting the biomechanics of human teeth, but further work is required to truly demonstrate similarity between the two.

The findings of the instantaneous stiffness analysis presented in Figure 8 further support the characterisation of dental complex biomechanics and their dependence on load rate. The K-means clustering algorithm is blinded to both RSAA and underlying load rate but is able to categorize the curves based on high- or low-rate loading based only on the curve features themselves. There is one curve from the higher-rate continuous loading schemes that is classified in the low-rate cluster but, as demonstrated in Appendix E, this categorization does not survive a higher resolution sorting of the curves. Instantaneous stiffness is an important characteristic of dental complex biomechanics because it can be continuously monitored during an extraction with the appropriate instrumentation, whereas peak force as a measure relies on completion of the extraction. This finding has practical implications for future development of vertical tooth extraction load schemes and devices. For example, the results of this analysis may be interpreted to provide a stiffness threshold (e.g. 150N/mm, approximately the transition from the low-rate cluster to the high-rate cluster at 50% of the loading region) that is used to limit the loading rate applied with an electromechanical control system. The continuously increasing stiffness behaviour and subsequent reduction near peak force highlights the nonlinearity of the system response and the importance of instantaneous measurement and feedback in the future development of extraction methods. In the context of immediate pre-clinical investigation, these findings also suggest that instantaneous stiffness measurement is an appropriate technique for studying the dental complex (and potentially other non-linear soft tissue systems) rather than the traditional practice of performing linear fits post-experiment and neglecting some aspects of the measured response (e.g. toe-in regions and/or yield).

The findings of the IFEA portion of this study updated the material parameters obtained in previous work [11] with a larger data set but obtained a very similar set of coefficients for the

PDL. As demonstrated in Figure 5-10, the coefficient-averaged solution among the three independent fits performed in this study agrees well with all three loading regimes considered (i.e. displacement-controlled, force-controlled, and intermittent loading). The updated coefficient-averaged solution causes slight changes in curve shape compared to the previous coefficient-averaged solution [11] and extends the time to peak force in all three cases. This effect is most appreciable in the intermittent displacement load group. Some changes in the IFEA solutions are to be anticipated with the inclusion of additional curves as the IFEA error function includes terms for the sum-of-squares error, peak force error, and time-to-peak-force errors from each individual curve that may influence the solution. The similarity among the IFEA solutions and the coefficient averages across loading regimes and the inclusion of additional curves suggests that the model is capturing the underlying physical behaviour of the system rather than independent spurious numerical results The quasi-linear viscoelastic model employed for the PDL does not capture the nonlinear viscoelastic behaviour of the PDL, which is a characteristic of the PDL that has been previously observed [30,32] and is demonstrated in this study in the increases in relaxation that occur throughout intermittent loading data sets. This is consistent with the findings of the previous IFEA study and suggests that, rather than a limitation on the data set, this is a limitation of the QLV model [11]. The QLV model may also explain the near-equilibrium creep behaviour observed in the prediction of the force-threshold tests which only partially matches the experimental findings. However, the QLV offers the advantage of being natively available in the FEBio software package and providing a functional representation of the basic viscoelastic behaviour of the PDL while only contributing two parameters to the optimization problem. Future work on this method can investigate other appropriate viscoelasticity models to better explain these phenomena but the QLV model employed in this study adequately captures the differences between the 2mm/min and 0.2mm/min groups and has demonstrated good prediction of the range of times to rupture observed during force-hold tests.

Qualitative assessment of CE-μCT images of extracted teeth revealed additional insight into the mechanism of PDL rupture that further indicate that the IFEA solution is replicating the physical behaviour of the PDL during tooth extraction. The peeling and denudement patterns highlighted in this study demonstrate the importance of the hard tissue boundaries in the biomechanics of the PDL during extraction load, particularly as a site of rupture initiation. This finding is consistent with the finite element model strain patterns published previously [11], wherein the interface-

adjacent elements strongly determine the rupture behaviour of the overall system. The pattern of denudement adjacent to large residual tissue thickness is consistent with the cross-sectional images of the human tooth following forceps extraction provided by Baschong et al in their study of cell viability [49], although the mechanism of loading and purpose of their imaging differs from this study. Due to the irreversible extension and damage of the tissue imaged in this study with no untested reference images, the CE-μCT reconstructions cannot be used to reliably reconstruct rupture formation and propagation. However, the patterns of flap formation and tooth surface denudement found throughout the CE-μCT images and demonstrated in Figures 5-8 and 5-9 are indicative of material behaviour that is consistent with the FE representation. The formation of a flap at the gingival edge of the PDL evidenced in Figure 9 is particularly similar to the FE model behaviour, which undergoes rupture initiation at this location. Similar patterns of tissue rupture are evidenced in Figure 8b, 8c, and apically in Figure 9a and 9b that are not reflected in the FE rupture pattern per se but are indicative that the concentration of strain at this boundary (which the model does reflect) is physically realistic. Attempting to gather comparative images before or during the extraction poses the risk of damaging or denaturing the tissue from prolonged x-ray exposure, which may influence the measured biomechanical outcomes. The in situ imaging of PDL rupture at the boundaries with the tooth or bone poses a significant technical challenge that remains outside the scope of the present work.

Results from FE simulations demonstrated the predictive power of the model by representing the displacement behaviour of the dental complex under constant sustained force, both with the PDL intact and with damage imposed by the insertion of a periotome. The FE model predicted rupture in both cases during the force-hold period, which is the middle ground of the three behaviours that were subsequently observed in the experimental model. This may be in part as a result of the QLV model behaviour, which in addition to neglecting some non-linearity of the system may also struggle to model the creep behaviour of a tissue when parameters are fit from relaxation data (and vice versa) [73]. Additionally, the predictions used the same 15mm root geometry from the model's inception despite the experimental data demonstrating dependence on RSAA. With no way to determine RSAA or root geometry without pre-extraction imaging this geometry was accepted but variations in tooth geometry may have influenced when each PDL ruptured. This may also explain the limited influence of damage volume and threshold in the apical and gingival damaged FE models. However, with variation of the damage thresholds, greater ranges

of behaviour could be modeled that encapsulated the times-to-rupture observed in the experimental cases.

Modelling damage as a void volume in addition to inclusion of a damaged zone improved the FE prediction of force-hold response in the apically damaged PDL. A range of gap depths and damage thresholds was modeled in silico without means to characterize the exact extent and nature of the damage imposed by the periotome despite the fixed depth of insertion. It is unlikely that tissue immediately adjacent to the periotome is undamaged by its insertion. Characterizing the exact nature and extent of such an injury is infeasible without the use of high-powered microscropy (e.g. synchrotron source phase contrast imaging). Despite this limitation, a range of simple changes to the FE model geometry and parameters were able to predict the range of behaviours in the apically-damaged experimental model in terms of both displacement rate and rupture time. This sensitivity further demonstrates the robustness of the FE model as a tool that, with further work and validation, can be extended to model a range of tooth geometries and extraction procedures.

Despite the limitations of the QLV and generalized geometry, the findings of this study suggest that an axisymmetric finite element model validated with a large, variable body of experimental data is a powerful tool for designing new vertical tooth extraction loading procedures and studying extraction biomechanics in different tissue conditions. The predictive capacity critically reduces the impact and costs of developing new vertical tooth extraction loading schemes. For example, the damage modelling method employed in this study surveyed a large range of damage conditions in a run of solver simulations that was completed in a number of days as opposed to utilizing laboratory experiments taking weeks and using extensive resources. Without data characterising the actual nature of periodontal injury caused the insertion of a periotome, this low-cost approach created a cluster of data that accurately captured changes in both complex stiffness and rupture behaviour demonstrated by the experimental model. A numerical-experimental-numerical modelling development loop utilizing this approach provides an evidence-informed approach to developing atraumatic extraction techniques while reducing obstacles such as cost and computational intensity.

5.5 Conclusion

This study characterized the biomechanical response of the ex vivo swine dental complex to vertical extraction loading at five initial loading rates and presented a finite element model based on this characterization. Experimental characterization demonstrated dependency of both peak extraction force and rising-side stiffness on the applied load rate, with peak force also depending strongly on tooth geometry determined by RSAA. The crosshead data obtained from 0.2mm/min, 2mm/min, and intermittent 2mm/min extractions was used to solve an IFEA problem determining PDL parameters for the axisymmetric finite element model of the dental complex. The resulting parameters were consistent among load rates and a coefficient-averaged solution predicted the force-time curves among all three load cases. The axisymmetric model using the determined PDL material parameters was used to predict constant-force extractions in the ex vivo model, which experimentally determined large variation in the rupture behavior. The finite element model was also applied to predict these force-hold extractions with damage induced in the apical and gingival PDL. The best predictions of the damaged periodontal response were obtained when the damage was modelled as a void with an adjacent damaged PDL volume, demonstrating good agreement with the displacement rates and rupture times obtained from a similarly-damaged ex vivo model. The biomechanical data and numerical model obtained by this study provide both an enhanced basic understanding of the biomechanics of vertical tooth extraction and useful tools for the modelling and development of new extraction devices and procedures.

References

1. Broers DLM, Dubois L, de Lange J, Su N, de Jongh A. Reasons for tooth removal in adults: a systematic review. International Dental Journal. 2022 Feb 1;72(1):52-7.Hiltunen K, Vehkalahti MM. Why and when older people lose their teeth: a study of public healthcare patients aged 60 years and over in 2007-2015. Gerodontology. 2023 Sep;40(3):326-33.
2. Broers DLM, Dubois L, de Lange J, Welie JV, Brands WG, Bruers JJ, de Jongh A. Financial, psychological, or cultural reasons for extracting healthy or restorable teeth. The Journal of the American Dental Association. 2022 Aug 1;153(8):761-8.
3. Bernal-Sánchez KK, Lara-Carrillo E, Velázquez-Enriquez U, Casanova-Rosado JF, Casanova-Rosado AJ, Morales-Valenzuela AA, Márquez-Rodríguez S, Medina-Solís CE, Maupomé G. Clinical and socio-demographic factors associated with dental extractions in a clinical sample. Brazilian Dental Journal. 2023 Dec 22;34:121-9.Supplement #1 – Additional Imaging Results
4. Alibrahim A, Al Salieti H, Alrawashdeh M, Darweesh H, Alsaleh H. Patterns and predictors of tooth loss among partially dentate individuals in Jordan: A cross-sectional study. The Saudi Dental Journal. 2023 Dec 27.
5. Beuling MG, Agterbos PC, van Riet TC, Ho JP, de Vries R, Kober J, de Lange J. Forces and movements during tooth extraction: A scoping review. Advances in Oral and Maxillofacial Surgery. 2023 Jan 7:100391.
6. Ahel V, Brekalo I, Ahel J, Brumini G. Measurement of tooth extraction forces in upper incisors. Collegium antropologicum. 2006 Mar 16;30(1):31-5.
7. Ahel V, Ćabov T, Špalj S, Perić B, Jelušić D, Dmitrašinović M. Forces that fracture teeth during extraction with mandibular premolar and maxillary incisor forceps. British Journal of Oral and Maxillofacial Surgery. 2015 Dec 1;53(10):982-7.
8. Lehtinen R, Ojala T. Rocking and twisting moments in extraction of teeth in the upper jaw. International journal of oral surgery. 1980 Oct 1;9(5):377-82.
9. Dietrich T, Schmid I, Locher M, Addison O. Extraction force and its determinants for minimally invasive vertical tooth extraction. Journal of the Mechanical Behavior of Biomedical Materials. 2020 May 1;105:103711.

10. Genna F, Paganelli C. Force–displacement relationship in the extraction of a porcine tooth from its socket: Experiments and numerical simulations. Journal of Mechanics of Materials and Structures. 2014 Dec 14;9(5):497-514.
11. Gadzella TJ, Westover L, Addison O, Romanyk DL. Inverse finite element analysis for an axisymmetric model of vertical tooth extraction. Submitted to the Journal of the Mechanical Behaviour of Biomedical Materials on February 23, 2024.
12. Gadzella TJ, Hynkova K, Westover L, Addison O, Romanyk DL. A novel method for simulating ex vivo tooth extractions under varying applied loads. Clinical Biomechanics. 2023 Dec 1;110:106116.
13. Chiba M, Ohshima S, Takizawa K. Measurement of the force required to extract the mandibular incisor of rats of various ages. Archives of Oral Biology. 1980 Jan 1;25(10):683-7.
14. Mohammadi SA. Association of inflammatory markers and growth factors with radiographically assessed wound healing of extraction sockets [MSc Thesis]. Omaha (USA): University of Nebraska Medical Center; 2023. Available from: https://digitalcommons.unmc.edu/etd/754/
15. Muska E, Walter C, Knight A, Taneja P, Bulsara Y, Hahn M, Desai M, Dietrich T. Atraumatic vertical tooth extraction: a proof of principle clinical study of a novel system. Oral Surg Oral Med Oral Pathol Oral Radiol. 2013;116(5):e303-10. doi: 10.1016/j.oooo.2011.11.037.
16. Hamed NA, Mohamed MH. Radiographic Evaluation of Bone Height Changes Around Immediately Placed Implant Retaining Mandibular Over-Denture in Atraumatic Tooth Extraction Cases. Egyptian Dental Journal. 2023 Jul 1;69(3):2035-43.
17. Schropp L, Wenzel A, Kostopoulos L, Karring T. Bone healing and soft tissue contour changes following single-tooth extraction: a clinical and radiographic 12-month prospective study. International Journal of Periodontics & Restorative Dentistry. 2003 Aug 1;23(4).
18. El-Kenawy MH, Ahmed WM. Comparison Between Physics and Conventional Forceps in Simple Dental Extraction. J Maxillofac Oral Surg. 2015;14(4):949-55. doi: 10.1007/s12663-015-0765-6.

19. Papadimitriou DE, Geminiani A, Zahavi T, Ercoli C. Sonosurgery for atraumatic tooth extraction: a clinical report. The Journal of prosthetic dentistry. 2012 Dec 1;108(6):339-43.
20. Sharma SD, Vidya B, Alexander M, Deshmukh S. Periotome as an Aid to Atraumatic Extraction: A Comparative Double Blind Randomized Controlled Trial. J Maxillofac Oral Surg. 2015;14(3):611-5. doi: 10.1007/s12663-014-0723-8.
21. Contractor MM, Bhate K, Londhe U, Awate S, Chhartriwala A, Samuel S. Efficacy of Periotome Versus Conventional Forceps Extraction in Socket Preservation and Reduction of Postoperative Pain: A Randomised Clinical Trial. Journal of Clinical & Diagnostic Research. 2023 Nov 1;17(11).
22. Makki AZ, Nassar AA, Alharbi WM, Bisharah WF, Alabdali MA, Alqurashi AM, Basandawa NA. Evaluation of post-extraction healing after atraumatic axial tooth extraction using Benex system II versus conventional extraction: Randomized control trial. The Saudi Dental Journal. 2021 Dec 1;33(8):923-8.
23. Hariharan S, Narayanan V, Soh CL. Split-mouth comparison of physics forceps and extraction forceps in orthodontic extraction of upper premolars. Br J Oral Maxillofac Surg. 2014;52(10):e137-40. doi: 10.1016/j.bjoms.2014.06.013.
24. Patel HS, Managutti AM, Menat S, Agarwal A, Shah D, Patel J. Comparative Evaluation of Efficacy of Physics Forceps versus Conventional Forceps in Orthodontic Extractions: A Prospective Randomized Split Mouth Study. J Clin Diagn Res. 2016;10(7):ZC41-5. doi: 10.7860/JCDR/2016/17724.8160.
25. Irshad F, Khan UQ, Memon ZA, Punjabi SK, Zaidi SA. Use of Physics Forcep Versus Conventional Forcep in Extraction of Mandibular First Molar: Physics Forcep Versus Conventional Forcep. Pakistan Journal of Health Sciences. 2023 May 31:123-8.
26. Tohar R, Alali H, Ansbacher T, Brosh T, Sher I, Gafni Y, Weinberg E, Gal M. Collagenase Administration into Periodontal Ligament Reduces the Forces Required for Tooth Extraction in an Ex situ Porcine Jaw Model. Journal of Functional Biomaterials. 2022 Jun 8;13(2):76.
27. Toms SR, Dakin GJ, Lemons JE, Eberhardt AW. Quasi-linear viscoelastic behaviour of the human periodontal ligament. J Biomech. 2002; 35(10):1411-1415. doi: 10.1016/S0021-9290(02)00166-5.

28. Pini M, Zysset PH, Botsis J, Contro R. Tensile and compressive behaviour of the bovine periodontal ligament. Journal of biomechanics. 2004 Jan 1;37(1):111-9.
29. Ho SP, Kurylo MP, Fong TK, Lee SS, Wagner HD, Ryder MI, Marshall GW. The biomechanical characteristics of the bone-periodontal ligament-cementum complex. Biomaterials. 2010 Sep 1;31(25):6635-46.
30. Oskui IZ, Hashemi A. Dynamic tensile properties of bovine periodontal ligament: a nonlinear viscoelastic model. Journal of Biomechanics. 2016 Mar 21;49(5):756-64.
31. Huang H, Tang W, Yang YU, Wu B, Yan B. Determination of viscoelastic properties of the periodontal ligament using nanoindentation testing and numerical modeling. Journal of Mechanics in Medicine and Biology. 2016 Sep 8;16(06):1650089.
32. Huang H, Tang W, Yang YU, Wu B, Yan B. Determination of viscoelastic properties of the periodontal ligament using nanoindentation testing and numerical modeling. Journal of Mechanics in Medicine and Biology. 2016 Sep 8;16(06):1650089.
33. Ho SP, Kurylo MP, Grandfield K, Hurng J, Herber RP, Ryder MI, Altoe V, Aloni S, Feng JQ, Webb S, Marshall GW. The plastic nature of the human bone–periodontal ligament–tooth fibrous joint. Bone. 2013 Dec 1;57(2):455-67.
34. Jang AT, Merkle AP, Fahey KP, Gansky SA, Ho SP. Multiscale biomechanical responses of adapted bone–periodontal ligament–tooth fibrous joints. Bone. 2015 Dec 1;81:196-207.
35. Lin JD, Jang AT, Kurylo MP, Hurng J, Yang F, Yang L, Pal A, Chen L, Ho SP. Periodontal ligament entheses and their adaptive role in the context of dentoalveolar joint function. Dental Materials. 2017 Jun 1;33(6):650-66.
36. Jang AT, Chen L, Shimotake AR, Landis W, Altoe V, Aloni S, Ryder M, Ho SP. A force on the crown and tug of war in the periodontal complex. Journal of dental research. 2018 Mar;97(3):241-50.
37. Najafidoust M, Hashemi A, Oskui IZ. Dynamic viscoelastic behavior of bovine periodontal ligament in compression. Journal of Periodontal Research. 2020 Oct;55(5):651-9.
38. Shibata T, Botsis J, Bergomi M, Mellal A, Komatsu K. Mechanical behavior of bovine periodontal ligament under tension-compression cyclic displacements. European journal of oral sciences. 2006 Feb;114(1):74-82.

39. Genna F, Annovazzi L, Bonesi C, Fogazzi P, Paganelli C. On the experimental determination of some mechanical properties of porcine periodontal ligament. Meccanica. 2008 Feb;43:55-73.
40. Najafidoust M, Hashemi A, Oskui IZ. Effect of temperature on dynamic compressive behavior of periodontal ligament. Medical Engineering & Physics. 2023 Jun 1;116:103986.
41. Uhlir R, Mayo V, Lin PH, Chen S, Lee YT, Hershey G, Lin FC, Ko CC. Biomechanical characterization of the periodontal ligament: Orthodontic tooth movement. The Angle Orthodontist. 2017 Mar 1;87(2):183-92.
42. Lin JD, Lee J, Özcoban H, Schneider GA, Ho SP. Biomechanical adaptation of the bone-periodontal ligament (PDL)-tooth fibrous joint as a consequence of disease. Journal of biomechanics. 2014 Jun 27;47(9):2102-14.
43. Papadopoulou K, Keilig L, Eliades T, Krause R, Jäger A, Bourauel C. The time-dependent biomechanical behaviour of the periodontal ligament—an in vitro experimental study in minipig mandibular two-rooted premolars. The European Journal of Orthodontics. 2014 Feb 1;36(1):9-15.
44. Oskui IZ, Hashemi A. Dynamic tensile properties of bovine periodontal ligament: a nonlinear viscoelastic model. Journal of Biomechanics. 2016 Mar 21;49(5):756-64.
45. Bosiakov S, Mikhasev G. Mathematical model for analysis of translational displacements of tooth root. Mathematical Modelling and Analysis. 2015 Jul 4;20(4):490-501.
46. Romanyk DL, Guan R, Major PW, Dennison CR. Repeatability of strain magnitude and strain rate measurements in the periodontal ligament using fibre Bragg gratings: an ex vivo study in a swine model. Journal of Biomechanics. 2017 Mar 21;54:117-22.
47. Knaup TJ, Dirk C, Reimann S, Keilig L, Eschbach M, Korbmacher-Steiner H, Bourauel C. Time-dependent behavior of porcine periodontal ligament: a combined experimental, numeric in-vitro study. American Journal of Orthodontics and Dentofacial Orthopedics. 2018 Jan 1;153(1):97-107.
48. Ansbacher T, Tohar R, Cohen A, Cohen O, Levartovsky S, Arieli A, Matalon S, Bar DZ, Gal M, Weinberg E. A novel computationally engineered collagenase reduces the force required for tooth extraction in an ex-situ porcine jaw model. Journal of Biological Engineering. 2023 Jul 17;17(1):47.

49. Baschong W, Weiss P, Imholz MS, Filippi A. Periodontal ligament on pulp-free root slices – an in vitro model for early tooth (re)integration. An exploratory study. Swiss Dent J. 2018 Nov 12;128(11):878-886. PMID: 30403326.
50. Heinonen V, Ruotsalainen TJ, Paavola L, Mikkonen JJ, Asikainen P, Koistinen AP, Kullaa AM. (2018) Alveolar bone remodeling after tooth extraction in irradiated mandible: An experimental study with canine model, Ultrastructural Pathology, 42:2, 124-132, DOI: 10.1080/01913123.2017.1422829
51. Provatidis CG. A comparative FEM-study of tooth mobility using isotropic and anisotropic models of the periodontal ligament. Medical engineering & physics. 2000 Jun 1;22(5):359-70.
52. McCormack SW, Witzel U, Watson PJ, Fagan MJ, Gröning F. Inclusion of periodontal ligament fibres in mandibular finite element models leads to an increase in alveolar bone strains. PLoS One. 2017 Nov 30;12(11):e0188707.
53. Uhlir R, Mayo V, Lin PH, Chen S, Lee YT, Hershey G, Lin FC, Ko CC. Biomechanical characterization of the periodontal ligament: Orthodontic tooth movement. The Angle Orthodontist. 2017 Mar 1;87(2):183-92.
54. Likitmongkolsakul U, Smithmaitrie P, Samruajbenjakun B, Aksornmuang J. Development and validation of 3D finite element models for prediction of orthodontic tooth movement. International journal of dentistry. 2018 Aug 30;2018.
55. Savignano R, Barone S, Paoli A, Razionale AV. FEM analysis of bone-ligaments-tooth models for biomechanical simulation of individual orthodontic devices. InInternational Design Engineering Technical Conferences and Computers and Information in Engineering Conference 2014 Aug 17 (Vol. 46285, p. V01AT02A081). American Society of Mechanical Engineers.
56. Su K, Yuan L, Du J. Bone remodeling under tooth loading. InTMS 2017 146th Annual Meeting & Exhibition Supplemental Proceedings 2017 (pp. 331-340). Springer International Publishing.
57. Amid R, Kadkhodazadeh M, Dehnavi F, Brokhim M. Comparison of stress and strain distribution around splinted and non-splinted teeth with compromised periodontium: A three-dimensional finite element analysis. Journal of Advanced Periodontology & Implant Dentistry. 2018;10(1):35.

58. Andreaus U, Colloca M, Iacoviello D. Coupling image processing and stress analysis for damage identification in a human premolar tooth. Computer methods and programs in biomedicine. 2011 Aug 1;103(2):61-73.
59. Papadopoulou K, Hasan I, Keilig L, Reimann S, Eliades T, Jäger A, Deschner J, Bourauel C. Biomechanical time dependency of the periodontal ligament: a combined experimental and numerical approach. European journal of orthodontics. 2013 Dec 1;35(6):811-8.
60. Nikolaus A, Currey JD, Lindtner T, Fleck C, Zaslansky P. Importance of the variable periodontal ligament geometry for whole tooth mechanical function: a validated numerical study. Journal of the mechanical behavior of biomedical materials. 2017 Mar 1;67:61-73.
61. Tuna M, Sunbuloglu E, Bozdag E. Finite element simulation of the behavior of the periodontal ligament: a validated nonlinear contact model. Journal of biomechanics. 2014 Sep 22;47(12):2883-90.
62. Natali AN, Pavan PG, Scarpa C. Numerical analysis of tooth mobility: formulation of a non-linear constitutive law for the periodontal ligament. Dental Materials. 2004 Sep 1;20(7):623-9.
63. Robinson D, Aguilar L, Gatti A, Abduo J, Lee PV, Ackland D. Load response of the natural tooth and dental implant: A comparative biomechanics study. The journal of advanced prosthodontics. 2019 Jun;11(3):169-78.
64. McCormack SW, Witzel U, Watson PJ, Fagan MJ, Gröning F. The biomechanical function of periodontal ligament fibres in orthodontic tooth movement. Plos one. 2014 Jul 18;9(7):e102387.
65. Natali, A. N., Carniel, E. L., Pavan, P. G., Sander, F. G., Dorow, C., and Geiger, M. (April 22, 2008). "A Visco-Hyperelastic-Damage Constitutive Model for the Analysis of the Biomechanical Response of the Periodontal Ligament." ASME. J Biomech Eng. June 2008; 130(3): 031004. https://doi.org/10.1115/1.
66. Ortún-Terrazas J, Cegoñino J, Santana-Penín U, Santana-Mora U, Perez del Palomar A. A porous fibrous hyperelastic damage model for human periodontal ligament: Application of a microcomputerized tomography finite element model. International Journal for Numerical Methods in Biomedical Engineering. 2019 Apr;35(4):e3176.

67. Maas SA, Ellis BJ, Ateshian GA, Weiss JA: FEBio: Finite Elements for Biomechanics. J Biomech Eng. 2012;134(1):011005
68. D'Errico, J. fminsearchbnd, fminsearchcon (), MATLAB Central File Exchange (2023). Available from: https://www.mathworks.com/matlabcentral/fileexchange/8277-fminsearchbnd-fminsearchcon
69. Moerman, KM. GIBBON: The Geometry and Image-Based Bioengineering Add-On. J Open Source Softw. 2018;3(22):506. doi: 10.21105/joss.00506
70. Wu B, Li N, Liu M, Cheng K, Jiang D, Yi Y, Ma S, Yan B, Lu Y. Construction of Human Periodontal Ligament Constitutive Model Based on Collagen Fiber Content. Materials. 2023 Oct 6;16(19):6582.
71. Ovy EG, Romanyk DL, Flores Mir C, Westover L. Modelling and evaluating periodontal ligament mechanical behaviour and properties: A scoping review of current approaches and limitations. Orthod Craniofac Res. 2022;25(2):199-211. doi: 10.1111/ocr.12527.
72. Su MZ, Chang HH, Chiang YC, Cheng JH, Fuh LJ, Wang CY, Lin CP. Modeling viscoelastic behavior of periodontal ligament with nonlinear finite element analysis. Journal of Dental Sciences. 2013 Jun 1;8(2):121-8.
73. Fung, YC. Biomechanics: mechanical properties of living tissues. 2nd Ed. New York (USA). Springer New York; 2013. Chapter 7, Bioviscoelastic Solids; p242-314.

6 Augmentation of an Atraumatic Extraction Device for Evidence-Based Extraction Protocols

This chapter completes Objective 3 of this thesis research by outlining the design of a computer interface for an instrumented Benex® extraction kit. The cognitive principles behind the design of the computer interface are presented. The interface is applied in ex vivo benchtop tests using the Benex® device on swine incisor samples prepared following the procedure outlined in Chapter 3 and Appendix A. This chapter demonstrates that the proof-of-concept interface is sufficient to allow the instrumented Benex® device to be used to perform tooth extractions following prescribed load schemes developed from the data provided in previous chapters.

6.1 Introduction

Previous measurements of tooth extraction biomechanics have focused on the forces applied with forceps due to their prevalence in performing routine extraction procedures. Attaching instrumentation to forceps is a considerable challenge due to their design and the size constraints of the oral cavity. Previous approaches include measuring the stress developed in the forceps handles with strain gauges [1] or airbags [2], both of which provide some insight into the forces and moments applied by the clinician. However, the applied forces and moments are translated to the dental complex through the frictional interface between the forceps jaws and the tooth, and act on the tooth in a combination of translational and rotational degrees of freedom. As a result, the action of these combined applied loads after transmission through the forceps interface and translation to the tooth's centre of rotation is not clear from the reported measurements. For example, pressure measurement at the forceps grips with airbags can identify the directions of moments applied by the clinician but cannot isolate individual force and moment components applied at the tooth surface. A robotic measurement system has been proposed as an alternative to better understand the kinetic and kinematic orientation of forceps movement during simulated extractions [3], but it remains unclear if this method can capture the translation of these loads to the dental complex because the measurements are also taken at the forceps grip. None of these instrumentation approaches have provided a characterization of extraction biomechanics sufficient to propose guidelines for extraction loading, nor have they been demonstrated to provide real-time measurement feedback to the clinician users towards implementing any such guidance.

Vertical tooth extraction with the Benex® device can be examined as a biomechanical loading case that does not share some of the limitations of forceps extraction. In vertical tooth extraction, the tooth root is loaded only along the direction of the attached cable (closely following the vertical axis of the tooth) [4] . The interface between the Benex® device and the tooth is a threaded connection that can be assumed to be much more rigid than the frictional grip applied with forceps, which in principle varies with the grip force. As a result, the transfer of load from the Benex® extraction device to the dental complex is more straightforward mechanically as compared to forceps, and involves no rotational transformations of forces to moments or vice versa. Vertical extractions with the Benex® device have been recorded with an attached load cell in response only to haptic feedback during the extraction, with clinicians judging the force level

applied to the tooth based on the resistance felt in turning the Benex® handwheel [4]. Similar to the work presented in Chapters 3 and 5, the study by Dietrich et al [4] was able to examine peak force as an indicator of extraction biomechanics, but this examination was performed after, not during, the extractions. Prior investigation of Benex® extractions have found that success of the extraction procedure is reduced by root size and complexity (which may be assessed prior to the extraction) [5]. However, the connections between root geometry, peak force, and extraction success have not been established between the findings of previous studies [4,5] and have only been investigated in the studies presented in Chapters 3 and 5. In this thesis chapter, a change to the operation of the instrumented Benex® device is proposed to create a feedback loop between the clinician and the instrumented Benex® device to allow for the pre-extraction planning of the applied extraction load and adherence to the planned procedure. The use of an instrumented device to provide feedback and guide vertical extractions based on force measurements has not been previously attempted due to the lack of biomechanical evidence to inform such procedures.

The work presented in Chapters 3-5 has provided the necessary data to preliminarily investigate instrumentation-guided vertical tooth extraction. The previous work in these Chapters has characterized the biomechanics of vertical tooth extraction in the ex vivo swine dental complex using both experimental and numerical approaches. The key findings of prior characterization towards informing instrument-guided extractions are: the sensitivity of the dental complex to load rate (Chapters 3 and 5); the non-linearity of the stiffness and viscoelastic behaviours of the dental complex (Chapters 4 and 5); and the predictable rupture behaviour of the PDL during various loads by the axisymmetric model implementing a visco-damage Arruda Boyce model (Chapters 4 and 5). The variation of dental complex response with loading regime has also been associated with the risk of tooth root fracture in the studies presented in the Chapters 3 and 5. Force-hold loading at a rate of 100N/min to thresholds of 175N or 200N has been proposed as a potential loading scheme that may reduce the peak force (and overall energy imparted to the dental complex) of vertical tooth extractions in the experimental swine model. The current chapter aims to demonstrate that an instrumented Benex® device such as that employed in the study by Dietrich et al. [4] can be used to achieve a force-hold loading scheme as a proof of concept for the application of biomechanically-derived loading schemes (which may be developed beyond the proposed force-hold scheme) with a clinical device.

The findings of Chapter 5 have established that there is a non-linear relationship between load and displacement throughout the extraction process, with demonstrated non-linear stiffness behaviours in the dental complex that depend on the applied loading rate. However, the instrumentation required for measuring the displacements imposed during extraction with a Benex® device (which would, in turn, permit the calculation and monitoring of instantaneous complex stiffness) is omitted from the version of the device used in this chapter. Displacement measurements have not been demonstrated for the Benex® devious previously, and further alteration of the device beyond the measurement of applied forces is omitted for the purpose of minimizing the impact on the device function and size (additional instrumentation increasing the mass and volume of the Benex® extractor). Omitting displacement-measuring instrumentation also reduces the required computational power of the interfacing computer (e.g. performing additional stiffness calculations and providing feedback to the user on how to interpret such outputs) which would increase the cost of the device unnecessarily and potentially negatively impact the complexity of operations during an extraction. Additional instrumentation may also change the operation of the Benex® device and reduce its familiarity to clinicians who have used previous versions of the instrumented device [5]. This is not to say that the measurement of only extraction force is not supported by the findings of Chapters 3 and 5. Peak extraction force has been demonstrated to be a good indicator of both the amount of energy imparted to the dental complex during an extraction and the risk of tooth extraction associated with that imparted energy. The completely force-controlled force hold schemes investigated in Chapter 5 also demonstrated promise for reducing the energy imparted during extraction, particularly when the PDL is mechanically compromised. Additionally, this chapter investigates the usefulness of providing instrumentation data as feedback to achieve a prescribed vertical tooth extraction load as an overall proof of concept that has not been previously investigated, and it is prudent to begin this investigation from an established device design.

The purpose of this chapter is to demonstrate a graphic computer interface as a proof of concept for using the load cell instrumented Benex® in a way that extends its capabilities from simply recording data to allowing the user to prescribe a load scheme and then follow it. In doing so, the importance of a biomechanically-informed approach to developing new load schemes for tooth extraction will be shown. The biomechanical characteristics of the dental complex investigated in Chapters 3 through 5 have demonstrated that an instrumentation system providing feedback to

guide extraction loading is necessary to improve extraction outcomes. The goal is to demonstrate the feasibility of such a system and lay the foundation for further device development that can include more complex loading factors, provide more complex calculated outputs guiding the extraction, and develop new load schemes outside the scope of those already developed in this thesis.

6.2 Methods

6.2.1 Physical Alteration of the Benex® Device

The adaptation of the Benex® extraction device to accommodate instrumentation with a load cell to detect extraction load, except for the design of a strain relief sensor housing, was completed prior to this thesis research. The arrangement of the Benex® device with these additional components is presented in Figure 6-1. The load cell housing was added as part of this thesis research to provide strain relief for the load cell cables. All other components were designed during previous research. The diameter of the FUTEK QLA401a pass-through button type load cell (FUTEK, Irvine CA, USA) used with this device is greater than the face of the connection in the Benex® device. For this reason, a tapered extension sleeve increasing to the load cell diameter is inserted between the Benex® device and the handwheel. A threaded extension is attached to the Benex® in place of the original handwheel that passes through the extension and load cell to accommodate a handwheel that is tapped at the appropriate diameter. The interior of the extension sleeve is hollowed to provide clearance for the thread extension.

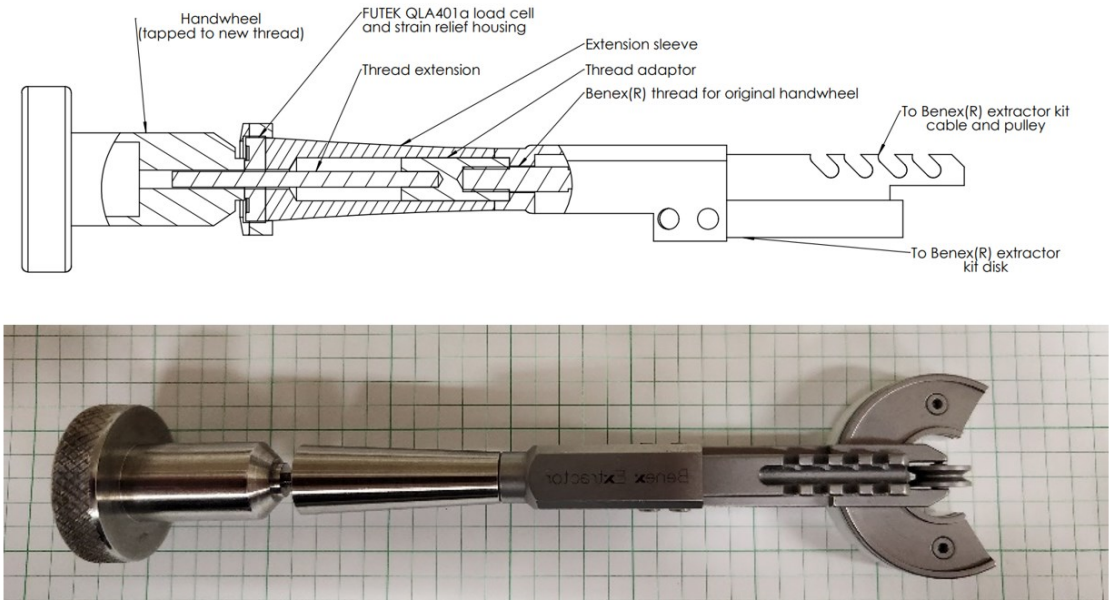

Figure 6-1: Top: annotated section view of the Benex® extension and load cell. Bottom: assembled Benex® extension (load cell and housing not shown)

During operation of the Benex® device, the handwheel is turned to create tension in the threaded slide. This tension is transmitted through the cable and pulley to the threaded insert and tooth. Opposing the imposed tension is compression between the contacting faces of the handwheel and the main body of the device. In the instrumented device, this compression occurs between the extension sleeve (through which the thread extension slides) and the handwheel. The load cell is placed between the handwheel and extension surfaces so that it can measure the compression as the handwheel is turned. The threaded extension, Benex® device slide, and tension cable are assumed to be sufficiently stiff that all tension measured at the handwheel is directly transmitted to the threaded insert and tooth root. The relationship between the applied torque, load at the tooth, and load cell instrumentation are demonstrated in Figure 6-2.

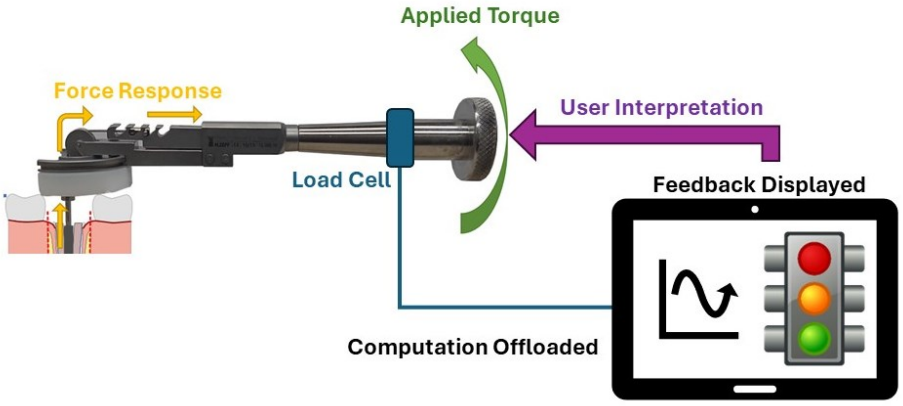

Figure 6-2: Diagram of the instrumented Benex(r) device and the control loop from the load cell to the computational interface and user action.

6.2.2 Computer Interface

The design of the interface is discussed in terms of the proximity compatibility principle (PCP) established by Wickens and Caswell [6], which provides a framework for understanding how data streams (e.g. load cell data), interface elements, and the user's cognitive load while performing a task or series of tasks interact. The pertinent core elements of the PCP can be summarized as follows:

- Anything that requires decision-making, attention, or memory retention from the user can be defined as "cognitive load";
- Spatial proximity among interface elements naturally correlates to cognitive proximity and association with the data streams they represent;
- Overcrowding of the interface space with congruent data streams and controls will cause confusion and frustration in the user;
- A single data source can have multiple streams represented in the interface based on an array of specific tasks that require multiple interpretations of the same data; and

Computational load, particularly the act of performing numerical comparisons, should be offloaded from the user while they are performing tasks under higher cognitive load such as having a conversation, operating multiple controls, or overseeing congruent tasks. Figure 6-2 demonstrates the intended interactions between the instrumented Benex® device to accommodate this offloading operation between the user and the computer interface. Two key tasks are required of the computer interface: to offload computational decision-making regarding

the loading regime from the user, and to display feedback that allows the user to take action (i.e. alter torque application) to meet the desired force level. Recording force data is included under the computational load undertaken by the computer interface.

The program underlying the computer interface combines a number of functional components that do not affect the use of the device but are necessary to collect and interpret data from the load cell. The load cell used in this study is a custom-manufactured FUTEK QLA401a pass-through button type load cell (FUTEK, Irvine CA, USA) which has been specifically designed to meet IP69 containment standards and can be sanitized in an autoclave – a quality vital to future clinical translation and use. FUTEK provides drivers and a dynamic link library to permit basic communication with the device using the Windows .NET framework. The .NET libraries can be accessed using IronPython, which is a limited Python 3 API for .NET. The IronPython script is subsequently controlled as a sub-routine program in Python 12.3, which provides access to the libraries used to process, record, and display load cell data along with all the interface control functions. The sample code for running the interface program and a list of the required dependencies is available in Appendix F.

The design of the graphic user interface is intended to isolate sources of data relating to the main tasks involved in using the instrumented Benex® device, namely setting up the test parameters (e.g. setting the desired load rate and force-hold threshold) and performing the test itself. These tasks have completely separate source flows of data - during setup, the data flow is from the user to the interface. Cognitive load is placed on the user by the selection of the experimental parameters with the calculation and graphical display of the entered load scheme offloaded to the computer. During the test, the flow of data is reversed, where the data source is the instrumented Benex® device which flows to the computer. The computer performs offloaded calculations comparing force data to the desired targets and providing feedback flow through the interface to the user. In this case, the only data stream from the instrumented Benex® device is from the load cell, and the offloaded calculations are simple comparisons between the target loading curve and the instantaneous readout from the load cell. This arrangement of data streams and calculations is relatively low in computational power requirement compared to other parameters that could be included in an extraction loading scheme, such as the calculation and comparison of instantaneous stiffnesses. The interface is coded to separate these tasks by having each occur in a

separate screen, creating a low degree of cognitive proximity between tasks and reducing the information access cost (IAC) [6] for the data in each separate stage by reducing potentially distracting elements. Within each window, interface elements associated with separate sub-tasks are arranged in close spatial configurations that can be used for the sub-task and then ignored. Throughout the workflow of a prescribed extraction, interface elements are selected that reduce the use of a keyboard because it is anticipated that procedures are performed while wearing gloves. Additionally, computer mice and touchscreens require much less dexterity to use and are easier to sanitize than keyboards.

The first window in the interface is used to set up the experimental parameters and data recording. A screen capture of this interface window is presented in Figure 6-3.

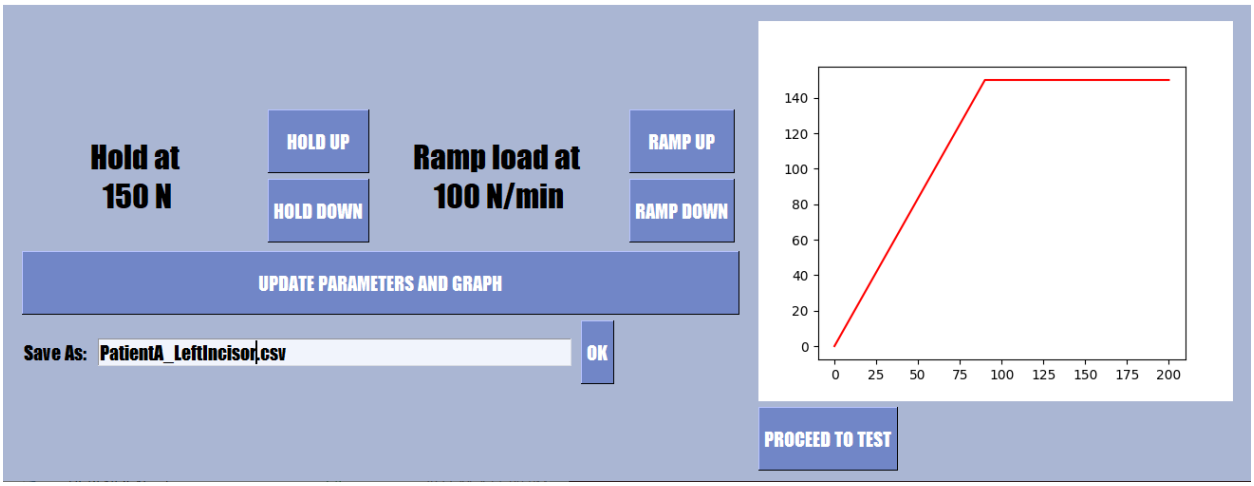

Figure 6-3: Screen capture of the first page for the Benex(r) interface. Dark blue features are single-press buttons.

Two parameters are needed to prescribe a force-hold loading scheme: the initial loading rate and the force threshold. The hold period length was not prescribed in this proof-of-concept version of the software. Each parameter has a set of toggles used to increase or decrease the values in increments of 25N(/min). A separate button plots the predicted force-time chart in the element to the right of this cluster. Below these controls is a text input box for entering a filename for saving the data. This is the only element in the interface that requires the use of the keyboard and can be circumvented because the program automatically enters the current date and time as a default file name. Another button accepts the entered filename text.

The second page, which is dedicated to performing the extraction itself, is demonstrated in Figure 6-4. The task of performing an extraction is subdivided into the tasks of taring the load cell, controlling the extraction, and receiving feedback for piloting the Benex® device. Each of these subtasks has elements with a high degree of nonintegrative similarity (i.e. they display the same data from the load cell but in different ways, for different purposes) and are arranged in close spatial proximity with the element required for that subtask. The numeric readout of the load cell is prominently displayed in the top left, immediately adjacent to the Tare and Gross function buttons. To the right of the screen is the cluster dedicated to controlling the extraction. This cluster features a plot which displays both the target load and load cell readings with buttons labelled “Stop”, “Start”, and “Pause” which allows the user to control the advance of the plot through the specified load curve. These controls also oversee data collection. The third element is a coloured indicator, or “stoplight”, which changes colour depending on how well the load cell reading matches the target load. The stoplight is yellow when the load is within 5% of the target, red when the load exceeds the target by more than 5%, and is otherwise green. The 5% threshold currently used is semi-arbitrary and may be altered depending on desired targets informed by a given clinical scenario. This feedback mechanism was placed in its own, high-contrast interface element because the force feedback will be used during the extraction procedure when cognitive load on the user from external sources such as monitoring patient condition will be at their highest. Placing this feedback data stream in its own element, rather than changing another element such as the text colour of the numeric readout or background of the plot, creates cognitive separation between tasks to avoid confusion and distraction in the user. Notably, this scheme for providing feedback to the instrumented Benex® user can accommodate any force-controlled loading scheme that can be expressed as a function of time and can accommodate built-in logic (such as in the force-hold scheme, which changes the target force function from a linear ramp to a constant value when the target load is met).

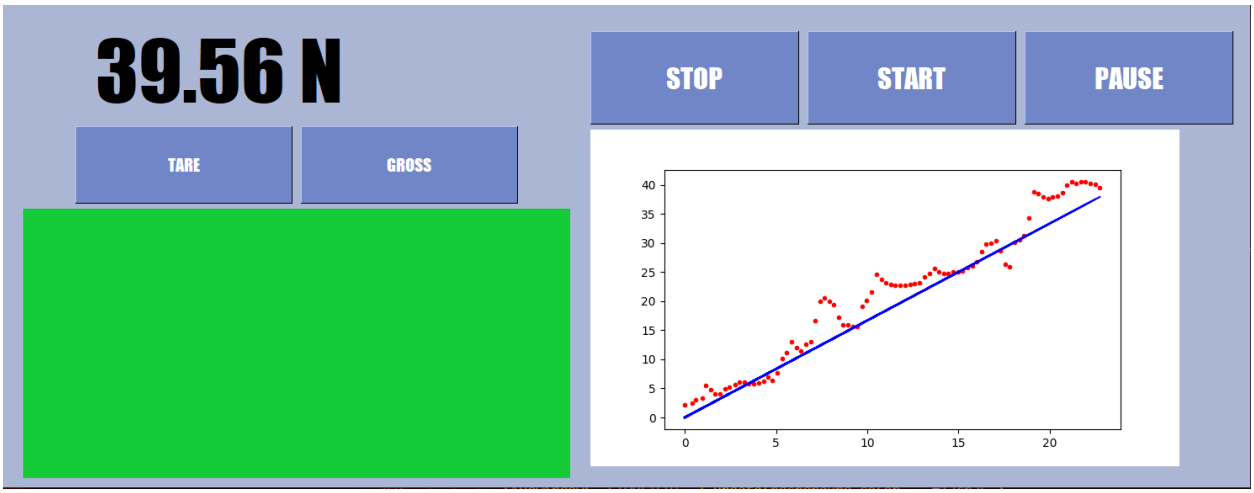

Figure 6-4: Screen capture of the second screen of the Benex(r) interface. The "stoplight" feature in the bottom left displays green in this capture. In the force-time plot (bottom right), the blue line is the target force profile and the red dots are the load cell measurements.

6.2.3 Ex Vivo Benchtop Tests

Ex vivo tests using swine incisors were performed to assess the interface as a proof-of-concept for assisting in controlling vertical tooth extraction. Swine incisors were prepared using the procedure developed in Chapter 3. Samples were still potted in dental stone to match the protocol adopted in Chapter 3. The Benex device was allowed to rest on the dental stone during the extraction (as demonstrated in Figure 6-5). The dental stone was machined as-needed to provide a stable mounting surface. Extractions were performed by a laboratory member with no clinical experience or training but who was familiar with the operation of the Benex® device from case video review and had never used the device to perform ex vivo extractions in the laboratory.

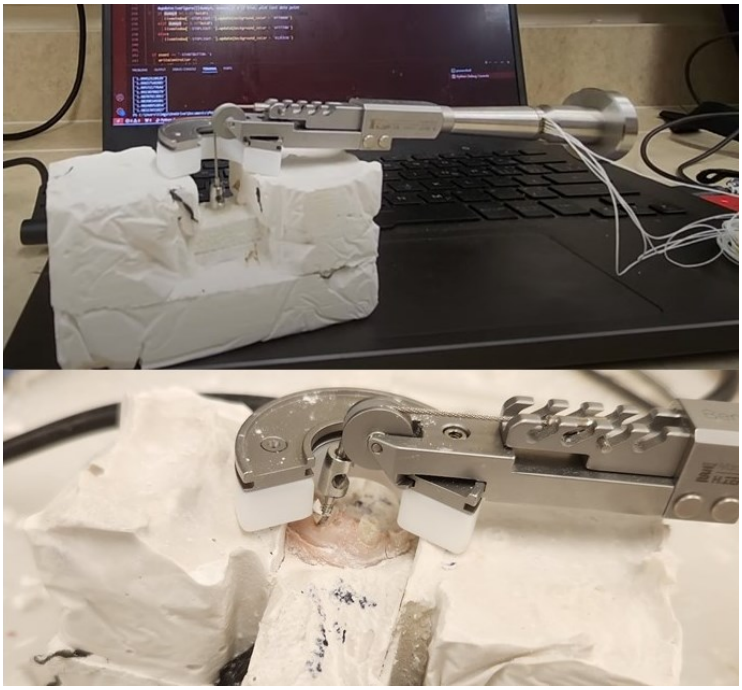

Figure 6-5: Top: the instrumented Benex® device resting on dental stone during a benchtop test on a simulated dental complex; Bottom: the Benex(r) extraction kit mounted to a potted dental stone sample with a fractured right swine incisor.

Two force thresholds (175N and 200N) were investigated at two different initial ramp rates (50N/min and 100N/min), resulting in a total of four load schemes that were investigated in this study. These load schemes were selected to match the force-hold load schemes developed in Chapter 5. The 50N loading rate was determined as half of the 100N/min load rate employed in Chapter 5 to determine if the instrumented device would be effective at slower rates requiring finer control of the Benex® handwheel. Three extractions were performed for each scheme (n=12 total). For each extraction scheme, the force-hold period was limited to 500s at which point the extraction load was increased at the operator's discretion until extraction of the tooth was completed. Post-hold loading at the operator's discretion consisted of targeted increases of 25-50N increments with indeterminate lengths of time at each increased force level depending on any perceived motion in the tooth based on the amount of rotation provided to the Benex® handwheel. Extractions were guided only using the computer interface running on a laptop with a USB mouse and keyboard.

6.3 Benchtop Testing Results

The force-time data collected during benchtop testing of the Benex® device and computer interface are shown in Figure 6-6.

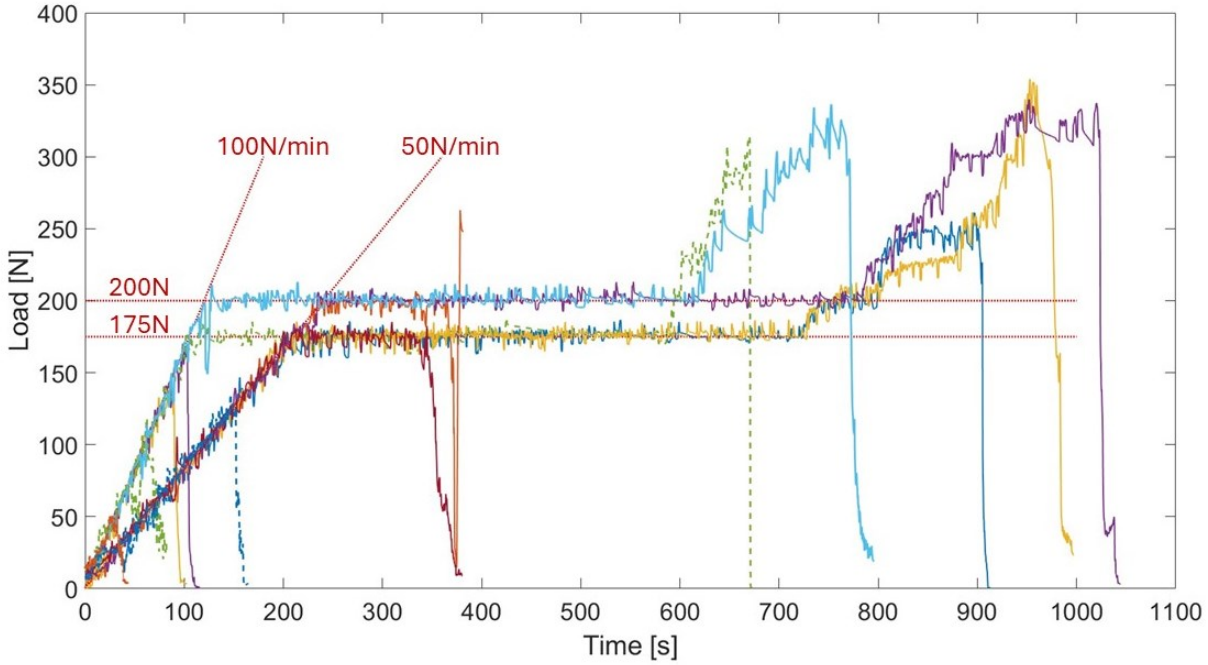

Figure 6-6: Force-time traces collected during ex vivo extractions with an instrumented Benex(r) device and updated computer interface. Each coloured curve indicates a separate extraction. Dashed coloured curves indicate extraction failure due to tooth root fracture.

One extraction was omitted due to a failure at the interface of the threaded Benex® screw and the tooth root which could not be recovered by re-drilling the root at a larger thread size. Three other extractions failed due to fracture of the tooth root during loading either in the initial ramp or post-hold phases. All three extraction behaviours observed in the previous ex vivo study on force-hold extraction schemes (Chapter 5) are present, with teeth releasing from the socket in the initial loading, force-hold, and post-hold loading phases. The frequency of extraction in each of these phases is summarized in Table 6-1.

Table 6-1: Frequency of extractions in different phases during benchtop instrumented Benex® extractions on ex vivo swine incisors (n=11 total). Failed extractions included in parentheses.

	Extraction Phase		
Load Scheme (Ramp / Hold)	**Pre-Hold**	**Holding**	**Post-Hold**
50N/min / 175N	0	1	2
50N/min / 200N	(1 failed due to root fracture)	1	1
100N/min / 175N	1	0	(1 failed due to root fracture)
100N/min / 200N	1 (1 failed due to root fracture)	0	1

The adherence of the measured force signal applied with the Benex® device to the target schemes is close in all cases, including those that resulted in failed extraction. Periodic deviations in force are present in all cases as the Benex® handle was released by the operator for frequent repositioning of the turning hand (Figure 6-7). The combination of the plot and stoplight elements guided the constant application of torque driving rotation of the Benex® handle during the force-hold period, but it was observed that maintaining constant torque against the resistance of the system caused rapid fatigue in the turning hand.

The force-time traces presented in Figure 6-7 are examples of how closely the target loading schemes were followed in this study. The 100N/min trace demonstrates close adherence of the device loading to the target curve during the loading phase, with small drops in force associated with the operator releasing the handwheel to reposition their hand. The 50N/min loading phase time trace is similarly adherent, with a sudden increase in force at approximately 95 seconds. This deviation from the loading curve demonstrates how the feedback elements of the interface are effective in communicating deviations from the target curve that may not be detected through haptic feedback alone, as the load in the Benex® device was quickly adjusted to return to the

target load. A similar deviation and correction are present in the 100N/min trace as it reaches the force-hold threshold of 200N.

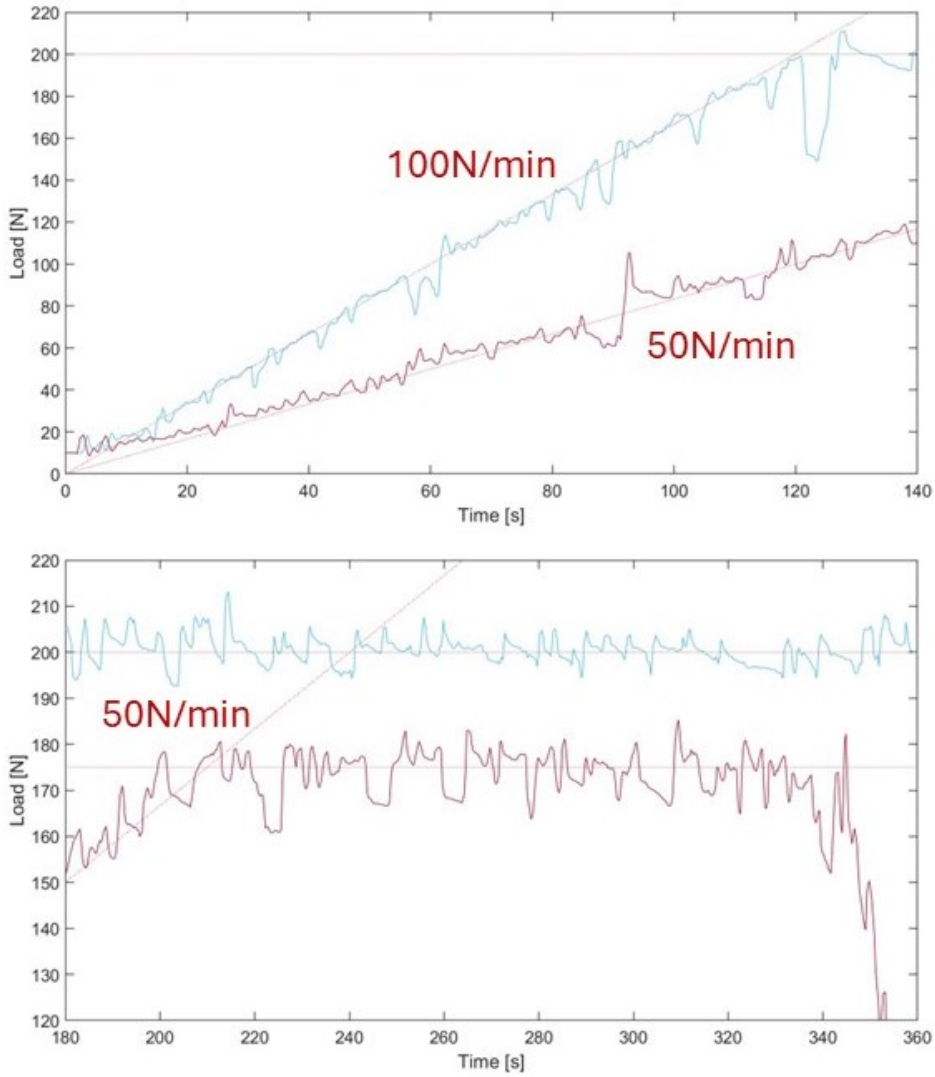

Figure 6-7: Isolated force-time traces from an extraction at 100N/min to 200N (blue) and at 50N/min to 175N (brown). Top: time traces during the loading phase; Bottom: time traces during the force-hold phase

The adherence of the device loading curves to the force-hold threshold targets is also subject to variation due to changes in the position of the operator's hand. There is a slight amount of backlash in the threaded components of the Benex® device resulting in drops in measured force when the handwheel is released. The 175N force-hold trace in Figure 6-7 is subject to larger changes in force as the dental complex underwent greater displacement, requiring larger

rotations to the Benex® handwheel and more frequent adjustment. In contrast, the 200N threshold trace demonstrates relatively stiff behaviour during the force-hold period, with more frequent (and lower force-reducing) adjustments.

6.4 Discussion

Previous efforts to introduce instrumentation in tooth extraction procedures have focused on gathering mechanical loading data from extraction forceps [1-3] and have faced challenges in translating the clinician-applied load at the forceps grips or along the forceps handles to the load state applied to the dental complex. These challenges have also limited the development and application of biomechanical guidelines for extraction procedures to improve clinical outcomes related to the damage caused by tooth extraction and the development of atraumatic extraction techniques. Vertical tooth extraction, specifically performed with a Benex® device, provides a clinical extraction case with a more direct relationship between measurable forces applied to the device [4] and the load distributed to the dental complex by largely eliminating rotational moments and transverse forces. Instead, the tooth root is loaded only along its primary long-axis with a rigid threaded connection between the device and the tooth root that eliminates the translation of remote loads to the tooth root's centre of rotation.

The purpose of this thesis chapter was to demonstrate proof-of-concept for vertical tooth extraction using the Benex® device with accompanying instrumentation and a computer interface that allowed for the application of extraction load following a prescribed loading regime. The application of the findings of Chapter 5 (the development of the force-hold loading scheme) in this benchtop study proves that the characterization data accumulated throughout this thesis can be used to develop new loading schemes. The prescribed loading regime in this chapter was expanded from Chapter 5 to include the 50N/min load rate, resulting in four combinations of load rate (100N/min and 50N/min) and maintained threshold (175N and 200N). The findings of Chapter 5 indicated that loading to 175N and 200N hold forces resulted in extraction before, during, or after a holding period of 500s, during which the dental complex underwent creep extension. This behaviour is reflected in the findings of this chapter, which demonstrate the same behaviours (Figure 6-6 and Table 6-1), although the loading applied after the 500s hold period in this chapter does not ramp at a constant rate. Instead, the force applied following the force-hold period is controlled arbitrarily by the user. The similarity between the

benchtop and material test frame results critically demonstrates that the experimental-numerical development loop from Chapter 5 can accurately predict the response of the dental complex when extraction load is applied with a clinical device, which confirms the validity of the biomechanically-informed approach to developing new extraction loading schemes.

The performance of the instrument-interface Benex® device is demonstrated through the ability of an operator with no previous clinical experience to perform vertical tooth extractions while closely following the prescribed loading schemes. Force-time data collected in all four extraction schemes (examples of which are presented in Figure 6-7) demonstrated good adherence between the force applied with the Benex® device and the target traces. The force-time traces measured from the Benex® device show small, regular deviations about the target load due to the operator loading the device by hand with frequent repositioning and some larger deviations due to over- or underloading the device. The example traces in Figure 6-7 also demonstrate that the computer interface was able to guide the user in recovering to the target load in these instances. In turn, this indicates that the combination of interface elements was appropriate for the benchtop testing case at providing the necessary feedback to the user. It was also observed that the force readout and plot elements were helpful when it was necessary to deviate from the prescribed load trace during post-hold loading. While this use of the interface does not completely offload decision-making from the user (as in the prescribed loading regimes when the "stoplight" element performs force comparisons and issues a stop-go set of signals directly to the user), it does show that a simple, but high-contrast and informative interface may be critical to allowing users to adapt to changing conditions or interpret external stimulus. For example, auditory feedback such as high-frequency cracks are important feedback that a Benex® operator receives which, based on their occurrences in the laboratory models presented in Chapters 3 and 5, may indicate fracture of the hard tissue, slip in the mechanical elements, or a number of other potential events have occurred. The force-time trace displayed on the computer interface can help interpret this signal (e.g. a click coupled with a large drop in the force plot indicating fracture of a hard tissue and failure of the extraction). This phenomenon was observed particularly in the post-hold loading phase of extractions, when the force feedback received haptically from the device was compared to all three interface elements during typical visual "sweeps" of the interface [6] as part of the cognitive task of determining if further torque should be applied.

By establishing the effectiveness of the instrumented Benex® device and the biomechanically-informed approach to prescribing vertical extraction load, the findings of this chapter provide the foundation for further development of extraction loading schemes. The interface and instrumentation used in this chapter do not measure displacement, disallowing the calculation of instantaneous complex stiffness as a controlling variable. The findings of Chapter 5 indicate that the instantaneous stiffness of the dental complex increases with higher load rates, which are associated with a greater risk of extraction failure due to tooth root fracture. Based on the findings of this chapter, a similar feedback mechanism to the "stoplight" implemented in this chapter could be used to guide schemes based on stiffness measurements. These load schemes have not been developed but the methods developed in previous Chapters may be used to devise the necessary parameters to define them. For example, numerical and physical experiments as demonstrated in Chapter 5 may be performed to determine a limiting stiffness threshold during loading that should not be surpassed in order to improve extraction success. The findings of this chapter demonstrate that in silico simulations and validation of the determined load schemes with the material test frame method are a viable path to develop load schemes for use with an appropriately-instrumented device. The force-hold loading scheme implemented in this chapter is a low-computational cost proof-of-concept for further development based on an instrumented device concept that has already been applied in clinical extractions [4]. Future work towards effective evidence-driven prescribed schemes will need to balance computational power requirements and the addition of further instruments to the Benex® device with the improved outcomes of a biomechanically-informed extraction procedure.

This proof-of-concept study of the tooth extraction computer interface illustrates some limitations for the benchtop testing method. A laptop with mouse and keyboard peripherals was used in this study but the use of the interface with a touchscreen device should be investigated. Touchscreen interfaces are much more straightforward surfaces to sanitize than both a mouse and keyboard and a Windows operating system (as was used in this study) should allow natively for the use of the touchscreen for typing when required. A touchscreen also reduces clutter and subsequently may improve uptake with clinician users, even during pre-clinical device development. This study also performed the extractions on ex vivo animal specimens without the spatial constraints of the oral cavity, allowing the benchtop user to freely look between the extracted tooth and computer screen in their periphery. Future work in pre-clinical testing of

instrumented extractions with this computer interface may need to consider the breadth of the visual field imposed by the oral cavity.

6.5 Conclusion

This proof-of-concept study demonstrated the design of a computer interface for force-instrumented vertical tooth extraction with the Benex® device. The proximity compatibility principle of interface design was demonstrated in the arrangement of computer interface elements to facilitate task flow through benchtop extractions. Three different feedback elements based on the measured extraction force were demonstrated on the computer interface to guide a novice user to perform ex vivo vertical tooth extractions following prescribed force-hold load schemes with good effect. This application of a computer interface specifically designed to guide vertical tooth extraction is a novel one, providing a foundation for the application of novel loading schemes in the design of clinical extraction procedures.

References

1. Lehtinen R, Ojala T. Rocking and twisting moments in extraction of teeth in the upper jaw. International journal of oral surgery. 1980 Oct 1;9(5):377-82.
2. Ahel V, Ćabov T, Špalj S, Perić B, Jelušić D, Dmitrašinović M. Forces that fracture teeth during extraction with mandibular premolar and maxillary incisor forceps. British Journal of Oral and Maxillofacial Surgery. 2015 Dec 1;53(10):982-7.
3. Riet TV, Graaf WD, Lange JD, Kober J. Analysis of movements in tooth removal procedures using robot technology. Plos one. 2023 May 18;18(5):e0285503.
4. Dietrich T, Schmid I, Locher M, Addison O. Extraction force and its determinants for minimally invasive vertical tooth extraction. Journal of the Mechanical Behavior of Biomedical Materials. 2020 May 1;105:103711.
5. Muska E, Walter C, Knight A, Taneja P, Bulsara Y, Hahn M, Desai M, Dietrich T. Atraumatic vertical tooth extraction: a proof of principle clinical study of a novel system. Oral Surg Oral Med Oral Pathol Oral Radiol. 2013;116(5):e303-10. doi: 10.1016/j.oooo.2011.11.037.
6. Wickens CD, Carswell CM. The proximity compatibility principle: Its psychological foundation and relevance to display design. Human factors. 1995 Sep;37(3):473-94.

7 Conclusion

The presented thesis demonstrates the thorough characterisation of the dental complex during vertical tooth extraction, from the development of novel ex vivo methods and numerical models through their implementation to the design and testing of extraction loading schemes with an instrumented clinical device. The purpose of this characterisation was to provide an engineering biomechanics approach to the understanding of vertical tooth extraction, currently absent in the literature, necessary for the advancement of atraumatic extraction devices and procedures. This was achieved through the completion of three objectives:

1. To experimentally characterize the mechanical behaviour of the ex vivo dental complex during controlled vertical tooth extraction and develop preliminary metrics for predicting procedure success;
2. To develop a generalizable finite element model of the dental complex that predicts the mechanics of tooth extraction for applications in future procedural and device development and validate it using the experimental characterisation data obtained in Objective 1; and
3. To apply the findings of Objectives 1&2 towards the improvement of atraumatic exodontia procedures by augmenting a clinical device with instrumentation and feedback mechanisms allowing the further investigation of extraction procedures based on the predictions of the experimental and numerical models.

The completion of Objective 1 depended on the development of a robust experimental method for characterizing vertical tooth extraction, which was completed in Chapter 3. This method improved on previous methods for simulating extraction [1-3] by implementing attachment parts directly taken from the Benex® vertical extraction kit and the adoption of a novel self-aligning apparatus. The removal of the tooth crown necessary to use the threaded insert and cable reduced the moment arm causing bending due to any eccentricities in loading direction, reducing the likelihood of brittle crack propagation relative to previous methods of drilling through the crown transversely [1]. This inclusion also improved the clinical relevance of the experimental model relative to previous methods [1-3]. Chapter 3 also introduced the mechanical metrics that were examined towards completing Objective 1. Peak force has been previously examined as a metric for the energy imparted to the dental complex during an extraction, but the analytical methods

described in Chapter 3 introduce the calculation of instantaneous stiffness during tissue extension (identified with video analysis) as a parameter of interest, further demonstrating the robustness of the experimental method.

The characterisation study presented in Chapter 5 applied this experimental method and demonstrated the sensitivity of the dental complex response to load rate. Higher peak forces and instantaneous stiffness behaviour were both associated with higher loading rates in force- and displacement-control. Higher rates were also associated with greater incidence of extraction failure. Failure cases tended to be longitudinal root fractures throughout the characterisation studies, with only two cases of bone fracture observed with post-extraction palpation (a single case, captured during testing) or imaging (noted in the post-hoc imaging only). RSAA was determined to increase peak extraction force to a similar extent as the imposed increases in load rate across the range of geometries in this study. The addition of geometric data (RSAA) expanded on previous findings [1-3], but this thesis was the first to examine geometric effects in direct relation to the influence of applied load on peak extraction force, which further fulfills Objective 1's aim of a complete biomechanical characterisation.

The completion of Objective 1 also included the illustration of rupture behaviour in the PDL demonstrated with CE- μCT in Chapter 5. It is well established that PDL rupture dominates the mechanics of tooth extraction but, in completing Objective 1, the presented work has begun to investigate the detailed mechanics of this process. The contributions of each tissue in the dental complex to its biomechanics could not be determined with the available imaging methods (e.g. surface level optical tracking during extraction and post-hoc μCT and CE- μCT). Instead, a robust characterization of the dental complex as a whole has been performed in this thesis with indicators of the importance of boundaries between tissues. The entirety of the complex response could be attributed to the PDL, but this is not a physically realistic assumption that neglects the extension of the hard tissues of the tooth and bone and should be approached cautiously given that microdamage accumulation and fracture of the hard tissues is a primary concern in extraction biomechanics. Even in manipulating only PDL parameters to fit dental complex responses in Objective 2, the representation of the hard tissues and extraction screw are important features of the axisymmetric FE model. Focusing on the PDL was required to be able

to fit the model parameters but future work should examine the sensitivity of the model to changes in the mechanical and damaging properties of other dental complex tissues.

Objective 2 was completed through the development of the numerical axisymmetric model of the dental complex proposed in Chapter 4. Completion of this objective depended greatly on the strength of the biomechanical characterisation performed under Objective 1, which was used in an IFEA solution process to determine PDL parameters. Initial IFEA solutions found in Chapter 4 revealed the optimization error function to be non-linear and non-convex throughout the domain. These characteristics were imposed in part by the attempt to include all three of hyperelastic, viscoelastic, and damage behaviours in the PDL model. Limiting the permissible domain for FE rupture to above the 50N transition time and the addition of quadratic terms for the peak force and time-to-peak force also contributed to this function behaviour. The importance of selecting a starting point for the optimization based on values from the literature was strongly demonstrated and the result was a set of locally-smooth optima that represented the experimental data.

The strengths of the FE model developed for Objective 2 were further demonstrated in Chapter 5. There was minimal adjustment to the PDL parameters when the IFEA process was repeated with the full characterisation data set. Some limitations of the axisymmetric model were demonstrated, such as the limited reflection of non-linear PDL viscoelasticity, but the proposed model was demonstrated to be successful at explaining the breadth of the characterisation data. The interfaces between the PDL and hard tissues are active sites of strain which the model formulation permits to damage and deform through the inclusion of a principal-strain-based damage criterion that downregulates the stress response of the elements as strain increases, effectively “softening” the interface. This reflects the findings of previous work on the literature that these are not abrupt boundaries but transition zones of structural and mechanical significance [4]. Future work into the nature of PDL rupture at these boundaries may provide insight into better representing these interfaces in the axisymmetric model. Notwithstanding this limitation, the strain-regulation damage formulation employed in this objective is sufficient for a generalizable predictive tool. The model demonstrates localised strain behaviour and rupture initiation at the tooth-PDL boundary that is strongly represented in the imaging findings of Objective 1, solidifying the physical relevance of the axisymmetric model.

The predictive power of the axisymmetric model has been demonstrated in the predictions of force-hold loading behaviours in Chapter 5, which is a critical step in the development of new loading regimes that fulfill Objective 3. A hypothetical force-hold loading scheme was proposed from biomechanical data (a process which has not been soundly demonstrated in the literature) and tested using the developed numerical model. The model predicted a middle-ground behaviour of rupture during the force-hold period that was reflected by subsequent validation with the experimental model, in which the PDL ruptured to complete extraction before, during, and after the force-hold period. Some variation in this behaviour was anticipated and was demonstrated through teeth being extracted at various stages in the experimental model. Similarly, the model was shown as a tool that can rapidly simulate a range of different conditions to predict an unknown condition, such as the damaged PDL tests performed in Chapter 5. The exact nature of the damage imposed by the periotome to the PDL could not be known, but range of conditions were simulated that encapsulated the rupture times and stiffness changes that were found in subsequent experimental testing. This predictive loop has not been demonstrated in the literature surrounding tooth extraction and was achieved with a relatively simple numerical model that did not require customization of the FE software or high-powered image processing.

Chapter 6 further cements the foundation for applying the data-driven approach of Objective 3 towards advancing vertical extraction techniques. The design and use of a computer interface that provides feedback to an instrumented Benex® device operator was demonstrated to allow the operator to follow a prescribed loading scheme. The difference between the computer interface and the recording and plotting functions provided with OEM instruments is that the interface was intentionally designed to facilitate the extraction process by offloading decision-making from the user. This software itself is simple in its implementation and can be adapted to other load-control extraction schemes. A novice operator was able to perform tooth extractions on the ex vivo model with varying loading parameters and precisely replicate the desired load traces. The results of the benchtop ex vivo extractions were similar to the experimental ex vivo and numerical predictions of behaviour under force-hold loading in that extractions completed in the pre-, during, and post-hold phases in the benchtop experiments. The similarity between the benchtop and material test frame experimental results (and their variation around the prediction of the numerical FE model) validates the evidence-based approach proposed in this thesis for developing new extraction loads, and highlights the necessity of both numerical and

experimental methods developed in Chapters 3-5. The completion of Objective 3 in Chapters 5 and 6 demonstrates the use of the numerical FE model to develop a new extraction scheme, its validation with the experimental characterisation method, and adaptation of instrumentation and feedback devices that allow the extraction scheme to be implemented on the benchtop. The result of this workflow is an evidence-informed novel extraction loading scheme with a validated instrumented clinical device that is sufficiently prepared for clinical testing. This thesis proves conclusively that the biomechanics approach, coupled with the appropriate instrumentation and feedback mechanisms, is a viable path towards improving extraction procedures.

7.1 Future work

Future work can add to the characterisation performed in Objective 1 in two ways. First, there is a technical challenge outside the scope of this thesis to be overcome in the in situ imaging of vertical extractions to determine the individual contributions of the tissues in the dental complex to its overall response. Some in situ methods discussed in Chapter 2 are capable of examining changes in PDL fibre alignment over small displacements but pose the risk of interfering with the mechanical outcomes of the experiments (e.g. by denaturing tissue through transmission X-ray exposure). Further advancement is required to balance the capture of tissue motion with the mechanical integrity of the experiment. Similarly, future work should seek to examine the role of the tissue interfaces in the denudement rupture behaviour demonstrated in the CE-μCT images gathered in Objective 1. This technological challenge that may be solved with higher-power imaging modalities such as synchrotron source phase contrast imaging that can capture the behaviour of laminar and penetrating fibrous structures at the hard tissue boundaries of the PDL.

The development of the axisymmetric model for Objective 2 did not include a method for varying the model geometry, which was found to be an important factor in Objective 1, but rather fit a single representative geometry to the entire cluster of gathered experimental data. This allows the model to be employed as a predictive tool for the mechanics of the ex vivo experiment without needing to attempt to predict individual variations in sample geometry. Instead, the model provides a good prediction for a range of extraction behaviours and, like all predictions, is subject to an amount of variance. Future work may examine the performance of the model under simple parameterizations of subject-specific geometry or extension to a fully 3D

subject-specific geometry, but introducing the complexities and computational expense of image processing and remeshing is antithetical to the aim of developing an accessible predictive tool.

As a proof-of-concept design for the application of biomechanically-derived loading schemes with a clinical device, the design concept presented in Chapter 6 lays the foundation for further development of extraction procedures and instruments. Future work originating from this proof of concept will consist of iterative interface design, adding and adjusting features to provide feedback to clinicians while maintaining the PCP philosophy adopted in the Chapter 6. Notably, the findings of Chapters 3 and 5 demonstrated that instantaneous stiffness was a measureable quantity sensitive to the underlying loading rate that may be control extraction procedures but the instrumentation necessary to measure stiffness (i.e. displacement) was not included in this thesis. Omitting these measurements allowed the proof-of-concept study to use a low-computational-cost interface based on a previously-implemented version of the instrumented Benex® device [5]. Implementing this interface concept in clinical practice and extending the measurement capabilities of the instrumented Benex® device are extended processes that requires further software development, hands-on feedback with clinicians, and the development of training materials that is outside the scope of the presented research.

7.2 Contributions

The key contributions of this thesis research are presented here divided into basic and applied scientific levels. The basic scientific contributions of the research are:

- An extensive data set describing the response of the ex vivo swine dental complex to vertical extraction load under varying load regimes, coupled with a set of imaging data that aids in describing patterns of PDL tissue rupture;
- Quantification of the effect of tooth geometry (represented by RSAA) and its relationship with applied load rate on affecting peak extraction force; and
- The finding that peak force and instantaneous stiffness are mechanical variables that respond to changes in applied load rate during extraction and are related to the success of the extraction procedure.

The applied scientific contributions of the research are:

- A novel experimental method for simulating vertical tooth extraction that improves on previous methods to realistically represent extraction loading and apply a high degree of experimental control, reflected in the sensitivity of the experiments and improvement in extraction rate representation over previous methods;
- A workflow for the application of post-extraction imaging for comparison to mechanical data gathered during tooth extraction;
- An experimentally-validated axisymmetric FE model of the dental complex that represents the dental complex under a variety of applied loading regimes, representing the complex behaviour of the PDL while maintaining simplicity and replicability as a tool for future use;
- The demonstrated application of the axisymmetric FE model to predict changes in tooth extraction procedure, both in the alteration of loading regime and physical changes to the dental complex (i.e. damage to the PDL); and
- Proof of concept of software interfaces for instrumented extraction devices as providing the feedback necessary to implement prescribed loading schemes that improve extraction outcomes, demonstrated in ex vivo benchtop tests with a clinical extraction device.

Overall, a significant advancement towards the improvement of atraumatic extraction procedures has been made with a sound scientific and engineering approach. This approach has relied heavily on the development of experimental and numerical methods that are neither mechanically complicated nor computationally intense but are capable of representing the biomechanics of tooth extraction nonetheless. The simple, effective power of these tools to inform the design of a clinical device and altered extraction biomechanics has also been clearly demonstrated. The biomechanical approach adopted here provides effective, accessible numerical models and experimental frameworks that can directly influence the clinical care received by the millions of Canadians experiencing edentulism.

References

1. Genna F, Paganelli C. Force–displacement relationship in the extraction of a porcine tooth from its socket: Experiments and numerical simulations. Journal of Mechanics of Materials and Structures. 2014 Dec 14;9(5):497-514.
2. Chiba M, Ohshima S, Takizawa K. Measurement of the force required to extract the mandibular incisor of rats of various ages. Archives of Oral Biology. 1980 Jan 1;25(10):683-7.
3. Tohar R, Alali H, Ansbacher T, Brosh T, Sher I, Gafni Y, Weinberg E, Gal M. Collagenase Administration into Periodontal Ligament Reduces the Forces Required for Tooth Extraction in an Ex situ Porcine Jaw Model. Journal of Functional Biomaterials. 2022 Jun 8;13(2):76
4. Ho SP, Kurylo MP, Grandfield K, Hurng J, Herber RP, Ryder MI, Altoe V, Aloni S, Feng JQ, Webb S, Marshall GW. The plastic nature of the human bone–periodontal ligament–tooth fibrous joint. Bone. 2013 Dec 1;57(2):455-67.
5. Dietrich T, Schmid I, Locher M, Addison O. Extraction force and its determinants for minimally invasive vertical tooth extraction. J Mech Behav Biomed Mater. 2020;105:103711. doi: 10.1016/j.jmbbm.2020.103711.

Complete List of References

Adeyemo WL, Ladeinde AL, Ogunlewe MO. Influence of trans-operative complications on socket healing following dental extractions. *J Contemp Dent Pract*. 2007;8(1):52-9.

Ahel V, Brekalo I, Ahel J, Brumini G. Measurement of tooth extraction forces in upper incisors. Collegium antropologicum. 2006 Mar 16;30(1):31-5.

Ahel V, Ćabov T, Špalj S, Perić B, Jelušić D, Dmitrašinović M. Forces that fracture teeth during extraction with mandibular premolar and maxillary incisor forceps. British Journal of Oral and Maxillofacial Surgery. 2015 Dec 1;53(10):982-7.

Alibrahim A, Al Salieti H, Alrawashdeh M, Darweesh H, Alsaleh H. Patterns and predictors of tooth loss among partially dentate individuals in Jordan: A cross-sectional study. The Saudi Dental Journal. 2023 Dec 27.

Amid R, Kadkhodazadeh M, Dehnavi F, Brokhim M. Comparison of stress and strain distribution around splinted and non-splinted teeth with compromised periodontium: A three-dimensional finite element analysis. Journal of Advanced Periodontology & Implant Dentistry. 2018;10(1):35.

An B, Zhang D. An analysis of crack growth in dentin at the microstructural scale. Mech Behav Biomed Mater. 2018; 81:149-160

Andreaus U, Colloca M, Iacoviello D. Coupling image processing and stress analysis for damage identification in a human premolar tooth. Computer methods and programs in biomedicine. 2011 Aug 1;103(2):61-73.

Ansbacher T, Tohar R, Cohen A, Cohen O, Levartovsky S, Arieli A, Matalon S, Bar DZ, Gal M, Weinberg E. A novel computationally engineered collagenase reduces the force required for tooth extraction in an ex-situ porcine jaw model. Journal of Biological Engineering. 2023 Jul 17;17(1):47.

Arruda, EM and Boyce, MC. A three-dimensional constitutive model for the large stretch behaviour of rubber elastic materials. J Mech Phys Solid. 1993; 41(2):389-412. doi: 10.1016/0022-5096(93)90013-6

Ashrafi M, Ghalichi F, Mirzakouchaki B, Zoljanahi Oskui I. Numerical simulation of hydro-mechanical coupling of periodontal ligament. Proceedings of the Institution of Mechanical Engineers, Part H: Journal of Engineering in Medicine. 2020 Feb;234(2):171-8.

Barone S, Paoli A, Razionale AV, Savignano R. Computer aided modelling to simulate the biomechanical behaviour of customised orthodontic removable appliances. International Journal on Interactive Design and Manufacturing (IJIDeM). 2016 Nov;10:387-400.

Baschong W, Weiss P, Imholz MS, Filippi A. Periodontal ligament on pulp-free root slices – an in vitro model for early tooth (re)integration. An exploratory study. Swiss Dent J. 2018 Nov 12;128(11):878-886. PMID: 30403326.

Becker W. Immediate implant placement: treatment planning and surgical steps for successful outcomes. *Br Dent J*. 2006;201(4):199-205. doi: 10.1038/sj.bdj.4813881.

Beertsen W, McCulloch CA, Sodek J. The periodontal ligament: a unique, multifunctional connective tissue. Periodontology 2000. 1997 Feb;13(1):20-40.

Bergomi M, Cugnoni J, Botsis J, Belser UC, Anselm Wiskott HW. The role of the fluid phase in the viscous response of bovine periodontal ligament. *J Biomech*. 2010;43(6):1146-52. doi: 10.1016/j.jbiomech.2009.12.020.

Bergomi M, Cugnoni J, Galli M, Botsis J, Belser UC, Wiskott HW. Hydro-mechanical coupling in the periodontal ligament: a porohyperelastic finite element model. *J Biomech*. 2011;44(1):34-8. doi: 10.1016/j.jbiomech.2010.08.019.

Bernal-Sánchez KK, Lara-Carrillo E, Velázquez-Enriquez U, Casanova-Rosado JF, Casanova-Rosado AJ, Morales-Valenzuela AA, Márquez-Rodríguez S, Medina-Solís CE, Maupomé G. Clinical and socio-demographic factors associated with dental extractions in a clinical sample. Brazilian Dental Journal. 2023 Dec 22;34:121-9.Supplement #1 – Additional Imaging Results

Beuling MG, Agterbos PC, van Riet TC, Ho JP, de Vries R, Kober J, de Lange J. Forces and movements during tooth extraction: A scoping review. Advances in Oral and Maxillofacial Surgery. 2023 Jan 7:100391.

Blanco J, Carral C, Argibay O, Liñares A. Implant placement in fresh extraction sockets. *Periodontol*. 2000. 2019;79(1):151-167. doi: 10.1111/prd.12253.

Bosiakov S, Mikhasev G. Mathematical model for analysis of translational displacements of tooth root. Mathematical Modelling and Analysis. 2015 Jul 4;20(4):490-501.

Broers DLM, Dubois L, de Lange J, Brands WG, Lagas MBD, et al. How dentists and oral and maxillofacial surgeons deal with tooth extraction without a valid clinical indication. PLoS ONE. 2023;18(1):1-10. doi: 10.1371/journal.pone.0280288

Broers DLM, Dubois L, de Lange J, Su N, and de Jongh A. Reasons for tooth removal in adults. Int Dent J. 2021;72(2022):52-57.

Broers DLM, Dubois L, de Lange J, Welie JV, Brands WG, Bruers JJ, de Jongh A. Financial, psychological, or cultural reasons for extracting healthy or restorable teeth. The Journal of the American Dental Association. 2022 Aug 1;153(8):761-8.

Bustad LK. Pigs in the laboratory. Sci Am. 1966 Jun;214(6):94-100. doi: 10.1038/scientificamerican0666-94. PMID: 5930599.

Canadian Dental Association. The State of Oral Health in Canada, March 2017. Available online: https://www.cda-adc.ca/stateoforalhealth/

Cattaneo PM, Cornelis MA. Orthodontic tooth movement studied by finite element analysis: an update. What can we learn from these simulations?. Current Osteoporosis Reports. 2021 Apr;19:175-81.

CEA, EDF, Open Cascade. SALOME 9 (Version 9.7). Issy-le-Moulineaux : Open Cascade. (2024). [Accessed June 24, 2020]. Retrieved from salome-platform.org.

Chiba M, Ohshima S, Takizawa K. Measurement of the force required to extract the mandibular incisor of rats of various ages. Archives of Oral Biology. 1980 Jan 1;25(10):683-7.

Chu TM, Liu SS, Babler WJ. Craniofacial biology, orthodontics, and implants. In: Basic and applied bone biology 2014 Jan 1 (pp. 225-242). Academic Press.

Cicciù M, Cervino G, Milone D, Risitano G. FEM Investigation of the Stress Distribution over Mandibular Bone Due to Screwed Overdenture Positioned on Dental Implants. Materials (Basel). 2018;11(9):1512. doi: 10.3390/ma11091512

Contractor MM, Bhate K, Londhe U, Awate S, Chhartriwala A, Samuel S. Efficacy of Periotome Versus Conventional Forceps Extraction in Socket Preservation and Reduction of Postoperative Pain: A Randomised Clinical Trial. Journal of Clinical & Diagnostic Research. 2023 Nov 1;17(11).

Corredor-Gómez JP, Rueda-Ramírez AM, Gamboa-Márquez MA, Torres-Rodríguez C, Cortés-Rodríguez CJ. An intramembranous ossification model for the in silico analysis of bone tissue formation in tooth extraction sites. Journal of Theoretical Biology. 2016 Jul 21;401:64-77.

Cunha MAGM, Lino PA, Santos TRD, Vasconcelos M, Lucas SD, Abreu MHNG. A 15-Year Time-series Study of Tooth Extraction in Brazil. *Medicine (Baltimore)*. 2015;94(47):e1924. doi: 10.1097/MD.0000000000001924.

D'Errico, J. fminsearchbnd, fminsearchcon (), MATLAB Central File Exchange (2023). Available from: https://www.mathworks.com/matlabcentral/fileexchange/8277-fminsearchbnd-fminsearchcon

Dezzen-Gomide AC, de Carvalho MA, Lazari-Carvalho PC, de Oliveira HF, Cury AA, Yamamoto-Silva FP, de Freitas Silva BS. A three-dimensional finite element analysis of permanent maxillary central incisors in different stages of root development and trauma settings. Computer methods and programs in biomedicine. 2021 Aug 1;207:106195.

Dietrich T. Minimally-invasive tooth extraction: doorknobs and strings revisited!. Dental update. 2013 May 2;40(4):325-30.

Dietrich T, Schmid I, Locher M, Addison O. Extraction force and its determinants for minimally invasive vertical tooth extraction. J Mech Behav Biomed Mater. 2020;105:103711. doi: 10.1016/j.jmbbm.2020.103711.

Dym H, Weiss A. Exodontia: tips and techniques for better outcomes. Dent Clin North Am. 2012;56(1):245-66. doi: 10.1016/j.cden.2011.07.002.

El-Kenawy MH, Ahmed WM. Comparison Between Physics and Conventional Forceps in Simple Dental Extraction. J Maxillofac Oral Surg. 2015;14(4):949-55. doi: 10.1007/s12663-015-0765-6.

Fard AM, Vakili-Tahami F. Fibrous soft tissues damage evaluation with a coupled thermo-visco-hyperelastic model. International Journal of Non-Linear Mechanics. 2020 Jan 1;118:103260

Fickl S, Zuhr O, Wachtel H, Bolz W, Huerzeler M. Tissue alterations after tooth extraction with and without surgical trauma: a volumetric study in the beagle dog. *J Clin Periodontol*. 2008;35(4):356-63. doi: 10.1111/j.1600-051X.2008.01209.x.

Fill TS, Carey JP, Toogood RW, Major PW. Experimentally determined mechanical properties of, and models for, the periodontal ligament: critical review of current literature. Journal Dent Biomech. 2011:312980.

Fill TS, Toogood RW, Major PW, Carey JP. Analytically determined mechanical properties of, and models for the periodontal ligament: critical review of literature. J Biomech. 2012;45(1):9-16. doi: 10.1016/j.jbiomech.2022.09.020

Fung, YC. Biomechanics: mechanical properties of living tissues. 2nd Ed. New York (USA). Springer New York; 2013. Chapter 7, Bioviscoelastic Solids; p242-314.

Gadzella TJ, Hynkova K, Westover L, Addison O, Romanyk DL. A novel method for simulating ex vivo tooth extractions under varying applied loads. J Clin Biomech. 2023;110:106116. https://doi.org/10.1016/j.clinbiomech.2023.106116.

Gei M, Genna F, Bigoni D. An interface model for the periodontal ligament. J. Biomech. Eng.. 2002 Oct 1;124(5):538-46.

Genna F, Annovazzi L, Bonesi C, Fogazzi P, Paganelli C. On the experimental determination of some mechanical properties of porcine periodontal ligament. Meccanica. 2008 Feb;43:55-73.

Genna F, Paganelli C. Force–displacement relationship in the extraction of a porcine tooth from its socket: Experiments and numerical simulations. Journal of Mechanics of Materials and Structures. 2014 Dec 14;9(5):497-514.

Genna F. A micromechanically-based, three-dimensional interface finite element for the modelling of the periodontal ligament. Computer Methods in Biomechanics and Biomedical Engineering. 2006 Aug 1;9(4):243-56.

Gholamalizadeh T, Moshfeghifar F, Ferguson Z, Schneider T, Panozzo D, Darkner S, Makaremi M, Chan F, Søndergaard PL, Erleben K. Open-Full-Jaw: An open-access dataset and pipeline for finite element models of human jaw. Computer Methods and Programs in Biomedicine. 2022 Sep 1;224:107009.

Gulabivala K, Ng YL. Tooth organogenesis, morphology and physiology. In: Endodontics (4th Edition). 2014 August (pp. 2-32). Mosby Elsevier.

Gupta M, Madhok K, Kulshrestha R, Chain S, Kaur H, Yadav A. Determination of stress distribution on periodontal ligament and alveolar bone by various tooth movements–A 3D FEM study. Journal of oral biology and craniofacial research. 2020 Oct 1;10(4):758-63.

Hamed NA, Mohamed MH. Radiographic Evaluation of Bone Height Changes Around Immediately Placed Implant Retaining Mandibular Over-Denture in Atraumatic Tooth Extraction Cases. Egyptian Dental Journal. 2023 Jul 1;69(3):2035-43.

Hämmerle CHF, Tarnow D. The etiology of hard- and soft-tissue deficiencies at dental implants: A narrative review. *J Periodontol*. 2018;89 Suppl 1:S291-S303. doi: 10.1002/JPER.16-0810.

Hariharan S, Narayanan V, Soh CL. Split-mouth comparison of physics forceps and extraction forceps in orthodontic extraction of upper premolars. Br J Oral Maxillofac Surg. 2014;52(10):e137-40. doi: 10.1016/j.bjoms.2014.06.013.

Heinonen V, Ruotsalainen TJ, Paavola L, Mikkonen JJ, Asikainen P, Koistinen AP, Kullaa AM. (2018) Alveolar bone remodeling after tooth extraction in irradiated mandible: An

experimental study with canine model, Ultrastructural Pathology, 42:2, 124-132, DOI: 10.1080/01913123.2017.1422829

Hiltunen K, Vehkalahti MM. Why and when older people lose their teeth: A study of public healthcare patients aged 60 years and over in 2007-2015. Gerodontology. 2023; 40: 326-333. doi: 10.1111/ger.12657

Ho SP, Kurylo MP, Fong TK, Lee SS, Wagner HD, Ryder MI, Marshall GW. The biomechanical characteristics of the bone-periodontal ligament-cementum complex. Biomaterials. 2010 Sep 1;31(25):6635-46.

Ho SP, Kurylo MP, Grandfield K, Hurng J, Herber RP, Ryder MI, Altoe V, Aloni S, Feng JQ, Webb S, Marshall GW. The plastic nature of the human bone–periodontal ligament–tooth fibrous joint. Bone. 2013 Dec 1;57(2):455-67.

Houg KP, Camarillo AM, Doschak MR, Major PW, Popwics T, Dennison Cr, Romanyk DL. Strain Measurement within an Intact Swine Periodontal Ligament. Journal of Dental Research. 2022;101(12):1474-1480. doi: 10.1177/00220345221100234

Huang H, Tang W, Tan Q, Yan B. Development and parameter identification of a visco-hyperelastic model for the periodontal ligament. Journal of the mechanical behavior of biomedical materials. 2017 Apr 1;68:210-5.

Huang H, Tang W, Yang YU, Wu B, Yan B. Determination of viscoelastic properties of the periodontal ligament using nanoindentation testing and numerical modeling. Journal of Mechanics in Medicine and Biology. 2016 Sep 8;16(06):1650089.

Hupp J, Ellis E, and Tucker MR. Contemporary oral and maxillofacial surgery. 7Th ed. Philadelphia, PA: Elsevier; 2019. Chapter 8: Principles of routine exodontia; p.106-134.

Irshad F, Khan UQ, Memon ZA, Punjabi SK, Zaidi SA. Use of Physics Forcep Versus Conventional Forcep in Extraction of Mandibular First Molar: Physics Forcep Versus Conventional Forcep. Pakistan Journal of Health Sciences. 2023 May 31:123-8.

Jang AT, Chen L, Shimotake AR, Landis W, Altoe V, Aloni S, Ryder M, Ho SP. A force on the crown and tug of war in the periodontal complex. Journal of dental research. 2018 Mar;97(3):241-50.

Jang AT, Merkle AP, Fahey KP, Gansky SA, Ho SP. Multiscale biomechanical responses of adapted bone–periodontal ligament–tooth fibrous joints. Bone. 2015 Dec 1;81:196-207.

John D'Errico (2021a). Movingslope(). Matlab Central File Exchange, retrieved July 30th, 2021. Available from: https://www.mathworks.com/matlabcentral/fileexchange/16997-movingslope

John D'Errico (2021b). SLM – Shape Language Modeling. Matlab Central File Exchange, retrieved July 30th, 2021. Available from: https://www.mathworks.com/matlabcentral/fileexchange/24443-slm-shape-language-modeling

Kaiser AH, Keilig L, Klein R, Bourauel C. Parameter identification for the simulation of the periodontal ligament during the initial phase of orthodontic tooth movement. Computer Methods in Biomechanics and Biomedical Engineering. 2021 Feb 17;24(3):333-48.

Karimi A, Razaghi R, Biglari H, Rahmati SM, Sandbothe A, Hasani M. Finite element modeling of the periodontal ligament under a realistic kinetic loading of the jaw system. The Saudi Dental Journal. 2020 Nov 1;32(7):349-56.

Karimi Dastgerdi A, Rouhi G, Dehghan MM, Farzad Mohajeri S, and Barikani HR. Linear momenta transferred to the dental implant-bone and natural tooth-PDL-bone contstructs under impact loading: a comparative in-vitro and in-silico study. Front. Bioeng. Biotechnol. 2020;8:54. doi: 10.3389/fbioe.2020.00544.

Karimi Dastgerdi A, Rouhi G, Dehghan MM, Farzad-Mohajeri S, Barikani HR. Linear Momenta Transferred to the Dental Implant-Bone and Natural Tooth-PDL-Bone Constructs Under Impact Loading: A Comparative in-vitro and in-silico Study. *Front Bioeng Biotechnol*. 2020;8:544. doi: 10.3389/fbioe.2020.00544.

Knaup TJ, Dirk C, Reimann S, Keilig L, Eschbach M, Korbmacher-Steiner H, Bourauel C. Time-dependent behavior of porcine periodontal ligament: a combined experimental, numeric in-vitro study. American Journal of Orthodontics and Dentofacial Orthopedics. 2018 Jan 1;153(1):97-107.

Komatsu K, Ohshima S, Chiba M. Measurement of the force required to extract the mandibular first molar from its socket in the dissected jaw of growing young rats. Gerodontology. 1990 Apr;9(1-3):3-7.

Korabi, R., Shemtov-Yona, K., Dorogoy, A. Rittel D. The Failure Envelope Concept Applied To The Bone-Dental Implant System. Sci Rep. 2017;7:2051. doi: 10.1038/s41598-017-02282-2

Leblebicioglu B, Hegde R, Yildiz VO, Tatakis DN. Immediate effects of tooth extraction on ridge integrity and dimensions. *Clin Oral Investig*. 2015;19(8):1777-84. doi: 10.1007/s00784-014-1392-1.

Lehtinen R, Ojala T. Rocking and twisting moments in extraction of teeth in the upper jaw. International journal of oral surgery. 1980 Oct 1;9(5):377-82.

Levin L, Day PF, Hicks L, O'Connell A, Fouad AF, Bourguignon C, Abbott PV. International Association of Dental Traumatology guidelines for the management of traumatic dental injuries: General introduction. Dental Traumatology. 2020 Aug;36(4):309-13.Saund D,

Liao Z, Chen J, Zhang Z, Li W, Swain M, Li Q. Computational modeling of dynamic behaviors of human teeth. Journal of biomechanics. 2015 Dec 16;48(16):4214-20.

Likitmongkolsakul U, Smithmaitrie P, Samruajbenjakun B, Aksornmuang J. Development and validation of 3D finite element models for prediction of orthodontic tooth movement. International journal of dentistry. 2018 Aug 30;2018.

Limjeerajarus N, Sratong-On P, Dhammayannarangsi P, Tompkins KA, Kamolratanakul P, Phannarus K, Osathanon T, Limjeerajarus CN. Determination of the compressive modulus of

elasticity of periodontal ligament derived from human first premolars. Heliyon. 2023 Mar 1;9(3).

Lin JD, Jang AT, Kurylo MP, Hurng J, Yang F, Yang L, Pal A, Chen L, Ho SP. Periodontal ligament entheses and their adaptive role in the context of dentoalveolar joint function. Dental Materials. 2017 Jun 1;33(6):650-66.

Lin JD, Lee J, Özcoban H, Schneider GA, Ho SP. Biomechanical adaptation of the bone-periodontal ligament (PDL)-tooth fibrous joint as a consequence of disease. Journal of biomechanics. 2014 Jun 27;47(9):2102-14.

Liu Y, Kerdok AE, Howe RD. A nonlinear finite element model of soft tissue indentation. International symposium on medical simulation. 2004 Jun 17; 67-76. Berlin, Heidelberg: Springer Berlin Heidelberg.

Maas SA, Ellis BJ, Ateshian GA, Weiss JA: FEBio: Finite Elements for Biomechanics. J Biomech Eng. 2012;134(1):011005

Maceri F, Marino M, Vairo G. A unified multiscale mechanical model for soft collagenous tissues with regular fiber arrangement. Journal of biomechanics. 2010 Jan 19;43(2):355-63.

Makki AZ, Nassar AA, Alharbi WM, Bisharah WF, Alabdali MA, Alqurashi AM, Basandawa NA. Evaluation of post-extraction healing after atraumatic axial tooth extraction using Benex system II versus conventional extraction: Randomized control trial. The Saudi Dental Journal. 2021 Dec 1;33(8):923-8.

Marchesseau S, Tobias Heimann T, Chatelin S, Willinger R , Delingette H. Fast porous visco-hyperelastic soft tissue model for surgery simulation: Application to liver surgery. Progress in Biophysics and Molecular Biology. 2010; 103(2–3):185-196. doi: 10.1016/j.pbiomolbio.2010.09.005.

Martinez Choy SE, Lenz J, Schweizerhof K, Schmitter M, Schindler HJ. Realistic kinetic loading of the jaw system during single chewing cycles: a finite element study. Journal of Oral Rehabilitation. 2017 May;44(5):375-84.

Martinez S, Lenz J, Schweizerhof K, Schindler HJ. A variable finite element model of the overall human masticatory system for evaluation of stress distributions during biting and bruxism. In10th European LS-DYNA Conference, Würzburg, Germany 2015.

McCormack SW, Witzel U, Watson PJ, Fagan MJ, Gröning F. Inclusion of periodontal ligament fibres in mandibular finite element models leads to an increase in alveolar bone strains. PLoS One. 2017 Nov 30;12(11):e0188707.

McCormack SW, Witzel U, Watson PJ, Fagan MJ, Gröning F. The biomechanical function of periodontal ligament fibres in orthodontic tooth movement. Plos one. 2014 Jul 18;9(7):e102387.

Mehari Abraha H, Iriarte-Diaz J, Ross CF, Taylor AB, Panagiotopoulou O. The mechanical effect of the periodontal ligament on bone strain regimes in a validated finite element model of a macaque mandible. Frontiers in bioengineering and biotechnology. 2019:269.

Moerman, KM. GIBBON: The Geometry and Image-Based Bioengineering Add-On. J Open Source Softw. 2018;3(22):506. doi: 10.21105/joss.00506

Mohammadi SA. Association of inflammatory markers and growth factors with radiographically assessed wound healing of extraction sockets [MSc Thesis]. Omaha (USA): University of Nebraska Medical Center; 2023. Available from: https://digitalcommons.unmc.edu/etd/754/

Mulimani P, Popowics TE. UNDERSTANDING PERIODONTAL TISSUE RESPONSES TO MECHANICAL LOAD THROUGH THE USE OF THE PIG MODEL, SUS SCROFA. EMBRACING NOVEL TECHNOLOGIES IN DENTISTRY AND ORTHODONTICS. 2019 Mar 1;1001:86.

Murray H, Clarke M, Locker D, Kay EJ. Reasons for tooth extractions in dental practices in Ontario, Canada according to tooth type. International Dental Journal. 1997 Feb;47(1):3-8.

Muska E, Walter C, Knight A, Taneja P, Bulsara Y, Hahn M, Desai M, Dietrich T. Atraumatic vertical tooth extraction: a proof of principle clinical study of a novel system.

Oral Surg Oral Med Oral Pathol Oral Radiol. 2013;116(5):e303-10. doi: 10.1016/j.oooo.2011.11.037.

Najafidoust M, Hashemi A, Oskui IZ. Dynamic viscoelastic behavior of bovine periodontal ligament in compression. Journal of Periodontal Research. 2020 Oct;55(5):651-9.

Najafidoust M, Hashemi A, Oskui IZ. Effect of temperature on dynamic compressive behavior of periodontal ligament. Medical Engineering & Physics. 2023 Jun 1;116:103986.

Nalla RK, Kinney JH, Ritchie RO. On the fracture of human dentin: is it stress-or strain-controlled? Journal of Biomedical Materials Research Part A: An Official Journal of The Society for Biomaterials, The Japanese Society for Biomaterials, and The Australian Society for Biomaterials and the Korean Society for Biomaterials. 2003 Nov 1;67(2):484-95.

Narooei K, Arman M. Generalization of exponential based hyperelastic to hyper-viscoelastic model for investigation of mechanical behavior of rate dependent materials. Journal of the mechanical behavior of biomedical materials. 2018 Mar 1;79:104-13.

Natali AN, Carniel EL, Pavan PG, Sander FG, Dorow C, Geiger M. A visco-hyperelastic-damage constitutive model for the analysis of the biomechanical response of the periodontal ligament. J Biomech Eng. 2008 Jun;130(3):031004. doi: 10.1115/1.2900415.

Natali AN, Pavan PG, Carniel EL, Dorow C. A transversally isotropic elasto-damage constitutive model for the periodontal ligament. *Comput Methods Biomech Biomed Engin*. 2003;6(5-6):329-36. doi: 10.1080/1025584031000163984O.

Natali AN, Pavan PG, Scarpa C. Numerical analysis of tooth mobility: formulation of a non-linear constitutive law for the periodontal ligament. Dental Materials. 2004 Sep 1;20(7):623-9.

Natali, A. N., Carniel, E. L., Pavan, P. G., Sander, F. G., Dorow, C., and Geiger, M. (April 22, 2008). A Visco-Hyperelastic-Damage Constitutive Model for the Analysis of the Biomechanical Response of the Periodontal Ligament. ASME. J Biomech Eng. June 2008; 130(3): 031004. https://doi.org/10.1115/1.

Naveh GR, Brumfeld V, Shahar R, Weiner S. Tooth periodontal ligament: Direct 3D microCT visualization of the collagen network and how the network changes when the tooth is loaded. Journal of structural biology. 2013 Feb 1;181(2):108-15.

Nejad RM, Moghadam DG, Moghadam MR, Aslani M, Moghaddam HA, Mir M. Fracture behavior of restored teeth and cavity shape optimization: Numerical and experimental investigation. Journal of the Mechanical Behavior of Biomedical Materials. 2021 Dec 1;124:104829.

Nihara J, Gielo-Perczak K, Cardinal L, Saito I, Nanda R, Uribe F. Finite element analysis of mandibular molar protraction mechanics using miniscrews. European journal of orthodontics. 2015 Feb 1;37(1):95-100.

Nikolaus A, Currey JD, Lindtner T, Fleck C, Zaslansky P. Importance of the variable periodontal ligament geometry for whole tooth mechanical function: a validated numerical study. Journal of the mechanical behavior of biomedical materials. 2017 Mar 1;67:61-73.

Oltramari PV, Navarro RL, Henriques JF, Capelozza AL, Granjeiro JM. Dental and skeletal characterization of the BR-1 minipig. The Veterinary Journal. 2007 Mar 1;173(2):399-407.

Ortún-Terrazas J, Cegoñino J, Pérez Del Palomar A. In silico study of cuspid' periodontal ligament damage under parafunctional and traumatic conditions of whole-mouth occlusions. A patient-specific evaluation. Comput Methods Programs Biomed. 2020 Feb;184:105107. doi: 10.1016/j.cmpb.2019.105107.

Ortún-Terrazas J, Cegoñino J, Santana-Penín U, Santana-Mora U, Del Palomar AP. Approach towards the porous fibrous structure of the periodontal ligament using micro-computerized tomography and finite element analysis. Journal of the mechanical behavior of biomedical materials. 2018 Mar 1;79:135-49.

Ortún-Terrazas J, Cegoñino J, Santana-Penín U, Santana-Mora U, Perez del Palomar A. A porous fibrous hyperelastic damage model for human periodontal ligament: Application of a microcomputerized tomography finite element model. International Journal for Numerical Methods in Biomedical Engineering. 2019 Apr;35(4):e3176.

Oskui IZ, Hashemi A, Jafarzadeh H, Kato A. Finite element investigation of human maxillary incisor under traumatic loading: Static vs dynamic analysis. Computer methods and programs in biomedicine. 2018 Mar 1;155:121-5.

Oskui IZ, Hashemi A. Dynamic tensile properties of bovine periodontal ligament: a nonlinear viscoelastic model. Journal of Biomechanics. 2016 Mar 21;49(5):756-64.

Otani T, Kobayashi M, Nozaki K, Gonda T, Maeda Y, Tanaka M. Influence of mouthguards and their palatal design on the stress-state of tooth-periodontal ligament-bone complex under static loading. Dental traumatology. 2018 Jun;34(3):208-13.

Otani T, Koga T, Nozaki K, Kobayashi Y, Tanaka M. Mechanical effects of distributed fibre orientation in the periodontal ligament of an idealised geometry. Computer Methods in Biomechanics and Biomedical Engineering. 2020 Nov 10;24(7):701-9.

Ou KL, Chang CC, Chang WJ, Lin CT, Chang KJ, Huang HM. Effect of damping properties on fracture resistance of root filled premolar teeth: a dynamic finite element analysis. International endodontic journal. 2009 Aug;42(8):694-704.

Ovy EG, Romanyk DL, Flores Mir C, Westover L. Modelling and evaluating periodontal ligament mechanical behaviour and properties: A scoping review of current approaches and limitations. Orthod Craniofac Res. 2022;25(2):199-211. doi: 10.1111/ocr.12527.

Papadimitriou DE, Geminiani A, Zahavi T, Ercoli C. Sonosurgery for atraumatic tooth extraction: a clinical report. The Journal of Prosthetic Dentistry. 2012 Dec 1;108(6):339-43.

Papadimitriou DEV, Geminiani A, Zahavi T, Ercoli C. Sonosurgery for atraumatic tooth extraction: a clinical report. J Prosthet Dent. 2012;108:339-343

Papadopoulou K, Hasan I, Keilig L, Reimann S, Eliades T, Jäger A, Deschner J, Bourauel C. Biomechanical time dependency of the periodontal ligament: a combined experimental and numerical approach. European journal of orthodontics. 2013 Dec 1;35(6):811-8.

Papadopoulou K, Keilig L, Eliades T, Krause R, Jäger A, Bourauel C. The time-dependent biomechanical behaviour of the periodontal ligament—an in vitro experimental study in

minipig mandibular two-rooted premolars. The European Journal of Orthodontics. 2014 Feb 1;36(1):9-15.

Patel HS, Managutti AM, Menat S, Agarwal A, Shah D, Patel J. Comparative Evaluation of Efficacy of Physics Forceps versus Conventional Forceps in Orthodontic Extractions: A Prospective Randomized Split Mouth Study. J Clin Diagn Res. 2016;10(7):ZC41-5. doi: 10.7860/JCDR/2016/17724.8160.

Pini M, Zysset PH, Botsis J, Contro R. Tensile and compressive behaviour of the bovine periodontal ligament. Journal of biomechanics. 2004 Jan 1;37(1):111-9.

Provatidis CG. A comparative FEM-study of tooth mobility using isotropic and anisotropic models of the periodontal ligament. Medical engineering & physics. 2000 Jun 1;22(5):359-70.

Puso MA, Weiss JA: Finite element implementation of anisotropic quasi-linear viscoelasticity using a discrete spectrum approximation. Journal of Biomechanical Engineering, 120(1):62-70, 1998.

Qian L, Todo M, Morita Y, Matsushita Y, Koyano K. Deformation analysis of the periodontium considering the viscoelasticity of the periodontal ligament. Dental Materials. 2009 Oct 1;25(10):1285-92.

Rahimi M, Mojra A. Numerical modeling of hyperfoam behavior of periodontal ligament in mechanical loading. In2019 26th National and 4th International Iranian Conference on Biomedical Engineering (ICBME) 2019 Nov 27 (pp. 82-87). IEEE.

Rao S, Arora H, Hameed S. A Threedimensional Finite Element Analysis of Stress Distribution in the Cortical Bone in Single Tooth Implant and Post Core-treated Tooth subjected to variable Loads. Int J Prosthodont Restor Dent 2017;7(1):8-16.

Riet TV, Graaf WD, Lange JD, Kober J. Analysis of movements in tooth removal procedures using robot technology. Plos one. 2023 May 18;18(5):e0285503.

Robinson D, Aguilar L, Gatti A, Abduo J, Lee PV, Ackland D. Load response of the natural tooth and dental implant: A comparative biomechanics study. The journal of advanced prosthodontics. 2019 Jun;11(3):169-78.

Romanyk DL, Guan R, Major PW, Dennison CR. Repeatability of strain magnitude and strain rate measurements in the periodontal ligament using fibre Bragg gratings: an ex vivo study in a swine model. Journal of Biomechanics. 2017 Mar 21;54:117-22.

Romanyk DL, Vafaeian B, Addison O, Adeeb S. The use of finite element analysis in dentistry and orthodontics: Critical points for model development and interpreting results. InSeminars in Orthodontics 2020 Sep 1 (Vol. 26, No. 3, pp. 162-173). WB Saunders.

Salem M, Westover L, Adeeb S, Duke K. An Equivalent Constitutive Model of Cancellous Bone With Fracture Prediction. J Biomech Eng. 2020; 142(12):121004. doi: 10.1115/1.4047080

Sangpradit K, Liu H, Dasgupta P, Althoefer K, Seneviratne LD. Finite-Element Modeling of Soft Tissue Rolling Indentation. IEEE Transactions on Biomedical Engineering. 2011; 58(12):3319-3327. doi: 10.1109/TBME.2011.2106783.

Savignano R, Barone S, Paoli A, Razionale AV. FEM analysis of bone-ligaments-tooth models for biomechanical simulation of individual orthodontic devices. In: International Design Engineering Technical Conferences and Computers and Information in Engineering Conference 2014 Aug 17 (Vol. 46285, p. V01AT02A081). American Society of Mechanical Engineers.

Schneider C, Zemp E, Zitzmann NU. Dental care behaviour in Switzerland. *Swiss Dent J*. 2019;129(6):466-478.

Schroeder KD. Human tooth diagram-en.svg from Wikimedia Commons. Licensed under CC-BY-SA 4.0.

Schropp L, Wenzel A, Kostopoulos L, Karring T. Bone healing and soft tissue contour changes following single-tooth extraction: a clinical and radiographic 12-month prospective study. International Journal of Periodontics & Restorative Dentistry. 2003 Aug 1;23(4).

Sharma SD, Vidya B, Alexander M, Deshmukh S. Periotome as an Aid to Atraumatic Extraction: A Comparative Double Blind Randomized Controlled Trial. J Maxillofac Oral Surg. 2015;14(3):611-5. doi: 10.1007/s12663-014-0723-8.

Shibata T, Botsis J, Bergomi M, Mellal A, Komatsu K. Mechanical behavior of bovine periodontal ligament under tension-compression cyclic displacements. European journal of oral sciences. 2006 Feb;114(1):74-82.

Sinescu C, Duma VF, Dodenciu D, Stratul S, Manole M, Draganescu GE. Mechanical properties of the periodontal system and of dental constructs deduced from the free response of the tooth. Journal of Healthcare Engineering. 2018 Sep 17;2018.

Su K, Yuan L, Du J. Bone remodeling under tooth loading. InTMS 2017 146th Annual Meeting & Exhibition Supplemental Proceedings 2017 (pp. 331-340). Springer International Publishing.

Su K, Yuan L, Yang J, Du J. Numerical simulation of mandible bone remodeling under tooth loading: A parametric study. Scientific reports. 2019 Oct 17;9(1):14887.

Su MZ, Chang HH, Chiang YC, Cheng JH, Fuh LJ, Wang CY, Lin CP. Modeling viscoelastic behavior of periodontal ligament with nonlinear finite element analysis. Journal of Dental Sciences. 2013 Jun 1;8(2):121-8.

Su, K., Yuan, L., Yang, J. et al. Numerical Simulation of Mandible Bone Remodeling under Tooth Loading: A Parametric Study. Sci Rep. 2019;9:14887. doi: 10.1038/s41598-019-51429-w

Tohar R, Alali H, Ansbacher T, Brosh T, Sher I, Gafni Y, Weinberg E, Gal M. Collagenase Administration into Periodontal Ligament Reduces the Forces Required for Tooth Extraction in an Ex situ Porcine Jaw Model. Journal of Functional Biomaterials. 2022 Jun 8;13(2):76

Toms SR, Dakin GJ, Lemons JE, Eberhardt AW. Quasi-linear viscoelastic behaviour of the human periodontal ligament. J Biomech. 2002; 35(10):1411-1415. doi: 10.1016/S0021-9290(02)00166-5.

Tuna M, Sunbuloglu E, Bozdag E. Finite element simulation of the behavior of the periodontal ligament: a validated nonlinear contact model. Journal of biomechanics. 2014 Sep 22;47(12):2883-90.

Uhlir R, Mayo V, Lin PH, Chen S, Lee YT, Hershey G, Lin FC, Ko CC. Biomechanical characterization of the periodontal ligament: Orthodontic tooth movement. The Angle Orthodontist. 2017 Mar 1;87(2):183-92.

Venni Heinonen, Timo J. Ruotsalainen, Lauri Paavola, Jopi J. Mikkonen, Pekka Asikainen, Arto P. Koistinen & Arja M. Kullaa (2018) Alveolar bone remodeling after tooth extraction in irradiated mandible: An experimental study with canine model, Ultrastructural Pathology, 42:2, 124-132, DOI: 10.1080/01913123.2017.1422829

Verna C, Dalstra M, Lee TC, Cattaneo PM, Melsen B. Microcracks in the alveolar bone following orthodontic tooth movement: a morphological and morphometric study. The European Journal of Orthodontics. 2004 Oct 1;26(5):459-67.

Wickens CD, Carswell CM. The proximity compatibility principle: Its psychological foundation and relevance to display design. Human factors. 1995 Sep;37(3):473-94.

Wu B, Fu Y, Shi H, Yan B, Lu R, Ma S, Markert B. Tensile testing of the mechanical behavior of the human periodontal ligament. BioMedical Engineering OnLine. 2018 Dec;17:1-1.

Wu B, Li N, Liu M, Cheng K, Jiang D, Yi Y, Ma S, Yan B, Lu Y. Construction of Human Periodontal Ligament Constitutive Model Based on Collagen Fiber Content. Materials. 2023 Oct 6;16(19):6582.

Wu B, Pu P, Zhao S, Izadikhah I, Shi H, Liu M, Lu R, Yan B, Ma S, Markert B. Frequency-related viscoelastic properties of the human incisor periodontal ligament under dynamic compressive loading. Plos one. 2020 Jul 13;15(7):e0235822.

Zhang YR, Du W, Zhou XD, Yu HY. Review of research on the mechanical properties of the human tooth. Int J Oral Sci. 2014 Jun;6(2):61-9. doi: 10.1038/ijos.2014.21.

Zhou J, Song Y, Zhang C, Shi X. Tensile creep mechanical behavior of periodontal ligament: A hyper-viscoelastic constitutive model. Computer Methods and Programs in Biomedicine. 2021 Aug 1;207.

Appendix A – Supplement to Chapter 3: Design of the Testing Apparatus and Method

Appendix A contains the details of the construction of a self-aligning apparatus for ex vivo vertical tooth extraction within a material test frame. The details of the preparation of swine mandibles for use in this apparatus is also detailed. Finally, the order of operations and characteristic results of stereo video analysis for determining periods of tissue loading during the experiments is discussed. This Appendix was published as supplementary material for Chapter 3 in the Journal of Clinical Biomechanics.

Design of the Experimental Apparatus

The base for the system is an Instron ElectroPuls E3000 material test system (Instron, Norwood, MA, USA). The custom apparatus, depicted in Figure A-1a, fixes to the base of the test frame through steel plates housing square clamp brackets (McMaster-Carr, MID Rail Supports - 1-1/2" Square Sleeve) which hold the guide rails for the self-alignment apparatus (McMaster-Carr, 1-1/2" Wide Guide Rail). Square sleeve bearing carriages (McMaster-Carr, 1-1/2"X3-1/8") traverse these rails to provide one degree of linear freedom and are connected by a steel plate. Atop the connecting plate and perpendicular to the square bearings is a track roller monorail (McMaster-Carr, 15.500X220mm) accommodating a high-load track roller carriage (McMaster-Carr). The combined action of this roller carriage with the square slider-bearings allows the system to traverse freely in the plane normal to the line of action of the test frame (demonstrated in Figure A-1c).

In addition to translation, the system utilizes an automotive universal joint (McMaster-Carr, Single U-Joint for 5/8X1-1/16" Shafts) mounted to the roller bearing carriage to provide two degrees of rotational freedom along the translating axes (Figure A-1c). These degrees of freedom allow the sample to rotate to a preferential loading direction without twisting about the loading axis. Atop the universal joint is the sample stage with a threaded hole pattern to accommodate fixing the sample clamps (Figure A-1b). The clamps are sheet aluminum alloy bent to wrap around the sample to the bottom surface of the sample stage.

Force and displacement data are captured by the test frame crosshead. The load cell used is an Instron 2527 Series dynamic load cell rated for 5kN. An aluminum extension and clevis-pinned block were machined to connect this load cell with the T-bar end of a Benex tension cable (Benex, Luzern, Switzerland). The opposing, flared end of the cable is used to connect to the threaded tooth anchor in the sample incisor. Two Basler AcA 1920-155um cameras (Basler AG, Ahrensburg, Germany) were fitted with 8mm Kowa lenses (Kowa Optimed Deustchland, Dusseldorf, Germany) inside the safety cage of the Instron test frame to capture simultaneous video streams of extraction simulations.

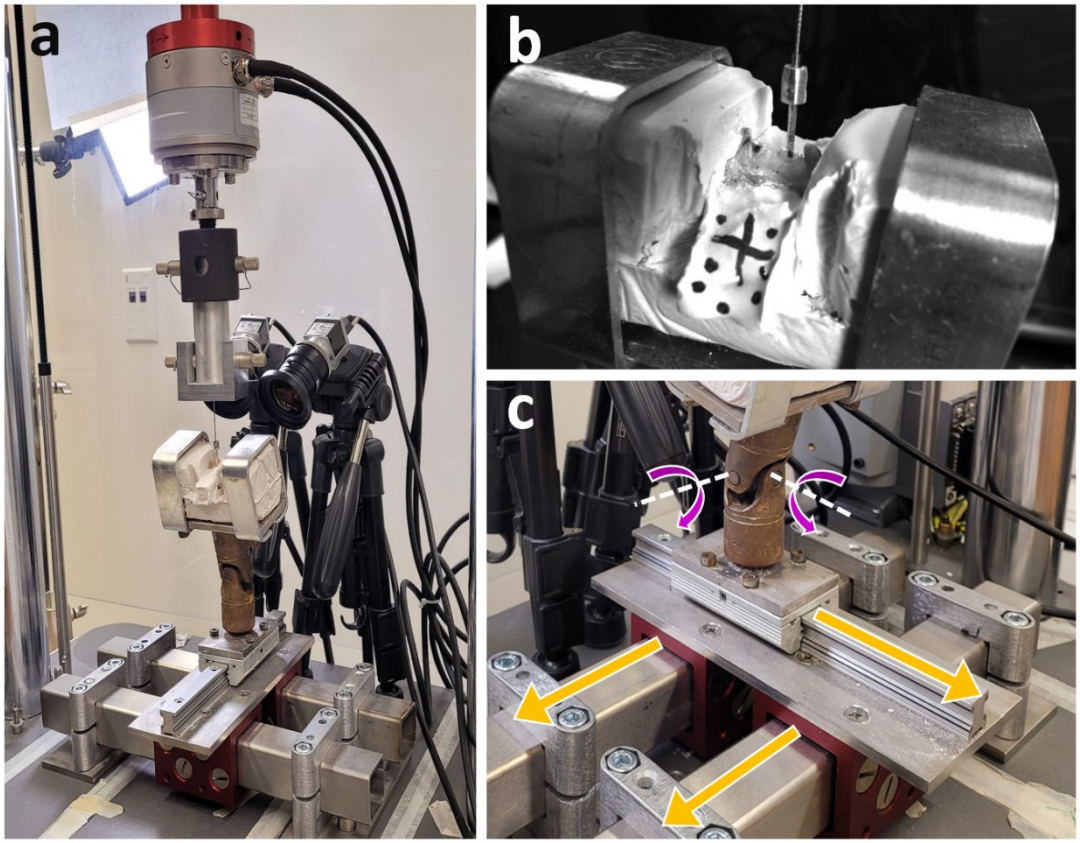

Figure A-1: The self-aligning test apparatus inside the test frame, showing a) the entire test apparatus. Force and displacement measurements are taken by the load cell and crosshead at the top of the image; b) image of a sample attached to the test apparatus with aluminum clamps. The incisor is attached to the crosshead with a screw implant and cable; c) an enlarged view of the self-aligning system motion elements. A monorail with bearing carriage and two square sleeve carriages provide linear motion (yellow arrows) and the universal joint allows for two axes of rotation (purple arrows).

Sample Preparation

Mandibles were removed from the freezer and thawed for 24 hours at 4°C prior to mechanical testing. The remainder of the procedure was performed at room temperature, approximately 21°C. The soft tissues of the cheek and tongue were removed using a scalpel to expose the underlying bone. An incision was made along the mucogingival junction to ensure that the gingiva remained intact. The scalpel blade was used to scrape away soft tissue below the mucogingival junction to expose the underlying bone. A marking was placed approximately 15mm below the lowest point of gingival attachment on the buccal side of the bone. A line was drawn from the distal surface of the second premolar to this point as the sectioning plane to be cut, as demonstrated in Figure A-2a). In this process, the apex of the incisors was removed from

the teeth to be extracted. This method was selected to remove high-curvature portions of the incisors not representative of human teeth, achieve an approximate root length similar to mature human teeth, and provide maximum stability during potting.

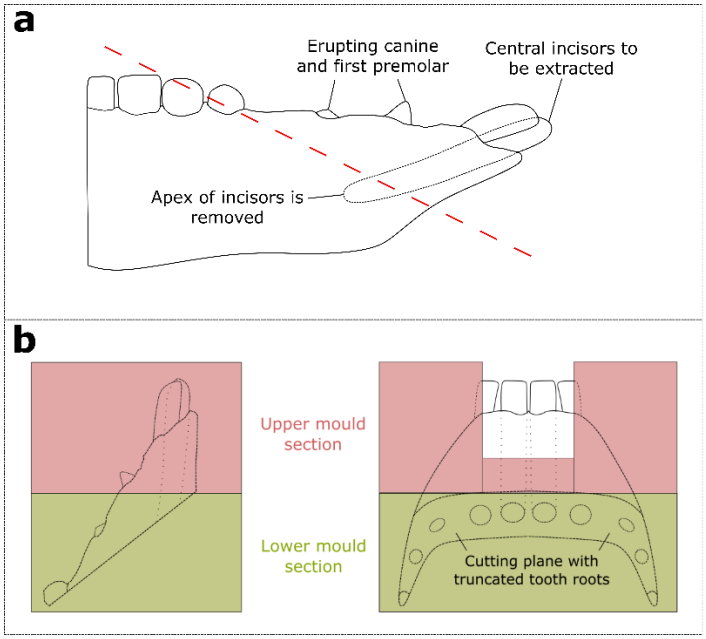

Figure A-2: Preparation of swine mandibles for extraction testing. a) a sagittal view diagram of the swine mandible, demonstrating the cutting plane through the bone and apex of the central incisors; b) Side view (left) and front view (right) sketches of the orientation of swine mandibles and teeth in dental stone pot. Green denotes dental stone poured in the lower section of the 3-piece mould and red denotes dental stone poured in the upper sections.

Samples were potted in Coecal III dental stone (GC Lab Technologies Inc., Alsip IL, USA). A custom mould was used with separable upper and lower sections to allow the formation of a U-shaped pot as depicted in Figure A-1b. The mandible specimen was angled within the pot to approximately align the axis of the incisor vertically with the two central incisors centered within the pot. To achieve this alignment, transparent acrylic sheet was cut by hand to pass over the lateral incisors and gingiva and hold the sample in place. These sheets prevented the dental stone from flowing over the central incisors, forming the interior of the "U" shape. Samples were covered with a PBS-soaked paper towel during cure times and other periods during which the tissue was not handled (e.g. between tests) to maintain hydration of the tissue.

Preparation of the teeth for extraction was performed by a dentist (KH). A periotome marked to depth of 2mm was used to sever the gingiva without luxation movements of tooth. A diamond

cylinder burr was used to remove approximately 2/3 of the clinical crown on each central incisor. The root canal was identified and then the screw hole was prepared with diamond coating twist drill (1.6 mm). A self-tapping anchor (2.1 mm) from the Benex extraction kit was inserted into an incisor with the provided screwdriver until firm attachment was achieved. Following preparation of the teeth, a permanent marker was used to make marks on the dental stone and tooth to assist in video tracking.

Video analysis

The purpose of video analysis was to distinguish periods of system self-alignment from periods dominated by relative motion of the tooth within the socket. Video calibration was performed in MATLAB using the Image Processing toolbox using the calibration sequences captured between tests.

Views acquired from each camera were analyzed separately from point tracking through reprojection. Exterior points of large drawn features on the tooth and dental stone surfaces were tracked to calculate the feature centroid which was then reprojected into 3-dimensionsal space. This method allowed for general tracking of motion between points between very dissimilar camera angles that did not permit automatic feature matching and differencing methods. The analysis of a single view is as follows:

- The MATLAB imadjust() function was used to improve the contrast of the greyscale images prior to point tracking;
- Points were detected in the first frame of the video using the detectMinEigenfeatures() function for a single feature;
- Detected points were tracked through the contrast-enhanced video to track the shape of the feature through the test;
- The centroid of the feature was calculated per-frame from the array of point locations;
- The planar locations of the feature centroids were reprojected based on the calibrated camera parameters; and
- The initial position of the centroid features were differenced to find their relative positions over time.

The features of interest for this analysis were the marker points placed on the tooth crown and dental stone during sample preparation. Examples of dental stone markings are visible in Figure A-1b. Comparison of the tooth feature to dental stone points provided two displacement-time traces that could be examined qualitatively to determine when tooth-PDL-bone extension

dominated relative to system alignment. Comparison among points on the dental stone helped confirm these results. The corresponding point in the video was then examined to confirm the centroid analysis. The frame indices in the crosshead displacement traces was then noted as the point of predominant tissue loading. This video analysis procedure was successfully applied to 16 of the 25 test extractions. Video analysis failed in the remaining cases due to data storage failure or the occlusion of necessary marker in one of the camera views by the surrounding dental stone.

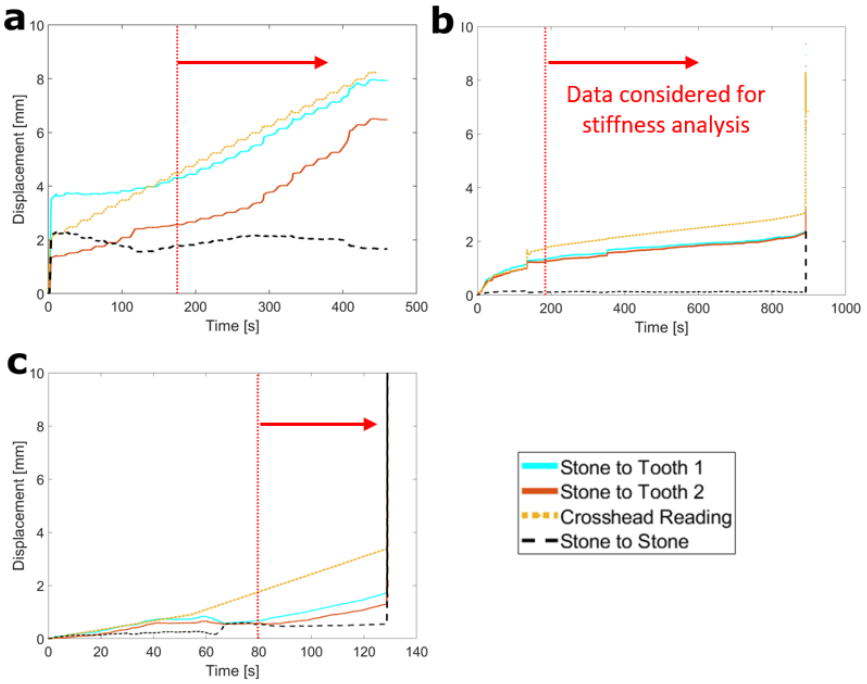

Figure A-3: Displacement traces acquired from the test frame crosshead and video analysis. Each subfigure is a representative curve taken from a single extraction under: a) intermittent loading; b) force control; and c) displacement control. Vertical dashed lines indicate the identified point where tooth displacement begins to dominate, beyond which data is considered in stiffness analysis. "Stone to Tooth" indicates displacement of the extracted tooth relative to two points measured on the dental stone. "Crosshead Reading" indicates displacement measured by the material test frame. "Stone to Stone" curves are the relative displacement between features tracked on the dental stone. Crosshead displacements tend to overpredict the displacements estimated from video views, with the relative displacement between stone features stabilizing after system alignment.

17 of 24 tooth extraction videos were successfully analyzed to identify periods dominated either by system self-alignment or tissue extension. Failure to analyze video occurred in some cases due to light quality, feature occlusion, and hardware limitations related to writing the complete

video files for longer trials. As demonstrated in Figure A-3, crosshead displacements tended to be higher than those observed with video because the crosshead displacements include movement due to system alignment. Stone-to-stone displacements tended to stabilize during tissue-dominated regions but were not always zero or constant, indicating that self-alignment continued in these periods. This was also observed during review of the video footage.

Video analysis of the simulated extractions suggests that the self-alignment system functions well to align the periodontal complex to a preferential loading direction, indicated by the difference in magnitude but similarity in trends between crosshead and video displacement measures. Qualitative review of the video also identified events not fully explained by crosshead data, such as large drops in force (potentially associated with tissue rupture) corresponding to changes in alignment of the system. These features tended to correspond to discontinuities in the displacement curves, as in Figure A-3b at approximately 425 seconds.

Appendix B – Supplement to Chapter 4: Preparation of the Experimental Data for Fitting

Appendix B discusses the rationale and method for aligning force-time data acquired during different extraction experiments using the self-aligning apparatus. This is a necessary step to performing IFEA fits of a single FE model response to multiple sets of data. This Appendix was accepted for publication with Chapter 4 of this thesis.

The self-aligning apparatus employed for the collection of experimental data comprises of linear and rotational motion elements that allow potted samples to self-align to a preferential loading direction with the intention of reducing unrealistic out-of-line bending that may cause hard tissue fractures. An example of the extremity of this motion is depicted in Figure B-1.

Figure B-1: Two video frames demonstrating self-alignment of potted samples in the experimental apparatus. Left: alignment at the outset of loading; Right: alignment after 50N transition.

This alignment motion occurs at low force levels across a different period for each trial, as evidenced in the experimental data presented in Figure B-2. The transition from alignment motion to extension of the tissue occurs over a range of several hundred seconds. A single FE model cannot be fit to meet this range of data, especially because the displacement of the apparatus is outside the boundaries of the modelled system.

It is also unclear what the displacement within the boundaries of the dental complex will be during system alignment – the entirety of the low-load displacement cannot be ascribed to the alignment motion, either. However, all force measured by the crosshead in this period is transmitted through the dental complex. A transition force of 50N was determined to be the threshold at which all curves had transitioned from self-alignment to tissue extension. Data above this threshold and below the peak force was extracted for analysis (yellow curves in Figure B-.2). The time at which each curve passed the 50N threshold was averaged to determine a common transition time. The difference between the transition time and each curve was then used to translate each curve to the common point, preserving each individual curve shape and peak force beyond this new transition as demonstrated by the blue curves in Figure B-.2. A linear increase in force was assumed for the alignment period before transition in all cases and was not included in the SSE calculation for IFEA optimization.

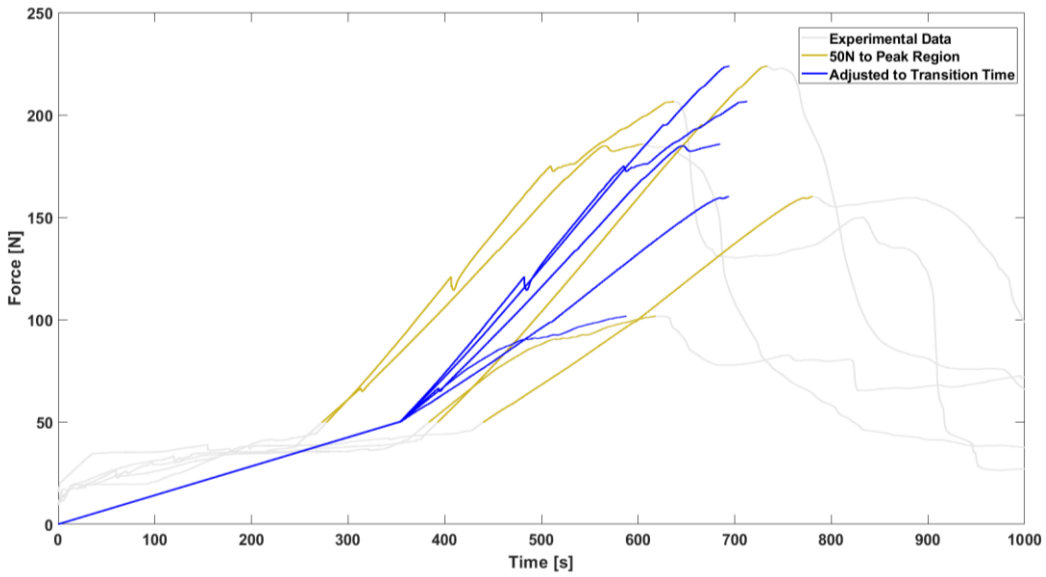

Figure B-2: Crosshead force-time traces acquired from ex vivo swine extractions. Loading regions selected for fitting are highlighted and translated to a common 50N transition point.

The multi-curve inverse method demonstrated sensitivity in early testing to experimental curves with exceptionally low stiffness or peak force. However, a quantitative measure was required in order to determine outlier curves for exclusion from the analysis. The challenge with calculating a confidence interval for the distribution of the experimental curve is that it requires the test traces to be the same length. For this analysis, each force-time curve was extended to the length of the longest curve at its peak value, as demonstrated in Figure B-3. As Figure B-3 demonstrates, even when its peak force is included in the calculation of the 95% confidence interval, the lowest curve (in green) falls outside these bounds. For this reason, the curve was excluded from the analysis.

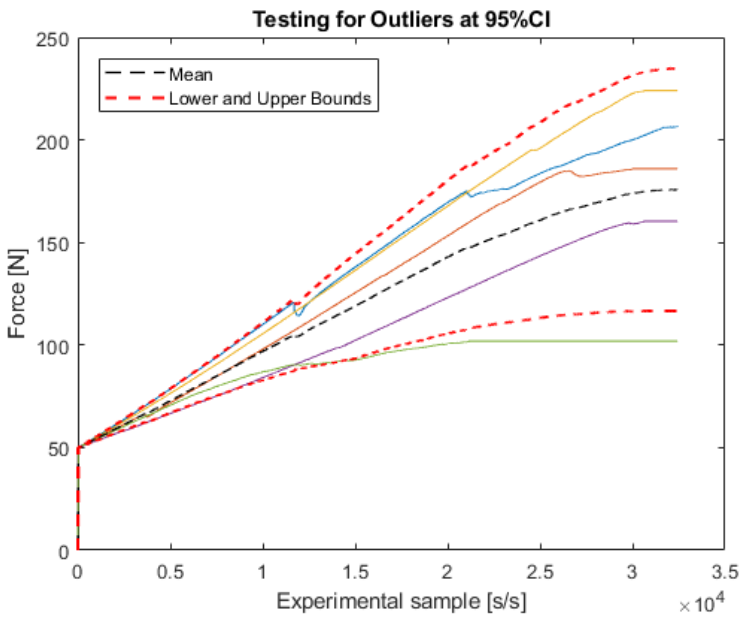

Figure B-3: Force-time curves for 0.2mm/min extractions with the mean and 95% confidence intervals calculated for the full domain. Each coloured curve represents a separate test extraction.

Appendix C – Supplement to Chapter 4: Material Parameter Sensitivity Analyses

Appendix C outlines several global material parameter sensitivity studies performed using the method developed in Chapter 4 of this thesis. Local variations in the hyperelastic and viscoelastic material parameters of the PDL material model are tested. The initial guess sensitivity of the IFEA procedure developed in Chapter 4 is also demonstrated in a study relating the initial guess, material parameters, and resulting error function values. This Appendix was accepted for publication with Chapter 4 of this thesis.

A demonstration of the sensitivity of the axisymmetric finite element (FE) model to the PDL material parameters is required to assess the validity of the model and the inverse FE optimization that was used to determine these parameters. Key indicators of issues with the model in such an analysis are strong discontinuities in model response as small perturbations are made local to the optimization solution and no observable effect on model response if variables are removed completely. Most parameters for the model are only assessed locally because removing them does not allow the material model to be evaluated. However, damage and viscoelasticity can both be assessed in this manner. Damage limits are needed for the basic function of the model (e.g. predicting peak force) and so the model response without them is omitted.

Sensitivity to Changes in Hyperelastic Parameters

The Arruda-Boyce hyperelastic model has three parameters: the initial modulus μ, the chain number N (which is also the square root of the locking stretch λ_L), and the bulk modulus k. Each parameter in the model has a physical meaning corresponding to the statistical representation of random walk chains, unlike other models that may contain an unspecified number of terms. However, assessing the sensitivity of and interaction amongst these parameters remains a necessity to prove the continuity of the optimization error function.

The sensitivity of each IFEA solution was assessed independently. The three Arruda-Boyce parameters were each varied by 10% of the solution value. In Figures C-1-3, these results are plotted in the first row of each figure. Chief interest is in the interactions among initial modulus and the remaining two parameters. In the second row, each plot represents a level of μ (90%, inverse solution, and 110%) and N is varied over the 90-110% range. Similarly, in the third row, k is varied within levels of μ but with the curve endpoints enlarged as there was little effect on the overall curve shape.

As anticipated, the greatest sensitivity appears to be to the initial modulus, μ. Across all three cases there are large changes in the curve shape and end time as a result of the 10% variation with this parameter demonstrating the most consistently high percent-changes to the curve endpoint with 10% variation, often ranging from 2-3.5%. The next most influential parameter is chain number, N. N appears to more strongly influence the peak predicted force whereas initial

modulus influences both peak force and the time at which peak force occurs. This trend persists at all levels of μ in the interactions with N. Finally, k appears to have a minor influence on the curve endpoint without strongly influencing the overall curve shape, except in the 2mm/min case in which it has an influence similar to modulus. This is to be anticipated as the deviatoric response of the material should be dominated by the chain-link model terms. In all cases and interactions, the variations are consistent and appear centered about the IFEA solution. This confirms the continuity of the underlying model at the determined solution based on these parameters.

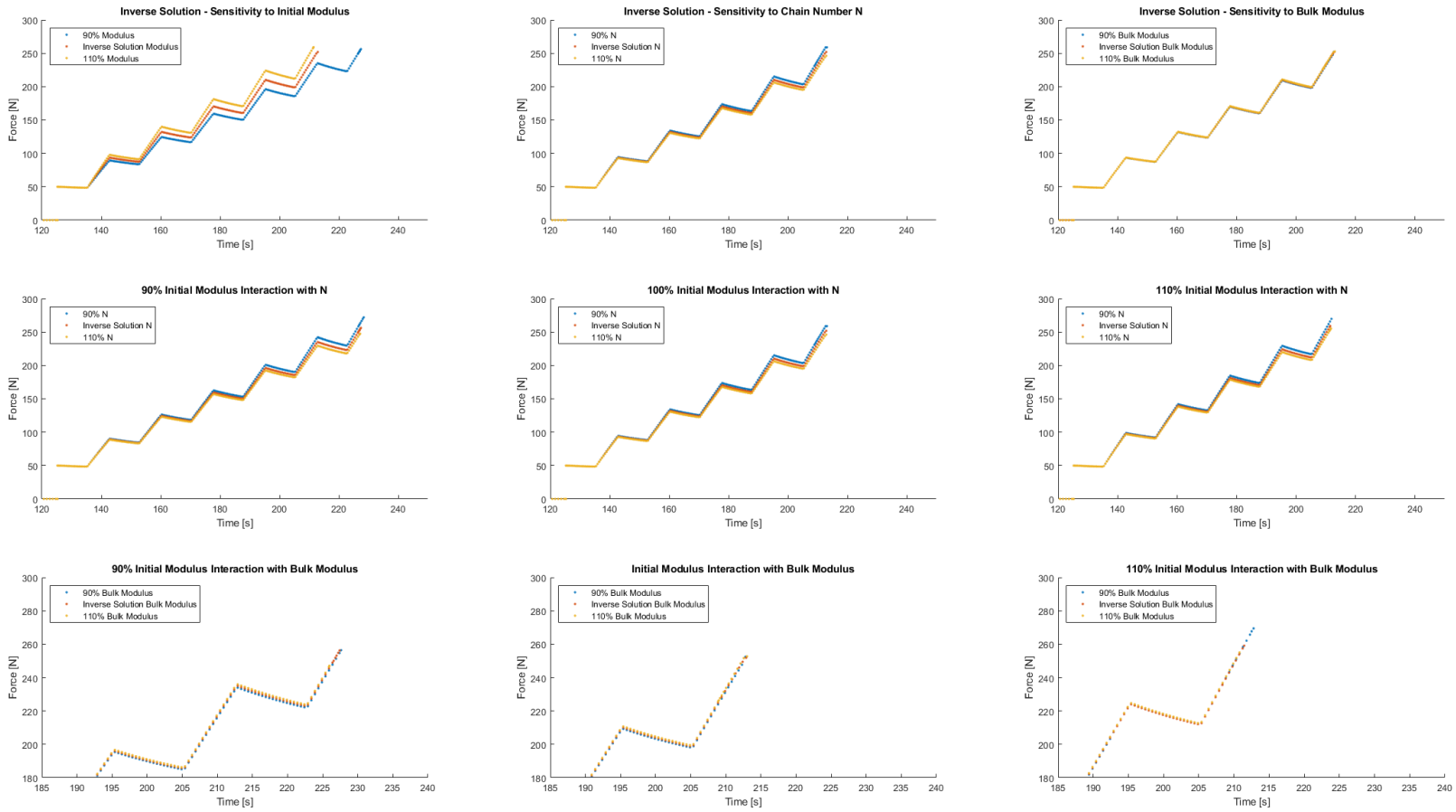

Figure C-1: Hyperelastic parameter sensitivity results for the intermittent displacement loading case

Table C-1: Sensitivity analysis results for the intermittent displacement loading case

Peak Force	Modulus		N		Bulk		Viscoelastic Constant	
% Varied	[N]	% Change	[N]	% Change	[N]	% Change	[N]	% Change
-10%	256.2	1.7	258.8	2.8	252.4	0.2	249.1	-1.1
0				251.8				
10%	259.1	2.9	246.1	-2.3	252.7	0.4	254.8	0.4

Time @ Pk. F	Modulus		N		Bulk		Viscoelastic Constant	
% Varied	[s]	% Change	[s]	% Change	[s]	% Change	[s]	% Change
-10%	227.4	6.8	213.1	0.1	212.8	0.0	212.8	0.0
0				212.9				
10%	211.5	-0.7	212.9	0.0	213.0	0.1	212.8	0.0

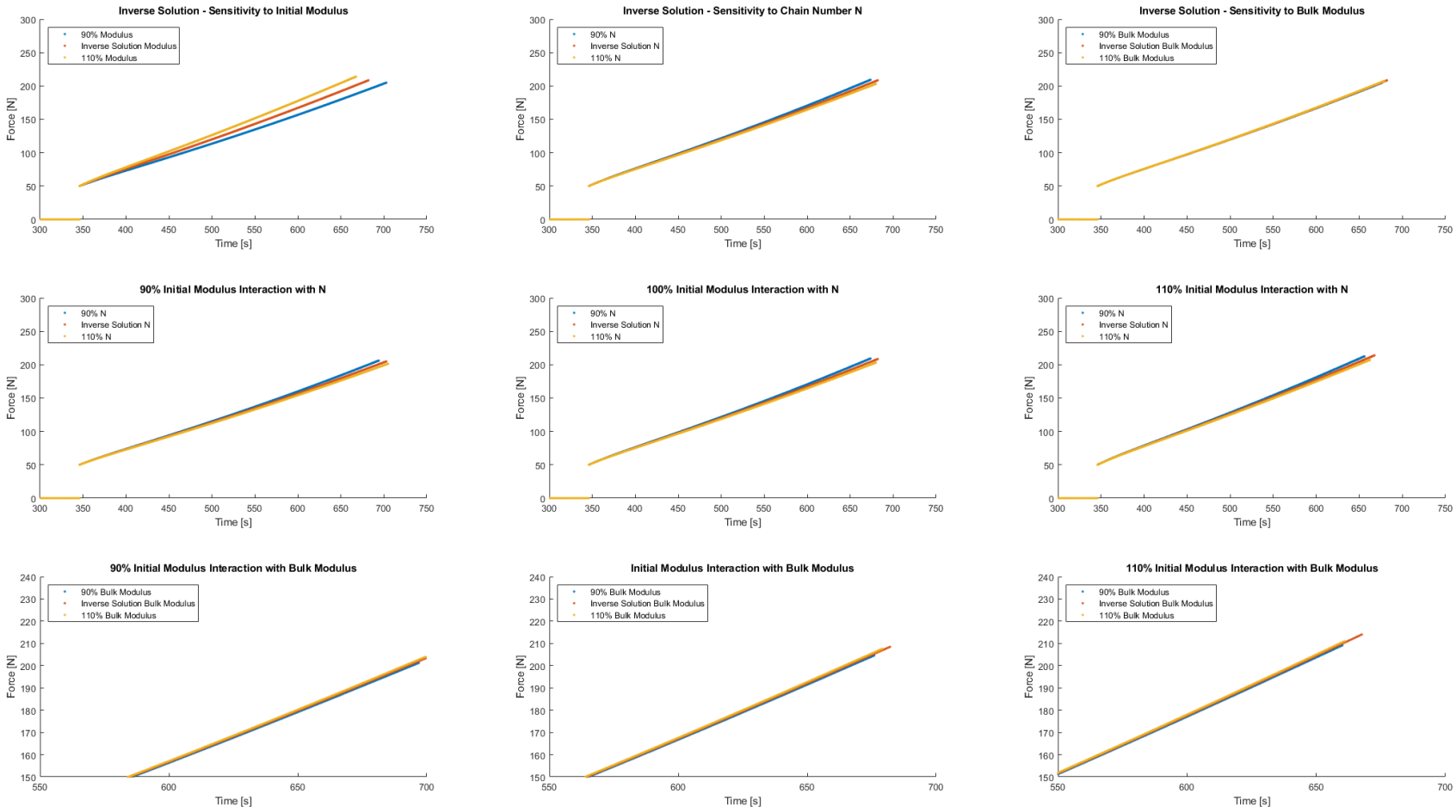

Figure C-2: Hyperelastic parameter sensitivity results for the 0.2mm/min loading case

Table C-2: Sensitivity analysis results for the 0.2mm/min load case

Peak Force	Modulus		N		Bulk		Viscoelastic Constant	
% Varied	[N]	% Change	[N]	% Change	[N]	% Change	[N]	% Change
-10%	204.9	-1.7	209.4	0.4	204.6	-1.9	208.7	0.1
0				208.5				
10%	214.0	2.7	203.1	-2.6	207.6	-0.4	211.9	1.6

Time @ Pk. F	Modulus		N		Bulk		Viscoelastic Constant	
% Varied	[s]	% Change	[s]	% Change	[s]	% Change	[s]	% Change
-10%	702.9	3.0	673.8	-1.2	676.0	-0.9	683.6	0.2
0				682.1				
10%	667.6	-2.1	679.8	-0.3	679.1	-0.4	687.6	0.8

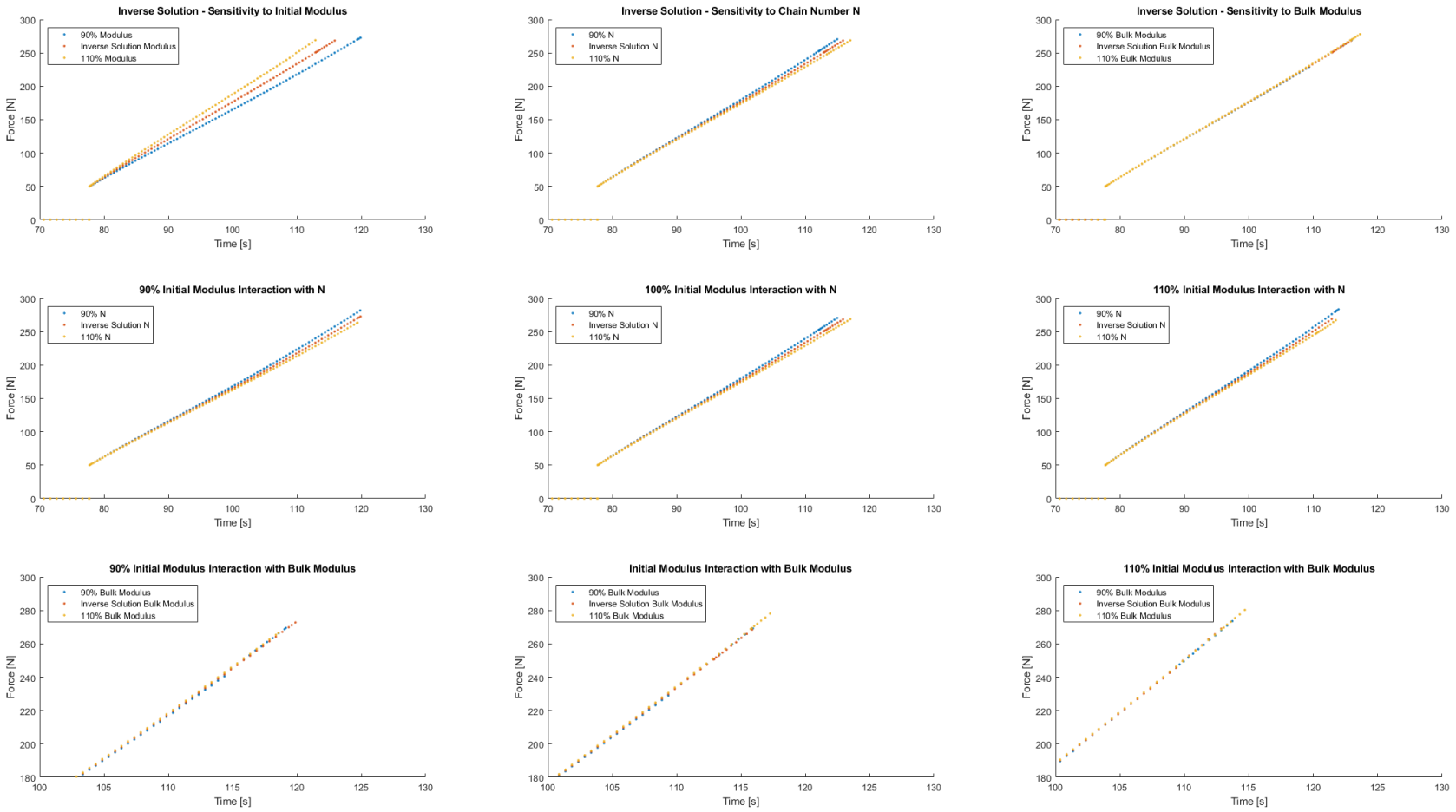

Figure C-3: Hyperelastic parameter sensitivity results for the 2mm/min loading case

Table C-3: Sensitivity analysis results for the 2mm/min loading case

Peak Force	Modulus		N		Bulk		Viscoelastic Constant	
% Varied	[N]	% Change	[N]	% Change	[N]	% Change	[N]	% Change
-10%	272.8	1.6	270.6	0.8	269.3	0.3	266.0	-0.9
0				268.5				
10%	269.1	0.2	268.8	0.1	278.1	3.6	277.3	3.3
Time @ Pk. F	**Modulus**		**N**		**Bulk**		**Viscoelastic Constant**	
% Varied	**[s]**	**% Change**	**[s]**	**% Change**	**[s]**	**% Change**	**[s]**	**% Change**
-10%	119.9	3.5	115.0	-0.8	115.9	0.1	116.2	0.3
0				115.9				
10%	112.9	-2.6	117.0	1.0	117.3	1.2	116.6	0.7

Sensitivity to Changes in Viscoelastic Constant

The necessity of the addition of viscoelasticity to the PDL model needs to be examined because two of the three cases studied with IFEA are for constanat-rate loading in force- and displacement-control schemes. The importance of viscoelasticity is demonstrated in Figure C-4, which compares the IFEA solution for intermittent displacement loading with the same solution but with no viscoelasticity ($g = 0$). There are two features of note in the differences between the presented curves: obviously, the curve with no viscoelasticity does not demonstrate relaxation in the displacement-controlled holding periods, and there is a notable difference in the peak force behaviour of the two simulations. It is clear that viscoelasticity is necessary for this case because the model cannot capture the shape of the experimental data. The damage limit SED_{max} would also need to be increased dramatically in this case to approximate the peak force behaviour of the experimental data. Given the agreement between the inverse value and estimates from the literature, this is not a desirable compromise. The viscoelasticity should then be maintained across all loading cases for purposes of consistency.

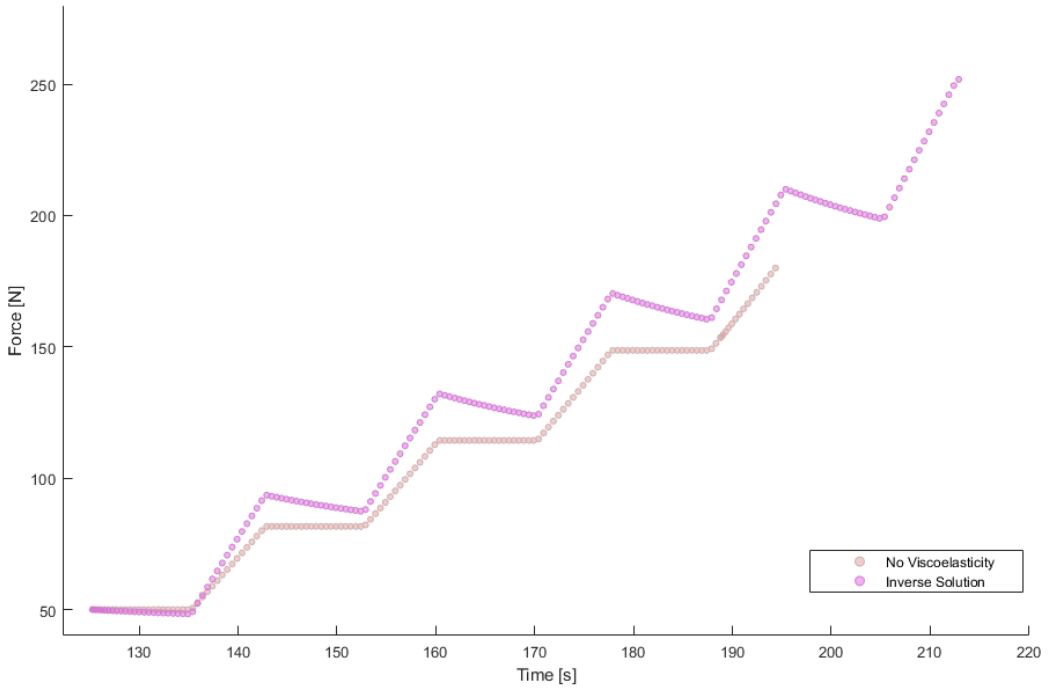

Figure C-4: Comparison of the coefficient-averaged IFEA solution with viscoelasticity with one generated using no viscoelasticity ($g = 0$)

The local sensitivity of all three load cases was then investigated around the coefficient-averaged solution. The viscoelastic coefficient was varied between 90-110% of the solution value and the force-time responses demonstrated in Figures C-5-7. Similar to the hyperelasticity sensitivity, the 0.2mm/min curves show relatively less sensitivity than the other loading schemes and all loading schemes demonstrate smooth, continuous variance about the minimum obtained with the inverse solution.

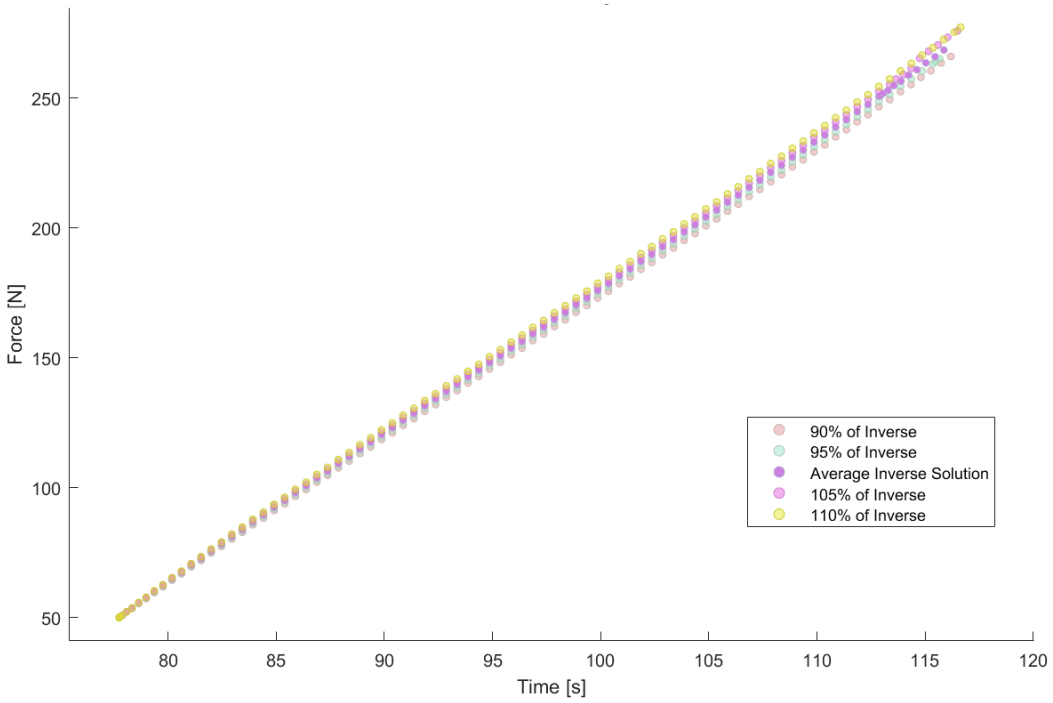

Figure C-5: Viscoelastic constant sensitivity results for 2mm/minute loading

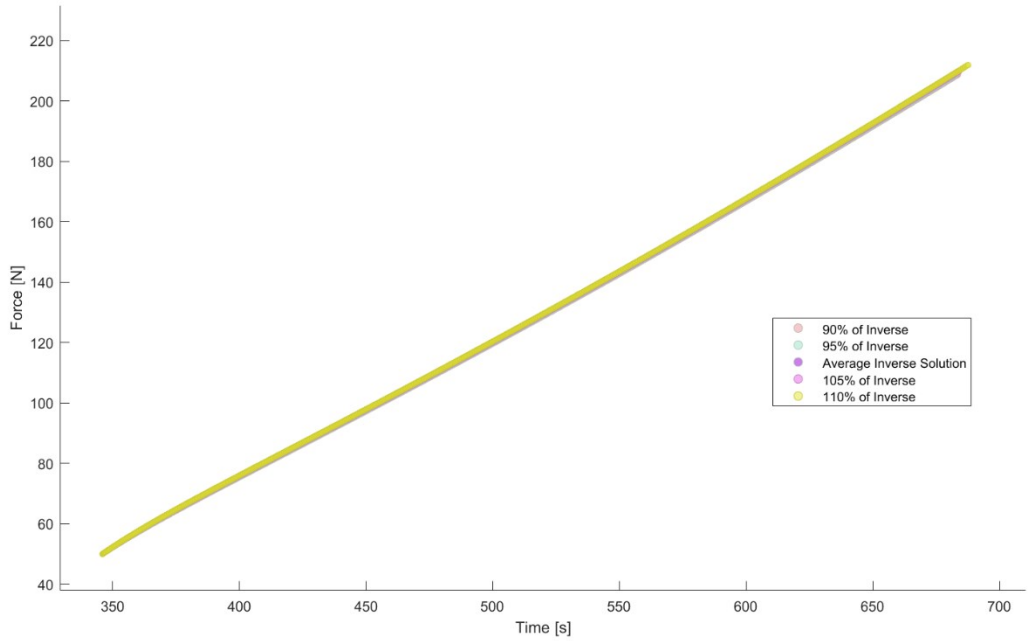

Figure C-6: Viscoelastic constant sensitivity results for 0.2mm/minute loading

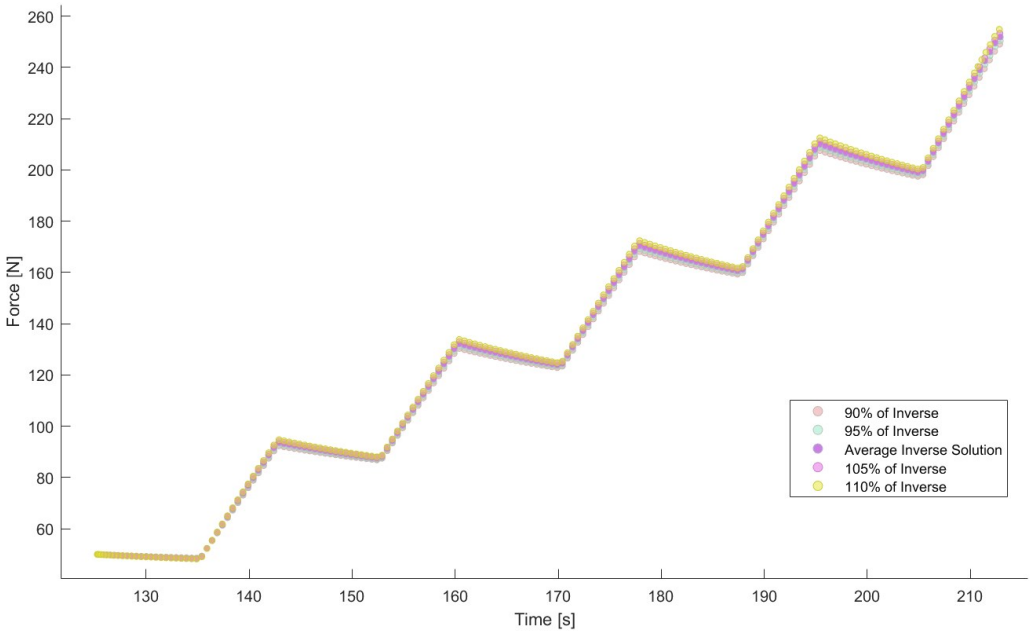

Figure C-7: Viscoelastic constant sensitivity results for intermittent displacement loading

Initial Guess Sensitivity

The initial guess sensitivity of the IFEA problem more directly assesses the behaviour of the IFEA optimization than it does the performance of the model. Initial guess values within the bounds of physical permissibility above the original values (given in Table S2.1). Each model was permitted to run to convergence. In the case that the model failed to converge within 4 weeks of runtime without a solution that fit the experimental data, it was noted as "No Convergence". In the case that the model did not converge in this period but a) had a solution that fit the data, and b) was demonstrating very little change in the material parameters, it was interpreted that this solution had converged to a local minimum. These solutions were reported as normal.

The results of the initial guess sensitivity study demonstrate that the IFEA problem is sensitive to large changes in the initial guess and that the method itself is sufficiently sensitive to find minima within the problem domain. Across all initial guesses, converged solution parameters range in relative change from the initial guess from 0.2% to 150%. Many of these relative changes are lower for the baseline initial guess compared to the upper and modified upper initial guesses, but this is likely due to the physical basis for the baseline initial guess. For example, the initial modulus μ changes no more than 10% from the baseline initial guess for any of the three test cases but the other initial guesses demonstrate changes in this parameter of up to 65.5% to find a converged solution. Notably, the converged values for initial modulus are similar in magnitude even when the initial guess is doubled, indicating that the value returned by averaging the coefficient value across the baseline guess cases is physically realistic and best explains the behaviour of the system. A similar trend can be observed for the damage-limiting strain energy SED_{max}.

Table C-1: Tabulated resulting parameters and errors at convergence for three initial solutions to the IFEA problem

Initial Guess	g		τ		μ		N		k		SED_{min}		SED_{max}		Converged Error
Upper	**1**		**50**		**1**		**20**		**15**		**0.5**		**7.5**		
	Value	% Change	Value	% Change	Value	% Change	Value	% Change	Value	% Change	Value	% Change	Value	% Change	
0.2mm/min	No Convergence														
2mm/min	0.998	-0.2	55.6	11.2	0.345	-65.5	21.6	8.0	18.1	20.7	0.804	60.8	4.79	-36.1	1.60E+07
Intermittent	No Convergence														
Modified Upper	**0.75**		**35**		**0.75**		**15**		**13**		**0.5**		**7.5**		
	Value	% Change	Value	% Change	Value	% Change	Value	% Change	Value	% Change	Value	% Change	Value	% Change	
0.2mm/min	0.602	-19.7	32.8	-6.3	0.455	-39.3	21	40.0	15.8	21.5	0.641	28.2	5.39	-28.1	4.50E+08
2mm/min	0.354	-52.8	41.3	18.0	0.462	-38.4	17.4	16.0	14.9	14.6	0.543	8.6	8.295	10.6	1.87E+07
Intermittent	0.109	-85.5	41.285	18.0	0.607	-19.1	20.86	39.1	12.234	-5.9	1.172	134.4	9.261	23.5	2.74E+04
Baseline	**0.5**		**20**		**0.5**		**10**		**10**		**0.1**		**5**		
	Value	% Change	Value	% Change	Value	% Change	Value	% Change	Value	% Change	Value	% Change	Value	% Change	
0.2mm/min	0.57	14.0	20.7	3.5	0.45	-10.0	9.51	-4.9	10.2	2.0	0.246	146.0	5.86	17.2	2.44E+05
2mm/min	0.586	17.2	19.3	-3.5	0.505	1.0	9.58	-4.2	9.7	-3.0	0.129	29.0	5.71	14.2	1.90E+05
Intermittent	0.527	5.4	20.4	2.0	0.463	-7.4	10.6	6.0	9.63	-3.7	0.25	150.0	6.2	24.0	2.43E+04

The results of the initial guess sensitivity study also demonstrate that the physically-based baseline initial guess results in the lowest error function values at convergence. The higher error values from different initial guesses suggest the existence of local minima throughout the IFEA problem domain. It is unsurprising that the convexity of the IFEA error function is disrupted in this way given the large number of parameters (7) and the non-linear interactions among the parameters (as demonstrated in Figures C1-3). The baseline initial guess was informed by physically-representative values from the literature rather than randomly selected for this reason. The similarity of solution parameters across each load case despite the capability of the optimization scheme to impose large changes (as demonstrated in this supplemental study) and the good performance of the load-case-averaged solution at explaining the behaviour of the dental complex across these cases confirms this decision.

Conclusion

The sensitivity of the axisymmetric finite element model of the dental complex has been assessed in two ways: first, the sensitivity of the model to local variations in the IFEA solution parameters was investigated; second, the sensitivity of the IFEA process to large changes in initial guess has been demonstrated. The findings of these investigations demonstrate smooth local sensitivity about the converged IFEA solution and some global dependency on initial guess that influences both the IFEA solution and converged value of the optimization error function. It is unsurprising to find that the optimization error function is not strictly convex and contains local minima for problems fitting soft tissue parameters, particularly one with a large number of parameters with non-linear interactions amongst them (e.g. between initial modulus and chain number). Confidence in the presented IFEA solution arises from the demonstrated local sensitivity about the baseline initial guess which was formulated from the literature; the much lower error function at convergence for this initial guess compared to the local minima found by other initial guesses; the capacity of the optimization algorithm to drive large changes in parameters (up to 87%) when necessary to drive towards a local minimum; and the similarity in solution parameters found for the IFEA problem across three different loading regimes. These factors combined illustrate an IFEA method that is sensitive to local minima but capable of locating a candidate global error minimum when a well-informed initial guess is provided, resulting in a solution that well represents the underlying physical behaviour of the dental complex rather than a spurious numerical result.

Appendix D – Supplement to Chapter 4: Mesh Sensitivity Analysis

Appendix D contains a mesh sensitivity analysis investigating the PDL mesh refinement applied to the axisymmetric FE model developed in Chapter 4. The overall model response (rupture time) and local element behaviours (principal strain) are investigated. This study was performed before the complete development of the visco-damage hyperelastic model employed in Chapter 4 and uses a principal strain criterion to govern the damage of the PDL material. This Appendix was accepted for publication with Chapter 4 of this thesis.

The mesh sensitivity analysis was performed early in the model development using the visco-damage-hyperelastic model with a principal strain damage criterion (rather than one using strain energy density). The damage-limiting strain ϵ_{max} was set to 1.52.

Four target element sizes were tested for mesh convergence. Only elements at the boundaries of the PDL (interface elements) were refined with the target body size for the PDL remaining at 0.05mm. The behaviour of the model as interface element target size was reduced to a minimum of 0.02mm, which was the practical limit of the mesh solver stability.

The two leading elements nearest to the occlusal/superior corner of the PDL-tooth boundary were examined because this location is engaged throughout loading and is the initiation site of simulated PDL rupture. Two elements at a location 1mm inferior to this corner on the PDL-tooth interface were also examined for strain behaviour. The results of the convergence study are demonstrated in Table D-1 and Figure D-1.

Table D-1: Mesh Convergence Study Results By Target Interface Element Size

Interface Element Size [mm]	Numer of PDL Elements	Leading Element Strain at Rupture		1mm Inferior Element Strain at Rupture		Simulation End Time	
		Value	% Change	Value	% Change	Value [s]	% Change
0.02	60194	1.09	8.1	0.42	6.9	33.8	5.6
0.03	46791	1.19	2.8	0.45	16.5	35.9	12.0
0.04	38867	1.22	16.1	0.54	3.8	40.8	1.6
0.05	33588	1.46		0.56		41.4	

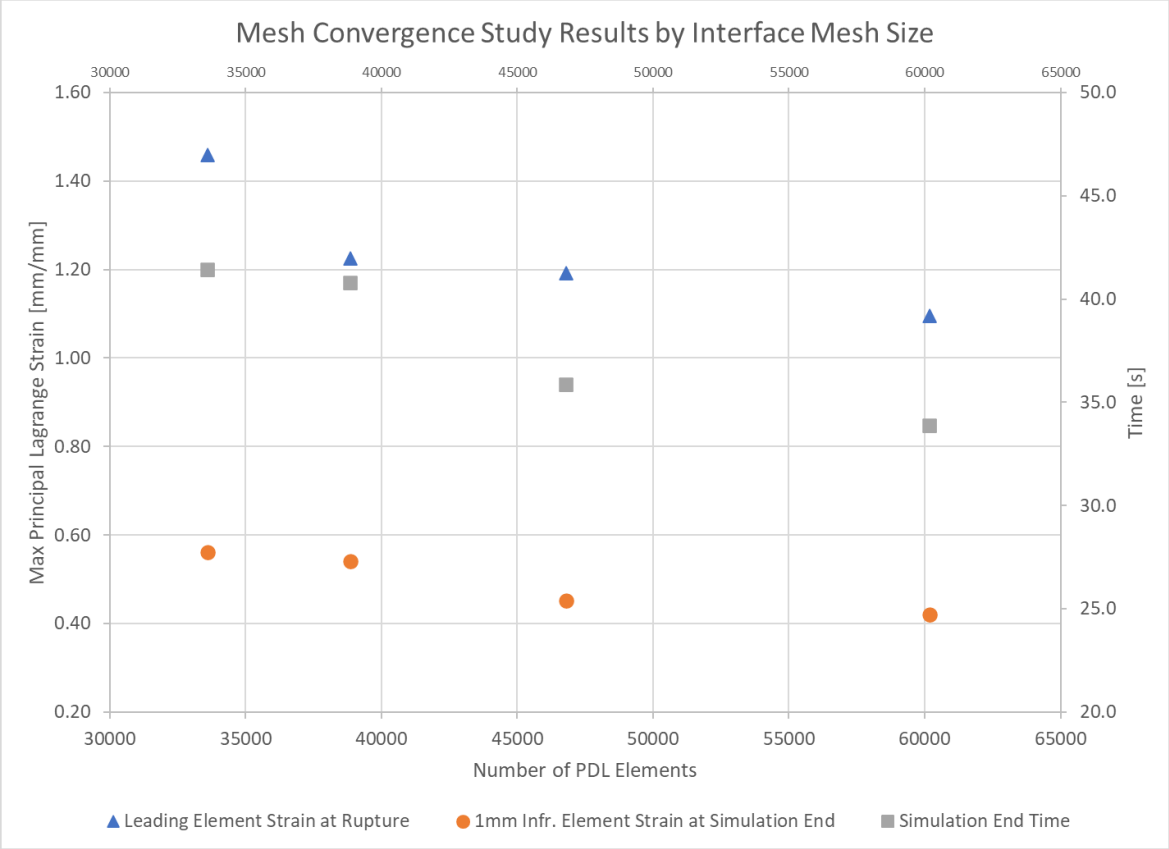

Figure D-1: Mesh convergence study results

The leading element interface strains (Figure D-2) demonstrate a continuing increase as the number of elements in the mesh decreased, which is an expected behaviour for these elements as they are directly adjacent to an infinitely sharp corner at the boundary of two materials. We anticipate a stress/strain singularity may occur because of this geometry and material dissimilarity. The behaviour of the elements 1mm inferior to this location represent the overall behaviour of the PDL body and demonstrate the converging trends anticipated for mesh independent behaviour (Figure D-3). At an interface mesh size of 0.02mm, there is a change in both maximum principal strain at the 1mm inferior elements and simulation end time less than 10% relative to a mesh size of 0.03mm, indicating that the mesh behaviour is converging and the overall system behaviour is isolated from the singularity at the leading edge. 0.02mm was also the lowest mesh size that could still yield a numerically-stable solution. As a result of the converging behaviour and stability restrictions, the 0.02mm interface target element size was selected for the model.

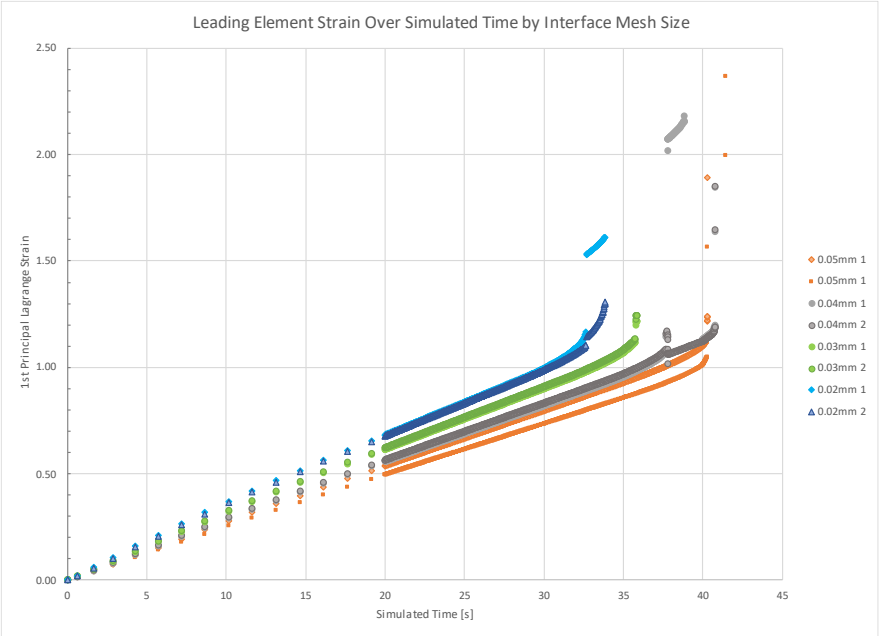

Figure D-2: 1st Principal Strain Behaviour of Leading Edge Elements by Mesh Size. Elements numbered 1 and 2 indicate two elements selected on either symmetry plane at the same location.

The leading element behaviour over time for the various mesh sizes in Figure D-2 reflects the singularity behaviour demonstrated in Figure D-1, with changing strain rates and time to rupture as mesh size decreases. The behaviour of the 1mm inferior elements (Figure D-3), however, contrasts this behaviour and shows that the overall system behaviour is not strictly dependent on these leading-edge elements. It is evident that the strain rate in the 1mm-inferior elements is independent of the refinement mesh size as the different cases all follow the same trend with differing rupture times at the end of the simulation. These trends are as anticipated for mesh convergence while containing a geometric singularity at the sharp corner of the leading edge and indicate that the overall system behaviour is not strongly mesh-dependent. This further strengthens the decision to use the 0.02mm mesh size at converging simulation end time.

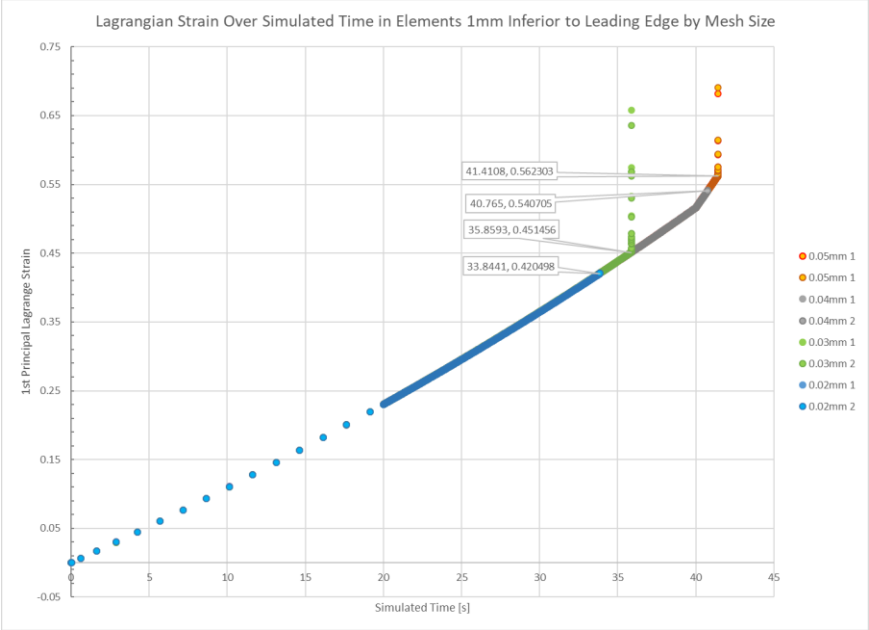

Figure D-3: 1st Principal Strain Behaviour of Elements 1mm Inferior to the Leading Edge by Mesh Size. Elements numbered 1 and 2 indicate two elements selected on either symmetry plane at the same location.

Appendix E – Supplement to Chapter 5: Investigation of K-means algorithm sorting of instantaneous stiffness curves

This appendix outlines an investigation of the robustness of the K-means algorithm method for sorting instantaneous stiffness curves. This study repeats the analysis using various cluster numbers to validate the method and its findings based on load rate. The data used in this study are the stiffness curves and K-means algorithm clusters originally devised in Chapter 5.

The purpose of the additional K-means analysis is to examine the factors that influence the sorting of tooth extraction stiffness curves by the K-means algorithm. In principle, the K-means algorithm sorts curves by closeness to cluster kernels based on Euclidean distance at every point in the curve domain, thereby capturing differences in both the stiffness magnitudes and overall shape of the curves. However, the reliability of this method at detecting systematic differences among the load rate groups (rather than random variations) has not been examined. The method for this examination is to decimate the data set into finer clusters by increasing the number of clusters from 4 to 6 and then to 8, re-performing the analysis with 50,000 random restarts for every case. The resulting clusters are then plotted separately and colour-coded so that each load rate has its own colour. Systematic differences in stiffness will survive this decimation, with the lower- and higher-stiffness clusters being subdivided without curves crossing over. Clusters resulting from grouping of random variations will not survive decimation, with blending of curves from both primary clusters in the decimated groups.

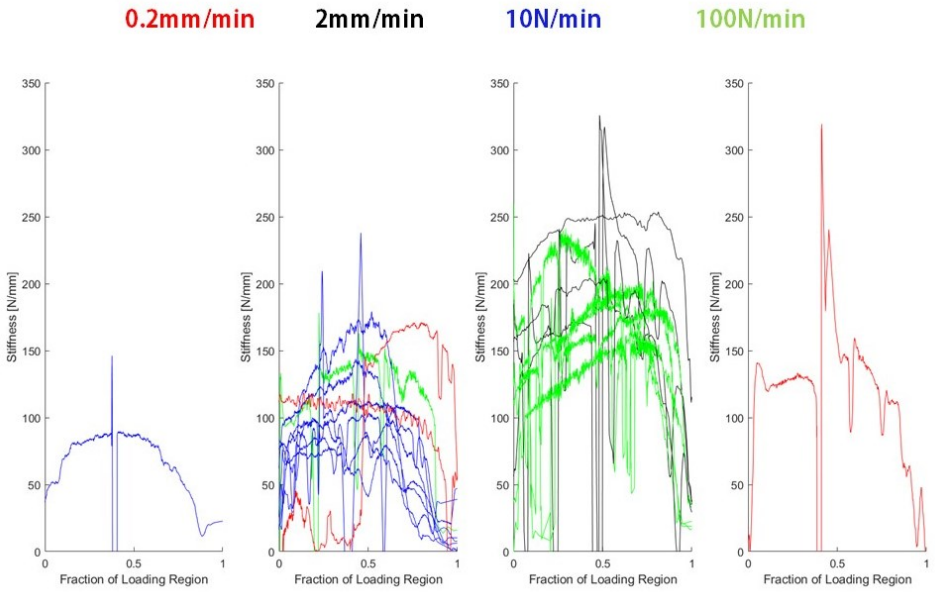

Figure E-1: K-Means Stiffness Cluster Results for 4 Clusters. Each sub plot is a cluster with colour identifying the load rate at which a stiffness curve was obtained.

The K-means results for four clusters (Figure E-1) demonstrate the sorting of the stiffness curves by load rate. The centre-left curve contains 0.2mm/min (red) and 10N/min curves (blue) with a single 100N/min curve (green) on the higher side of the cluster. The centre-right cluster is the higher main cluster composed entirely of 100N/min and 2mm/min curves (black). Separating the

clusters into separate plots also highlights the disruptions that may drive the two single-curve clusters away from the others. Some rapid motion (such as tissue rupture or shift in the self-aligning system) caused large drops and then spikes in stiffness in the two curves that were isolated.

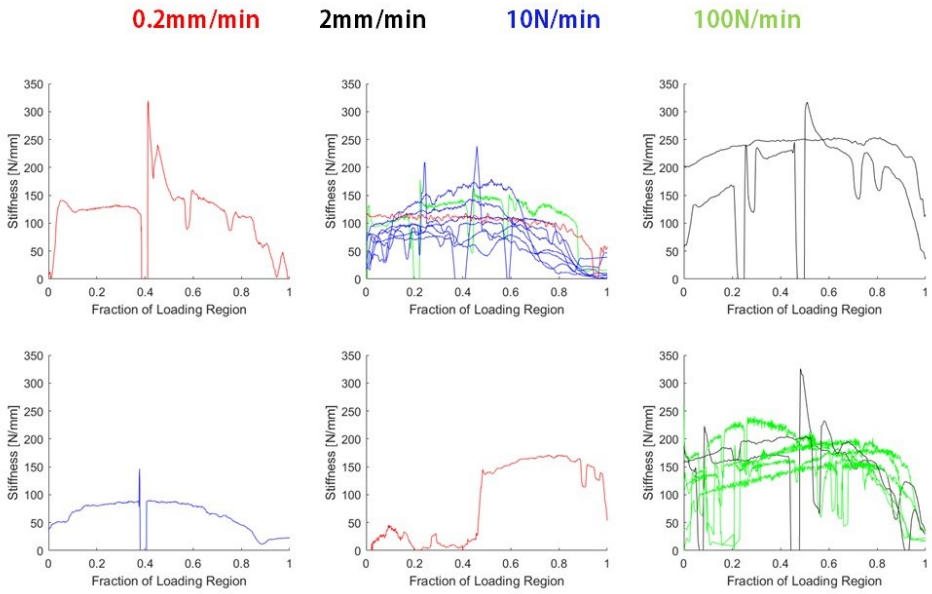

Figure E-2: K-Means Stiffness Cluster Results for 6 Clusters. Each sub plot is a cluster with colour identifying the load rate at which a stiffness curve was obtained.

Both primary clusters survive decimation into 6 clusters (Figure E-2) by sub-division into two additional clusters. In the higher cluster, two 2mm/min curves are sorted into their own cluster at higher stiffness than the remainder of the cluster. A single 0.2mm/min curve with a prolonged low-stiffness region is isolated from the remainder of the lower main cluster.

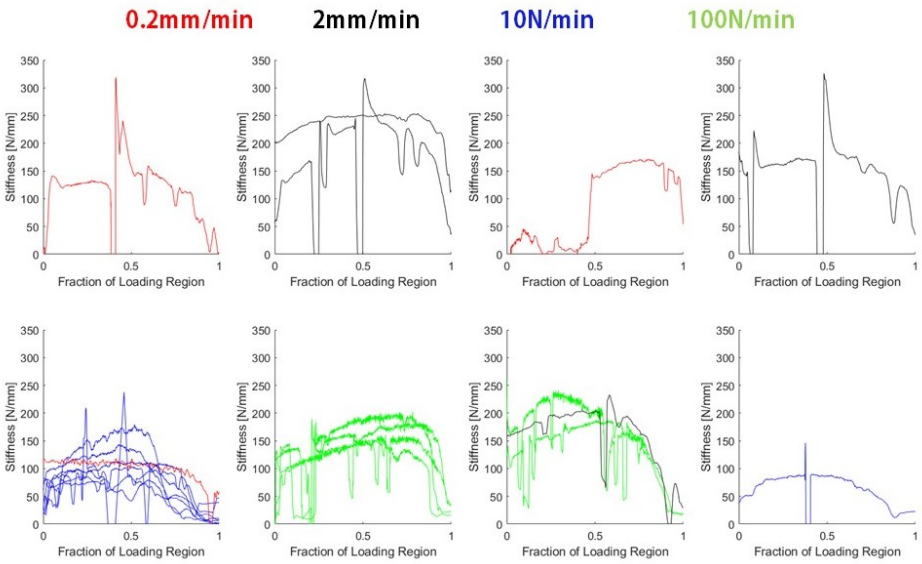

Figure E-3: K-Means Stiffness Cluster Results for 8 Clusters. Each sub plot is a cluster with colour identifying the load rate at which a stiffness curve was obtained.

Both primary clusters survived the decimation to 8 clusters with the exception of a single curve, which moved from the lower cluster to the higher cluster. This curve was the 100N/min curve that was sorted into the lower cluster, visible in that cluster in Figures E-2 and E-1. Additional single-curve clusters are identified along with a split of the higher of the two main clusters.

This analysis confirms that the clusters obtained from the initial 4-cluster K-means algorithm sorting are driven by the systematic differences in stiffness curves based on their underlying load rate rather than random variances. In both decimation steps the clusters are preserved almost perfectly, with only one 100N/min curve moving from the lower main cluster to a higher cluster when the number of clusters in the analysis is doubled. This finding indicates that it is likely random variation in stiffness that caused this curve to be sorted into the lower cluster in the 4-curve analysis but that overall, the differences among load groups are much stronger than these random variances.

Although this decimation analysis shows that systematic differences among stiffness curves can be observed at higher cluster numbers, the results of the 4-cluster analysis are still most appropriate for studying the overall trends in stiffness among load groups. Only four loading regimes are included in the data provided to the K-means algorithm and, although the algorithm is completely blinded to this information, there is no physical basis for the inclusion of more

clusters than there are loading regimes. The decimation analysis presented here should be carefully considered as a post-hoc analysis to the four-cluster analysis rather than equivalent in relevance to the physical experiment.

Appendix F – Supplement to Chapter 6: Interface Codes and Dependencies

Appendix F contains the information needed to install the appropriate Python environment to run the instrumentation interface developed in Chapter 6. A list of required dependencies is included, along with two separate Python scripts that govern the FUTEK load cell and generate the interface windows. The IronPython script governing the load cell is controlled by the Python script for the interface and should be installed in a directory with the FUTEK DLL files as described below.

Installed Packages

The following software packages need to be installed on a Windows 10 operating system (or later) to operate the interface:

1. IronPython 2.7.12 - https://ironpython.net/download/
    - Install this in its own directory. IronPython runs in its own environment and can be kept outside your Visual Studio environment
2. Python 3.12 - https://ironpython.net/download/
    - It is recommended to install Visual Studio Code, which will install Python and all its backend requirements. It also provides a shell environment and debugging help.
    - The following libraries can be installed for Python in either the Visual Studio shell or the windows terminal. Python should include the latest version of pip, which can be used to install and unpack all of these:
        - PySimpleGUi
        - Tkinter
        - Matplotlib
        - Datetime
        - csv
        - re
3. Futek device dynamic library (DLL) - https://media.futek.com/content/futek/files/downloads/futek-usb-dll.zip
    - This DLL needs to be accessed by the IronPython script for managing the device. Unpack it in the same location as IronPython and make sure the script points to the right location

With any open-source project, there can be a number of hidden dependencies that are not well documented based on the assumption that a complete development package is already installed. The following distributions can be installed using Visual Studio tools:

4. Visual Studio C++ distributables (2022, 2019, 2017, 2013)
5. .Net Core and .NET framework

Futek Device Control Code - IronPython Environment

```
import wpf
import clr
import System
clr.AddReferenceToFileAndPath(r"C:\Users\timga\IPyth\FUTEK\AnyCPU\FUTEK_USB_DLL.d
ll")
clr.AddReferenceByPartialName("IronPython")
import FUTEK_USB_DLL
from FUTEK_USB_DLL import USB_DLL
from System.Windows import Application, Window
from IronPython.Compiler import CallTarget0
import time
import sys

# Initialize important variables
deviceSerNo = "723794" #Change this if we have to!

class deviceObj:
    oFTUEKUSBDLL = FUTEK_USB_DLL.USB_DLL()
    Title = "Futek Load Cell in Background"
    oDLL = FUTEK_USB_DLL.USB_DLL()
    SerialNumber = ""
    DeviceHandle = ""
    Temp = ""
    OffsetValue = 0
    FullscaleValue = 0
    FullScaleLoad = 0
    DecimalPoint = 0
    UnitCode = 0
    UnitsText = ""
    Tare = 0.0
    NormalData = 0
    CalculatedReading = 0.0
    OpenedConnection = False #was defaulted false

def GetOffsetValue(deviceObj):
        while True:
            deviceObj.Temp =
deviceObj.oDLL.Get_Offset_Value(deviceObj.DeviceHandle)
            if deviceObj.Temp.isnumeric():
                break
        deviceObj.OffsetValue = int(deviceObj.Temp)
        return
```

```
        # <summary>
        # Gets the fullscale value by using the FUTEK DLL Method and
        # check if it's numeric and then parse it into integer
        # then store it into the memory
        # </summary>
def GetFullscaleValue(deviceObj):
    while True:
        deviceObj.Temp =
deviceObj.oDLL.Get_Fullscale_Value(deviceObj.DeviceHandle)
        if deviceObj.Temp.isnumeric():
            break
    deviceObj.FullscaleValue = int(deviceObj.Temp)
    return

    # <summary>
    # Gets the fullscale load by using the FUTEK DLL Method and
    # check if it's numeric and then parse it into integer
    # then store it into the memory
    # </summary>
def GetFullscaleLoad(deviceObj):
    while True:
        deviceObj.Temp =
deviceObj.oDLL.Get_Fullscale_Load(deviceObj.DeviceHandle)
        if deviceObj.Temp.isnumeric():
            break
    deviceObj.FullScaleLoad = int(deviceObj.Temp)
    return

    # <summary>
    # Gets the number of decimal places by using the FUTEK
    # DLL Method and check if it's numeric and then parse
    # it into integer then store it into the memory
    # </summary>
def GetDecimalPoint(deviceObj):
    while True:
        deviceObj.Temp = deviceObj.oDLL.Get_Decimal_Point(deviceObj.DeviceHandle)
        if deviceObj.Temp.isnumeric():
            break
    deviceObj.DecimalPoint = int(deviceObj.Temp)
    if deviceObj.DecimalPoint > 3:
        deviceObj.DecimalPoint = 0
    return

    # <summary>
    # Gets the unit code to later find unit needed for the device
```

```
    # by using the FUTEK DLL Method and check if it's numeric and
    # then parse it into integer and then store it into the memory
    # </summary>
def GetUnitCode(deviceObj):
    while True:
        deviceObj.Temp = deviceObj.oDLL.Get_Unit_Code(deviceObj.DeviceHandle)
        if deviceObj.Temp.isnumeric():
            break
    deviceObj.UnitCode = int(deviceObj.Temp)
    return

    # <summary>
    # Uses the UnitCode from the memory to find the correct
    # unit for the device
    # </summary>
    # <remarks>
    # For more information about unit code visit:
    #
http://www.futek.com/files/docs/API/FUTEK_USB_DLL/webframe.html#UnitCodes.html
    # </remarks>
def FindUnits(deviceObj):
    units = {
        0 : "atm", 1 : "bar", 2 : "dyn", 3 : "ft-H20", 4 : "ft-lb", 5 : "g", 6 :
"g-cm", 7 : "g-mm", 8 : "in-H20", 9 : "in-lb",
        10 : "in-oz", 11 : "kdyn", 12 : "kg", 13 : "kg-cm", 14 : "kg/cm2", 15 :
"kg-m", 16 : "klbs", 17 : "kN", 18 : "kPa", 19 : "kpsi",
        20 : "lbs", 21 : "Mdyn", 22 : "mmHG", 23 : "mN-m", 24 : "MPa", 25 : "MT",
26 : "N", 27 : "N-cm", 28 : "N-m", 29 : "N-mm",
        30 : "oz", 31 : "psi", 32 : "Pa", 33 : "T", 34 : "mV/V", 35 : "muA", 36 :
"mA", 37 : "A", 38 : "mm", 39 : "cm",
        40 : "dm", 41 : "m", 42 : "km", 43 : "in", 44 : "ft", 45 : "yd", 46 :
"mi", 47 : "mug", 48 : "mg", 49 : "LT",
        50 : "mbar", 51 : "degC", 52 : "degF", 53 : "K", 54 : "degRa", 55 : "kN-
m", 56 : "g-m", 57 : "nV", 58 : "muV", 59 : "mV",
        60 : "V", 61 : "kV", 62 : "NONE"
        }
    deviceObj.UnitsText= units.get(deviceObj.UnitCode, "Undefined")
    return

def objectSetup(deviceObj):
    GetOffsetValue(deviceObj)
    GetFullscaleValue(deviceObj)
    GetFullscaleLoad(deviceObj)
    GetDecimalPoint(deviceObj)
    GetUnitCode(deviceObj)
```

```
    FindUnits(deviceObj)

deviceObj = deviceObj()
deviceObj.SerialNumber = deviceSerNo
#print(deviceObj.SerialNumber)
deviceObj.oDLL.Open_Device_Connection(deviceObj.SerialNumber)

if deviceObj.oDLL.DeviceStatus == 0:
    print("Device OK!")
    deviceObj.OpenedConnection = True
    deviceObj.DeviceHandle = deviceObj.oDLL.DeviceHandle
    objectSetup(deviceObj)
    print("Device Units are in " + deviceObj.UnitsText)
else:
    print("Device Error " + str(deviceObj.oDLL.DeviceStatus))
    quit()

while True:
    deviceObj.Temp = deviceObj.oDLL.Normal_Data_Request(deviceObj.DeviceHandle)
    deviceObj.NormalData = int(deviceObj.Temp)
    deviceObj.CalculatedReading = deviceObj.NormalData - deviceObj.OffsetValue
    deviceObj.CalculatedReading /= float(deviceObj.FullscaleValue -
deviceObj.OffsetValue)
    deviceObj.CalculatedReading *= deviceObj.FullScaleLoad
    deviceObj.CalculatedReading /= float(pow(10, deviceObj.DecimalPoint))
    print(deviceObj.CalculatedReading)

    #if sys.stdin == b'SMELLY'":
        #print("smell")

    time.sleep(0.25)
```

Main Interface Code - Python 3.12 Environment

```
import PySimpleGUI as sg
from tkinter.filedialog import askdirectory
import matplotlib.pyplot as plt
import matplotlib.figure
import matplotlib
from matplotlib.backends.backend_tkagg import FigureCanvasTkAgg
from datetime import datetime, date
import time
import sys
import csv
import subprocess
import re


sg.theme('Mono Blue')
sg.set_options(font = 'Impact 15', button_element_size=(20, 2))

def updateStaticFigure(data):
    axes = fig.axes
    x = [i[0] for i in data]
    y = [i[1] for i in data]
    axes[0].cla()
    axes[0].plot(x,y,'r-')
    figure_canvas_agg.draw() # call the draw method
    figure_canvas_agg.get_tk_widget().pack() #I guess we need pack to send it to
GUI as well

global holdF
holdF = 50
global rampR
rampR = 100
global rampT
rampT = 0
dateStr = datetime.now().strftime("%Y-%m-%d.%H.%M")
defaultList = [dateStr, '.csv']
defaultName = "".join(defaultList)
saveFileName = defaultName
proceedControl = 0

# GUI layout Setup
leftLayout = [[sg.VPush()],
          [
           sg.Text(f'Hold at \n{holdF} N', k='-HOLDFTEXT-',
justification='center', font = ('Impact 25'), size = (15,2)),
```

```
           sg.Column([[sg.Button('HOLD UP', k = '-HOLDUPB-',
expand_x=True)],[sg.Button('HOLD DOWN', k = '-HOLDDOWNB-')]]),
           sg.Text(f'Ramp load at \n{rampR} N/min', k = '-RAMPRTEXT-', font =
('Impact 25'), justification='center', size=(15,2)),
           sg.Column([[sg.Button('RAMP UP', k = '-RAMPUPB-',
expand_x=True)],[sg.Button('RAMP DOWN', k = '-RAMPDOWNB-')]])
           ],
           [
              sg.Button('UPDATE PARAMETERS AND GRAPH', k = '-UPDATEB-',
expand_x=True)
           ],
           [sg.Text('Save As:', k='-SAVEHEAD-', justification='right'),
sg.Input(defaultName,k='-SAVENAME-' ), sg.B('OK', k='-FILENAMEBUTTON-')]
           ]

rightLayout = [[sg.VPush()],
              [sg.Canvas(k='-SETUPPLOT-')],
              [sg.Button('PROCEED TO TEST', k='-PROCBUTTON-')]
              ]

mainLayout = [[sg.Column(leftLayout), sg.Column(rightLayout)]]
errLayout = [[sg.Text('Nonzero Ramp Not Permissible')]]

# call window
windowName = sg.Window('Benex Interface 2023', mainLayout, finalize=True)

#matplotlib setup
fig = matplotlib.figure.Figure(figsize = (5,4))
fig.add_subplot(111).plot([],[]) # need this subplot always inside the matplotlib
figure item
figure_canvas_agg = FigureCanvasTkAgg(fig, windowName['-SETUPPLOT-'].TKCanvas) #
assign the tkinter object to the canvas in the layout
figure_canvas_agg.draw() # call the draw method
figure_canvas_agg.get_tk_widget().pack()

while True:
   event, values =  windowName.read() # get events from the window

   if event =='-FILENAMEBUTTON-':
      saveFileName = values['-SAVENAME-']

   if event == '-HOLDUPB-':
      holdF += 25
      if holdF >= 400:
         holdF = 400
```

```
      windowName['-HOLDFTEXT-'].update(f'Hold at \n{holdF} N')

   if event== '-HOLDDOWNB-':
      holdF -= 25
      if holdF <= 0:
         holdF=0

      windowName['-HOLDFTEXT-'].update(f'Hold at \n{holdF} N')

   if event== '-PROCBUTTON-':
      proceedControl=1
      windowName.close()

   if event == '-RAMPUPB-':
      rampR += 25
      if rampR >=300:
         rampR = 300
      windowName['-RAMPRTEXT-'].update(f'Ramp load at \n{rampR} N/min')

   if event == '-RAMPDOWNB-':
      rampR-=25
      if rampR <= 0:
         rampR=0
      windowName['-RAMPRTEXT-'].update(f'Ramp load at \n{rampR} N/min')

   if event== sg.WIN_CLOSED:
      break

   if event == '-UPDATEB-':
    if rampR==0:
       sg.Window('ERROR', errLayout)
    rampT = 60*holdF/rampR
    endTime=200
    if rampT>=150:
       endTime=600
    desiredRampList = [[0,0], [rampT,holdF], [endTime, holdF]]
    updateStaticFigure(desiredRampList)
    plt.cla()
    print(rampT)

print(saveFileName)
windowName.close()

if proceedControl==0: # this just stops the next window from opening so you can
actually end the program
```

```
   sys.exit()

# Define a layout for the new window
   # Right Layout
      # Stop Start Pause Reset at top
      # Live plot of force data overlaid with previous curve (if we keep it)
liveRight = [[ sg.VPush()],
             [sg.Button('STOP', k='-STOPBUTTON-', font = ('Impact 25'),
size=(15,2) ),sg.Button('START', k='-STARTBUTTON-', font = ('Impact 25'),
size=(15,2) ), sg.Button('PAUSE', k='-PAUSEBUTTON-', font = ('Impact 25'),
size=(15,2) )],
             [sg.Canvas(k='-LIVEPLOT-')]
            ]
   # Left Layout
      # Stoplight
      # Force Number Readout
liveLeft = [[sg.VPush()],
            [sg.Text(f'{holdF}', k='-READOUTTEXT-', justification='center', font
= ('Impact 72'), size = (10,1))],
           [sg.Push(), sg.Button('TARE', k='-TAREBUTTON-', size =(25, 3)),
sg.Button('GROSS', k = '-GROSSBUTTON-', size =(25, 3)), sg.Push() ],
           [ sg.Push(), sg.Canvas(k='-STOPLIGHT-', size=(650,320),
background_color='#d1a82a'), sg.Push()]
            ]

liveLayout = [[sg.Column(liveLeft), sg.Column(liveRight)]]

# Define the new window that combines these and initialize
liveWindow = sg.Window('Benex Interface 2023', liveLayout, finalize=True)

# Plot Setup
global plotTickr
plotTickr = 1

def setupLiveFigure():
   global figLive
   figLive = matplotlib.figure.Figure(figsize = (7,4))
   figLive.add_subplot(111).plot([],[])
   global figure_canvas_agg_Live
   figure_canvas_agg_Live = FigureCanvasTkAgg(figLive, liveWindow['-LIVEPLOT-
'].TKCanvas) # assign the tkinter object to the canvas in the layout
   figure_canvas_agg_Live.draw() # call the draw method
   figure_canvas_agg_Live.get_tk_widget().pack()

def updateLiveFigure(data, plotTickr):
```

```
    axes = figLive.axes

    if plotTickr >= 200:
       axes[0].cla()
       plotTickr = 1

    x = [i[0] for i in data]
    y = [i[1] for i in data]

    if x[0] <= rampT:
       targY = rampR*(x[0]/60)
       targXList = [0, x[0]]
       targYList = [0, targY]
    else:
       targY = holdF
       targXList = [rampT, x[0]]
       targYList = [holdF, holdF]

    axes[0].plot(x,y,'r.')

    axes[0].plot(targXList, targYList, 'b')
    plotTickr += 1
    figure_canvas_agg_Live.draw() # call the draw method
    figure_canvas_agg_Live.get_tk_widget().pack() #I guess we need pack to send
it to GUI as well
    return plotTickr

# Declare csv writing step based on name obtained from last window
fieldNames = ['Time', 'Force [N]']
writeController = 0 # This variable will control if we are writing to the file
and plot or not
dummyA = 10 # These dummies will be used to hold the place of sensor readings
dummyB = 20
numFiles = 0 # we'll use this to generate new files when the stop button is hit
oldFileName = saveFileName

## Open the CSV file and start the sensor process in the background
with open(saveFileName, 'w', newline='') as saveFile:
   writer = csv.DictWriter(saveFile, fieldnames=fieldNames, restval='NaN') # Feed
parameters into dictionary writer object
   writer.writeheader()

   saveFile.close()

ironPyLocation = 'C:/Users/timga/IPyth/ipy.exe'
```

```
sensProcLoc = 'C:/Users/timga/IPyth/futekDevice.py'
sensorProcess = subprocess.Popen([ironPyLocation, sensProcLoc], stdout =
subprocess.PIPE, stdin = subprocess.PIPE)
setupLiveFigure()
startTime = datetime.now()
tareVal = 0

while True: # While loop that governs the control window
   event, values =  liveWindow.read(timeout=0.5) # Monitor for button presses
   # Read sensor process output
   timeNow = datetime.now()
   timeD = timeNow - startTime
   dummyA = timeD.total_seconds()

   output = sensorProcess.stdout.readline() # read the last line of the
subprocess output
   bitOutput = output.strip() # Strip it down to the bits
   procOutputString = bitOutput.decode('UTF-8') # Decode bits to a UTF8 string

   if event == sg.WINDOW_CLOSED:
      sensorProcess.kill()
      break

   try:
      procOutput = re.findall(r"[-=]?\d*\.\d+|\d+",procOutputString)
      print(procOutput)
      dummyB = 4.44822*float(procOutput[0])-tareVal
   except:
      print('Device Text: ' + procOutputString)

   liveWindow['-READOUTTEXT-'].update(f'{dummyB:.2f} N')


   if writeController ==1: # Conditional for plotting and csvwriting
      with open(saveFileName, 'a', newline='') as saveFile: # if true, append
data to current csvwrite object
         writer = csv.DictWriter(saveFile, fieldnames = fieldNames,
restval='NaN')
         writer.writerow({'Time':dummyA, 'Force [N]':dummyB}) # This is the line
that actually writes it out
         saveFile.close()

      print(plotTickr)
      plotTickr = updateLiveFigure([[dummyA, dummyB]], plotTickr) # if true, plot
last data point
```

```
      if dummyB >= 1.05*holdF:
         liveWindow['-STOPLIGHT-'].update(background_color = '#ff0000')
      elif dummyB >= 0.90*holdF:
         liveWindow['-STOPLIGHT-'].update(background_color = '#ffff00')
      else:
         liveWindow['-STOPLIGHT-'].update(background_color = '#13cb36')


   if event == '-STARTBUTTON-':
      writeController =1
      startTime = datetime.now()


   if event == '-GROSSBUTTON-':
      tareVal = 0

   if event =='-TAREBUTTON-':
      tareVal = dummyB

   if event =='-STOPBUTTON-': # Stop Button
      if writeController == 1:
         writeController = 0
          # kill this window
         newFileName = ''.join([str(numFiles), '_', oldFileName])
         numFiles +=1
         saveFileName = newFileName
         print(saveFileName)
         # Need to clear the graph and initiate the new file
         figLive.clf()
         figLive.add_subplot(111).plot([],[])


   if event =='-PAUSEBUTTON-': # Pause Button
      writeController = 0 # set conditional for plot/csvwrite object loop to
false
```